Spatial-temporal reconstruction of Amazon flood pulse and dry season length over the past century using tree rings and isotopes of floodplain tree species *Macrolobium acaciifolium*

Bruno Barçante Ladvocat Cintra

Submitted in accordance with the requirements for the degree of Doctor of Philosophy

The University of Leeds
School of Geography

March 2019

The candidate confirms that the work submitted is his/her own, except where work which has formed part of jointly-authored publications has been included. The contribution of the candidate and the other authors to this work has been explicitly indicated below. The candidate confirms that appropriate credit has been given within the thesis where reference has been made to the work of others.

Chapter 3:

Cintra, B.B.L., Gloor, M., Boom, A., Schöngart, J., Locosselli, G.M., Brienen, R. 2019. Contrasting controls on tree ring isotope variation for Amazon floodplain and terra firme trees. *Tree Physiology*. https://doi.org/10.1093/treephys/tpz009

BBLC (the candidate), RJB and AB collected samples. BBLC and AB did the laboratory analysis. BBLC analyzed the data. BBLC, RJB and MG wrote the manuscript. All authors contributed to the design and to the final version of the paper.

Chapter 4:

Cintra, B.B.L, Gloor, M., Schöngart, J. Boom, A. and Brienen, R.J. *In prep*. Effects of hydroclimatic variability on ring-widths of *Macrolobium acaciifolium* floodplain trees from different regions within the Amazon Basin.

BBLC collected the samples, analyzed the data and wrote the Chapter. RB and MG reviewed and provided critical feedback to the manuscript. All authors participated in the design of the study.

Chapter 5:

Cintra, B.B.L, Gloor, M., Schöngart, J. Boom, A. and Brienen, R.J. *In prep*. Oxygen isotope ratios in tree rings of *Macrolobium acaciifolium* reflect past climate during the dry and transitional seasons.

BBLC collected the samples, analyzed the data and wrote the Chapter. RB and MG reviewed and provided critical feedback to the manuscript. All authors participated in the design of the study.

Assertion of moral rights:

Acknowledgements

This Thesis is the result of the collaboration and effort of many researchers. Firstly, I would like to thank my internal supervisors Roel Brienen and Manuel Gloor for all the effort they put into revising and contributing to my work. In all times when I was challenged by the difficulties of carrying out a PhD research, both Roel and Manuel showed the patience and help which can be expected from good teachers. I have learned much from both of them, and value all the insights and suggestions that they made to contribute to my research. I also would like to thank Arnoud Boom for his lessons on the isotopes laboratory, for being extremely helpful with my isotopes analyses and for always being available to receive me. I value all the long science conversations we had in Leicester about the many possibilities of doing interesting research in different regions of the Amazon Basin. I also would like to thank Jochen Schöngart for all his teaching on the tree-ring science which prepared me to become a PhD candidate, and for the effort he put into organizing field work expeditions in Brazil.

The development of this Thesis would not have been possible without the funding from Brazilian National Council for Scientific Research through the Science Without Borders program, which funded both my scholarship and many necessary costs related to the development of this research (207400/2014-8). Therefore, I would like to thank the CNPq for the opportunity to study abroad and to contribute to high quality research that helps science advance both in Brazil and globally.

I would also to thank the opportunity to work with many Geographer and Ecologist colleagues who directly or indirectly contributed to my work either by helping me during field and lab work and/or by listening and providing valuable insight to my research, Beto, Carol Signori, Camila Farrapo, Chico Cruz, Francisco Diniz, Giuliano Locosselli, Michelle Kalamandeen, Jessica Baker, my wife Karina LL Melgaço Ladvocat, Santiago Clerici, Vitor Andrade and Vitor Lery. Also all my office mates whose hard work has always been inspiring, Josh, Owen, Scott, Andy, Lawrance, Junfan, Zac, Leam, Louise, Rui.

During this period, I also counted with the support of many friends who were part of my personal development and certainly influenced my ideals and thus my work. Therefore, I want to take this opportunity to mention the names of some of these very important people to me: Adriane, Andy, Alfredo, Andrea, Berna & Carol, Carol Signori, Fer, Marta, Matt, Francisco, Gustavo, Jack, Jess, Jimmy, Julia, Ju Aracaju, Luciene, Thiago and Suzanne.

Finally, I am extremely grateful to my family for all the support and love during this period which I have been away from them. My parents Marcia and Guy, my brothers Rafael and Gustavo, and especially my wife Karina for being always by my side and always giving me strength to move forward. It is also because of them that all the effort makes much sense and this journey would not have been the same without their love and support. Thank you.

Abstract

Climate observations for the Amazon Basin indicate the dry season is becoming drier and longer over recent decades. However, long-term climate data to put these trends in perspective are scarce for most of the Basin, thus hindering our understanding of spatial and temporal variability of the dry season in the Amazon region. I explored the potential of using tree ring-widths and oxygen isotopes in tree rings ($\delta^{18}O_{TR}$) of the floodplain tree species *Macrolobium acaciifolium* as a proxy for past climate conditions during the dry and transitional seasons, the growth period for floodplain trees. I sampled and analyzed wood cores of *M. acaciifolium* trees from floodplain forests located in western, central and southwest Amazon. *M. acaciifolium* presented clear ring definitions, but also frequent false rings requiring careful wood anatomic analysis and cross-dating. Despite these limitations, ring-formation dates estimated by cross-dating of ring-widths closely matched bomb-peak radiocarbon dating of tree-rings. Analysis of climate signals in ring-widths and $\delta^{18}O_{TR}$ revealed potential for reconstruction of past dry season climate conditions, but the strength and nature of climate relationships differed between sites. Ring-width chronologies showed stronger climatic signals at sites located in smaller river catchments from western and southwestern Amazon, where the terrestrial phase of the trees coincided with the peak of the dry season. In contrast, $\delta^{18}O_{TR}$ chronologies showed stronger climatic signals at the sites in western and central Amazon where growing conditions/seasons are wetter. Long-term increases in $\delta^{18}O_{TR}$ since 1970 suggest there has been a drying trend during the dry season of the Amazon Basin, consistent with climate observations for this period. This Thesis shows that floodplain trees growing at sites in smaller catchments with mild dry seasons have the greatest potential as proxies for dry season climate. More studies exploring potentials of different floodplain species, including slow-growing old trees, are recommended.

Contents

List of Tables

List of Figures

Abbreviations

$\delta^{18}O_{air}$ - Oxygen isotope composition of atmospheric vapour

$\delta^{18}O_{SUB}$ – oxygen isotope composition of photo assimilates

$\delta^{18}O_{lw}$ - Oxygen isotope composition of the leaf lamina water

$\delta^{18}O_{sw}$ - Oxygen isotope composition of plant source water

$\delta^{18}O_{es}$ - Oxygen isotope composition at the evaporative sites in the leaf (e.g. stomata and mesophyll spaces)

$\delta^{18}O$ – oxygen isotope composition

$\delta^{18}O_{TR}$ - Average oxygen isotope composition of tree ring cellulose

$\Delta^{13}C$ – carbon isotope discrimination

$\delta^{13}C_{plant}$ - Carbon isotope composition in plant tissues

$\delta^{13}C_{atm}$ - Carbon isotope composition in atmospheric CO_2

$\wp$ - Peclet Number

ϕ - proportion of oxygen in photo assimilates that exchanges with stem water during cellulose synthesis

a - Fractionation during CO_2 diffusion through stomata

b - Fractionation due to isotopic discrimination during carboxylation

A - Assimilation rate of CO_2 during photosynthesis

AMO – Atlantic Multidecadal Oscillation

Avg - average

C – molar concentration of water

c_a - Atmospheric CO_2 partial pressure

c_i - Leaf internal CO_2 partial pressure

CRU – Climate Research Unit

D - Diffusion rate of $H_2{}^{18}O$ in water

e_a - Atmospheric vapour pressure

e_i - Leaf internal saturated vapour pressure

e_{sat} - Saturated vapour pressure

E – Leaf transpiration

ENSO – El Niño Southern Oscillation

GCM – General circulation models

g_s – stomatal conductance to CO_2

g_{s0} - Maximum stomatal conductance

g_{sMax} - Maximum stomatal conductance

g_{sW} – stomatal conductance to water

g_m – mesophyll conductance

g_{m25} - mesophyll conductance at 25°C

g_b - Leaf boundary layer conductance

ITC – inter-series correlation

IRMS – Isotope ratio mass-spectrometer

L – the length of the path from the stomata into the leaf veins

PDO – Pacific Decadal Oscillation

precip. - Precipitation

NSC – Non-structural carbohydrates

FP - Floodplain

MS – mean sensitivity of ring-width series

TF – terra firme

P - Atmospheric pressure

$p_x p_{ex}$ - Proportion of enriched water in the cell (p_x) and proportion of oxygen exchanged with water in the cell during cellulose synthesis (p_{ex})

ε_k - Kinetic fractionation factor during diffusion of H_2O from stomata to the atmosphere

ε^* - Equilibrium fractionation during evaporation of $H_2{}^{18}O$

ε_{wc} - Fractionation of oxygen during synthesis of sugars in the leaf

ITCZ - Intertropical Convergence Zone

R – Isotope ratio

$\bar{R}$ - mean of all pair-wise correlations

RH – Relative humidity

RuBisCO - Ribulose-1,5-bisphosphate carboxylase/oxygenase

SST – sea surface temperature

STN – standardized ring-width series

SNIRH-ANA – Sistema Nacional de Informações Hidrológica/Agência Nacional das Águas

SENHAMI – Servício Nacional de Meteorología y Hidrología del Peru

TNA – Tropical North Atlantic

TRMM - Tropical Rainfall Measuring Mission

TSA – Tropical South Atlantic

T_{leaf} - Leaf temperature

T_{air} – air temperature

T – temperature

TS – time series

u – Velocity of the advective transport of water from leaf veins to stomata VPD - Atmospheric vapour pressure deficit

U - Wind speed

VPD_0 - Average vapour pressure deficit over the growing season

VSMOW – Vienna Mean Standard Ocean Water

W - Leaf lamina diameter

Chapter 1 **Introduction**

1.1. Background

The Amazon Basin and its extensive area of continuous tropical rainforests are an important component of the global climate system. This region in tropical South America constitutes one of the three major centres of deep atmospheric convection on Earth, alongside tropical Africa and the tropical Western Pacific, and is connected to the global atmospheric circulation via the Walker and Hadley atmospheric circulation cells (Garreaud et al., 2009). The direct influence of the Intertropical Convergence Zone (ITCZ) and the intense atmospheric convection over the Amazon region result in high rainfall amounts, contributing almost 20% of the global freshwater discharge into the Oceans (Salati and Vose, 1984; Richey et al., 1986, Callede et al., 2010). These wet and warm climate conditions sustain the world's largest wetland areas and the largest continuous tropical rainforest, representing almost half of all tropical forests and harbouring the world's most diverse forest ecosystems (ter Steege et al., 2013; Slik et al., 2015; Antonelli et al., 2018).

To a large extent, the contribution of the Amazon Basin to the global climate system is owed to its extensive forest areas. Over the 5 million km^2 of rainforest landscape, forest trees recirculate water to the atmosphere through evapotranspiration (Salati et al., 1979; Costa and Foley, 1999; Spracklen et al., 2012), alter the atmospheric chemistry (Arneth et al., 2010) and produce biogenic aerosols that promote cloud formation (Pöschl et al., 2010; China et al., 2018). Thereby the forests act as a source of rainfall over South America (Salati et al., 1979; Henderson-Sellers et al., 2002; Marengo, 2005). It is estimated an average 30% of all precipitation within the Basin originates from evapotranspiration, with this number reaching over 50% during the dry season in the southwest of the Amazon (Van Der Ent et al., 2010; Spracklen et al., 2012; Harper et al., 2014; Zemp et al., 2014; Zemp et al., 2017).

Besides playing an important role for the global hydrological cycle, Amazon forests also affect global climate conditions by exchanging greenhouse gases with the atmosphere. Due to the high temperature and productivity of tropical ecosystems, tropical wetlands are among the main sources of methane to the atmosphere (Belger et al., 2011; Bloom et al., 2012; Pangala et al., 2013), with Amazon wetland forests and peatland swamps releasing an estimated 47 million tons of methane annually to the atmosphere (Kirschke et al., 2013; Pangala et al., 2017). On the other hand, tree growth in the Amazon forest removes from the atmosphere an estimated 380 million tons of carbon per year (Phillips et al., 2009; Beer et al., 2010; Pan et al., 2011; Brienen et al., 2015). Due to the large amounts of carbon the forests remove from the atmosphere, it is considered that they currently function as a terrestrial carbon sink (Malhi et al., 2008; Brienen et al., 2015; Feldpausch et al., 2016), thereby helping to slow down atmospheric CO_2 growth and decelerate global warming (Dixon et al., 2006; Pan et al., 2011; Le Quéré et al., 2015).

The relevance of the natural Amazon ecosystems and the services provided by them often clash with the economic development in this region (Davidson et al., 2012; Nobre et al., 2016). The Amazon region is an important component of the economies of eight countries in South America and is home to over 20 million people who depend on its resources for agriculture, transport, energy production and different aspects of their livelihood (Stickler et al., 2013; Marengo et al., 2013; Magrin et al., 2014; Pinho et al., 2015). While the region is mostly scarcely populated and its natural landscape largely preserved, expanding human occupation has caused relatively rapid changes in the natural forest landscape, especially since 1970s with the Brazilian national integration plans (Nobre et al., 2016). The primary causes of these changes are the construction of roads, agriculture and logging (Fearnside, 2005; Soares-Filho et al., 2006; Nepstad et al., 2014; Chen et al., 2015) and the construction of dams (Melack and Wang, 1998; Manyari and de Carvalho, 2007; Tundisi et al., 2014; de Resende et al., 2018), all of which are often followed by expanding human occupation and consequent deforestation and increased frequency of forest fires (Aragão et al., 2007; Nepstad et al., 2014; Flores et al., 2017). Today nearly 20% of

the Amazon's original forest cover are already lost, especially in the south and southeast, on the so-called deforestation arc.

The effects of these drastic alterations in the natural forest landscape go beyond its obvious immediate impacts for the natural environment and the biodiversity in the region. They may also have consequences for the hydroclimatic conditions of the Amazon, and potentially for global warming. While small-scale deforestation may lead to slightly increased precipitation over deforested areas (Roy and Avissar, 2002), removal of more than 20% of the forest cover has led to drier and warmer climate conditions in deforested regions of the Amazon (Gash and Nobre, 1997; Butt et al., 2011; Dubreuil et al., 2012; Randow et al., 2015; Spracklen and Garcia-Carreras, 2015) and altered river runoff patterns (Costa et al., 2003; Coe et al., 2011). Meso-scale modelling studies supported by satellite images suggest these effects are caused by reduction in evapotranspiration from the forest and consequent alterations in cloud formation and moisture transport over the deforested region (Wang et al., 2009; Spracklen et al., 2012). Such alterations also potentially delay the onset of the wet season, contributing to a longer and more intense dry season (Fu et al., 2013; Spracklen and Garcia-Carreras, 2015; Wright et al., 2017). The scenario of hydroclimatic changes due to deforestation in the Amazon is further aggravated by the effects of global warming due to increasing atmospheric CO_2 levels, which alters large-scale atmospheric circulation and potentially intensifies climatic extremes in the Amazon (Flato et al., 2013).

Such a scenario of deforestation and extreme climatic conditions would have significant impacts for the human population in the Amazon region (Betts et al., 2008; Marengo et al., 2013; Magrin et al., 2014; Pinho et al., 2015). For example, during years with anomalously wet climate, entire villages have been completely submerged by floods and/or were cut off from food and medical supplies, while at the same time vector- and water-borne diseases propagate more rapidly (Singer and Castro, 1995; Vittor et al., 2006; Marengo et al., 2013; Brondízio et al., 2016). On the other end of climatic extremes, during dry years, there is an elevated number of respiratory health

issues associated with smoky atmospheric conditions caused by large-scale forest fires (Anderson et al., 2011, Smith et al., 2014). Drier than usual climate conditions also cause reductions in agricultural production and fishery resources with severe economic risk for local farmers (Moran et al., 2006; Brondizio and Moran, 2008; Anderson et al., 2011; Röpke et al., 2017), and reduce hydropower generation potential, hampering the already controversial hydro-energetic planning of the region (Stickler et al., 2013).

Besides affecting human living conditions in the region, extreme climatic conditions resulting from both deforestation and global warming have profound effects for the Amazon forests at a large-scale (Betts et al., 2008; Davidson et al., 2012; Feldpausch et al., 2012). The occurrence of severe droughts over the last three decades (Marengo and Espinoza, 2015) led to widespread mortality of trees in the Amazon region (Nepstad et al., 2007; Phillips et al., 2009; Costa et al., 2010; Allen et al., 2010; Lewis et al., 2011; Brienen et al., 2015; Feldpausch et al., 2016), affected the CO_2 exchange between the forest and the atmosphere (Gatti et al., 2014; Humphrey et al., 2018), increased the risk and scale of fire propagation in the forest (Alencar et al., 2005; Aragão et al., 2007; Flores et al., 2017; Schöngart et al., 2017) and led to a decline of the net carbon accumulation in forest biomass (Brienen et al., 2015; Feldpausch et al., 2016). In addition to drought, unusually high river levels over the last decade may have negative impacts for seasonal floodplain forests. As different floodplain tree species have different levels of flood tolerance (Parolin et al., 2004; Junk et al., 2010), alterations of the river's hydrological regime may subject floodplain trees to flood levels beyond their adaptive capacity. This may potentially lead to large scale forest dieback in these ecosystems (Assahira et al., 2017; de Resende et al., 2018), which represent roughly 20% of all Amazon forests (Junk et al., 2014). These impacts of droughts and floods may result in the release of substantial amounts of carbon from the forest to the atmosphere, which in turn may provide a positive feedback on regional and global climate change (Andreae et al., 2004; Aragão et al., 2018).

As deforestation in the Amazon is progressing, global atmospheric CO_2 continues to increase steadily and extreme droughts and floods in the region seem to become more frequent, there is growing need to understand and predict the evolution of hydroclimatic conditions of the Amazon over the coming decades. Early General Circulation Models (GCM) predicted that large-scale deforestation in the Amazon would likely lead to drier climate conditions and longer dry seasons (Shukla et al., 1990; Nobre et al., 1991; Henderson-Sellers et al., 1993; Costa and Foley, 2000). Although these early simulations tended to overestimate the regional effects of deforestation in comparison with predictions by more detailed mesoscale models (Roy and Avissar, 2002; da Silva and Avissar, 2006; Costa et al., 2007; Sampaio et al., 2007; D'Almeida et al., 2007; Costa and Pires, 2010; Medvigy et al., 2011), they raised concerns that such changes could drive large-scale mortality of Amazon forests, accelerating global warming through the release of substantial amounts of carbon to the atmosphere (Cox et al., 2000; Cox et al., 2004; Malhi et al., 2008; Nobre et al., 2009) and possibly result in climate changes in different parts of the globe (Gedney and Valdes, 2000; Werth and Avissar, 2002; Avissar and Werth, 2005; but see also Lorenz et al., 2016). More recent GCMs are becoming increasingly more realistic and capable in predicting climate changes in the Amazon due to both deforestation and increasing atmospheric CO_2. As a general consensus (or "model democracy" as stated by Boisier et al., 2015), the GCMs which are part of the Coupled Model Intercomparison Project Phases 5 and 6 (CMIP5 and CMIP6) still suggest the Amazon may undergo a drying trend, with a possible prolonged dry season (Boisier et al., 2015; Fernandes et al., 2015), increased frequency of climate extremes due to an intensification of monsoonal circulation (Kitoh et al., 2013), and increased (decreased) inundation in the northwest and central (east and southeast) of the Amazon (Sorribas et al., 2016). However, there are large discrepancies between different model predictions, and the uncertainties of model predictions for the Amazon region are still large.

Only few GCM predictions suggest a mechanism which may be consistent with the recent trends and observations in the hydrological cycle of the Amazon (Kitoh et al.,

2013; Fernandes et al., 2015; Li et al., 2016; Hua et al., 2019). These observations do not show a drying trend in the Amazon, but rather point to an hydroclimatic intensification of the region (Gloor et al., 2013; Gloor et al., 2015; Barichivich et al., 2018). This intensification has resulted in increased precipitation during the wet season in the northwest of the Amazon, increased Amazon river runoff and small decreases in precipitation during the dry season in the south and east of the Amazon (Gloor et al., 2013; Gloor et al., 2015; Barichivich et al., 2018). Rather than being caused by internal changes in climate due to deforestation, these changes have been attributed to external climate forcing related to decadal variability in the sea surface temperatures of the surrounding Ocean basins, with a central role of the Tropical Atlantic sea surface temperatures, and possible aggravation due to global warming (Barichivich et al., 2018). Nevertheless, the climate conditions in the Amazon Basin are spatially and temporally heterogeneous and there are still large uncertainties regarding how different regions in the Amazon may be affected by potential climatic changes resulting from both deforestation, global warming and also natural climate variability related to large-scale climate cycles. In particular, there is not much consensus about the evolution of the dry season length and intensity in the Amazon (Boisier et al., 2015). Some studies suggest that deforestation is already leading to longer and/or drier dry seasons in the Amazon (Fu et al., 2013; Marengo and Espinoza, 2015; Spracklen and Garcia-Carreras, 2015; Khanna et al., 2017).

The uncertainties in the predictions the future climate conditions in the Amazon may be partially attributed to incomplete understanding of the mechanisms that drive spatial and temporal climate variability in the Amazon. Such incomplete understanding is caused by a lack of reliable hydroclimatic data for more than 30 years in most of the region. Thus, a significant contribution for this field may be achieved by obtaining more information about past hydrologic conditions in the Amazon, and identifying the regional differences in the climate variability. Obtaining information about past dry season climate variability in different sub-basins of the Amazon is the main objective of this thesis, which examines whether and how to use tree rings of Amazon floodplain trees as proxies for past dry season climate. In the

following sections, I will detail the main characteristics of the hydroclimatic variability in the Amazon, highlighting the main gaps of knowledge and how we can contribute to this field through the use of different proxies for past climate conditions.

1.2.Climate variability in the Amazon Basin

Spatial and seasonal climate variability of the Amazon Basin are related to large-scale atmospheric circulations over South America which are part of a monsoon-like pattern known as the South American Monsoon System (Zhou and Lau, 1998; Vera et al., 2006). To a large extent, these atmospheric changes result from the seasonal shift in the mean latitudinal position of the Intertropical Convergence Zone (ITCZ), which shifts seasonally from approximately 9^{o}N in the boreal summer to 2^{o}N in the austral summer (Schneider et al., 2014).

The development of the Summer Monsoon in South America is characterized by the following processes: i) a strengthening of the trade winds from the Tropical North Atlantic, ii) intensification of the convective centre over most of central South America, iii) development of a high level anti-cyclonic circulation (the Bolivian high) over the Altiplano region and the low level low (the Chaco Low) to the east of the Andes over Bolivia; iv) intensification of the low level south American jet on the east site of the Andes, which brings moisture from the Amazon to the south and south-east of south America; v) and the development of a band of cloudiness and precipitation from the southern Amazonia to the Atlantic Ocean off the southeast coast of Brazil known as the South Atlantic Convergence Zone (Zhou and Lau, 1998; Marengo, 2004; Vera et al., 2006; Garreaud et al., 2009; Liebmann, 2011).

The atmospheric circulation associated with the South American Monsoon System results in high moisture inflow into the Amazon Basin via the trade winds from the Atlantic and in an intense atmospheric convection over the Basin. The resulting hydrological cycle of the Amazon Basin is characterized by generally wet conditions with an average 2400mm rainfall per year over the entire catchment. During the summer monsoon, when the mean latitudinal position of the ITCZ shifts southward,

South America receives more than 70% of its total annual precipitation (Vera et al., 2006). In the southern regions of the Amazon Basin, year-round precipitation may also have contributions from the advection of extra-tropical moisture from low level anti-cyclonic excursions from the south, which may account for a significant portion of the total precipitation during the dry season, after the summer monsoon retreats (Garreaud and Wallace, 1998; Hurley et al., 2016; Ovando et al., 2016).

Retreat of the South American Summer Monsoon starts when the mean latitudinal position of the ITCZ shifts northward, causing a reduction of the moisture inflow via the trade winds from the Tropical Atlantic, and a weakening of the atmospheric convection over the Amazon and central South America. This results in a significant reduction in precipitation amounts, with most of South-America presenting a well-defined annual dry season. While this dry season may last up to 6 months in some regions of the Amazon Basin, the total annual rainfall amounts and seasonality are spatially variable across this large region (Figure 1.1).

1.2.1. Climate seasonality and the flood pulse of Amazon Rivers

In general, the north-western regions of the Amazon Basin are the wettest, with annual rainfall up to 3500mm well distributed throughout the year. Towards the south and southeast of the Basin, total annual precipitation tends to decrease, with total annual precipitation of 1700mm in some regions. In these regions, most of the precipitation is concentrated in the wet season, with up to 5 months with less than 100mm of rainfall (Figure 1.1).

One of the consequences of the seasonal variations in rainfall in the Amazon is its effects on the levels and discharges of Amazon rivers. During the transition from the dry to the rainy season, the increases in rainfall amounts over the whole Basin are followed by increases in the discharge amounts of the rivers and a significant rise in the river levels. Between the lowest and the highest phases, river levels may vary up to 6m small Amazon tributaries, i.e. upstream in the sub-basins of the Amazon, and up to 15m in the main stream of the Amazon River.

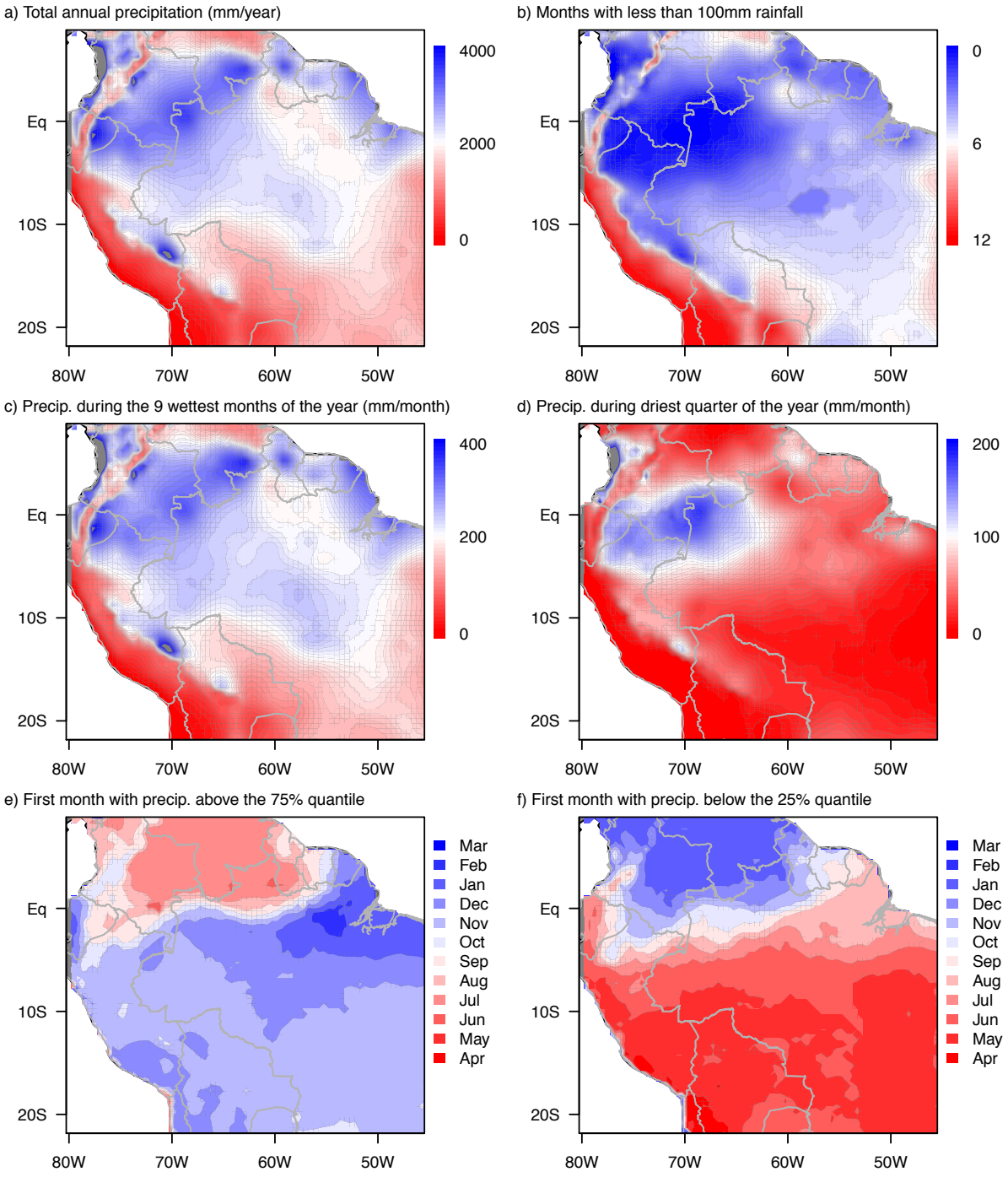

Figure 1.1. Spatial and seasonal variation of precipitation in the Amazon. (a) Variation in total annual precipitation, (b) number of months with less than 100 mm of rainfall, (c) mean monthly precipitation during the 9 wettest months of the year, (d) mean monthly precipitation during the 3 driest months of the year, (e) wet season starting month and (d) dry season starting month. All calculations based on long-term means of each grid point individually. Data from CRU TS 4.00 Climatology, 1980-2015 A.D.

Such seasonal fluctuations in the river levels are known as the annual flood pulse of Amazon Rivers. The flood pulse results in the seasonal inundation large areas along the river banks, where the seasonal floodplain forests occur (Figure 1.2).

The spatial and temporal hydroclimatic variations in the Amazon are of high ecological importance for the region. In non-flooded areas, the dry season length and intensity are strong determinants of large-scale patterns of forest tree species distribution (Souza et al., 2016; Esquivel-Muelbert et al., 2017), forest structure and biomass stocks across the basin (Malhi et al., 2004; Phillips et al., 2004; Quesada et al., 2012; Schietti et al., 2016). In contrast, distinct ecosystems exist in the floodplains of the Amazon, where the flood pulse is the dominant determinant of species distributions and forest structure. These differences in the factors that limit tree growth also influence how different forest ecosystems in the Amazon respond to climate variability at inter-annual and longer time scales. In the next sections, I will detail some of the main aspects of the climate variability in the Amazon at different time scales.

1.2.2. Inter-annual climate variations in the Amazon

On a year-to-year basis, climate in the Amazon is influenced by variations in the amount of moisture inputs into the basin via the trade winds from the Atlantic Ocean, and by the intensity of the atmospheric convection over the region. Both moisture inflow and convection intensity may be enhanced or suppressed by influences of the sea surface temperatures of the tropical eastern Pacific and tropical Atlantic oceans. Warm SSTs in these oceans may alter convective activity and the direction of the trade winds that bring moisture in to the Amazon, thereby affecting rainfall patterns in the Basin (Costa and Foley, 1999; Foley et al., 2002; Marengo, 2004; Marengo et al., 2008; Marengo, 2009; Yoon and Zeng, 2010; Gloor et al., 2013; Gloor et al., 2015; Barichivich et al., 2018).

One of the strongest controls of the inter-annual variation of climate in the Amazon Basin is the El Niño Southern Oscillation (ENSO), which is related to the Walker

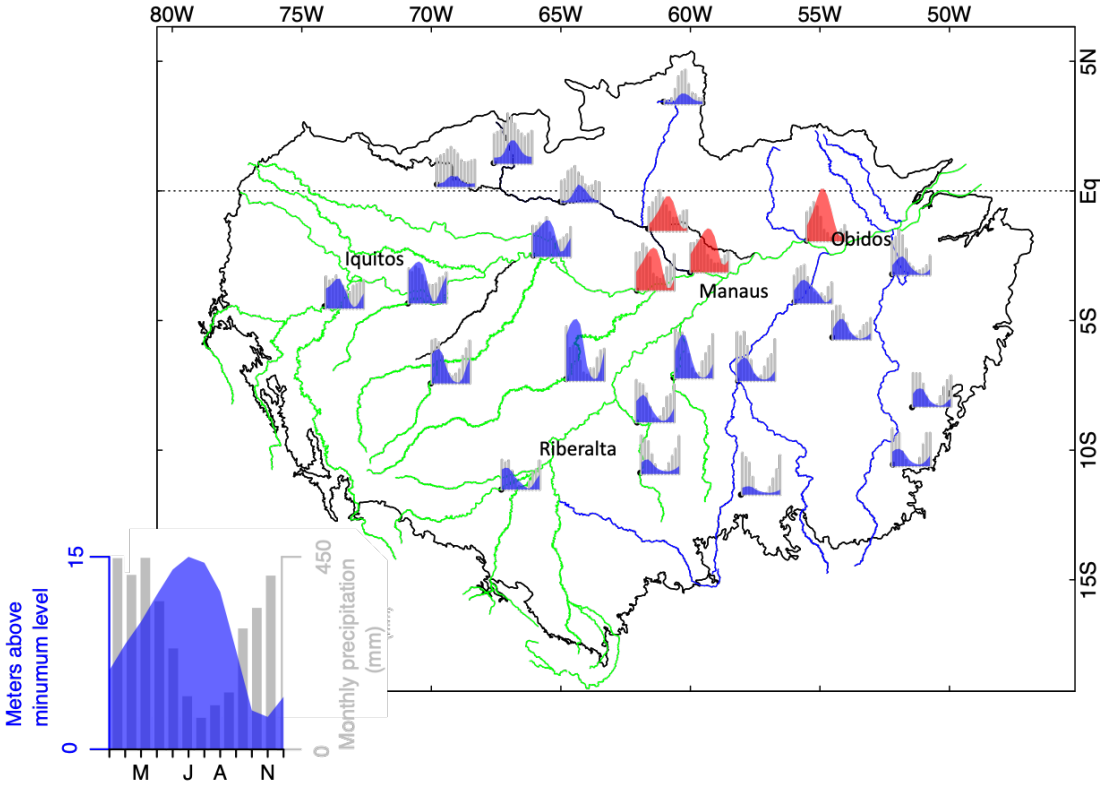

Figure 1.2. Map of the Amazon basin highlighting the rivers with blackwater that originate in the Guiana shields (black lines), "white" water that originate in the Andes (green lines) and clear water which originate in the Brazilian and Guiana shields (blue lines). Hydrographs show the seasonality in precipitation (gray bars) and river level (blue shading) for various rivers across the basin. Red hydrographs indicate locations where the seasonality of the river levels lags the seasonality of local rainfall by 2 or more months. Data from hydroclimatic stations from the Brazilian Water Agency (ANA), from 1990 to 2015 A.D.

Circulation over the Pacific Ocean and tropical South America. During "neutral" years of the ENSO, the trade winds over sea level of the tropical Pacific are favoured by a zonal (east-west) temperature difference of the SST, with warm waters in the west and cooler waters in the east. These temperature differences create a pressure gradient between the cool east SST (high pressure) and warm west SST (low pressure) which is in the same direction as the trade winds. Under these conditions, the Walker Circulation over the tropical Pacific has two main convection centres, one over the Amazon Basin and one over the western tropical Pacific, and a main centre of subsidence over the central-eastern tropical pacific (Foley et al., 2002).

During the La Niña phase of the ENSO, when SST of the central-eastern tropical Pacific are colder than average, the trade winds over the Pacific are intensified, the Walker

Circulation is strengthened, and atmospheric convection over the Amazon is increased. This leads to increases of precipitation over the region and river discharges in the Amazon (Figure 1.3cd). During the El Niño phase of the ENSO, when SSTs of the central-eastern tropical Pacific Ocean are warmer than average, the trade winds are weakened. The main convection centres shift to the central tropical Pacific, resulting in subsidence of dry air over the Amazon Basin, which suppresses the atmospheric convection over this region (Aceituno, 1988; Foley et al., 2002). This reduces the precipitation over the region (Figure 1.3), causing intense droughts such as those observed in 1912, 1926, 1982, 1990, 1994, 1997 (Foley et al., 2002; Marengo, 2009; Espinoza et al., 2011; Barichivich et al., 2018).

Although ENSO is a main control of climatic variability in the Amazon, its effects vary spatially and it does not explain the interannual climatic variability over the entire Amazon (Marengo, 2004; Marengo, 2009; Yoon and Zeng, 2010; Marengo and Espinoza, 2015) (Figure 1.3a,b). The Influence of ENSO on rainfall is pronounced in the northern and eastern portions of the Basin (Sombroek, 2001; Marengo, 2004; Marengo, 2009; Espinoza et al., 2011), but less so in the southern sectors. Inter-annual rainfall variability in the Amazon may also be affected by the SST gradient of the tropical Atlantic Ocean (Hastenrath and Heller, 1977; Marengo, 2004; Cox et al., 2008; Yoon and Zeng, 2010; Gloor et al., 2013; Marengo and Espinoza, 2015; Gloor et al., 2015; Barichivich et al., 2018). For example, the drought of 1964, 1979, 2005 and 2010 were not associated with ENSO, but to warmer-than-usual SST of the tropical region of the Atlantic Ocean North of the equator (Tropical North Atlantic, 80^{o} to 20^{o}W, 8^{o} to 22N) in comparison to SST of the Tropical South Atlantic (35^{o}W to 10^{o}E, 24^{o}S to 2^{o}N) (Yoon and Zeng, 2010; Marengo et al., 2012) – Figure 1.3.

The effect of warm SSTs of the Tropical Atlantic on Amazon rainfall has been attributed to shifts in the position of the Intertropical Convergence Zone, affecting the moisture inflow into the Amazon (Marengo et al., 2008; Marengo, 2009; Yoon and Zeng, 2010). Warmer than usual SSTs of the Tropical North Atlantic are

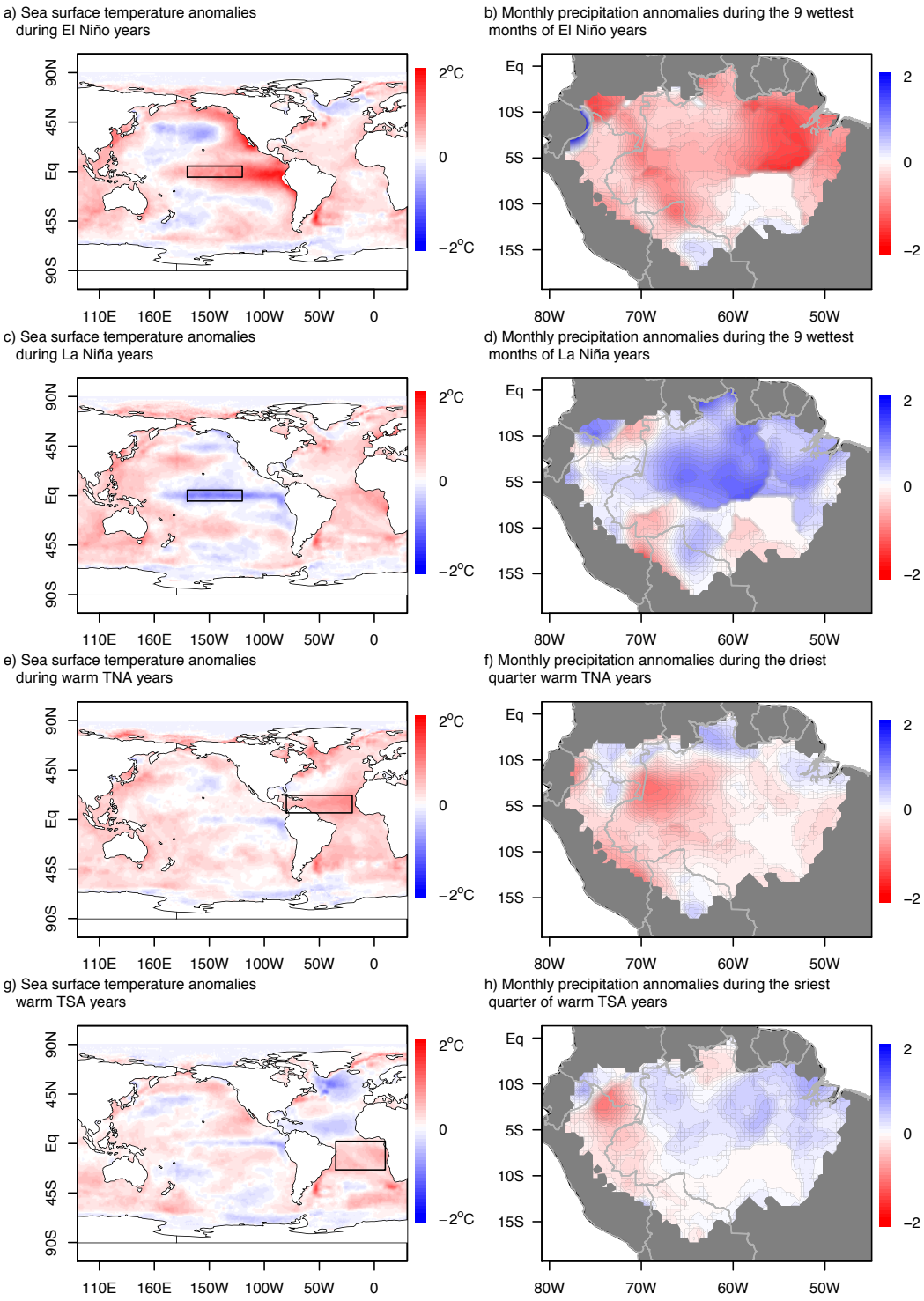

Figure 1.3. Sea surface temperature anomaly patterns (SSTA) and effects on Amazon rainfall. (a) SSTA in El Niño years and associated (b) wet season rainfall; (c) SSTA in La Niña years and associated (d) wet season rainfall anomalies; (e) SSTA during the warm phase of the Tropical North Atlantic and associated (f) dry season rainfall anomalies; (g) SSTA during the warm (cold) phase of the Tropical South (North) Atlantic and associated (h) dry season rainfall anomalies. Polygons in SST maps (left panels indicate the position of the Nino3.4 region (a,b), of the Tropical North Atlantic region (e) and of the Tropical South Atlantic region (g). Color scale in (b,d,f,h) are in standard deviations from the mean. Wet and dry periods were calculated from each grid point separately. Rainfall data from CRU TS 4.00 climatology and SST data from HadSST1 climatology, 1980-2017 A.D.

associated with precipitation reductions in the basin mainly during the dry season and the southwest of the Amazon Basin. For example, the drought of 2005 which was related to warmer than usual SSTs of the TNA affected mostly the southern and western sections of the Basin, and although it started during the rainy season, it was stronger during the dry season (Marengo et al., 2008; Yoon and Zeng, 2010). In contrast, warm SSTs of the tropical south Atlantic have been related to increases in precipitation in the southern sectors of the Amazon (Marengo, 2004; Marengo, 2009) and reduced Amazon river discharge to the Atlantic Ocean (Espinoza et al., 2011; Gloor et al., 2015). Thus the effects of the Tropical Atlantic SST gradients differ from the effects of ENSO, both spatially and seasonally (Marengo et al., 2008; Marengo, 2009; Yoon and Zeng, 2010)

These large-scale controls also affect the hydrological discharge of Amazon rivers, which drain rainfall from large catchment areas. Various studies have also looked at records of river flow and rainfall in sub-basins of the Amazon which show variable and sometimes opposing short-term (decadal) trends during the 20th century (Gentry and Lopez-Parodi, 1980; Marengo et al., 1998; Costa and Foley, 1999; Marengo et al., 2004; Espinoza Villar et al., 2009). These studies show the complexity of the different controls that affect decadal variability of climate in the Amazon, with differences in the controls between the northern and southern portions of the basin (Figure 1.4). Climatic and river records which span ~ 100 years indicate that the Amazon hydrological cycle is intensifying, with increases in precipitation in the north and north west of the Amazon and a decrease in the south and southeast (Marengo, 2009; Gloor et al., 2013; Barichivich et al., 2018). These differences in the climate between the north and the south of the Basin reflect the different mechanisms that control inter-annual climate variability in different regions of the Amazon basin.

1.2.3. Multidecadal climate variations in the Amazon

Multidecadal hydrometeorological variations in the Amazon basin are also attributed to the interaction of SSTs in the tropical Pacific and Atlantic Oceans (Marengo, 2004;

Marengo, 2009; Barichivich et al., 2018). The SSTs of the Pacific Ocean oscillate on multidecadal cycles known as the Pacific Decadal Oscillation (PDO) (Zhang et al., 1997). The PDO is characterized by a warm and a cool phase, which are related to the SST gradient between the northern Pacific and the tropical Pacific. Each phase lasts approximately 28 years. During the cool phase, the northern Pacific Ocean SST is warmer than average and the equatorial SST is cooler than average. The opposite warm phase of the PDO is characterized by cooler than average SST in the northern Pacific Ocean and warmer than average SSTs in the equatorial Pacific Ocean. A cold or warm phase of the PDO may last 20-30 years, resulting in multidecadal variations in climatic conditions and river discharge in the Amazon Basin (Marengo, 2004; Marengo, 2009). The warm phase of the PDO is associated with drier periods in the Amazon, and with the occurrence of more frequent El Niño events, for example during the period from 1978 to 1996 when three strong El Niño events occurred (Marengo, 2009).

Long term trends in Amazonian rainfall have also been attributed to SST gradients in the Atlantic Ocean (Marengo, 2009; Yoon and Zeng, 2010; Gloor et al., 2015; Barichivich et al., 2018). For example, a warming trend in the tropical South Atlantic before the 1975 was related to more precipitation in the southern Amazon (Costa and Foley, 1999; Marengo, 2009). Approximately from that period until now, the inverse trend has been occurring, with a multi-decadal warming of the Tropical North Atlantic (Gloor et al., 2013; Servain et al., 2014; Gloor et al., 2015). This warming of the Tropical North Atlantic in part reflects the decadal variability of the SST of the north Atlantic, the Atlantic Multidecadal Oscillation, which has been suggested to be an important mechanism controlling the variability of the South American Monsoon system (Chiessi et al., 2009). The Atlantic Multidecadal Oscillation is a decadal variability of the SST of the North Atlantic which has a cycle of approximately 65yrs (Kerr, 2000; Enfield et al., 2001). It is closely linked to an interoceanic transfer of warm water from the Indian to the Atlantic Ocean via the Agulhas region in the south of Africa (Biastoch et al., 2009; Biastoch et al., 2015), which has intensified over the last 30yrs, possibly as a consequence of global warming (Biastoch and Böning, 2013).

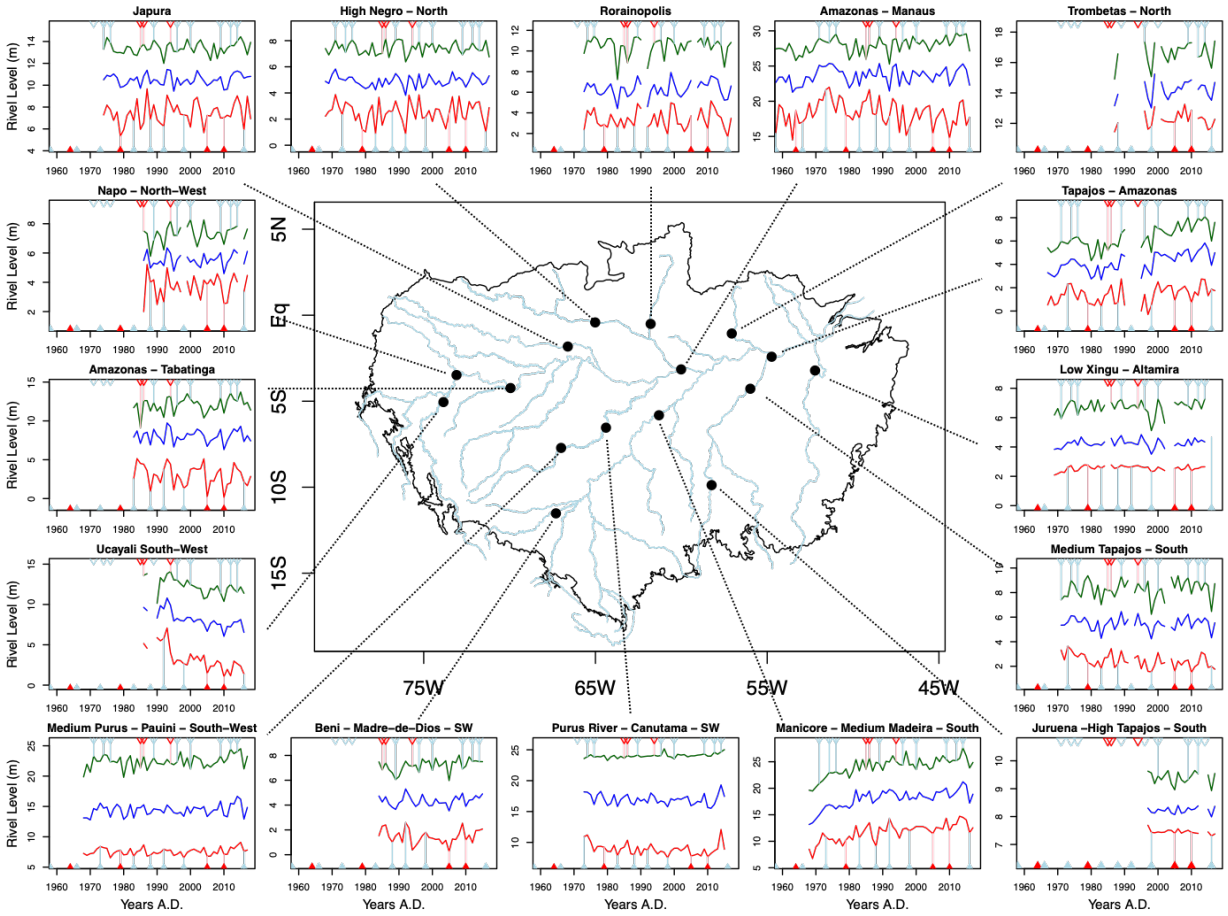

Figure 1.4. River-level anomalies in some of the major Amazon rivers recorded from hydrological stations in the Amazon Basin. The locations of the stations are indicated as black dots in the map. For each station, the annual maximum (green), mean (blue) and minimum (red) are shown. In each graph, blue triangles in the bottom (top) indicate El Niño (La Niña) years and red triangles in the bottom (top) indicate years with anomalously warm sea surface temperatures in the Tropical North (South) Atlantic Region.

Such interaction between these two Ocean basins has been pointed as one of the main causes for the recent warming trend of the tropical North Atlantic, and in an increased trans-basin SST difference between the tropical Atlantic and Pacific Ocean. This increasing trans-basin SST gradient resulted in a strengthening of the Walker Circulation (McGregor et al., 2014), and consequently led to the progressive intensification of the hydrological cycle of the Amazon Basin over the last 30yrs (Gloor et al., 2013; Gloor et al., 2015; Barichivich et al., 2018).

It is clear that the hydrological cycle of the Amazon cannot be explained solely by the effects of one external control. It is rather controlled by an interaction between the

different Ocean Basins (Barichivich et al., 2018). Although the ENSO is undoubtedly a strong control of the hydrological cycle in the Amazon at inter-annual scales, the recent studies discussed above show that the Atlantic Ocean plays a central role, both in the decadal variability of the hydrological cycle of the Amazon and likely in longer time scales (Chiessi et al., 2009).

1.3. Use of proxies for past climate variability in the Amazon

Past Amazon climate variability has been explored using proxy records extending back over time-scales of hundreds to thousands of years. For example, the concentration of different iron-oxides in terrigenous sediments off the Atlantic Coast of South America (the Ceara rise) show millennial scale variations in Amazon river runoff between glacial and interglacial periods for 1 million years (Harris and Mix, 1999). While this is a unique record in terms of its reach into the past, it is also of very coarse resolution.

Numerous other proxy records for hydrology of the Amazon basin and South America have a significantly shorter reach, spanning approximately 5 to 25 thousand years, but have higher resolution, on the order of decades. These proxies generally reveal the susceptibility of the hydrological cycle in South America and in the Amazon to the latitudinal shifts of the Intertropical Convergence Zone driven by variations in the summer insolation and the earth's precessional cycle. They are based on (1) oxygen isotopes in calcite of speleothems from several parts of Brazil (Cruz et al., 2005; Cruz et al., 2006; Cruz et al., 2009; Stríkis et al., 2011; Wang et al., 2017) and Peruvian/Bolivian Andes Mountains (van Breukelen et al., 2008; Reuter et al., 2009; Cruz et al., 2009; Kanner et al., 2013; Wang et al., 2017), with the longest records from Cruz et al. (2009), spanning 126 thousand years, and from Wang et al. (2017), spanning 45 thousand years, (2) oxygen isotopes in glaciers from the Andes (Thompson et al., 1995; Thompson et al., 2000) which reach back to 25 thousand years, (3) several proxy types from lake sediments from the Andes (Baker et al., 2001; Wolfe et al., 2001), (4) carbon isotopes in organic molecules of peat bogs as indicators of past temperature variability (Skrzypek et al., 2011; Engel et al., 2014), (4) oxygen

isotopes in foraminifera in the discharge region of the Amazon River (Maslin and Burns, 2000) and of the La Plata River (Chiessi et al., 2009), (5) and in iron oxides of marine sediments in the Cariaco Basin off the Venezuelan coast (Haug et al., 2001). In many cases these proxies also have annual resolution for a time window spanning few hundred years up to a few thousand years (Hoffmann et al., 2003; Black et al., 2007; Vimeux et al., 2009; Bird et al., 2011; Thompson et al., 2013; Novello et al., 2016).

While these records are long and provide valuable information, they are often hard to obtain, as is the case for ice cores, or very rare in the Amazon basin, as is the case of speleothems and lake sediments. There is only one speleothem record for the Amazon (Wang et al., 2017), which is located in the east of the Basin, while to date there are no speleothem records in the central Amazon region. Thus, they do not provide a spatially resolved climate reconstruction within the basin, and accurate proxies of Amazon hydrology over the recent past with annual resolution are still scarce. Records for different regions within in the Amazon are still needed to assess effect of large-scale climate controls on the hydrology of different regions of the Amazon Basin. Such assessment could potentially be achieved using tree-rings as proxies for past climate variability in the Amazon.

1.3.1. Tree rings as proxies for climate variation in the Amazon

While in temperate zones the formation of annual tree-rings as a consequence of cambial dormancy during winter months is well known, tropical trees are generally not expected to form annual rings as tropical climates are usually year-round favourable to tree growth. Since the early 20th century, studies have already proven that tropical trees form annual rings (Berlage, 1931; Bormann and Berlyn, 1981; Schöngart et al., 2002). However, it was not until recent decades that tropical tree ring records started being applied more widely for climate reconstructions. Applications of tree-ring research in the tropics is still debated and their use is not without complications, as many tree species do not form visibly distinct rings or form false and wedging rings which are often not easily detected. The formation of annual

rings in tropical trees was firmly proved with the use of radiocarbon dating (Worbes, 2002) . The formation of annual rings in the tropics is attributed to seasonal variations in rainfall (Bormann and Berlyn, 1981; Borchert, 1999; Fichtler et al., 2003; Lisi et al., 2008; Fichtler and Worbes, 2012). Where trees in a given population respond similarly to inter-annual climate variability climate, the ring-widths can be cross-dated. This has widened the possibility for extending our knowledge on past climatic variability in tropical regions. Many tree ring chronologies have been developed in the tropics and have been shown to be a useful tool for reconstruction of past wet rainfall variability in the Tropical South America (Worbes, 1999; Brienen and Zuidema, 2005; Brienen et al., 2010; López and Villalba, 2011; Ramírez and del Valle, 2012; Locosselli et al., 2013; Locosselli et al., 2016; Lopez et al., 2017; Granato-Souza et al., 2018), and other tropical regions from Africa and southeast Asia (Fichtler et al., 2004; Schöngart et al., 2006; Buckley et al., 2007; Mendivelso et al., 2014; Gebrekirstos et al., 2014; Pumijumnong et al., 2014). Besides their applications for climate reconstructions, tropical tree rings are also becoming increasingly applied for other purposes, such as the development of sustainable forest management plans (Brienen and Zuidema, 2006; Brienen and Zuidema, 2007; Schöngart et al., 2008; De Ridder et al., 2013; Rosa et al., 2017), ecological studies (Brienen and Zuidema, 2006; Mendivelso et al., 2013; Cintra et al., 2013) and forest regeneration studies (Rozendaal et al., 2010; Vlam et al., 2014).

Use of tree rings as proxies for climate variability has the benefit that they are easily obtained, and not limited to specific locations, as is the case for peat and speleothems, for example. Thus, tree ring studies potentially provide spatially resolved information of past climatic variability for hundreds of years, depending on tree longevity. Tropical trees can potentially reach ages up to 2000 years (Condit et al., 1995; Chambers et al., 1998), although to this date there are no tree ring chronologies that reach that far back in time in South America. One limitation of the use of tree rings for climate reconstructions is that tree growth in the tropics is restricted to the wet season. Thus, information contained in tree rings does not provide climate variability of the dry season. An exception to this are trees from

floodplain forests, which have a distinct ecology from other forest types, and grow during the dry season. A large portion of the Amazon basin is composed of different types of seasonally flooded forests, where trees can only grow when they are out of the water during the low stage of the rivers, which usually coincides at least partially with the dry season. Such trees may therefore potentially provide valuable information about the past dry season climatic variability in different regions of the Amazon basin.

1.3.2. Floodplain forests in the Amazon

Floodplain forests are ecosystems subject to seasonal flooding caused by the annual cycle of river level fluctuations. These ecosystems occur in areas along the main tributaries of the Amazon river and in floodplain lake systems. They cover approximately 500 thousand km^2 in the Amazon, which is equivalent to 15% of all Amazon forests (Junk et al., 2011; Melack and Hass, 2010). Amazonian floodplain forests are classified into two major types, *várzeas* and *igapós* (Prance, 1979; Junk et al., 2011). These differ from each other in their areas of occurrence, their tree species composition and forest dynamics (Wittmann et al., 2002; Wittmann et al., 2004; Parolin and Wittmann, 2010; Wittmann et al., 2012). *Várzea* forests occur on fertile soils associated with rivers that originate in the Andes, i.e. “white water rivers” (Figures 1.2 and 1.5). They are the most productive and dynamic floodplain forest types in the Amazon (Schöngart et al., 2010). They are areas of high endemism (Wittmann et al., 2004; Wittmann et al., 2006; Wittmann et al., 2012), hosting the most tree diverse floodplain ecosystems in the world (Parolin and Wittmann, 2010). In contrast, the *igapó* forests occur on nutrient poor or white sand soils associated with “black water rivers” that originate in the Guianan and Brazilian shields (Prance, 1979; Junk, 1989; Junk et al., 2011) (Figures 1.2 and 1.5). They are the least productive and dynamic floodplain forest ecosystems of the Amazon and are less species rich than *várzea* forests (Junk et al., 2010; Parolin and Wittmann, 2010; Junk et al., 2015; de Sousa Lobo et al., 2019).

Amazon floodplain forests are distinct from other forests in the Amazon in their tree species composition and ecophysiology (Nebel et al., 2001; Wittmann et al., 2004; Wittmann et al., 2012). Floodplain tree species exhibit a variety of morphological and physiological adaptations which allow them to tolerate the floods (Worbes 1997; Schöngart et al., 2002; Parolin et al., 2004; Parolin, 2009; Parolin and Wittmann, 2010). They remain flooded for a period of 50 days to over 200 days per year, with flooding heights of up to 9 meters in the lower elevations (Wittmann et al., 2004) (Figure 1.6).

Figure 1.5. The encounter of the waters from the Amazonas River and Negro River at Manaus. On the areas flooded by the Amazonas River and its tributaries (brown waters in the picture) that originate in the Andes, *várzea* forests can be found. On the areas flooded by rivers that originate in the Guianan Shields, as the Negro River (dark water in the picture), or in the Brazilian shields, *igapó* forests can be found. Photo by Bruno BL Cintra.

Despite the diverse adaptations of trees to flooding, all floodplain tree species investigated to date completely stop growing during most of the flooded period, and grow mainly during the terrestrial phase (i.e. non-flooded period) (Schöngart et al., 2002). The complete cessation of tree growth induced by the flooding conditions is thought to be because tree roots are unable to take up water in anoxic soil conditions imposed by the floods. Soil hypoxic conditions prevent root aerobic respiration,

reduces root cell cytosolic pH, inhibits plant osmotic regulation and the activity of proteins which mediate root hydraulic conductivity (Zhang and Tyerman, 1991; Zhang and Tyerman, 1999; Tournaire-Roux et al., 2003; Chaumont et al., 2005; Bailey-Serres and Voesenek, 2008).

Although all floodplain tree species have evolved to tolerate the anoxic conditions imposed by the floods, the level of flood tolerance varies between species, with most species adapted to live in specific elevational positions along the flooding gradient and only few species occurring along the entire gradient (Nebel et al., 2001; Schöngart et al., 2005). Hence, the annual flood pulse itself is the most important driver of spatial variation in floodplain forest structure and species distributions (Junk, 1989; Wittmann et al., 2004; Junk et al., 2010; Assis et al., 2015; Muscarella et al., 2018). For this reason, floodplain forests may be severely impacted by alterations in the hydrological regime of rivers. In extreme cases, hydrological alterations caused construction of hydroelectric dams lead to large-scale tree mortality and have long-lasting impact on species distributions in the floodplains (Assahira et al., 2017; de Resende et al., 2018; de Sousa Lobo et al., 2019) (Figure 1.7).

Similarly to other forest ecosystems in the Amazon, the carbon cycle of floodplain forests is closely coupled to the regional hydrological cycle of the Basin. However, as the river level fluctuations follow local rainfall seasonality – with a lag of 1-3 months (Figure 1.2) – the terrestrial phase of floodplain forests occurs mostly during the dry season and/or in the transition to the wet season. Thus, the peak of floodplain productivity and carbon uptake is during the dry season, when trees are not flooded, and thus they absorb carbon from the atmosphere when carbon uptake by other Amazonian forest ecosystems is at its lowest. Moreover, due to such control of the rivers' hydrological regime on tree growth in floodplain forests, ecosystem responses and the feedbacks to varying climate conditions differ between floodplain and non-flooded forests. In years with reduced wet-season rainfall amounts, the terrestrial phase of floodplain trees is longer, trees have extended growing periods and can grow more (Schöngart et al., 2002; Schöngart et al., 2004). In contrast, in years with

increased precipitation, the growing phase is shorter and trees grow less. This contrasts, for example, with non-flooded forests, which are negatively (positively) impacted by reductions in precipitation amounts during dry (wet) years (Phillips et al., 2009). Thus, understanding how different ecosystems may have been affected by climate variability in the past may be a useful way to understand how they will respond to ongoing and future climate changes.

Figure 1.6. Images of floodplain forests during the terrestrial phase (top) and during the flooded phase. Photo by Bruno BL Cintra.

The fact that floodplain trees are seasonally flooded is interesting from the dendrochronology point of view, as flooding provides a very well defined growing season for the trees. Complete cessation of growth induced by the flooding ultimately leads to the cambial dormancy and to formation of distinct wood anatomical features that allow the identification of tree ring boundaries (Worbes, 2002). As river fluctuations exhibit a regular annual cycle, tree rings in floodplain trees are also expected to be annual and can be used as proxies for past variability of the controls of tree growth (Worbes, 2002; Schöngart et al., 2002; Assahira et al.,

2017). Therefore, floodplain trees are suitable for dendrochronology studies (Schöngart et al., 2002; Dezzeo et al., 2003; Worbes, 2004; Schöngart et al., 2005).

The dendrochronological potential of floodplain trees only started being explored in recent decades. Because floodplain trees grow during the dry season, they potentially provide complementary climate information to that obtained from terra firme trees. For two floodplain tree species in particular, *Piranhea trifoliata* and *Macrolobium acaciifolium*, tree-ring chronologies have been shown to be related to the length of the period that trees stay out of the water, i.e. the length terrestrial phase (Schöngart et al., 2004; Assahira et al., 2017). Such information is useful for deriving closely related information to the past variability of hydrological regime of Amazonian rivers, i.e. the minimum level of the rivers annually. In addition, as the seasonality of the river levels is caused by the seasonality in rainfall over the catchment area of the rivers, the length of the terrestrial phase can provide an analogous measure of to dry season length in different sub-basins of the Amazon.

Besides their potential for standard dendrochronological analysis, floodplain trees may also provide interesting proxies for past dry season intensity (i.e. precipitation amounts) through the analysis of isotope ratios in their tree rings. Isotopes analyses of carbon and oxygen are becoming increasingly used in dendrochronology (McCarol and Loader, 2004; Sleen et al., 2017), and have shown promising results for reconstructing wet season rainfall in non-flooded Amazon trees (Hietz et al. 2004; Fichtler et al. 2010; Bowman et al., 2013; Baker et al., 2015; Baker et al., 2016). Carbon isotopes provide useful information about leaf gas exchange regulations and assimilation rates (Farquhar et al., 1982; Farquhar et al., 1989; Seibt et al., 2008), use of carbohydrate reserves (Helle and Schleser, 2004; Gessler et al., 2014), tree's responses to rising atmospheric CO_2 (Saurer et al., 2004; Sleen et al., 2015) and to local climate conditions (Leavit and Long, 1991; Ferrio and Voltas, 2005; Ohashi et al., 2009; Gebrekirstos et al., 2009; Brienen et al., 2011). Oxygen isotopes are interesting for climate reconstruction because they reflect different aspects of the hydrological cycle. In Chapter 4 I analyzed both carbon and oxygen isotopes in tree rings and

provide a detailed description of theory and models for both isotopes. As I am mainly interested in the potential of using oxygen isotopes in tree rings of floodplain trees to study the hydrological cycle in the Amazon, in the next section I will detail how oxygen isotopes are related to the hydrological cycle and how they can be used in tree rings for past climate reconstruction.

Figure 1.7. Image showing large-scale mortality of trees downstream from the hydroelectric dam from Balbina, in the State of Amazonas, Brazil. The cause of the death of the trees was attributed to changes in the hydrological regime of rivers, which imposed longer flooding periods than the trees were adapted to (Assahira et al., 2017). Photo by Bruno B L Cintra.

1.3.3. Oxygen isotopes ratios and the hydrological cycle

Isotope ratio (R) is the ratio of the abundance of a rarer isotopic form in relation to the higher abundance of the common isotopic form. In the case of oxygen for example, ^{18}O and ^{17}O are stable isotopes and exist naturally, but just like other uncommon stable isotopes, they are rare compared to the common ^{16}O form. ^{16}O represents 99.759%, while ^{18}O represents only 0.204% of the oxygen in the atmosphere, and ^{17}O is even rarer than ^{18}O.

The isotopic ratios of a substance are commonly expressed relative to the isotopic ratio of a standard substance, expressed as δ (in ‰). In the case of the oxygen, the ratio between the rare form ^{18}O to the common form ^{16}O in a substance

($^{18}R_s$=[^{18}O]/[^{16}O]) is expressed in relation to the same ratio in a conventional standard, the Vienna Standard Mean Ocean Water (VSMOW – Craig, 1961; Gonfiantini, 1978; Hut, 1987), which is based on distilled ocean water from different parts of the world. The oxygen isotope composition is then commonly expressed as $\delta^{18}O$, and calculated as

$$\delta^{18}\mathrm{O} = \left(\frac{^{18}\mathrm{R}_s}{^{18}\mathrm{R}_{VSMOW}} - 1\right) * 10^3‰$$

The definition above uses oxygen isotopes only for explanation purposes. It is used equally for any other isotope, except that for each isotope a specific standard for isotope ratios is used.

The isotopic ratio of any substance is not necessarily constant. For example, when the physical state of a substance changes, fractionation of its isotopic composition may occur. Fractionation (Δ) is any process that changes the isotopic ratio (or the δ) of a substance. There are basically two types of fractionation, *equilibrium* and *kinetic. Equilibrium fractionation* is a process when two substances interchange isotopes until an equilibrium is reached, resulting in a constant difference of the isotopic signal between the two substances. An example of equilibrium fractionation is when a surface of liquid water exchanges isotopes with the saturated atmosphere. In this case, the resulting fractionation depends only on the temperature of the water and vapour in contact (which control the diffusion rates of both isotopes), and can be measured as (Bottinga and Craig, 1969)

$$\varepsilon^* = 2.644 - 3.206 * \left(\frac{10^3}{T}\right) + 1.534\left(\frac{10^6}{T^2}\right) ‰$$

Where ε^* is the enrichment factor and *T* is the temperature. This equation results in a fractionation of 8.77‰ at 30°C and decreasing fractionation at higher temperatures.

Kinetic fractionation on the other hand occurs when the reaction involving molecules containing two or more isotope forms is unidirectional. In this case, isotopic

equilibrium is not achieved and the resulting fractionation depends on the ratio of the reaction rates of each isotope form. Following the same example above, *kinetic* fractionation would occur if the atmosphere is not saturated, and the water molecules evaporating from the water are constantly removed by the wind. *Kinetic* fractionation is also very common during the chain of biochemical reactions that lead to the synthesis of diverse organic tissues in the plant (Sternberg, 2008). The resultant δ from a fractionation process usually depend on the temperature-dependent reaction rates and on the nature of the reaction itself.

$\delta^{18}O$ is useful for hydrological studies because water containing ^{16}O and ^{18}O have slightly different evaporation and condensation rates, and thus $\delta^{18}O$ of water reflects hydroclimatic processes that affect the physical state of the water. $H_2{}^{16}O$ evaporates faster and $H_2{}^{18}O$ condenses faster. Thus, vapour formed from water evaporating from the ocean is more depleted in heavy isotopes (i.e. has a lower $\delta^{18}O$) and the water left in the Ocean. In contrast, rain drops formed by condensation of vapour are more enriched in ^{18}O (i.e. has a higher $\delta^{18}O$) than the vapour left in the air. A schematic representation of the fractionating processes taking place from the evaporation of water from the Ocean until the formation of rain is presented in Figure 1.8.

Isotopic fractionation of water evaporating from the ocean occurs at near-equilibrium. Water and vapour exchanging molecules at equilibrium will result in the vapour from the atmosphere containing less ^{18}O than the water in the Ocean. The water evaporated from the Ocean will carry the isotopic signal and form the clouds. Thus, the $\delta^{18}O$ of precipitation is first determined by the $\delta^{18}O$ of the vapour in saturated air masses entering the continent originated by evaporation of ocean waters. The temperature of condensation influences the fractionation during the formation of rain drops. Thus in temperate regions, where seasonal variation in temperature is large, interannual variations in temperature are the main factor driving interannual variations in $\delta^{18}O$ of rainfall water (Dansgaard, 1964; Araguás-Araguás et al., 2000). However, in lower latitude regions such where precipitation is mainly convective and seasonal and inter-annual variations in temperature are

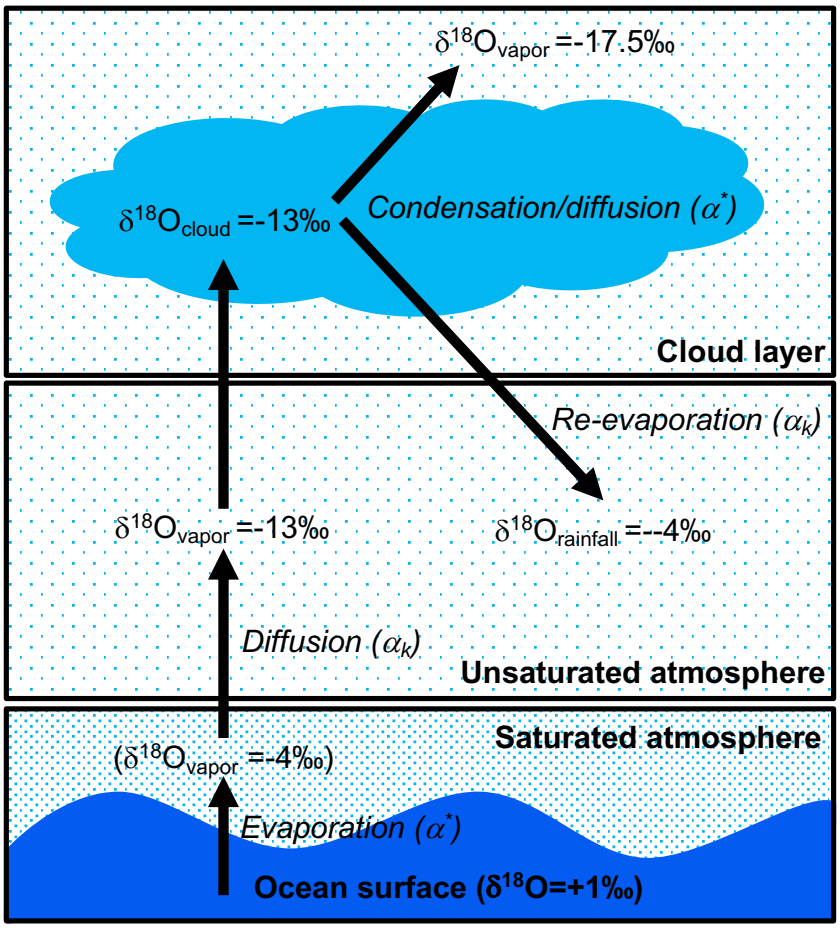

Figure 1.8. Schematic representation of the processes affecting the $\delta^{18}O$ of water from evaporation from the Ocean until precipitation from clouds. Texts in italic indicate equilibrium (α^*) and kinetic (α_k) fractionating processes. Texts in bold indicate large water reservoirs. Modified from Gat et al. 2001.

comparatively small, rainfall $\delta^{18}O$ is not related to interannual variation in temperatures. In low-latitude regions, inter-annual variations in rainfall $\delta^{18}O$ are related to two mechanisms, the amount effect (i.e. Risi et al., 2008) and the rainfall history over the trajectory of air parcels (Dansgaard, 1964; Salati et al., 1979; Schubert and Jahren, 2015).

During heavy convective rainfall events, fast condensation rates result in the formation of rain drops with relatively low $\delta^{18}O$. Rain drops falling through a saturated atmosphere undergo diffusive equilibration with the vapour (equilibrium fractionation), which may contribute to a similar $\delta^{18}O$ between the rain drops and the vapour. Depletion of $\delta^{18}O$ in the rainwater can be observed during a single rainfall event and may be stronger with heavier precipitation (Lee and Fung, 2008). In

contrast, as $H_2{}^{18}O$ condenses faster, slow condensation rates during light precipitation events result in the formation of rain drops with higher $\delta^{18}O$. Rain drops may undergo further fractionation at non-equilibrium (kinetic) conditions as they fall through a dry atmosphere and partially re-evaporate. Partial re-evaporation of rain drops contribute to increase their $\delta^{18}O$ (Lee and Fung, 2008; Risi et al., 2008; Villacís et al., 2008). Such difference between the $\delta^{18}O$ of rainfall during heavy and light rainfall events is known as amount effect.

In addition to the amount effect, the rainfall history over the trajectory of air parcels may also be an important determinant of the $\delta^{18}O$ in rainfall in regions distant from the coast. Because water containing heavy isotopes condenses faster, the vapour in the air becomes more depleted in ^{18}O after every rainfall event. Consequently, successive rainfall events progressively deplete the clouds of heavy isotopes, effectively a Rayleigh distillation (Dansgaard, 1964; Salati et al., 1979). As clouds become progressively depleted, rainfall $\delta^{18}O$ also tends to become depleted, which is known as rainout (Figure 1.9). This results in an inland gradient of $\delta^{18}O$ depletion of water, i.e. rainfall close to the coast – upwind the atmospheric flow – has higher $\delta^{18}O$ than rainfall far from the coast – downwind the atmospheric flow (Salati et al., 1979) – Figure 1.9. Because the amount is stronger during heavier or longer precipitation events, the inland gradient of cloud ^{18}O depletion tends to be steeper in years with more rainfall, and vice versa. Such rainout upwind of the atmospheric flow is an important determinant of interannual variations of $\delta^{18}O$ in precipitation in the Amazon basin (Salati et al., 1979; Matsui et al., 1983; Vuille and Werner, 2005; Villacís et al., 2008; Baker et al., 2016).

The inland gradient of $\delta^{18}O$ depletion in rainfall water in the Amazon is of approximately 1.5 ‰ per 1000km (Salati et al., 1979). This is actually less than in other parts of the world, where this gradient generally in the order of 2‰ per 1000km (Rozanski et al., 1993). This is thought to be due to the rainfall recycling promoted by the forest (Salati et al., 1979; Salati and Nobre, 1991; Gat and Matsui, 1991).

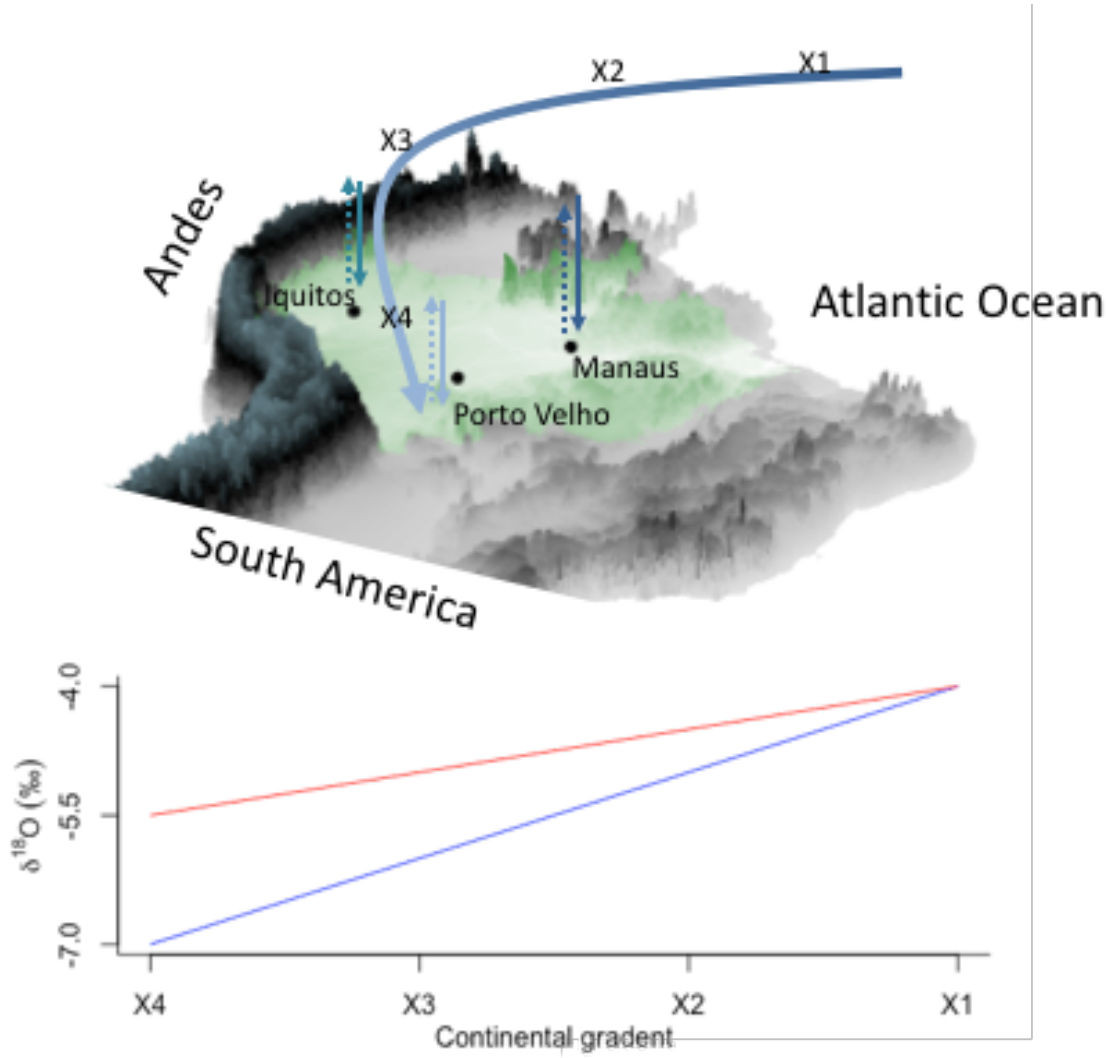

Figure 1.9. Schematic representation of the inland gradient of meteoric water ^{18}O depletion. Darker (lighter) blue shades indicate higher (lower) $\delta^{18}O$ in cloud and rainfall. Vertical solid lines represent rainfall and vertical dotted lines represent evapotranspiration from the forest. The area of the Amazon Basin is highlighted in green. The graph below shows conceptually the change in rainfall $\delta^{18}O$ along the inland gradient (X1,X2,X3,X4) during rainy (blue line) and drier years (red line). The graph shown is adapted from Salati et al. (1979, their Fig 4).

The recycling of rain occurs through partial evaporation from open water bodies as lakes and river, through total evaporation of water intercepted by the forest canopy (non-fractionating because no water is left) and through evapotranspiration by the leaves. While the evaporation from open bodies is fractionating, i.e. produces vapour that is more depleted in ^{18}O than the water left behind, total evaporation of water intercepted in the canopy is non-fractionating as it completely returns all water molecules to the atmosphere. Water transpired by the leaves is also considered to

have the same isotopic composition as the water that entered the leaves, as it also returns all water molecules to the atmosphere.

Due to rainfall recycling via canopy interception and evapotranspiration, recycled rain carries the local climatic $\delta^{18}O$ to other regions of the Amazon, downwind of the atmospheric flow. This process is even more important during the dry season when a significant portion of the rainfall comes from recycled water through evapotranspiration with very limited moisture inputs from the ocean (Salati et al., 1979; Victoria et al., 1991; Zemp et al., 2014). Therefore, the isotopic signal in dry season precipitation in western/southwestern regions of the Amazon carry mainly a signal of soil water $\delta^{18}O$ transpired by plants, and should indicate the degree of water recycling.

If the $\delta^{18}O$ of the dry season rainfall indeed contains mainly a signal of evapotranspiration, physiological changes in evapotranspiration due to increased atmospheric [CO_2] should be most easily detected during the dry season. In different parts of the world, increased atmospheric CO_2 levels has led to an increased water use efficiency of the plants, i.e. plants transpire less for the same photosynthesis production (Saurer et al., 2004; Hietz et al., 2005; Nock et al., 2010; Brienen et al., 2011; Franks, 2013; Sleen et al., 2015). However, evidence for such plant physiological effects on the Amazon hydroclimatic system remains scarce. The analysis climate proxies of floodplain trees that potentially record the $\delta^{18}O$ of dry season rainfall may bring additional insights to this field.

1.3.4. Tree-ring $\delta^{18}O$ as an archive of the hydrological cycle

$\delta^{18}O$ in the cellulose of tree rings reflects the $\delta^{18}O$ in the source (rain) water, and all fractionating steps that occur until the incorporation of the oxygen from water fixed in the organic molecules of plant tissues. A brief synthesis of the whole path is as follows: first, water for each rainfall event mixes with water that was already in the soil until the soil is saturated with water (Brooks et al., 2010; Evaristo et al., 2015). Thus, the water that plants take up is not expected to reflect the $\delta^{18}O$ of any single

precipitation event, but rather integrates the $\delta^{18}O$ of successive rainfall events. Soil water uptake by the roots is considered to be non-fractionating for oxygen isotopes (Luo and Sternberg, 1992; Dawson and Ehleringer, 1993) and thus the water entering the leaves through the xylem is considered to have the same isotopic composition as soil water (but see also Vargas et al., 2017). The oxygen isotopic composition of water entering the leaves is then altered at the sites of evaporation in the leaf inter-cellular spaces, where it undergoes evaporative enrichment. Further alterations of the oxygen isotopic ratio occur during the synthesis of carbohydrates during photosynthesis and during the synthesis of cellulose. In both situations, metabolized carbohydrates exchange oxygen with water present in the cells (Barbour, 2007; Sternberg, 2008).

As tree ring $\delta^{18}O$ reflects the $\delta^{18}O$ of the water used by the trees, many studies from temperate regions have revealed the potential of using $\delta^{18}O$ in tree rings as proxies for past conditions of temperature (Libby et al., 1976; Burk and Stuiver, 1981; Saurer et al., 1997; Anderson et al., 1998; Rebetez et al., 2003; Danis et al., 2006; Treydte et al., 2007; Reynolds-Henne et al., 2007; Edwards et al., 2008; Saurer et al., 2008; Saurer et al., 2012), relative humidity (Burk and Stuiver, 1981; Robertson et al., 2001; Danis et al., 2006; Edwards et al., 2008; Roden et al., 2009; Voelker et al., 2014) and precipitation amounts (Ramesh et al., 1986; Masson-Delmotte et al., 2005; Treydte et al., 2006; Treydte et al., 2007; Reynolds-Henne et al., 2007; Roden and Ehleringer, 2007; Liu et al., 2012). These studies revealed not just the potential of this tool for climate reconstructions, but also showed that the plant responses to the local climate conditions can significantly alter the environmental signal contained in the $\delta^{18}O$ of the tree rings. Analysis of $\delta^{18}O$ in tree rings started being applied for climate reconstruction studies with tropical tree-rings more recently, and comparatively fewer studies have been done in the tropics so far. Many of these studies reveal high potential for use of oxygen isotopes for climate reconstruction in the tropics (Miller et al., 2006; Kahmen et al., 2008; Managave et al., 2011; Baker et al., 2015), but also few studies reveal challenging interpretations of these proxies (Poussart et al., 2004; Poussart and Schrag, 2005; Ballantyne et al., 2011; Pons and Helle, 2011; Schollaen

et al., 2013; Ohashi et al., 2015). Despite recent advances in the use of oxygen isotopes in the tropics, to my knowledge no studies have performed a detailed assessment of how the tree-ring isotope models and theory developed for temperate trees performs for tropical environments, which is a field that still requires further development.

One of the main factors affecting variations of the oxygen composition of tree rings is the enrichment of the source water in the leaves (Farquhar and Lloyd, 1993; Roden and Ehleringer, 1999; Barbour and Farquhar, 2000; Roden et al., 2000; Cernusak et al., 2002; Cernusak et al., 2005; Farquhar et al., 2007). The degree of enrichment depends on two opposing fluxes in the leaf: the flux of source water entering the leaves through the xylem and the back-diffusion of the $H_2{}^{18}O$ from the sites of evaporation (i.e. stomata and intercellular spaces) through the leaf lamina. In a highly transpiring leaf there is a high flux of water coming from the xylem which will lead to an average leaf water $\delta^{18}O$ close to that of water entering the leaf. If transpiration decreases, the incoming flux of depleted water from the xylem is reduced, allowing more water containing heavy isotopes to diffuse from the stomata and intercellular spaces through the leaf lamina, which raises the average $\delta^{18}O$ of leaf lamina water. The resultant $\delta^{18}O$ of the leaf water depends mainly on transpiration flux in the leaf, which is in turn determined by stomatal conductance and air humidity. The $\delta^{18}O$ of carbohydrates synthesized in the leaf ($\delta^{18}O_{SUB}$) will be approximately $\delta^{18}O$ 27‰ higher than the $\delta^{18}O$ of leaf water ($\delta^{18}O_{lw}$). During cellulose synthesis, a part of the ^{18}O in the photosynthetically fixed carbohydrates is exchanged with xylem water through carbonyl hydration (Luo and Sternberg, 1992). This ^{18}O reinforces the source water signal in the cellulose. Thus, the cellulose $\delta^{18}O_c$ will reflect not only the $\delta^{18}O_{SUB}$, but also the $\delta^{18}O$ of the water in the stem at the moment of the cellulose synthesis.

Usually the $\delta^{18}O$ in the cellulose will have values around 27‰, with a variation of ±4‰ which should depend on the species analyzed. However, high seasonal variations in temperature and the relative humidity may have effects over the vapour enrichment of the water on the leaf, resulting in a seasonal variation that does not

correspond entirely to rainfall $\delta^{18}O$. Therefore, it is important to correctly interpret the data based on known $\delta^{18}O$ variability in precipitation water from the region, to be able to detect potential sources of variations in the cellulose $\delta^{18}O$. One useful way to study the contribution of source water $\delta^{18}O$ vs leaf water enrichment is through the use of tree-ring isotope models. For all processes that lead to the incorporation of the $\delta^{18}O$ in the cellulose, numeric models have been developed. These are explained in detail in the Chapter 3 of this thesis.

1.4. Thesis Objectives

The overarching aim of this research is to use tree rings and oxygen isotopes in the tree rings of *Macrolobium acaciifolium* as a proxy for past variability in dry season climate. In order to achieve this goal, the following research questions were addressed:

- What climatic factors influence tree growth of *M. acaciifolium* growing under different climatic conditions in the Amazon Basin?
- Can the ring-widths of *M. acaciifolium* tree from different regions within the Amazon basin be used as proxies for the past dry season climate?
- What is the relative contribution of source water $\delta^{18}O$ vs leaf water enrichment to the $\delta^{18}O$ signal in tree rings of *M. acaciifolium* trees, and does this differ for trees growing in different climatic conditions?
- Can $\delta^{18}O$ in the tree rings of *M. acaciifolium* be used as a proxy for past dry season precipitation in the Amazon Basin?
- What are the main climatic controls (e.g. sea surface temperatures) affecting both ring-widths and tree-ring $\delta^{18}O$ in *M. acaciifolium* trees growing in different regions within the Amazon Basin?
- What can be inferred from long-term trends in $\delta^{18}O$ of tree rings of *M. acaciifolium* growing in different locations and under climatic conditions?

1.5. Thesis Outline

In Chapter 1 of this thesis I present a review of the literature of relevance for the development of this thesis, and present an outline the thesis objectives and research questions.

The Chapter 2 of this thesis I explain in detail the technical procedures and methodological choices for the development of this Thesis.

In Chapter 3 the I explored the controls of the intra-annual variations of both carbon and oxygen isotopes in the tree rings of two species: *Macrolobium acaciifolium*, which is the floodplain tree species of interest for this thesis, and *Cedrela odorata*, a terra firme species for which tree ring $\delta^{18}O$ has been previously studied.

In Chapter 4, ring-width chronologies of *M. acaciifolium* from three regions in the Amazon Basin were developed, and their potential for reconstructing past variability of river levels and local dry season climate conditions was explored.

In Chapter 5, tree-ring $\delta^{18}O$ chronologies of *M. acaciifolium* were developed for the same sites as in Chapter 4, and their potential for reconstructing past variability of dry season climate conditions at local and large-scales was explored.

In Chapter 6 I summarize the main research achievements of this Thesis, discuss the potentials and limitations of the proposed approach to reconstruct past dry season climate in the Amazon, and propose research directions to improve this field.

Chapter 2 **Overview of Methods**

2.1. Species selection

For the development of this research a widely occurring Amazon floodplain species was chosen, *Macrolobium acaciifolium* (Figure 2.1). This species presents phenological and physiological adaptations to the flood pulse. It sheds its leaves during the flooded period (i.e. is a brevi-deciduous species) and is capable of using anaerobic metabolism during a short period after the roots become flooded (Worbes, 1997; Schöngart et al., 2002; Parolin et al., 2004). Wood densities range from ~0.4 to 0.5 g cm^{-3} and reported annual growth rates vary from ~1.5 mm in nutrient poor black water floodplains (*igapó*) to ~2.6 mm in nutrient rich white water floodplains (*várzea)*. Trees from *igapós* achieve much higher ages (mean 268±118 years) due to their low growth rates compared to ages achieved in *várzeas* (mean 135±27 years, Schöngart et al., 2005). *M. acaciifolium* forms very clear rings (Figure 2.1) that have been shown to be annual by dendrochronological methods and radiocarbon dating (Assahira et al., 2017, Schöngart et al., 2005). Previous studies have shown that the ring-width chronologies of this species are correlated with the duration of the non-flooded period, i.e. the period when the river levels are below the trees' topographic position (Schöngart et al., 2005, Assahira et al., 2017, Batista et al., 2018).

2.2. Field work

Field work was carried out at three seasonal floodplain sites, selected to differ in the geographic origin of the catchment area of the river that floods them. One site is located at the western end of the Basin at the Marañon River, Peru (74°05'30''W, 4°29'30''S), one at a northern sub basin at the Negro River, Brazil (60°38'45''W, 2°40'10''S), and one in a southern sub basin at Sena river, which is within the Madre de Dios floodplains, Bolivia (67°20'36''W, 11°40'41''S) – Figure 2.2.

In addition to these three sites, one sample from a várzea forest in Leticia (-4º 30' 00''N, -70º 00' 00''E), collected by Dr. Arnoud Boom (University of Leicester) was used for the analysis carried out in Chapter 3. The site from Leticia is geographically close and presents similar hydroclimate to the sites in western Amazon (see Figure 3.1 in Chapter 3).

Figure 2.1. *Macrolobium acaciifolium* tree in an igapó forest from central Amazon floodplains. (a) Image of the whole tree, (b) image of the bark of the tree and (c) image of the leaves and fruits of the tree. In (d-e) tree-rings of *M. acaciifolium* are shown as (d) reflective scan of a sample, (e) film scan of a thin cut (100μm) from the same sample, taken with a core microtome, (f) blue reflection of the same sample, enhancing the wood density variations within rings, (g) cellulose extracted from the wood. In (a) the red arrow indicates the height of the last flooding event, which left a darker shade on the submerged part of the tree trunk.

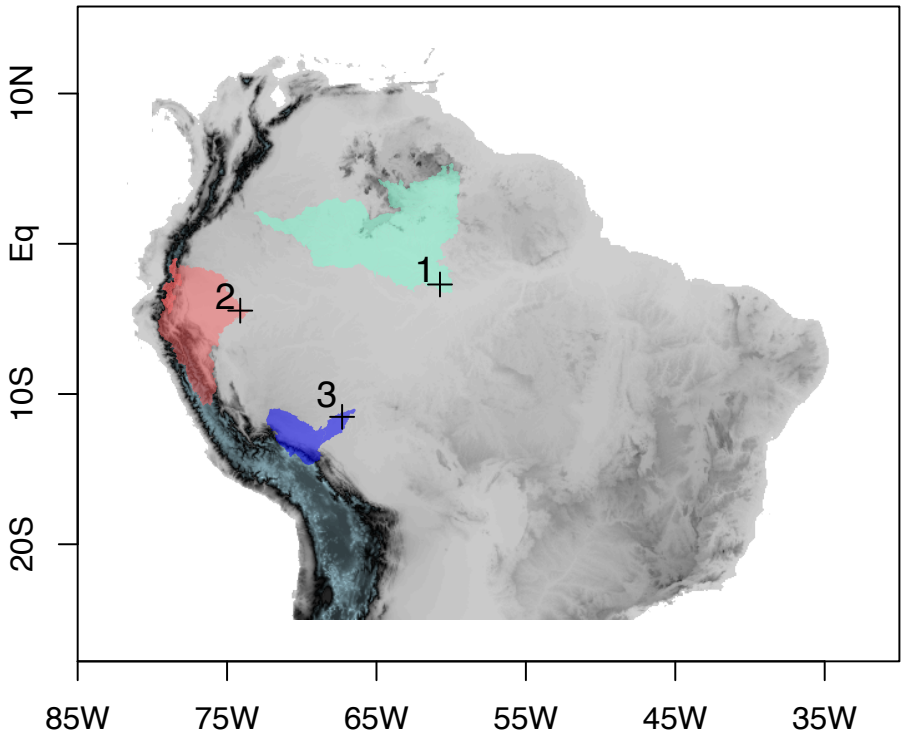

Figure 2.2. Location of the three sites were wood samples of *M. acaciifolium* were collected for this thesis. (1) southwest Amazon, Bolivia, (2) western Amazon, Peru and (3) central Amazon, Brazil.

2.3. Sample collection and preparation:

At each of the three sites shown in Table 2.1, 40-50 individuals of *M. acaciifolium* were sampled, adding up to a total of 335 cores from 145 trees. Trees of varying diameter classes were sampled to avoid common biases present in tree ring data-sets that focus on the largest individuals in a population (i.e. big-tree selection bias, Brienen et al., 2012, Bowman et al., 2012) (Figure 2.3). From each tree 2-3 cores were taken using 5 and/or 10 mm increment borers.

From every core sample, thin slices were cut using a core microtome (Gärtner et al., 2010) (Figure 2.4). The thin slices were mounted on glass slides and scanned as film with an Epson Scanner V700, which generates a projection image of a scanned sample. All scans were made at a resolution varying from 3200-3500 dpi (~50 kilopixel mm^2). The sample scans were then used for ring width measurements using the open-access software ImageJ, ObjectJ plugin - Tree Ring Project, available online at (https://sils.fnwi.uva.nl/bcb/objectj/examples/TreeRings/, Vischer and Nastase,

2017). The choice for measuring the tree ring widths using ImageJ rather than more standard measurement devices such as TSAP was because (1) better visualization of the tree rings in the samples scanned as films compared to the raw wood material; (2) ObjectJ provides a very good platform for visual crossdating, allowing the visualization of multiple samples at the same time; (3) no need to mark directly on the wood, which helps to preserve the samples, (4) all ring marking and measurements are saved in the images and can be easily accessed for later verification without the need to return to the lab and (5) using an image analysis software allows decomposition of colour components of the images to enhance visualization of wood anatomical features that define the tree rings.

Table 2.1. Hydrological features of the flood-pulse and the dry season rainfall on the sampling sites. Catchment areas are relative to the approximate position of the sampling site. Dry season is here defined as the period with cumulated monthly rainfall equal to 100 mm or less. Data from the SNIRH/ANA and from SENHAMI. Numbers in parenthesis beside each site correspond to the site numbers in Figure 2.2.

Sampling site	central amazon (1)	western Amazon (2)	southwest Amazon (3)
Floodplains	Negro	Marañon	Madre-de-Dios
Soil	Clayey	Clayey	Sandy
Vegetation	*Igapó* forests	*Várzea* forests	No floristic data
Annual rainfall (1980-2015A.D.)	1700-3000mm	1700-3700mm	1500-2000mm
Dry season length	3	0	5
Dry season precipitation (mm/month)	82	No dry season	53
Full Catchment area (km^2)	705 000	390 000	128 000
Flood pulse amplitude (cm)	1020 (Manaus, 1980-2017 A.D.)	682 (Nauta, 2000-2017 A.D.)	1132 (Riberalta, 1990-2017 A.D.)
Terrestrial phase (months)	Sep-Feb	May-Dec	Apr-Nov
Mean flood pulse amplitude (m)	9.5	7.1	5.3
Months between peak dry season and lowest river level	2-3	0	1

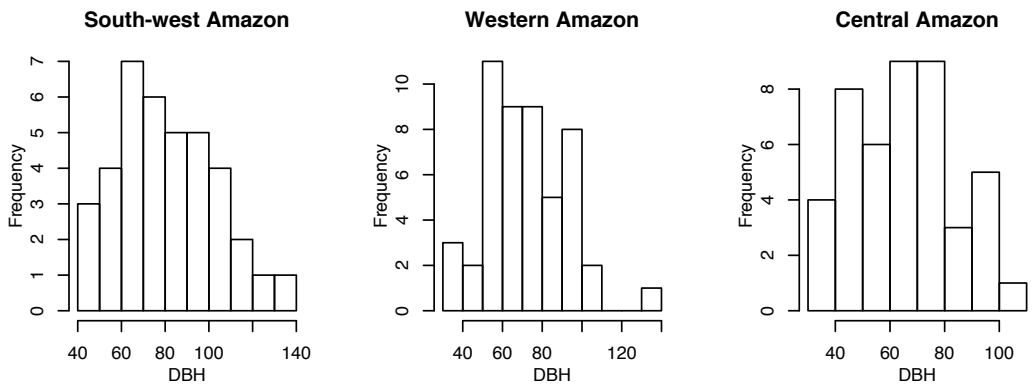

Figure 2.3. Histograms showing the frequency distribution of the diameter at breast height (1.3m, DBH) of all *Macrolobium acaciifolium* trees sampled at each site.

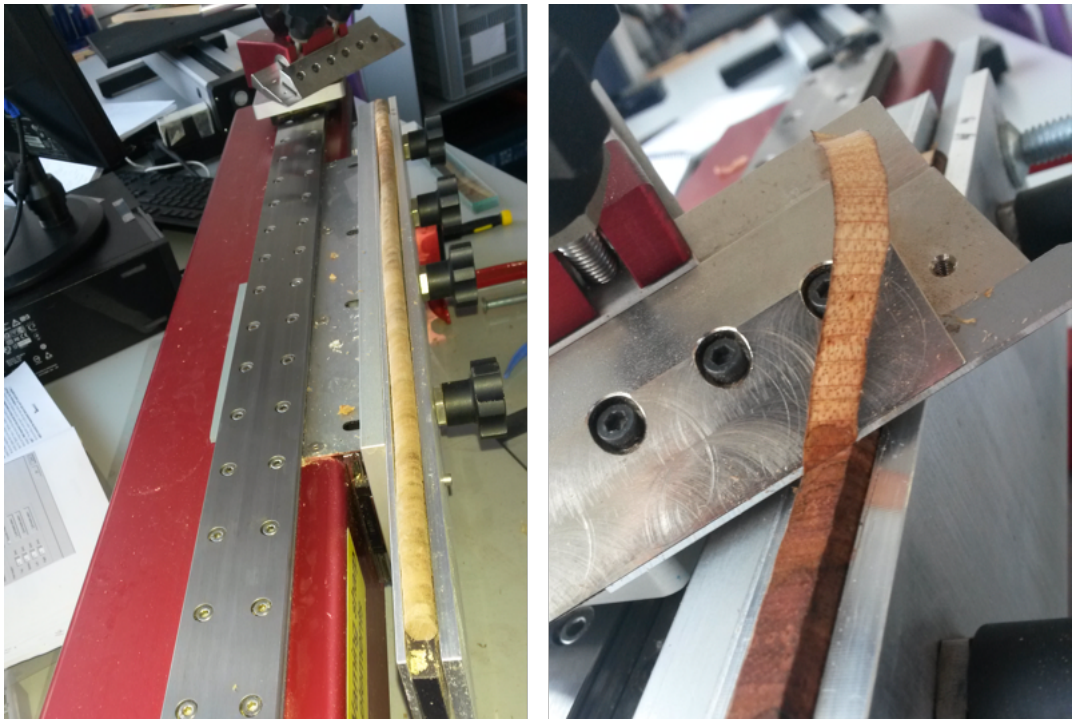

Figure 2.4. Image detailing the use of a core microtome to cut thin slices from tree ring samples. The image on the right details the moment the slices are being cut.

2.4. Tree ring measurements and crossdating

Time series of variables measured from tree rings of different trees can be aligned (or synchronized) in order to evidence a common pattern which may be driven by fluctuations in climate and/or growing conditions. The process of aligning information obtained from tree rings is called crossdating (Douglass, 1914; Fritts, 1971; Briffa and Jones, 1990; Speer, 2010). Crossdating can be done by identifying the anatomical features that define ring-boundaries, measuring one or more

variables in each ring, and comparing the time series of variation obtained for each tree. The most commonly measured variable in tree rings are ring-widths, but useful information can also be obtained from measuring other variables such as vessel area (Fonti et al., 2007; Locosselli et al., 2013), concentration of chemical compounds (Poussart et al., 2006), or the isotopic composition in the wood (McCarol and Loader, 2004; Sleen et al., 2017). Variables measured in successive rings are set out as time series which are aligned according to the year of formation of each tree ring. When different trees present a common variability, aligning the time series of the trees should exhibit a clear pattern of variability common to all trees, which may be evident in annual, decadal or longer time-scales. For example, ring-widths can be crossdated when different trees in a population present similar growth responses to variations in climate or growing conditions.

As the time series of measurements taken from the tree rings are synchronized according to the year of formation of the tree rings, one indispensable condition for crossdating is that the periodicity of ring formation is annual. Annual ring formation in lowland tropical trees is usually caused by seasonally occurring droughts or floods, as is the case for seasonally flooded forests in the Amazon (Worbes et al., 2002, Dezzeo et al., 2005). However, crossdating tree ring measurements is often challenging for tropical tree species due to formation additional (false) or unclear (missing) ring boundaries in few years. Therefore, an accurate cross-dating requires that such false or missing rings are detected and accounted for in different trees.

Accounting for the presence of false and missing rings in tropical trees is possible when tree rings are analyzed on multiple radii across the cross-section of the tree trunks. When entire disc samples of tree trunks are available, false and missing rings can be detected by visually analyzing tree ring across the entire cross-section of the tree trunks. However, disc samples are often not available, as is the case in the present thesis. Here I used only wood cores sampled with increment borers, which required that two or more cores were sampled from each tree to allow detection of false or missing rings. Such comparison was done first visually, by comparing the

wood anatomy of different cores from the same tree and counting the number of rings between pointer rings – i.e. rings which were very narrow or with distinct anatomical features (Schweingruber et al., 1990). Comparison of ring measurements was also done statistically, by comparing and correlating different segments of the time series obtained from each core. Such comparison was done using the time series produced by the direct measurements from the tree rings, or the time series may also be standardized (see next section) in order to evidence the high-frequency variability in the time series.

Once the presence of false and/or missing rings is accounted for, a mean series can be produced for each tree by averaging the information measured in each tree ring from different cores. The average series of each tree can then be compared and the strength of the common variability among different trees can be estimated with different statistical tools, which are described in the next section.

In the Chapter 4 of this thesis, I crossdated ring-widths measured from cores of *Macrolobium acaciifolium* trees. A subset of cores with the best results from the crossdating process were then selected for isotopes measurements in Chapter 5. The entire process of ring-width crossdating used in this thesis is schematically summarized in Figure 2.5 (e.g. Wills et al., 2011), and is described as follows.

Macrolobium acaciifolium tree rings can primarily be identified by marginal (or terminal) parenchyma bands, furthermore variations in wood density and vessel distribution are often visible and improve identification of ring boundaries (Worbes, 2004; Schöngart et al., 2005) (Figure 2.6). False and wedging rings may occur in this species as a result of short term flood periods during the growing season. Such short term flooding periods may occur in successive years leading to repeated formation of double parenchyma bands (Figure 2.6a).

As a first step for the construction of tree-ring chronologies, ring-widths of each core were measured with careful attention to anatomic features that indicated potential false rings. To detect false rings, each sample (core) was visually inspected for

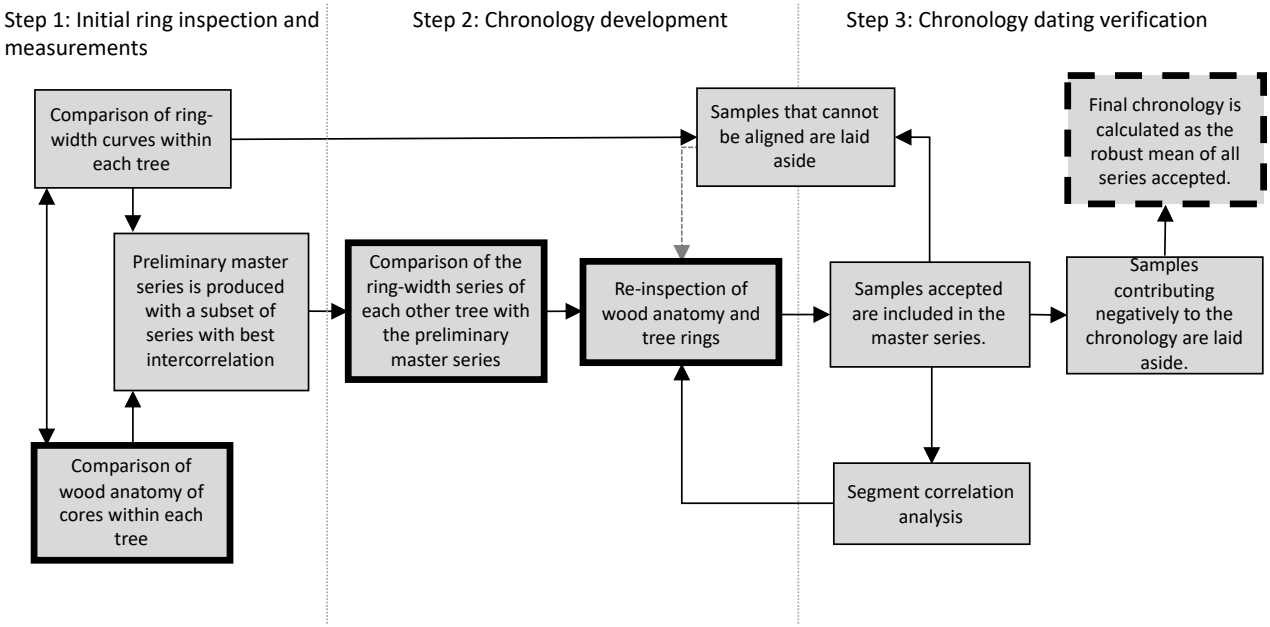

Figure 2.5. Schematic diagram showing the step-by-step crossdating approach used in this thesis. Boxes in bold indicate steps that are most time-consuming of the process, indicating the central attention given to the anatomical analysis of tree rings. Gray dashed line indicates tasks performed after steps 1-3 are completed. Tasks are repeated until no additional samples are included in the chronology.

discontinuous parenchyma bands, repeatedly occurring double parenchyma bands, wedging parenchyma bands and parenchyma bands which did not follow the variations in wood density and vessel distribution. Whenever these features were found they were considered as potentially false rings. Such identified potentially false rings were then further investigated first by visual and correlation coefficients between segments of different radii of each tree (Figure 2.6b). Wood features that had been identified as potential false rings were excluded when they were not present in all radii of a tree.

2.4.1. Detrending of ring-width series

After measuring the ring-widths of all cores and excluding identified false rings, the radii of each tree were averaged to produce a mean ring-width series per tree. The raw ring-width series exhibit multidecadal trends arising from both ontogenetic effects (Voelker et al., 2011) and/or from periods of canopy release and suppression (Brienen and Zuidema, 2006). Such trends are superimposed over the climatic effects over tree growth and can be removed to improve the climatic signals in the ring-width series.

To do this, two standard dendrochronological methods were used to estimate a trend curve which is removed from each individual ring-width series. The first of the two methods applied consists of estimating an age-dependent growth curve estimated at the population level, thus the same trend is removed from all trees (i.e. regional standardization curve detrending, Briffa et al., 1992) – Figure 2.7. After producing a regional curve for each of sites sampled, it was clear that trees analyzed in this thesis presented large variability in the decadal trends, which in most cases did not follow the mean curve produced for each site. Therefore, this method was not considered suitable for this particular dataset.

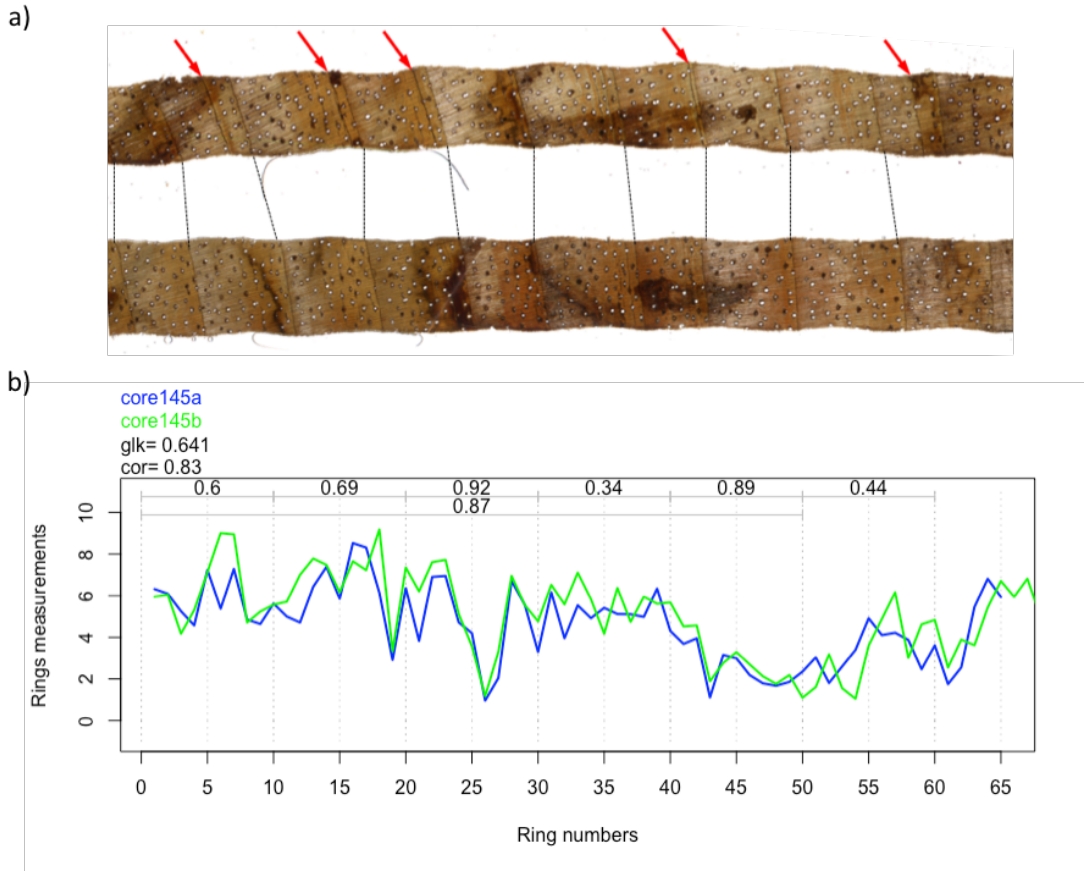

Figure 2.6. (a) Corresponding segments of two samples from a single tree, with red arrows indicating the presence of discontinuous/double parenchyma bands which only occur in one of the two samples and which do not follow the wood density and vessel distribution variations. (b) Raw ring-width series of the two cores shown above. The segments shown in (a) correspond to the rings 31-40 in the series shown in (b). Numbers above the series indicate correlation coefficients for different segments within the two series.

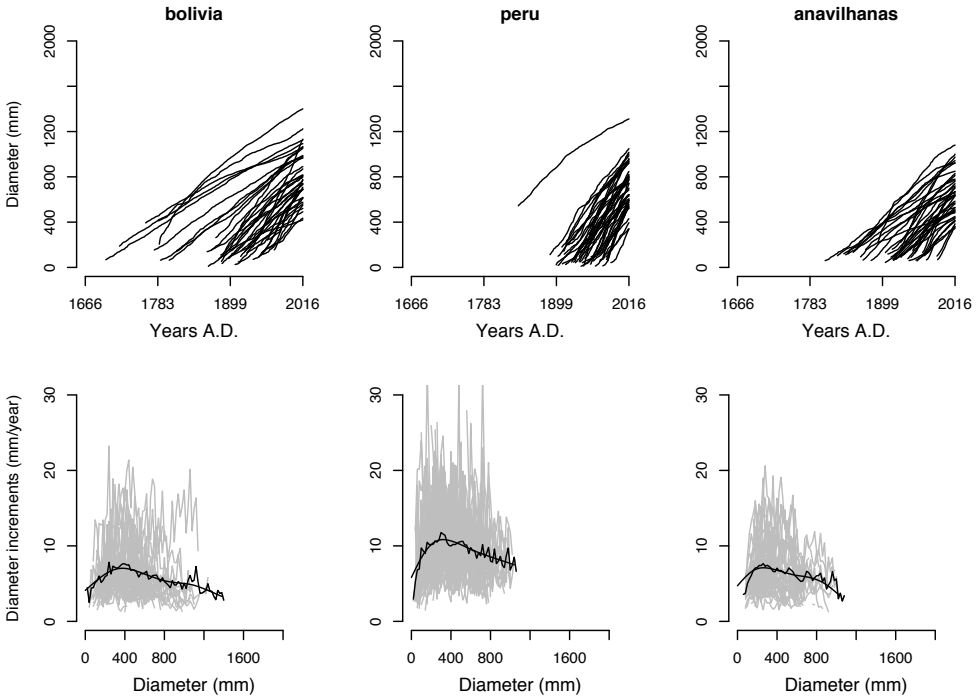

Figure 2.7. Construction of regional standardization curves showing the high variability of the growth trends for each site.

The second method consists of estimating a trend for the ring-width series of each tree separately, and thus a different curve is removed from each tree. The individual trends can be estimated by calculating a 5-year moving average, fitting a negative-exponential model or by fitting a smooth spline for each series (Cook and Peters, 1981) (Figure 2.8).

Estimating and removing a trend curve from the ring-width series produces one detrended or standardized (STN) series of each tree. This process is called ring-width detrending. Each method produces different detrended curves which may be more suitable for different tree ring datasets.

2.4.2. Resolving autocorrelation in the STN series

Detrending the ring-width series as described above generates series with normal distribution, which is necessary for parametric statistical analysis such as correlations with climate variables (Book and Briffa, 1990). However, STN series often present a persistent autocorrelation structure, i.e. the values of one year are correlated with the values of previous years. If the ring-width series are to be related to

environmental variables through regression analysis, this autocorrelation can be removed. The procedure of removing the autocorrelation in the series is called pre-whitening (Cook, 1982). Autocorrelation models of 1-3 orders (i.e. 1-3 years back in time) are calculated and the model with the lowest Akaike Information Criterion is selected. The residuals of the autocorrelation models of each STN series are used as the residual (RES) series.

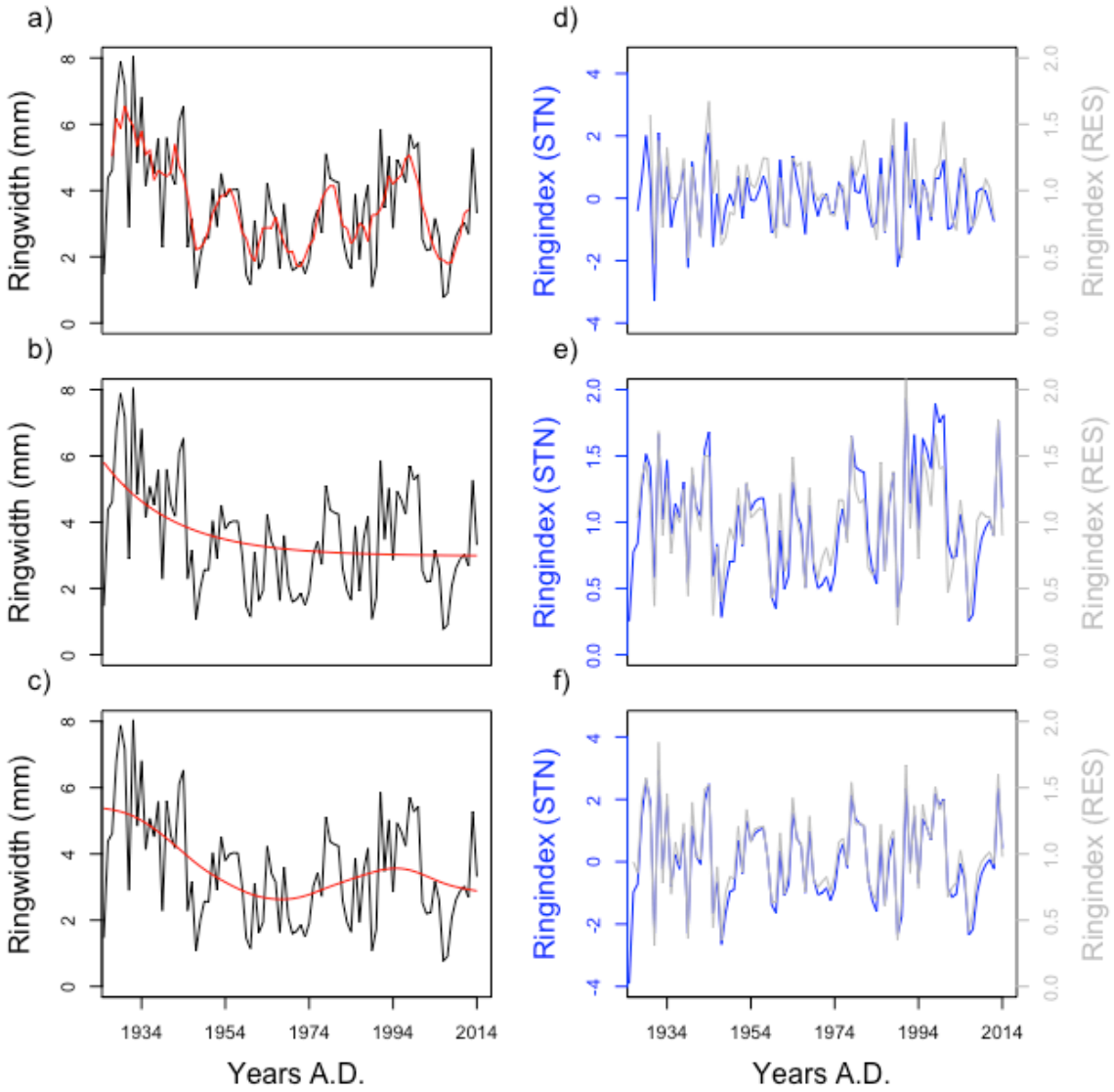

Figure 2.8. Example of different approaches to detrend a ring-width series. In panels (a-c), the black lines are the raw-ring-width series and the red lines are the removed trend. In panels (d-f), blue lines are the detrended black lines from panels (a-c), and the gray line is the detrended series after removing autocorrelation with an autoregressive modelling. (a,d) Detrending by applying a 5-moving average, (b,e) detrending by fitting a negative exponential model, (c,f) detrending by applying a smooth spline fitting.

2.4.3. Verifying the signal-strength and dating of chronology

If the trees in the chronology have a strong common response to climate variations and their tree rings were well dated, it is expected that the resulting STN/RES series will present a strong common variability. This common variability can be statistically assessed through statistical measures which are listed and described here:

- the average of all pairwise correlations of each series,

$$\bar{R} \equiv \frac{1}{\frac{n(n-1)}{2}} \sum_{i=1}^{n} \sum_{j>i}^{n} r_{i,j}$$

where $r_{i,j}$ is the Pearson's correlation coefficient between ring-widths of trees *I* and *j* and *n* is the total number of tree series in the chronology;

- the $\bar{R}_{\text{eff}}$, which takes into account the number of cores taken from each tree and the correlation between them

$$\bar{R}_{eff} \equiv \frac{\bar{R}}{\bar{R}_{wt} + \left(\frac{1 - \bar{R}_{wt}}{c.eff}\right)} \quad ,$$

where $\bar{R}_{\text{wt}}$ is the mean of the correlations between the ring-width series from cores of the same tree over all trees, and c.eff is a measure of the effective number of cores per tree as (Briffa and Jones, 1990):

$$c_{eff} \equiv \left(\left(\frac{1}{n}\right) \sum_{i}^{n} \left(\frac{1}{n.cores_i}\right) \right)^{-1} \quad ,$$

with *n.cores* as the number of cores in each tree;

- the average of the correlations of each series with the mean of all others (inter-series corr.),

$$Itc = \sum_{i}^{n} \frac{r_{i,i*}}{n}$$

where *i** is the mean of all ring-width of all trees excluding tree *I*;

- and the expressed population signal (EPS) (Wigley et al., 1984; Briffa and Jones, 1990)

$$EPS = \frac{n\bar{R}_{eff}}{1+(n-1)\bar{R}_{eff}} \quad ,$$

Which is a measure of the signal strength relative to the replication in the chronology (Wigley et al., 1984; Speer et al., 2010). See Chapter 4 for details on the calculation of each of these parameters.

In addition to these standard dendrochronology statistics, I also considered the mean sensitivity of the ring-width chronologies, even though it is often described as not being a robust statistical analysis of time series (Bunn et al., 2013). The mean sensitivity was defined as (Biondi and Qeadan, 2008)

$$MS = \frac{2}{n-1}\sum_{t=2}^{n}\frac{|w_t - w_{t-1}|}{w_t + w_{t+1}}$$

where *n* is the length of the series and *w* is the widths of the tree rings in the series.

The common variability of the chronology can be weakened by incorporation of trees with dating errors due to undetected false rings during the initial analysis of wood anatomy and radii comparison. To detect possible false rings still in the chronology I compared each STN series with the mean series of the best trees in the chronology. The best trees were selected based on the dating confidence and on their signal strength. To select trees based on their signal strength, the EPS was repeatedly calculated, each time removing one individual series – effectively bootstrapping the average series. After this is done for all trees, the removed tree that resulted in the largest increase of the EPS is excluded. This procedure was repeated until the maximum EPS was achieved or until a minimum of 15 trees were left in the dataset. Comparing each STN series with the average series of the best trees in the data set allowed the identification of trees that could still present dating errors.

An initial exploratory analysis of the dataset used in this thesis showed that extracting the residuals from a 5yr moving average curve fitted to the ring-width series resulted in the highest EPS for two of the three sites sampled here (Table 2.2). However, this approach removed all variation at the decadal scale which may also be driven by climate. Therefore this approach was not used for producing the ring-width chronologies in this study. The other detrending approach that led to the best results for all three sites was to extract the residuals of a smooth spline fit to the ring-width series (Table 2.2). Therefore, this detrending method was chosen to develop the ring-width chronologies which are shown in Chapter 4.

Table 2.2. Descriptive statistics for chronologies produced for each site using different methods of ring-width standardization (STN) and applying autocorrelation modelling after standardization (RES). Statistical measures shown are EPS (expressed population signal), average correlation between all trees ($\bar{R}$ and $\bar{R}_{eff}$), average correlation between cores of the same tree over all trees ($\bar{R}_{wt}$), and the number of trees included in the chronology (n). All calculations done before segment correlation analysis, over a period of 100 years. Details on the ring-width standardization and calculation of descriptive statistics are explained in the text.

Western Amazon						
		EPS	$\bar{R}_{eff}$	$\bar{R}$	$\bar{R}_{wt}$	n
5 yr moving average	STN	0.90	0.17	0.14	0.57	45
	RES	0.84	0.10	0.08	0.45	45
Negative exp. Model	STN	0.84	0.10	0.09	0.63	45
	RES	0.85	0.11	0.09	0.49	45
Smooth spline	STN	0.87	0.13	0.11	0.60	45
	RES	0.85	0.11	0.09	0.46	45
southwest Amazon						
		eps.eff	rbar.eff	rbar.bt	rbar.wt	n.trees
5 yr moving average	STN	0.74	0.08	0.07	0.43	34
	RES	0.70	0.06	0.06	0.54	34
Negative exp. Model	STN	0.75	0.08	0.07	0.42	34
	RES	0.76	0.09	0.08	0.52	34
Smooth spline	STN	0.76	0.08	0.07	0.40	34
	RES	0.76	0.08	0.07	0.40	34
central Amazon						
		eps.eff	rbar.eff	rbar.bt	rbar.wt	n.trees
5 yr moving average	STN	0.82	0.17	0.14	0.48	23
	RES	0.80	0.15	0.12	0.41	23
Negative exp. Model	STN	0.83	0.17	0.15	0.58	23
	RES	0.81	0.16	0.13	0.46	23
Smooth spline	STN	0.83	0.18	0.15	0.52	23
	RES	0.80	0.14	0.12	0.42	23

Finally, the dating of each tree in the chronology was verified through segment correlation analysis (Holmes et al., 1982). This analysis consisted in first dividing each series into overlapping segments of equal lengths and correlating each segment with the average of the of the same segment of all other series. When one segment was not significantly positively correlated with the average of the other trees, correlation coefficients were re-calculated for lagged versions of the segment. If one of more lagged versions of the segment were significantly correlated with the average of the other trees, the sample was inspected again to verify if a possible dating error could be detected in the wood anatomy.

The final indexed ring-width chronology was calculated as the robust mean of either the STN series or the RES series (Speer et al., 2010). The final chronology was then assessed one last time by repeating the procedure of bootstrapping of the tree ring series tree and recalculating the EPS. At this stage, any removed series that result in a significant improvement of the EPS were excluded from the chronology. The results of the final chronologies produced for each site are shown and discussed in detail in Chapter 4.

All detrending and cross-dating were done in R 3.3.1 (R Core Team 2016) using the package dplR (Bunn, 2010).

2.5. Verifying chronology dating by radiocarbon bomb-peak dating

An efficient method to verify the dating of the final chronologies produced is to perform radiocarbon (^{14}C) dating of tree rings. ^{14}C dating provides estimates of the date of ring formation which are especially accurate for rings formed after 1955, when a sharp peak in the atmospheric concentration of radiocarbon was created after nuclear bomb tests performed during 1945-1963 (Dai and Fan, 1986). After this period, nuclear bomb tests stopped with the Test Ban Treaty, and the atmospheric radiocarbon concentration declined rapidly due to continuous emissions of ^{14}C-depleted carbon from fossil fuel burning. The evolution of the atmospheric radiocarbon concentration since then (the bomb-peak ^{14}C curve) has been analyzed

for different parts of the world (Hua et al., 2013). Due to the large differences in radiocarbon concentration between successive years following 1955, the radiocarbon concentration in wood tissues of successive tree rings formed after 1955 can be used as a tracer for the year of formation of the tree rings, with an accuracy of ±1-2 years depending on the year of formation of the tree ring (Worbes, 2004; Wills et al., 2011; Andrew-Hayles et al., 2015; Baker et al., 2017).

For this thesis, the radiocarbon dating of 27 rings of 9 different trees (3 rings per tree) was done as an independent method of verifying the dates of the tree rings after crossdating. For this analysis, it was important to analyze more than one ring per tree. This is because the atmospheric radiocarbon concentration after 1955 shows a sharp increase up to approximately 1963 and then decline more gradually until the present date, which results that every radiocarbon measurement may have at least two possible dates on the atmospheric radiocarbon curve. This uncertainty can be resolved when the radiocarbon ages of more than one ring from the same tree are analyzed. The results of these analyses are shown in Chapter 4.

2.6. Sample preparation for isotope analysis

In addition to measuring ring-widths, the isotopic composition oxygen and carbon of the tree rings of selected wood cores was also measured. The isotopic composition in the wholewood, i.e. raw material, reflects the isotopic composition of different wood components, weighed by their proportional masses in the wood material. Several studies show that the isotopic compositions of different wood components like cellulose, lignin and lipids may be very different, and that their variations in the wood are often correlated (Epstein et al., 1976, Schleser et al., 2015, Li et al., 2011, Loader et al., 2003). While the isotopic composition of individual wood components isolated may show very similar time series, the isotopic composition of wholewood may be affected simply by variations in the wood composition (e.g. proportion of early and late-wood) between different years or with tree ages (Epstein et al., 1976). This will dampen the environmental signal in the isotopic composition. For this reason, many studies using isotopes ratios in tree rings for climate reconstruction

analyze the isotopic composition of cellulose tissues in the tree rings, extracted from wholewood tissues. For the purposes of this study, the isotope composition of tree rings was also based on cellulose extracted from wholewood – except for one $\delta^{13}C$ series which had previously been analized, details in Chapter 3. Cellulose was chosen because part of the oxygen in the cellulose molecules originates from stem water present in the cell during cellulose synthesis – through carbonyl hydration (Sternberg et al., 2008 and references therein). Thus, the isotopic signal of cellulose is expected to retain climatic signals contained in the source water $\delta^{18}O$.

For isotope analysis of tree ring samples, cellulose was extracted directly from wood cross-sectional slices following the procedure of Kagawa et al. (2015): cross-sectional slices of 1-4mm thickness and 6-8 cm length were cut from the core samples with a circular diamond saw blade and packed in TEFLON perforated sheets (Figure 2.9). Cellulose was then extracted from the raw wood material following the chemical procedure of Wieloch et al. (2001).

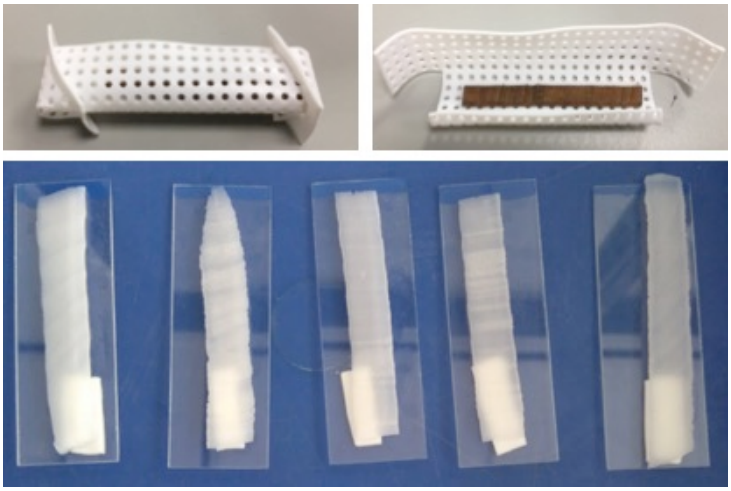

Figure 2.9. Image of the sample preparation for cellulose extraction. Top picture shows a cross-sectional lath of 2mm thickness and 6cm length packed in a foldable package of perforated Teflon sheet, before cellulose extraction. Bottom picture shows several samples after chemical extraction of cellulose from cross-sectional laths.

The procedure for cellulose extraction starts with two rounds of 2h immersions of the samples in a 5% NaOH solution, followed by four rounds of 8h immersion in a 7.5% $NaClO_2$ solution. Samples were washed with hot distilled water at the end of the first two rounds and the last four rounds. This resulted in cellulose slices which

were then air dried for 2 hours, frozen and freeze dried at -50°C for 72 hours. Once dried, the cellulose slices, for which the tree ring structure was still visible, were cut into individual tree rings. Cellulose samples were packed into silver (0.5±0.05 mg) and tin (1.0±0.1 mg) capsules oxygen and carbon isotopes analyses, respectively. Capsules containing the cellulose samples were pyrolyzed at 1400°C and their isotope ratio determined in an element analyzer and an isotope ratio mass spectrometer (Sercon 20-20 IRMS) with analytic precision of 0.15‰ for oxygen isotopes and 0.05‰ for carbon isotopes. Oxygen isotope ratios are expressed relative to the Vienna Standard Mean Ocean Water (V-SMOW) and carbon isotope ratios are expressed relative to Pee Dee Belemnite standard. All isotope analyses were carried out at the University of Leicester, under supervision of Dr. Arnoud Boom.

2.7.Climate data sources

Hydrological data of river at each sampling site was obtained from the Brazilian *Sistema Nacional de Informações Hidrológicas,* from the Peruvian *Servicio Nacional de Meteorología y Hidrología del Peru* and from collaborators in Bolivia. For the site in western Amazon, Rainfall data from local stations was not available for all sites. Thus for analysis purposes, for all sites data of local precipitation was also obtained from global precipitation datasets: Climate Research Unit (CRU TS 4.0.1) of the University of East Anglia, Global Precipitation Climatology Center (climatedataguide.ucar.edu/climate-data/gpcc-global-precipitation-climatology-centre) of the National Oceanic and Atmospheric Administration (NOAA) and from the Tropical Rainfall Measuring Mission (TRMM 3B42, http://trmm.gsfc.nasa.gov/data_dir/data.html) of the NASA Goddard Space Flight Center. Data of cloud cover, temperature and vapour pressure deficit (VPD) were also obtained from CRU TS 4.0.1. The $\delta^{18}O$ of precipitation water was obtained from the Global Network of Isotopes in Precipitation (GNIP), via the Water Isotopes System for Data Analysis, Visualization and Electronic Review (WISER, http://nds121.iaea.org/wiser/index.php). SST from the Equatorial Pacific and (El Niño regions 1+2, 3, 4 and 3.4) and Tropical Atlantic (North and South) were be obtained

from the Global Precipitation Climatology Center (GPCC, climatedataguide.ucar.edu/climate-data/gpcc-global-precipitation-climatology-centre) of the NOAA, and PDO monthly indices from the Joint Institute for the Study of the Atmosphere and Ocean from the Washington University (http://jisao.washington.edu/pdo/).

Chapter 3 Contrasting controls on tree ring isotope variation for Amazon floodplain and terra firme trees

Abstract

- Isotopes in tropical trees rings can improve our understanding of tree responses to climate. We assessed how climate and growing conditions affect tree-ring oxygen and carbon isotopes ($\delta^{18}O_{TR}$ and $\delta^{13}C_{TR}$) in four Amazon trees. We analyzed within-ring isotope variation for two terra firme (non-flooded) and two floodplain trees growing at sites with varying seasonality.
- We find distinct intra-annual patterns of $\delta^{18}O_{TR}$ and $\delta^{13}C_{TR}$ driven mostly by seasonal variation in weather and source water $\delta^{18}O$. Seasonal variation in isotopes was lowest for the tree growing under the wettest conditions. Tree ring cellulose isotope models based on existing theory reproduced well observed within-ring variation with possible contributions of both stomatal and mesophyll conductance to variation in $\delta^{13}C_{TR}$.
- Climate analysis reveal that terra firme $\delta^{18}O_{TR}$ signals were related to basin-wide precipitation indicating a source water $\delta^{18}O$ influence, while floodplain trees recorded leaf enrichment effects related to local climate. Thus, intrinsically different processes (source water vs. leaf enrichment) affect $\delta^{18}O_{TR}$ in the two different species analyzed. These differences are likely a result of both species-specific traits and of the contrasting growing conditions in the floodplains and terra firme environments.
- Simultaneous analysis of $\delta^{13}C_{TR}$ and $\delta^{18}O_{TR}$ support this interpretation as it shows strongly similar intra-annual patterns for both isotopes in the floodplain trees arising from a common control by leaf stomatal conductance, while terra firme trees showed less covariation between the two isotopes. Our results are interesting from a plant physiological perspective and have implications for climate reconstructions as trees record intrinsically different processes.

3.1. Introduction

Intra-annual, high-resolution oxygen and carbon isotopes are increasingly being used for a multitude of applications, including climate reconstructions (Barbour et al., 2002; Ohashi et al., 2009; Roden et al., 2009; Fichtler et al., 2010; Managave et al., 2011), age and growth rate determinations in ringless tropical trees (Poussart et al., 2004; Poussart and Schrag, 2005; Pons and Helle, 2011), and for studying seasonality in growth and use of carbohydrate reserves (Helle and Schleser, 2004; Ohashi et al., 2009; Fichtler et al., 2010; Gulbranson and Ryberg, 2013). A prerequisite for using tree-ring isotope records is an understanding of the underlying physiological processes affecting tree-ring isotope ratios.

Much progress in our understanding has been made over the past decades for temperate trees (McCarroll and Loader, 2004). In comparison, isotope studies of tropical trees remain scarce, despite their great potential to improve our understanding of tree functioning and for climate reconstructions (Sleen et al., 2017) and the importance of these vast forests for the global carbon cycle (Phillips et al., 2009; Beer et al., 2010; Pan et al., 2011; Brienen et al., 2015). There is little information about what processes dominate variation of tree ring oxygen and carbon isotopes ($\delta^{18}O_{TR}$ and $\delta^{13}C_{TR}$) in tropical environments, and how this varies between different tropical tree species.

Oxygen isotope signals in tree rings are mostly the result of variation in source water $\delta^{18}O$ and evaporative leaf enrichment (Dongmann et al., 1974; Roden and Ehleringer, 1999; Farquhar et al., 2007; Cernusak et al., 2016). In tropical trees oxygen isotopes have been shown to reflect both processes (Miller et al., 2006; Kahmen et al., 2011; Brienen et al., 2011; Bowman et al., 2013; Schollaen et al., 2013), but which of these effects dominates and under which conditions remains poorly known. Specifically, the contribution of leaf water enrichment to the final $\delta^{18}O_{TR}$ may vary between species and environments, due to variation in leaf transpiration arising from specific differences in leaf traits (e.g. varying path lengths, Kahmen et al., 2008;

Holloway-Phillips et al., 2016) and/or site humidity levels (Barbour and Farquhar, 2000; Barbour et al., 2002; Kahmen et al., 2011).

Carbon isotope ratios in tree rings are affected by the ratio between photosynthetic assimilation rate and conductance to CO_2. The conductance of CO_2 from outside the leaf to the sites of photosynthesis consists of stomatal conductance, g_s and mesophyll conductance, g_m which both affect $\delta^{13}C_{TR}$ (Farquhar et al., 1982; Seibt et al., 2008; Farquhar and Cernusak, 2012). As g_s is often sensitive to water availability, $\delta^{13}C_{TR}$ has been shown to reflect drought levels at relatively dry sites in the tropics (Gebrekirstos et al., 2009; Fichtler et al., 2010; Brienen et al., 2011). Mesophyll conductance, g_m is temperature dependent in many tree species and therefore variations in leaf temperature may also affect $\delta^{13}C_{TR}$ (Seibt et al., 2008; Griffiths and Helliker, 2013; von Caemmerer and Evans, 2015). Other studies show that $\delta^{13}C_{TR}$ signals also vary as a result of post-photosynthetic processes, specifically usage of carbon reserves (Helle and Schleser, 2004; Eglin et al., 2010; Gulbranson and Ryberg, 2013; Gessler et al., 2014).

A useful approach to understand what processes are reflected in isotope signals is simultaneous analysis of variations of $\delta^{18}O_{TR}$ and $\delta^{13}C_{TR}$ in tree ring cellulose. This is because stomatal conductance response to low humidity may affect both leaf ^{13}C discrimination and leaf water ^{18}O enrichment, potentially leading to co-variation of $\delta^{13}C_{TR}$ and $\delta^{18}O_{TR}$ (Step 1 in Figure 3.1a and Step 2 in Figure 3.1b). This approach has, for example, been used to assist in the interpretation of carbon isotope signals in leaves of temperate trees (Scheidegger et al., 2000), and allowed at least a partial separation of leaf level fractionation processes from the other fractionating effects on $\delta^{18}O_{TR}$ and $\delta^{13}C_{TR}$ (Barbour et al., 2002; Barnard et al., 2012; Roden and Farquhar, 2012; Roden and Siegwolf, 2012) (Figure 3.1).

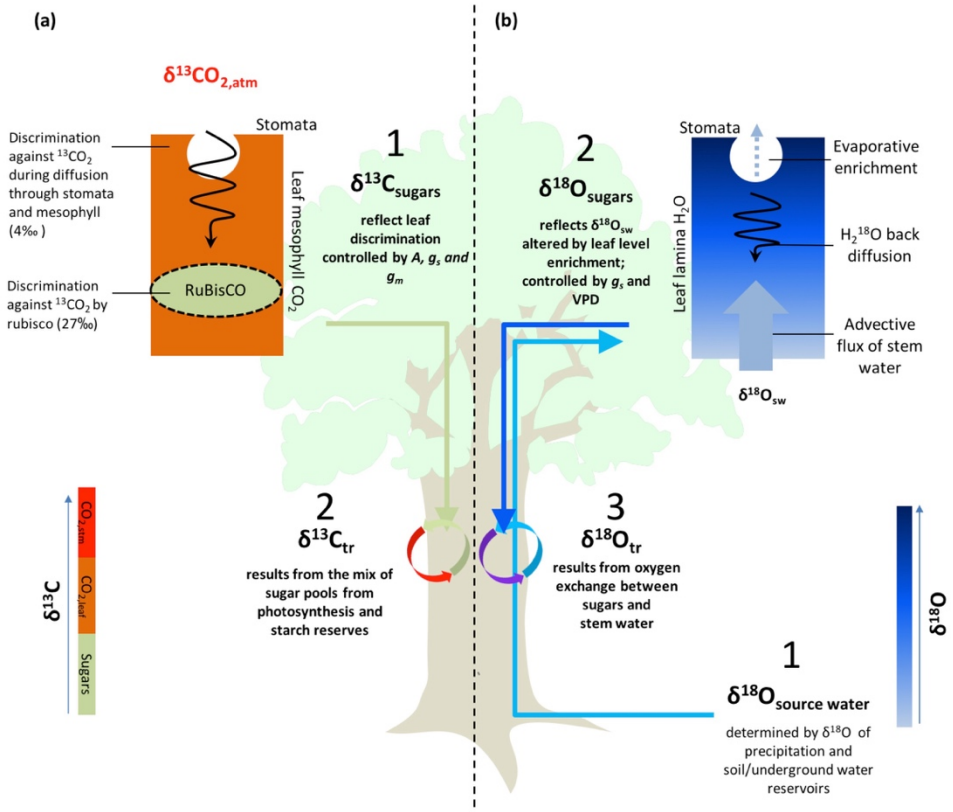

Figure 3.1 Illustration of the main processes driving isotope signals in tree rings. Left diagram illustrates the two main processes affecting $\delta^{13}C_{TR}$, which are (1) leaf level carbon isotope discrimination controlled by photosynthetic assimilation (A) and stomatal conductance (g_s), and (2) mixing of $\delta^{13}C$ signals from leaf sugars and starch reserves into tree ring cellulose. Right diagram illustrates the three processes affecting $\delta^{18}O_{TR}$, which are (1) variation in source water $\delta^{18}O$, (2) enrichment of the source water signal in the leaf due to evaporation, and (3) exchange of oxygen between stem water and sugars before incorporation into tree ring cellulose.

Here we analyze which processes affect isotopic variation in tree rings of Amazonian trees, using a dual isotope approach with intra-ring resolution. This approach allows us to assess at a fine temporal scale how tree-ring isotopic compositions reflect the trees' responses to varying weather conditions during the growing season. We chose two tree species growing under very different environmental conditions in the western and southwestern Amazon basin: the deciduous species *Cedrela odorata* (Meliaceae) from terra firme (non-flooded) forests which grow primarily during the wet season

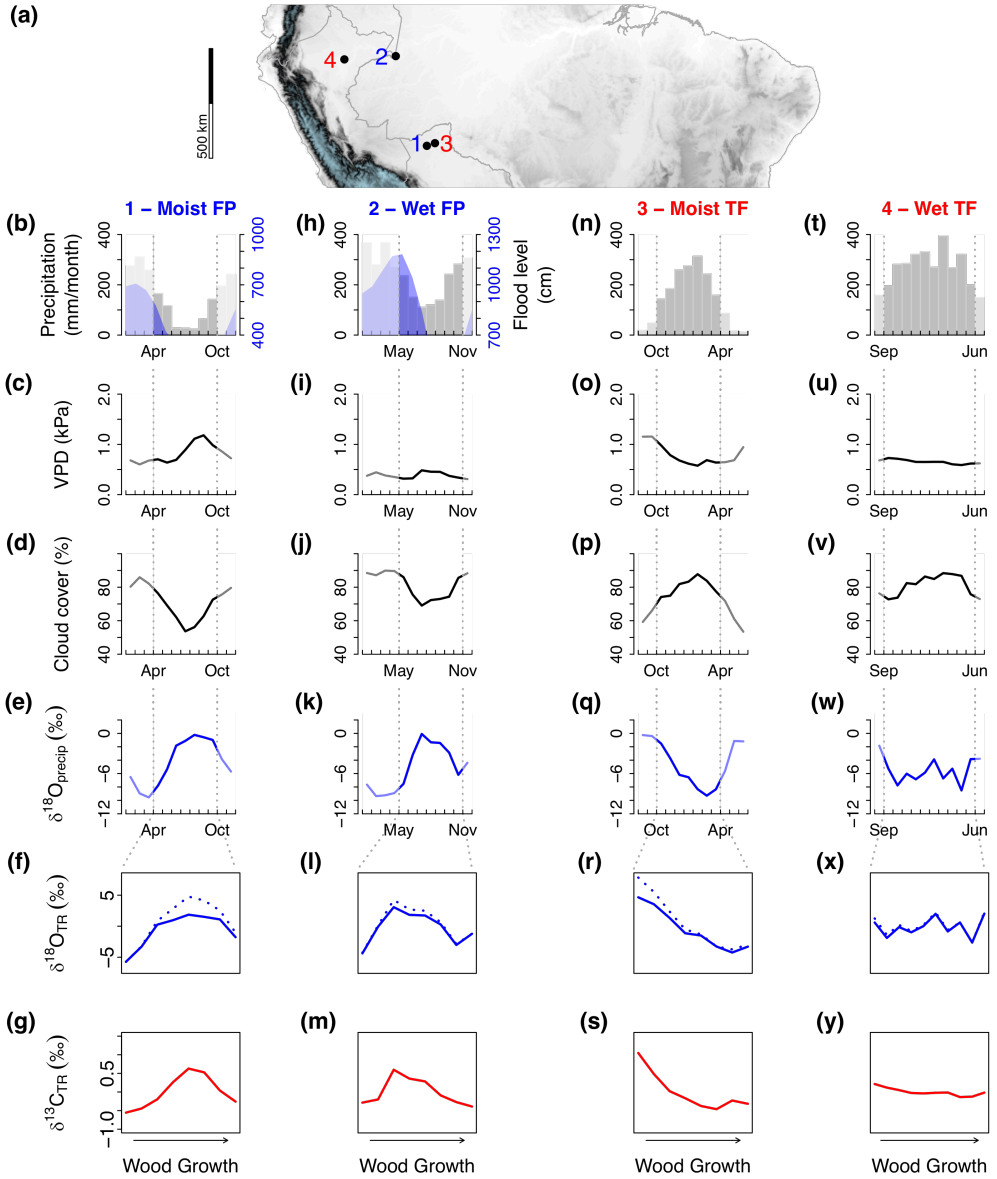

Figure 3.2. Map with the sampling sites (panel a) and annual cycles of climatic variables (panels b–e, h–k, n–q, t–w) and predicted intra-annual tree ring isotopes (panels f–g, l–m, r–s, x–y) for the two floodplain (FP) and the two terra firme (TF) sites. Annual cycle of monthly precipitation (grey bars) and river flood level (blue, showing levels above tree base) (top row), monthly vapour pressure deficit (second row), monthly cloud cover (third row), monthly $\delta^{18}O$ in precipitation (fourth row), predicted $\delta^{18}O$ in tree rings (solid line for effects of only source water $\delta^{18}O$ and stippled line for added effects of leaf water enrichment) (fifth row), and predicted $\delta^{13}C$ in tree rings, ignoring post photosynthetic processes (lowermost row). The vertical dashed lines indicate the assumed growing seasons for each site – see details in section Data Analysis. Climatic data shown are from CRU TS 4.00. Rainfall $\delta^{18}O$ data are from the GNIP database. River level data are from the Brazilian Hidroweb-SNIRH database and from the ORE-HYBAM database for the Peruvian site.

(Dünisch et al., 2003; Brienen et al., 2012; Costa et al., 2013; Brienen et al., 2015; Baker et al., 2017); and the brevi-deciduous species *Macrolobium acaciifolium* (Fabaceae) from floodplain ecosystems, which grows when river stage levels are low, i.e. during the dry season (Schöngart et al., 2002; Schöngart et al., 2005; Assahira et al., 2017). The original motivation for looking at these contrasting environments was that terra firme trees would record wet season and floodplain dry season climate variation. We chose these species because both are spatially widespread (ter Steege et al., 2013), grow in contrasting conditions and produce distinct annual rings (Fig. I.1 in Appendix I). For both species, we investigate two trees from two sites at a high intra-ring resolution (four trees in total). The sites were selected to differ in precipitation amount and seasonality (Figure 3.2).

Our objectives are (1) to compare observed and expected intra-annual patterns of carbon and oxygen isotope within their tree rings based on existing mechanistic understanding; (2) to assess the role of local climate and hydrological conditions and species differences on the intra-annual cycles of $\delta^{18}O_{TR}$ and $\delta^{13}C_{TR}$ and (3) to assess to what degree the dual-isotope approach may indicate what the main climatic and physiological drivers of variation in both isotopes at the intra-annual level are.

3.2. Isotopes in tree rings: theory and modelling

3.2.1. Carbon isotopes

Atmospheric CO_2 is the source of carbon for terrestrial trees. During CO_2 uptake by a leaf, four fractionating processes are of importance: CO_2 diffusion through the stomata and through the leaf mesophyll (i.e. cell membranes and cytoplasm), photorespiration and isotopic fractionation during the carboxylation reaction due to higher chemical affinity of the enzyme RuBisCO for $^{12}CO_2$ compared to $^{13}CO_2$ (Step 1 in Figure 3.1a). These processes result in lower average plant organic ^{13}C compared to the atmosphere, or a positive atmosphere-plant isotope discrimination (Δ)

$$\Delta^{13}C \equiv \frac{R_{atm}-R_{plant}}{R_{plant}} \cdot 10^3 = (\delta^{13}C_{atm} - \delta^{13}C_{plant})/(1 + \frac{\delta^{13}C_{plant}}{1000}) \qquad [1]$$

Here $R \equiv \frac{N_{rare}}{N_{abundant}}$ with N_{rare} the number of molecules of the rare isotope compound and $N_{abundant}$ the number of molecules of the abundant isotope compound in a sample, and with $\delta(permille, ‰) \equiv (\frac{R_{sample}}{R_{std}} - 1) \cdot 10^3$, where R_{std} is the isotope ratio of an internationally recognized standard. Farquhar et al. (1982) formulated a model to predict this discrimination that considers fractionation during diffusion through stomata and through the mesophyll, during carboxylation and fractionation due to photorespiration:

$$\Delta^{13}C = a\left(\frac{c_a - c_i}{c_a}\right) + a_m\left(\frac{c_i - c_c}{c_a}\right) + \mathrm{b}\left(\frac{c_c}{c_a}\right) - f\Gamma^*/c_a \qquad [2]$$

where c_i is CO_2 partial pressure inside leaf intercellular space, c_a is CO_2 partial pressure in air, c_c is the CO_2 partial pressure in the chloroplast, a (= 4.4‰) is the fractionation caused by slower diffusion of $^{13}CO_2$ compared to $^{12}CO_2$ through stomata, a_m (=1.8‰) is the fractionation during CO_2 diffusion through the mesophyll, b (= 30‰) is fractionation during carboxylation caused by discrimination of RuBisCO against $^{13}CO_2$ inside the leaf, *f* (=12‰) is the discrimination due to photorespiration and Γ^* is the CO_2 compensation point in the absence of day respiration (see also Seibt et al., 2008).

The model predicts that if c_c is close to c_a, then discrimination is primarily due to non-equilibrium fractionation associated with carboxylation (≈b). If, on the other hand, CO_2 in the leaf is being drawn down by assimilation and c_c drops, then the carboxylation reaction causes an increase of the $^{13}CO_2$ to $^{12}CO_2$ ratio inside the leaf (a Rayleigh distillation, step 1 in Figure 3.1a). The consequent enrichment of CO_2 inside the leaf offsets the effects of fractionation by carboxylation and lowers the net discrimination slightly towards the value for fractionation by diffusion (≈a). For plants, the magnitude of fractionation thus depends on the CO_2 partial pressure difference $c_a - c_c$ between the outside and inside of the leaf. This difference is controlled by the ratio between carbon assimilation rate (A) and CO_2 flux in the leaf via $A = g_{sC}\left(\frac{c_a - c_i}{P}\right) = g_m\left(\frac{c_i - c_c}{P}\right)$, which expresses that at steady state, assimilation

rate A is equal to diffusive CO_2 flow though stomata and into the chloroplast. Here P is atmospheric air pressure, g_{sC} is the stomatal conductance to CO2 and g_m is the mesophyll conductance to CO_2. Equation 4 may then be expressed as

$$\Delta^{13}C = a + (b - a)\frac{c_i}{c_a} - (b - a_m)\left(\frac{A}{c_a g_m}\right) - f\Gamma^*/c_a \quad [3]$$

Isotope ratios of sugars produced in the leaf may undergo alterations before being incorporated in wood tissue by processes such as respiration, re-fixation of respired CO_2, and production and remobilisation of carbon reserves, primarily starch (e.g. Cernusak et al., 2009; Treydte et al., 2014). In particular, for some deciduous trees wood formation before leaf flush requires the mobilization of non-structural carbohydrate reserves (NSC, step 2 in Figure 3.1a). NSC reserves which have accumulated by the end of the previous growing seasons are usually enriched in ^{13}C in comparison with new photosynthesis assimilates (Brugnoli et al., 1988; Damesin and Lelarge, 2003). Thus the use of stored NSC during the growing season may lead to higher $\delta^{13}C$ in initial tree ring sections (Helle and Schleser, 2004; Skomarkova et al., 2006; Ohashi et al., 2009; Gulbranson and Ryberg, 2013; Gessler and Treydte, 2016), and possibly in other ring sections as well (Eglin et al., 2010). These post-photosynthetic processes may partially decouple the $\delta^{13}C_{TR}$ signal from current years' leaf fractionation processes, potentially dampening the climatic signal in $\delta^{13}C_{TR.}$

In summary two processes contribute to intra- and interannual variation in $\delta^{13}C_{TR}$: (i) ^{13}C discrimination during leaf carbon uptake and photosynthesis and (ii) carbon remobilization from non-structural carbon reserves. $\delta^{13}C_{TR}$ derived from reserves is enriched with ^{13}C and for deciduous species tends to be used primarily during the initial phase of tree ring formation. ^{13}C discrimination at the leaf level is controlled by the ratio of CO_2 inside the leaf to CO_2 in air. If this ratio is low – either because of low stomatal/mesophyll conductance to CO_2 associated with high vapour pressure deficit (VPD) or low temperatures, or due to high assimilation rates - discrimination will be small and vice versa.

3.2.2. Oxygen isotopes

More processes contribute to $\delta^{18}O$ variation in tree ring cellulose ($\delta^{18}O_{TR}$) compared to $\delta^{13}C_{TR}$. First, $\delta^{18}O_{TR}$ is related to the isotopic composition of source water ($\delta^{18}O_{sw}$), which may originate from rainfall and/or from underground water (step 1 in Figure 3.1b). $\delta^{18}O_{sw}$ may change in the soil by fractionation during evaporation. Water is taken up from the soil by roots without fractionation (Ehleringer and Dawson, 1992). Xylem water entering the leaf has thus the same $\delta^{18}O$ as soil water. In the leaf, water will get enriched in $H_2{}^{18}O$ compared to stem water due to preferential evaporation of light water, $H_2{}^{16}O$ (Craig and Gordon, 1965; Dongmann et al., 1974). Average leaf water $\delta^{18}O$ ($\delta^{18}O_{lw}$) depends on the extent of ^{18}O enrichment of water at the sites of evaporation within the leaves ($\delta^{18}O_{es}$), and on how much $H_2{}^{18}O$ diffuses from the sites of evaporation through the leaf lamina, which depends on transpiration (Farquhar and Lloyd, 1993, Farquhar et al., 2007; Cernusak and Kahmen, 2013). Transpiration is driven by leaf to air vapour pressure difference (VPD) modulated by stomatal conductance (which itself may depend on VPD) (step 2 in Figure 3.1b). Sugars produced in the leaf carry with them the ^{18}O enriched leaf water signal ($\delta^{18}O_{lw}$) until they are broken down during cellulose synthesis, when they exchange oxygen isotopes with water in the stem (step 3 in Figure 3.1b).

The roles of the above-mentioned processes have been incorporated into models. The earliest model for $\delta^{18}O$ at the leaf sites of evaporation is from Dongmann et al. (1974) based on a model of Craig and Gordon (1965) for fractionation during the process of evaporation from a water surface. The Dongmann model considers a water flow from roots to the stomata to the atmosphere, equilibrium fractionation ε^+ during evaporation from tissue in the stomata, and kinetic fractionation ε_k during diffusion of molecules from the leaf to the atmosphere through stomata. The resulting model for the isotopic signature at the site of evaporation $\delta^{18}O_{es}$ is (same as eq. 1. of Sternberg, 2009, but algebraically rearranged)

$$\delta^{18}O_{es} = (\delta^{18}O_{sw} + \varepsilon_k)\left(\frac{e_i - e_a}{e_i}\right) + \varepsilon^+ + \delta^{18}O_a\left(\frac{e_a}{e_i}\right) \quad [4]$$

e_i and e_a are the intracellular and ambient vapour pressure, respectively; $\varepsilon_k = \frac{32g_s^{-1}+21g_b^{-1}}{g_s^{-1}+g_b^{-1}} \sim 26.5‰$ is the kinetic isotopic fractionation of diffusion through stomata and boundary layer, g_b is the leaf boundary layer conductance (Farquhar et al., 1989); $\varepsilon^+ = 2.644 - 3.206\left(\frac{10^3}{K}\right) + 1.534\left(\frac{10^6}{K^2}\right) = 9.57‰$ (at 20°C) is the temperature dependent isotopic equilibrium fractionation between vapour and water at the evaporation site inside the stomata, where T is the leaf temperature in Kelvin. At higher temperatures ε^+ tends to decrease, but this effect is relatively small (Bottinga and Craig, 1969).

To interpret the model it is helpful to express leaf transpiration through stomata as $E = gs * \frac{ei-ea}{P} = gs * \frac{VPD}{P}$ where $VPD \equiv e_i - e_a$ is leaf to air vapour pressure difference (or 'deficit') and *P* is the atmospheric pressure. Thus, if VPD ~ 0, there is no leaf to air water flow and thus no flow from the stem into the leaves. In this case, $\delta^{18}O_{es}$ is just the sum of atmospheric $\delta^{18}O_a$ (e_i/e_a = 1) and the equilibrium fractionation ε^+ of evaporation inside the stomata. If in contrast there is a flow of water from the leaf via stomata to the atmosphere (i.e. when VPD > 0) and thus also a flow of stem (source) water to the stomata, then there is also a contribution to $\delta^{18}O_{es}$ from source water $\delta^{18}O_{sw}$ and from kinetic fraction ε_k during diffusion of water molecules through the stomatal opening – see Figure 3.3a.

The Dongmann model (1974) described above tends to overestimate leaf water $\delta^{18}O$. Farquhar and Lloyd (1993) suggest that this is because average leaf water $\delta^{18}O$ is a mixture of $\delta^{18}O$ at the evaporative site ($\delta^{18}O_{es}$) and in the source water ($\delta^{18}O_{sw}$). The relative contribution of $\delta^{18}O_{es}$ and $\delta^{18}O_{sw}$ to average leaf water $\delta^{18}O$ ($\delta^{18}O_{lw}$) depends on the degree of back-diffusion of isotopes from the evaporation site along the water-stream from veins to stomata. The lower the water flow, the more important is the effect of back-diffusion and vice versa. The importance of back-diffusion can be measured by the Péclet number

$$\wp \equiv \frac{Advection}{Diffusion} = \frac{u}{D/L}, \qquad [5]$$

the ratio of advective water transport (velocity *u*, which can be expressed using transpiration as $u = \frac{E}{C}$ where c is concentration of water e.g. in moles m^{-3}) by the water stream from soil to air via stomata and the counteracting diffusive transport (D molecular diffusivity of water and *L* the length of the path from stomata into leaf veins (see also Cernusak and Kahmen, 2013). Farquhar and Lloyd (1993) formulated a model of this effect which predicts $\delta^{18}O$ in the leaf within a distance *L* along veins from the evaporative site:

$$\delta^{18}O_{lw} = \delta^{18}O_{sw} + (\delta^{18}O_{es} - \delta^{18}O_{sw}) * \frac{(1-e^{-\wp})}{\wp} \quad [6]$$

The term $\alpha = \frac{(1-e^{-\wp})}{\wp}$ determines the contribution of $\delta^{18}O_{es}$ to $\delta^{18}O_{lw}$, resulting from back diffusion. According to this model if transport via advection of stem water to the evaporation site is much faster than the counteracting diffusive transport - i.e. when $\wp$ is large - $\delta^{18}O$ of leaf water is close to $\delta^{18}O$ of source (stem) water. If in contrast transport by advection of stem water is less than by back-diffusion then $\delta^{18}O$ of leaf water will be close to $\delta^{18}O_{es}$ (since $\frac{(1-e^{-\wp})}{\wp} \rightarrow 1$ for $\wp \rightarrow 0$) – Figure 3.3b,d. Thus, because the advective flux is given by transpiration, E, the contribution of $\delta^{18}O_{es}$ to $\delta^{18}O_{lw}$ is controlled by both stomatal conductance to water, g_{sw} and VPD (Figure 3.3b-d). Since transpiration is linearly proportional to VPD, small changes in g_{sw} have a large effect on net transpiration (and thus on $\delta^{18}O_{lw}$) when VPD is large (see Figure 3.3).

Finally, tree ring cellulose $\delta^{18}O$ ($\delta^{18}O_{TR}$) depends on post-photosynthetic fractionation, which occurs when sugars exchange oxygen with stem water during cellulose synthesis (step 3 in Figure 3.1b). According to Sternberg (2009) this fractionation can be parameterised as:

$$\delta^{18}O_{tr} = \phi(\delta^{18}O_{sw} + \Delta) + \left((1-\phi) * (\delta^{18}O_{sub})\right) \quad [7]$$

Here ϕ (~ 0.4) is the proportion of oxygen from sugars that exchanged with stem water during this process, Δ is the average fractionation of the oxygen that exchanged with stem water, and $\delta^{18}O_{sub}$ is the $\delta^{18}O$ of sugars which did not exchange

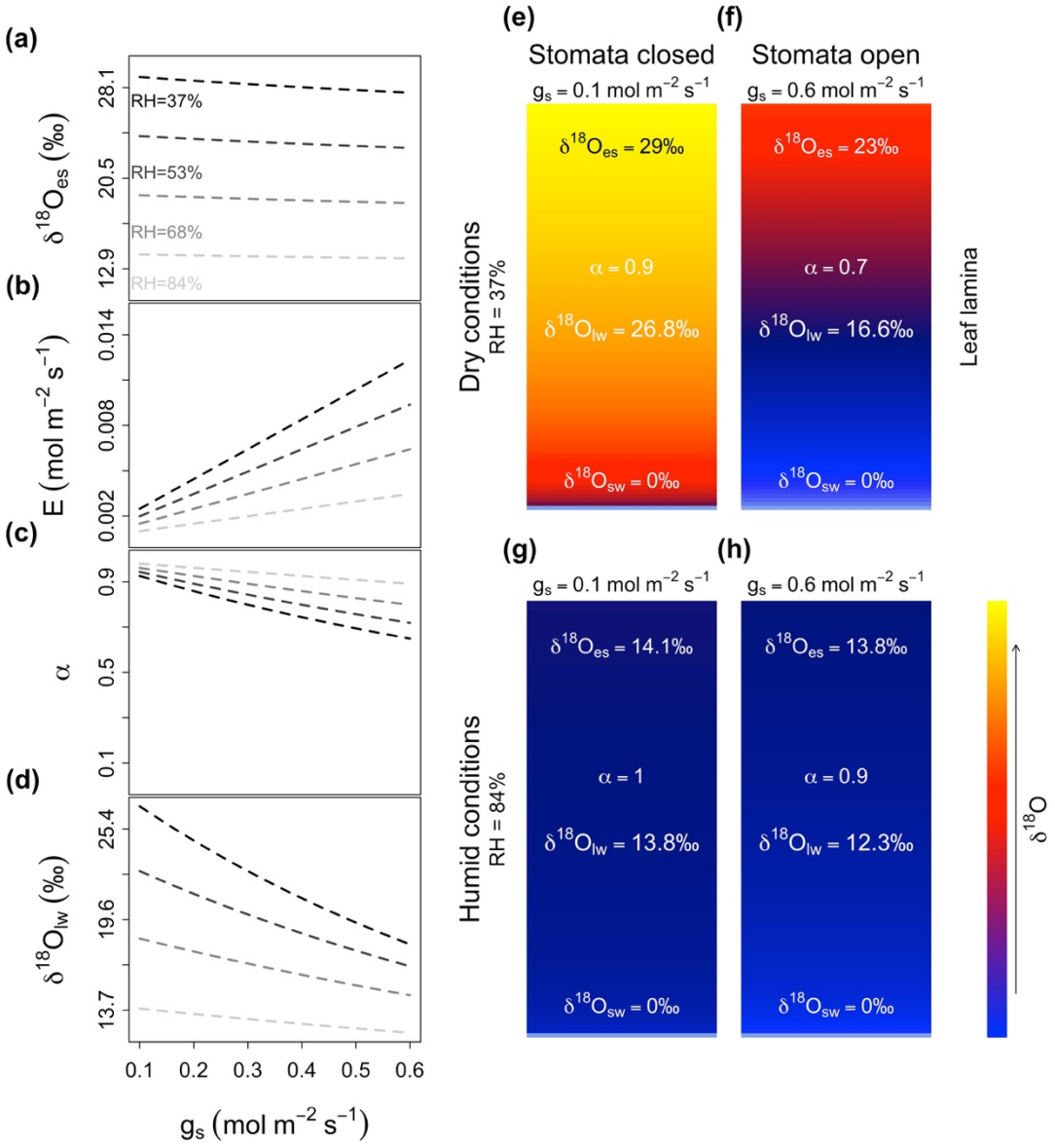

Figure 3.3. Predicted effects of stomatal conductance (g_s) on leaf water $\delta^{18}O$ at four different levels of relative humidity (RH). Modelled relationship between g_s and $\delta^{18}O$ of water at the sites of evaporation ($\delta^{18}O_{es}$) (panel a), g_s and leaf transpiration (E) (panel b), g_s and "mixture" of source water with water from the sites of evaporation (alpha=$\left(\frac{(1-e^{-\varphi})}{\varphi}\right)$, panel c), and g_s and mean leaf water $\delta^{18}O$ ($\delta^{18}O_{lw}$) (panel d). Panels e-h illustrate predicted $\delta^{18}O$ gradients between incoming leaf water ($\delta^{18}O_{sw}$) and $\delta^{18}O$ at sites of evaporation ($\delta^{18}O_{es}$) for low relative humidity (top panels, e,f) and high relative humidity (lower panels) and for low (left panels) and high stomatal conductance (right panels).

with water during cellulose synthesis. Therefore, ϕ tends to reinforce the source water $\delta^{18}O$ signal in tree ring cellulose, without completely erasing the leaf water enrichment signal. Experiments have shown that approximately 40% of the sugars exchanges oxygen with stem water before incorporation into cellulose, with variations between different tree species (DeNiro and Cooper, 1989; Luo and Sternberg, 1992; Cernusak et al., 2005; Sternberg et al., 2006). In summary, three processes control $\delta^{18}O_{TR}$: (i) source water $\delta^{18}O$, (ii) enrichment of source water in the leaf during evaporation, which depends on VPD and leaf transpiration rates (see Figure 3.3), and (iii) the degree of exchange of oxygen in exported sugars with stem water during cellulose synthesis. The degree of leaf enrichment increases linearly with increasing VPD, but also depends on transpiration rate (due back-diffusion), and is thus related to g_{sW} and VPD. The sensitivity of leaf enrichment to g_{sW} is predicted to be highest under high VPD or low relative humidity (see Figure 3.3).

We thus expect that intra-annual variation of $\delta^{18}O_{TR}$ will be primarily influenced by the seasonal cycle of source water or precipitation $\delta^{18}O$, which varies quite strongly over trees' growing season (Figure 3.2e,k,q,w). Leaf level enrichment processes will add to this 'background' variation by causing enrichment which is expected to be greater under higher VPD and expected to be more strongly modulated by g_{sW} under drier conditions (see Figure 3.3).

3.3. Methods

3.3.1. $\delta^{18}O_{TR}$ and $\delta^{13}C_{TR}$ predictions

To make our expectations more quantitative we have used the tree ring-isotope models described in section *Isotopes in tree rings: theory and modelling* to predict the sensitivity of intra-annual variation in both isotopes to weather conditions during the tree's growing seasons. Climatic variables that influence these predictions were VPD, temperature, and source water $\delta^{18}O$. Our predictions also depend on estimated responses to g_s and g_m to the climatic variables. For both isotopes, stomatal conductance to water and CO_2 were calculated as a function of VPD via

$g_{sW} = 1.6g_{sC} = g_{sMax}\left(\frac{1}{1+\left(\frac{VPD}{VPD_{mean}}\right)}\right)$. Here g_{sMax} (0.5 mol m^2 s^{-1}) is an assumed value for maximum g_{sW} and VPD_{mean} is the long-term mean of VPD during the growing season of each tree. For $\delta^{13}C_{TR}$, g_m was estimated as a linear function of temperature via $g_m = g_{m25}(0.44 + 0.058T)$ (Evans and von Caemmerer, 2013), where g_{m25} is the g_m at 25°C and T is temperature in Celsius. As g_m is highly variable between species (von Cammerer and Evans, 2015) and we have no information about g_m for neither of the species in this study, we considered an assumed of g_{m25} = 0.19 mol m^2 s^{-1} for both species. For $\delta^{13}C_{TR}$ predictions, we ignored carbon remobilization, as we lacked sufficient insight to quantify these processes. We also did not consider any seasonal variations in the growth rates of the trees, as we lack information on growth rhythm during the growing season for the two tree species at the study sites. Further details of the models and parameters used for predictions of $\delta^{18}O_{TR}$ and $\delta^{13}C_{TR}$ can be found in Table I.2 in Appendix I.

3.3.2. Sites and species selection

Terra firme sites and species

Two terra firme sites (i.e, non-flooded) differing in total annual rainfall were selected for this study (Figure 3.2a); a wet site in the Peruvian Amazon with total annual precipitation of 2500 mm (-4° 54' 00'' N, -73° 47' 59.62''E), and a moist site in the Bolivian Amazon with 1700mm annual precipitation (-10° 59' 60''N, -65° 00' 00''E). Precipitation in the moist site is highly seasonal, dropping below 100 mm $month^{-1}$ for up to 5 months per year, while mean monthly precipitation in the wet terra firme site rarely drops below 100 mm.

The species we choose for terra firme forests, *Cedrela odorata,* grows during the wet season and stops growing at the onset of the dry season, when it sheds its leaves (Dünisch et al., 2003; Costa et al., 2013). New leaf flush occurs several weeks later at the end of the dry season (Dünisch et al., 2003; Brienen and Zuidema, 2005). Previous studies on *Cedrela odorata* from the south west of the Amazon basin have shown

that $\delta^{18}O_{TR}$ reflects rainout processes up-wind of the growth site, and thus are a good proxy for basin-wide rainfall in the Amazon (Brienen et al., 2012; Baker et al., 2016).

Seasonal floodplain sites and species

Várzea forests are one of the most representative seasonal floodplain forests supporting annual flooding of up to 7m (Wittmann et al., 2012). Two várzea floodplain sites were selected, a 'wet floodplain site' in the Colombian Amazon receiving 2600 mm of annual precipitation (-4° 30' 00''N, -70° 00' 00''E), and a 'moist site' in the Bolivian Amazon receiving 1700 mm of annual rainfall (-11° 33' 30''N, -67° 18' 54''E).

Macrolobium acaciifolium, the species chosen for this environment renews its canopy during the flooded period, which lasts for approximately 6 months, after which growth restarts, often when trees are still flooded (Schöngart et al., 2002). Growth rates are highest in the beginning of the terrestrial phase just after the flooding recedes and stops once the trees get flooded due to anoxic conditions around the roots (Schöngart et al., 2005). The terrestrial phase starts at the peak of the dry season in the wet floodplain site and during wet-dry season transition at the moist floodplain site. This species forms annual rings which follow the annual cycle of the flood-pulse of the rivers (Schöngart et al., 2005, Assahira et al., 2017).

3.3.3. Tree ring sampling and Isotopes analysis

For each *C. odorata* tree we cut a disc, and 10mm cores were extracted from *M. acaciifolium* trees. One of the selected *C. odorata* trees is part of a published oxygen isotopes chronology which has been validated by radiocarbon dating (Baker et al., 2017).Tree rings were microscopically identified by wood anatomical features. For two samples of each species (one sample per site, see Figure 3.2), 9-11 rings were cut into thin segments of 0.02 – 3mm for the intra-annual high resolution analysis. Very thin segments of 0.02 mm were cut using a core microtome (Gärtner and Nievergelt, 2010). On average, rings were separated into 10 to 22 sections parallel to ring boundaries, although for a few very narrow rings only five sections could be cut. For

Macrolobium acaciifolium, six additional samples were cut into three even-sized segments for the intra-annual medium resolution analysis. This was done to assess the representativeness of the floodplain trees for the general patterns in these environments. Three of these six additional samples are from the moist floodplain site and the other three are from a wet floodplain site located 500km upstream of the wet floodplain site shown in Figure 3.2.

Cellulose was extracted from the wood using the Brendell et al. (2000) method, except for *C. odorata* from moist terra firme site where cellulose was extracted following Wieloch et al. (2011). Only the carbon isotope series from the west Amazonian floodplain was based on whole-wood. Samples were freeze-dried and weighed in precision balance to pack 0.5±0.05mg of samples in silver capsules for $\delta^{18}O$ analysis and 1±0.1mg tin capsules for $\delta^{13}C$ analysis. Isotope analysis was done at the University of Leicester using an Isotopes Mass Spectrometer (Sercon 20-20 IRMS) with precision of 0.15‰.

3.3.4. Climate data

Local monthly precipitation, vapour pressure, temperature and cloud cover data for all sites were obtained from Climate Research Unit (CRU TS 4.00 0.5° resolution). Daily river stage data from the sites in Colombia and Bolivia were obtained from the nearest river gauging stations through the Hidroweb portal (http://www.snirh.gov.br/hidroweb/) from the Brazilian National System of Hydric Resources Information (SNIRH). As there were no local station data available for the site in Peru, we used instead monthly river data from the virtual river gauging station data from ORE-HYBAM.

The $\delta^{18}O$-data for precipitation were obtained from the Global Network of Isotopes in Precipitation and in the Global Network of Isotopes in River (GNIP and GNIR), accessed through the Water Isotopes System for Data Analysis, Visualization and Electronic Review (WISER, http://nds121.iaea.org/wiser/index.php). For the Bolivia

site, we complemented this with monthly precipitation $\delta^{18}O$ data (Gloor and Brienen, unpublished data).

Seasonal changes in climate were calculated for the same calendar years of the analyzed tree rings at each site. Figure 3.2 shows the seasonal changes in monthly precipitation, inundation (floodplain sites only), VPD, cloud cover and rainfall $\delta^{18}O$ for all studied sites.

3.3.5. Data analysis

For each site, seasonal changes in intra-ring $\delta^{18}O_{TR}$ and $\delta^{13}C_{TR}$ were predicted using the available climatic data (see *Climate data*) from the site-specific growing seasons. Site-specific growing seasons were defined for each tree using the available information on growth rhythms for the *M. acaciifolium* (Schöngart et al., 2002) and *C. odorata* (Dünisch et al., 2003; Costa et al., 2013). These vary considerably between the terra firme (wet site: September-June; moist site: October-April) and floodplain sites (wet site: May-November; moist site: April-October). The model inputs used for the tree-ring isotopes predictions are presented in Table I.2 in Appendix I.

Co-variation between observed isotope records was assessed using Pearson correlation coefficient. To assess the effect of inter-annual variation in climate on tree ring isotopes, we calculated mean isotope values for the complete ring. We then related the inter-annual variation in $\delta^{13}C$ and $\delta^{18}O$ for the full ring to local temperature, rainfall and cloud cover during the entire growing season of the trees. We did not consider VPD for these analyses, as the available data may not be accurate enough at the inter-annual level. In addition to local climate variables, we also considered Amazon basin-wide precipitation, which has been shown to influence local precipitation $\delta^{18}O$ (Baker et al., 2016). Amazon basin-wide precipitation was calculated as the spatially integrated mean precipitation for the hydrological basin (see Baker et al. 2016). These analyses were done for the 4 trees with high intra-annual resolution.

In order to further explore the effects of seasonal climate variation on tree ring isotopic composition, we also calculated the dry season length and climate means over moving periods of 2 to 8 months across the trees' growing seasons. Dry season length was defined as in Marengo et al. (2001) and calculated using daily rainfall data from Tropical Rainfall Measuring Mission (TRMM 3B42 0.25 ^{o} resolution). These climate means were correlated with mean isotope values for the whole ring and with the mean isotope values for 3 intra-ring segments. For these analyses, the six *M. acaciifolium* oxygen series with medium intra-ring resolution were also included.

All analyses were done using the data analysis tool R, version 3.2.3.

3.4. Results

Predicted $\delta^{13}C_{TR}$ and $\delta^{18}O_{TR}$ patterns for each site showed different contributions from seasonal changes in $\delta^{18}O_{sw}$, VPD and temperature, and from estimated responses of g_{sW} and g_m. For $\delta^{18}O_{TR}$ most of the predicted variation comes from $\delta^{18}O_{sw}$, but leaf water enrichment caused by changes in VPD and g_{sW} responses also contribute significantly to predicted $\delta^{18}O_{TR}$ for the two trees growing at the drier sites (i.e., the moist floodplain and moist terra firme site, see Figure 3.2f,l,r,x and Figure I.2 in Appendix I). Using two different assumptions for effective pathlength (L) we also note that pathlength significantly affects the Péclet effect, especially under low relative humidity (see Figure I.3 in Appendix I, see also Holloway-Phillips et al. 2016, Kahmen et al. 2008). For our predictions however, we did not vary pathlength, as we had no species specific data on path lengths and predicted contributions of leaf water enrichment to $\delta^{18}O_{TR}$ thus reflects only site differences in VPD and g_{sW} (not pathlength difference).

For $\delta^{13}C_{TR}$, g_{sC} responses to VPD contributed to most of the predicted $\delta^{13}C_{TR}$ variations in all trees, except for the *C. odorata* from the wet terra firme site, which showed weak $\delta^{13}C_{TR}$ variations (Figure 3.2g,m,s,y). Temperature effects over g_m also contributed significantly to the predicted $\delta^{13}C_{TR}$ patterns for *M. acaciifolium* from the

moist floodplain site – where seasonal temperature variations were biggest – but showed little contribution for the other trees (Figure I.4 in Appendix I).

Table 3.1. Summary the general isotopes sampling and isotopic patterns within rings for each tree from floodplains (FP) and terra firme (TF) sites.

	Macrolobium acaciifolium		*Cedrela odorata*	
	Moist FP	Wet FP	Moist TF	Wet TF
$\delta^{18}O_{TR}$				
total number of samples	129	196	128	90
number of rings	11	9	11	9
avg samples per ring	12	22	12	10
Mean observed variation within rings variation (max – min, ‰)	4.33±1.63	5.24±1.46	4.61±1.42	4.33±1.75
Mean predicted variation within rings (max – min, ‰)	10.6	8.45	11.9	4.94
avg correlation between within-ring patterns	0.52	0.31	0.32	0.22
$\delta^{13}C_{TR}$				
total number of samples	129	228	129	90
number of rings	11	10	11	9
avg samples per ring	12	23	12	10
Mean observed variation within rings (max – min, ‰)	1.86±0.9	1.84±0.56	1.41±0.61	1.27±0.28
Mean predicted variation within rings (max – min, ‰)	1.2	0.85	1.65	0.35
avg correlation between within-ring patterns	0.33	0.64	0.23	0.07
$\delta^{18}O$~$\delta^{13}C$ correlations				
Avg. corr. Coef.	0.73	0.38	0.22	0.03
Number of correlated patterns within different rings	7	5	2	1

Observed within-ring $\delta^{18}O_{TR}$ variation matches the predicted patterns very well in all four trees with high intra-ring resolution (Figure 3.4 – blue lines), although the within-ring amplitude was about two times lower for the observed patterns (4-5‰) compared to predictions (~10‰, see Table 1). The observed $\delta^{13}C_{TR}$ patterns matches predictions quite well in the two *C. odorata* trees from the terra firme sites and for the *M. acaciifolium* tree from the moist floodplain site (Figure 3.4b,c and right panels – red lines), but less well for the *M. acaciifolium* tree from the wet floodplain sites (Figure 3.4a,d and right panels –red lines). The observed average amplitude for $\delta^{13}C_{TR}$ is similar to predictions (~ 1 ‰). $\delta^{13}C_{TR}$ in the initial section of individual rings was frequently higher than predicted in the *M. acaciifolium* from the wet floodplain and in some years for the *C. odorata* from moist terra firme, both of which show pronounced $\delta^{13}C_{TR}$ increases of up to 2‰ across ring boundaries (Figure 3.4b,c – red lines).

Comparison of $\delta^{13}C_{TR}$ and $\delta^{18}O_{TR}$ time series showed strong common features for some trees but less so for others. Within-ring $\delta^{13}C$ and $\delta^{18}O$ cycles in the floodplain trees were correlated in several years, especially at the moist site (Figure 3.4a, Table 1). In contrast, the terra firme trees only showed significant correlations between $\delta^{18}O_{TR}$ and $\delta^{13}C_{TR}$ in those rings with exceptionally large within-ring variations (Figure 3.4c and Table 1).

We also note that the $\delta^{18}O$ time series of the two terra firme trees showed very similar patterns both on short and longer time scales (Figure I.5 in Appendix I).

The regression analysis between climate variables and the tree-ring isotopes series revealed various significant correlations. For the two moist sites (terra firme and floodplain), we found that mean inter-annual ring $\delta^{13}C$ was negatively correlated with local precipitation during the driest period of their growing seasons (Figure 3.5). No climatic effects on tree ring $\delta^{13}C$ were found for the trees from the wet sites. Inter-annual mean ring $\delta^{18}O$ variation of the two *M. acaciifolium* trees from the floodplain sites was positively correlated with cloud cover during the growing season ($p<0.1$),

while $\delta^{18}O$ of the *C. odorata* trees from the terra firme sites was negatively correlated with Amazon wide precipitation amounts (Figure 3.5).

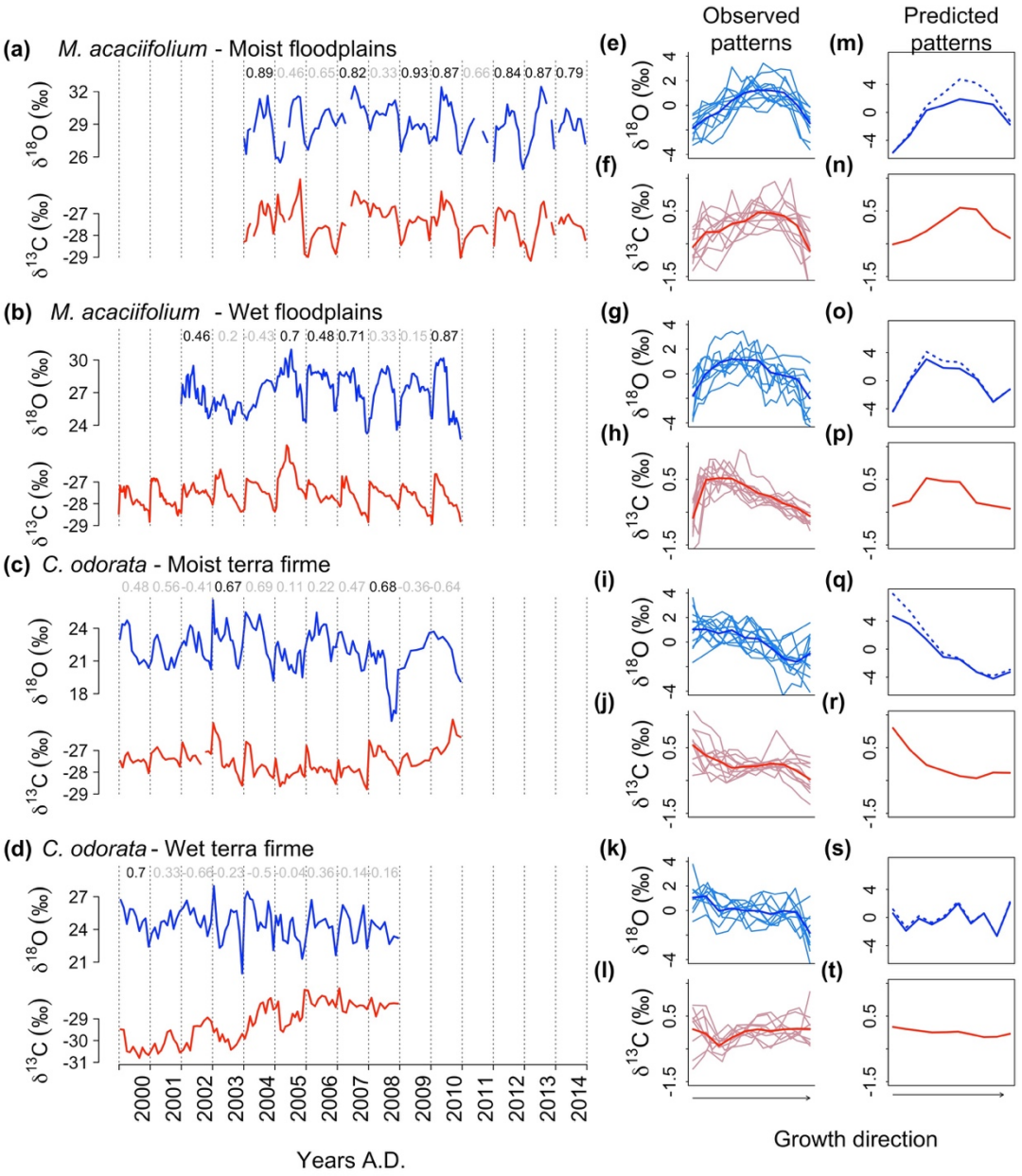

Figure 3.4. Observed high resolution series of $\delta^{18}O_{TR}$ (blue lines) and $\delta^{13}C_{TR}$ (red lines) (left panels), and observed (middle panels) and predicted (right panels) intra-annual cycles for the four study trees. The values at the top of the left side panels indicate the correlation coefficients between the $\delta^{18}O$ and $\delta^{13}C$ variations within each ring, with significant values in black. The solid blue and red lines in middle panels are the mean intra-annual cycles over all rings. Solid blue line in right panels represent the effects of only source water $\delta^{18}O$ and stippled blue line indicates the added effects of leaf water enrichment. Note that the scale of the tree-ring $\delta^{18}O$ predictions is larger than that for the observations (see the Discussion section for details). $\delta^{18}O$ and $\delta^{13}C$ values are from α-cellulose, except for the $\delta^{13}C$ series from Wet FP, which is from wholewood.

Additional significant correlations with climate variables were found for specific ring segments and for shorter periods of 4-8 months within the growing season, showing the same overall pattern described above. Here we show correlations for sequentially moving windows of 4 and 6 months duration, as these summarize the patterns observed for both longer and shorter time spans (see Figure I.6 in Appendix I). These analyses included 3 additional *M. acaciifolium* trees per site (Figure I.7 in Appendix I). For the *M. acaciifolium* trees from the wet floodplain site, average tree ring $\delta^{18}O$ was also higher when the dry season started earlier (corr. Coef=0.59, $P<0.05$) or was longer (corr. Coef=0.64, $P<0.05$). Finally, for all trees the isotopic composition of specific ring segments showed generally correlations with more climate variables compared to mean ring isotopic time-series.

3.5. Discussion

3.5.1. High-resolution intra-ring variation in $\delta^{13}C$ and $\delta^{18}O$.

Our results show that the observed intra-annual $\delta^{13}C_{TR}$ patterns agree reasonably well with the predicted $\delta^{13}C_{TR}$ patterns, and that $\delta^{13}C_{TR}$ variations thus follow seasonal variation in vapour pressure deficit (since our model does not include NSC reserve remobilization). For the floodplain species *M. acaciifolium*, within-ring variation in $\delta^{13}C_{TR}$ shows strong positive peaks in $\delta^{13}C_{TR}$ in the initial or middle sections of the ring. These $\delta^{13}C_{TR}$ peaks coincide with the drier conditions at the initial and middle periods of the growing season at the wet and moist site, respectively. In the moist terra firme tree, we find decreases in $\delta^{13}C_{TR}$ from the initial to the final sections of the ring, which is consistent with steadily decreasing water stress as the rainy season progresses. As predicted, we find a rather constant mean $\delta^{13}C_{TR}$ at the wet terra firme site due to generally humid conditions throughout the growing season of this tree (Figure 3.4). Thus, observed $\delta^{13}C_{TR}$ patterns are largely consistent with expected plant stomatal responses to changes in VPD during the growing season of each tree. Our model also included temperature effect on g_m. This effect slightly improved the match between predicted and observed $\delta^{13}C_{TR}$ patterns for the *M. acaciifolium* trees from the moist floodplain site (Figure 3.4 and Figure I.4 in Appendix

I). For this tree, we also noted that seasonal temperature variations predict relatively large variation in $\delta^{13}C_{TR}$ due to mesophyll conductance without requiring any change in g_{sC} (see Figure I.4e in Appendix I). While this effect is only predicted in one tree, it shows that the temperature effects on g_m could significantly influence seasonal variations in $\delta^{13}C_{TR}$ and may be more important to C-isotope discrimination than generally assumed (Griffiths and Helliker, 2013; von Caemmerer and Evans, 2015).

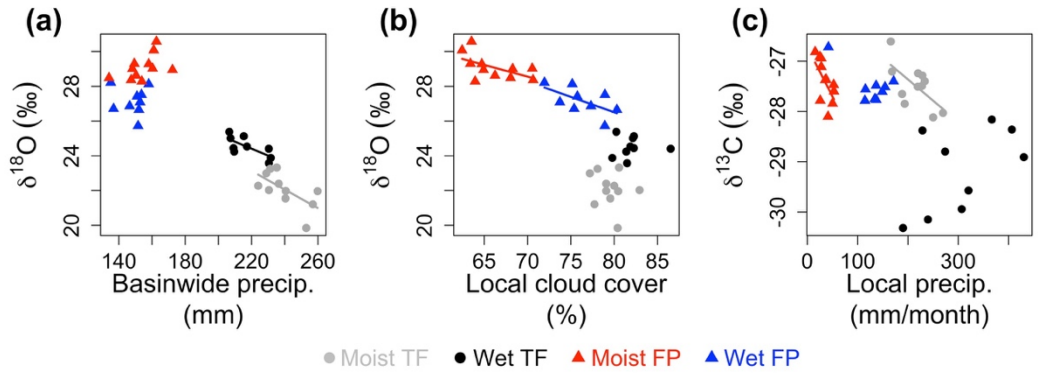

Figure 3.5. Summary of the climate effects on inter-annual variation in $\delta^{18}O_{TR}$ and $\delta^{13}C_{TR}$. Relation between $\delta^{18}O_{TR}$ and basin-wide precipitation (panel a), $\delta^{18}O_{TR}$ and local cloud cover (panel b) and $\delta^{13}C_{TR}$ and local precipitation (panel c). Mean climate variables were calculated over trees' respective growing seasons (see methods). Regression lines show significant ($p< 0.05$) relationships between isotopes and climate. $\delta^{18}O$ and $\delta^{13}C$ values are from α-cellulose, except for the $\delta^{13}C$ series from Wet FP, which is from wholewood.

In addition to climate effects, we expected to observe effects of NSC remobilization on intra-annual $\delta^{13}C_{TR}$. Both investigated species completely change their leaves annually and remain leafless for several weeks (*C. odorata*) or some days (*M. acaciifolium*) (Schöngart et al., 2002; Dünisch et al., 2003). We thus expected sharp increases in $\delta^{13}C_{TR}$ values at tree ring boundaries in the records of all trees, related to starch dependent stem growth before initial leaf flush. We only observe clear sharp increases in $\delta^{13}C_{TR}$ for *M. acaciifolium* from the wet floodplain site (Figure 3.4b). As these sharp increases occurred exactly across the ring boundaries, and as peak $\delta^{13}C_{TR}$ due to climate was predicted to occur later in the season (see Figure 3.4p), we suspect these patterns may be due to use of NSC at the start of the growing season. We also find smaller peaks early in the rings of *C. odorata* from the moist site. *C. odorata* is indeed known to use starch from the previous year for stem growth at the

beginning of the growing season (Dünisch and Puls, 2003). Thus, the data provide some evidence for carbon r80emobilization effects, but these effects are not consistent between the two trees of each species and seemingly unrelated to deciduousness. Other studies in the tropics similarly show that the effect is not always evident in deciduous species (Poussart et al., 2004; Ohashi et al., 2009; Fichtler et al., 2010) and can also be seen in evergreen trees (Schleser et al., 2015). More work is needed to understand C-remobilisation effects on tree ring $\delta^{13}C_{TR}$.

Observed intra-annual $\delta^{18}O_{TR}$ patterns match very well our predictions for all four trees. They follow the changes in precipitation $\delta^{18}O$ and predictions for leaf water enrichment over the respective growing season for each tree (Figure I.2 in Appendix I). The observed amplitude however is much lower (4-5‰) than that predicted by the two combined effects (10-15‰). It is also lower than the single effect of precipitation $\delta^{18}O$, but matches the amplitude arising from leaf water enrichment (Figure I.2 in Appendix I). For the source water contribution, one would indeed expect a somewhat lower amplitude in $\delta^{18}O_{TR}$ compared to rainfall $\delta^{18}O$, as plants use soil water which is expected to show less seasonal variation. This is because water from successive precipitation events mix in a larger reservoir in the soil (Brooks et al., 2010; Evaristo et al., 2015), and this effect is not included in our predictions. $\delta^{18}O_{TR}$ results alone can thus not discern between leaf level processes and source water influences. Further analysis of the climate signals and covariation between $\delta^{18}O_{TR}$ and $\delta^{13}C_{TR}$ in the next sections provide more insights about the dominant drivers of $\delta^{18}O_{TR}$ for each of the studied trees.

3.5.2. Relations between inter-annual variation in tree ring isotopes and climate

$\delta^{13}C_{TR}$ in three trees reflected local precipitation during the driest part of the growing season (Figure I.6 in Appendix I). This is consistent with known effects of water availability on leaf ^{13}C-isotope discrimination as trees close their stomata to prevent water loss when soil moisture and relative humidity are low (Farquhar and Sharkey, 1982). It is also consistent with observations of negative correlations between $\delta^{13}C$

and precipitation for tropical trees growing at relatively dry sites (e.g. Gebrekirstos et al., 2009, Fichtler et al., 2010, Brienen et al., 2012). The only tree for which we do not find a relationship with precipitation in the expected direction is the *C. odorata* tree growing at the wet terra firme site. This is probably because the site is so wet (precipitation rarely drops below 100mm per month). We have no explanation for the observed positive correlation between precipitation and $\delta^{13}C$ in this tree.

The relations between climate variables and tree ring oxygen isotopes suggests that different dominant drivers control inter-annual variation in $\delta^{18}O$ in the two species; in the *M. acaciifolium* floodplain trees $\delta^{18}O$ covaries with temperature, cloud cover, local precipitation and dry season length, while for the two *C. odorata* terra firme trees $\delta^{18}O$ covaries with basin-wide precipitation amount (Figure 3.5, Figure I.6 in Appendix I). Temperature, cloud cover and precipitation may reach increasingly stressful levels when the dry season is longer, and probably affect $\delta^{18}O$ in floodplain trees primarily via their effects on evaporative leaf water enrichment above source water $\delta^{18}O$. Leaf water enrichment depends on water vapour pressure of the atmosphere, air temperature, isotopic composition of atmospheric water, leaf temperature, and stomatal conductance (Barbour et al., 2000; Barbour, 2007; Kahmen et al., 2008; see Figure 3.1). Surprisingly, tree ring $\delta^{18}O$ for both floodplain trees correlates most strongly with cloud cover, and this pattern is still consistent in the analysis including the six trees with medium intra-ring resolution oxygen series (Figure I.6 in Appendix I). This may be because reduced cloud cover during the dry season may lead to higher leaf temperatures (Doughty and Goulden, 2009), lower air humidity (Quaas, 2012), and thus raised leaf-to-air vapour pressure difference (VPD) and consequently, reductions in stomatal conductance (Lloyd and Farquhar, 2008). Overall, these results are consistent with theory and experimental studies of the effects of local moisture conditions over leaf water enrichment and $\delta^{18}O_{TR}$ variations (Barbour et al., 2000; Barbour and Farquhar, 2000; Barbour, 2007; Cernusak et al., 2016).

For the terra firme trees which grow during the wet season, tree ring $\delta^{18}O$ is mainly influenced by Amazon basin-wide precipitation (Figure 3.5), and less by local climate (Figure I.6 in Appendix I). This suggests that the tree ring $\delta^{18}O_{TR}$ signal is a precipitation $\delta^{18}O_{TR}$ signal. Precipitation $\delta^{18}O_{TR}$ in turn is the result of the cumulative effects of all precipitation events upwind from the sites. This is because heavy water isotopes are gradually removed at each precipitation event during moisture transport from the tropical Atlantic to the study sites, precipitation will be more depleted in $\delta^{18}O$ during years with more rain over the Amazon assuming incoming $\delta^{18}O_{TR}$ does not vary from year to year (Salati and Vose, 1984; Vimeux et al., 2005; Villacís et al., 2008). These results are consistent with the known precipitation $\delta^{18}O$ influence on $\delta^{18}O_{TR}$ in *C. odorata* tree rings (Brienen et al., 2012; Baker et al., 2015; Baker et al., 2016). In line with this is the coherence in $\delta^{18}O_{TR}$ patterns within rings (intra-annually) observed for the two terra firme sites, *C. odorata trees* from Bolivia and Peru, which are ~1000 km apart (Figure I.5 in Appendix I). These results demonstrate that source water is the dominant influence on tree ring $\delta^{18}O$ for these *C. odorata* trees. We note however that $\delta^{18}O$ for *C. odorata* tree at the moist site showed some (weak) correlations with local precipitation during the start of the growing season (Figure I.6 in Appendix I), consistent with weak local effects observed in longer tree ring $\delta^{18}O_{TR}$ series from the same site in Bolivia (Brienen et al., 2012). Also consistent with this is predicted contribution of leaf enrichment to $\delta^{18}O_{TR}$ in initial ring sections of this tree, caused by relatively dry conditions during the start of the growing season (Figure 3.4q). In all, for these *C. odorata* trees, source water is the dominant signal, with possible weak influences of local precipitation at the start of the growing season for the moist trees. Although we do not have replications for these trees, these results are consistent with previous studies which show that mean interannual tree-ring $\delta^{18}O$ variations of *C. odorata* trees from different sites (including our same Moist Terra Firme site) are driven by source water $\delta^{18}O$ (Brienen et al., 2012; Baker et al., 2015; Baker et al., 2016).

3.5.3. Dual-isotope analysis

A striking property of the isotope records is the strong intra- and inter-annual co-variation between carbon and oxygen isotopes in the floodplain *M. acaciifolium* trees (See Figure 3.4, Table 3.1 and Figure I.8 in Appendix I). This covariation is particularly strong for the *M. acaciifolium* tree from the moist floodplain site with highly similar features in the intra-annual patterns (Figure 3.4a), and also good correlations between mean annual $\delta^{13}C_{TR}$ and $\delta^{18}O_{TR}$ (Figure I.8 in Appendix I). Such strongly co-varying patterns suggest a common driver. The one common process for $\delta^{13}C_{TR}$ and $\delta^{18}O_{TR}$ is the response of stomatal conductance to water status of the soil plant continuum and vapour pressure deficit. These results thus strongly support the climate-$\delta^{18}O_{TR}$ analysis for this species which suggests that variation in $\delta^{18}O_{TR}$ is primarily controlled by leaf ^{18}O enrichment, and that the initial source water signal is dampened in the final tree ring $\delta^{18}O$ signal.

In contrast, in the two terra firme trees, the $\delta^{18}O_{TR}$ and $\delta^{13}C_{TR}$ records of each tree are generally uncorrelated (Figure 3.4c,d), indicating that they are not both primarily influenced by stomatal conductance effects on leaf ^{13}C-discrimination and/or on leaf ^{18}O enrichment. This decoupling of variation in $\delta^{13}C_{TR}$ and $\delta^{18}O_{TR}$ in this species could be due to a lack of control of stomatal conductance on $\delta^{13}C_{TR}$, $\delta^{18}O_{TR}$ or both. As we observe a weak negative relation between $\delta^{13}C_{TR}$ and precipitation only at the moist site and an opposite relation at the wet site, control of stomatal conductance on leaf ^{13}C-discrimination seems to be weaker in *C. odorata*. While this is one possible explanation, a more plausible reason for the lack of covariation between $\delta^{18}O_{TR}$ and $\delta^{13}C_{TR}$ is that $\delta^{18}O_{TR}$ in this species mainly records variation in source water $\delta^{18}O$ and only weak local climate effects, as we showed here (Figure I.6a in Appendix I) and also in Brienen et al. (2012). This lack of ^{18}O leaf enrichment signals in $\delta^{18}O_{TR}$ for *C. odorata* may be due to either low levels of leaf enrichment above the source water in the leaf, or because any occurring leaf isotope enrichment is not transferred to the final tree ring $\delta^{18}O$ in this species because of extensive exchange of leaf exported sugar with stem water during cellulose synthesis

(Sternberg, 2008). The former explanation, a lack of leaf enrichment, could be due to species-specific leaf traits, such as higher leaf transpiration rates and/or longer effective path lengths reducing strongly the effect of back diffusion on average leaf $\delta^{18}O$ (Kahmen et al., 2008; Cernusak and Kahmen, 2013; see also Figure I.3 in Appendix I).

Apart from purely species-specific effects, differences in the leaf enrichment contributions to $\delta^{18}O_{TR}$ for the four trees could also be influenced by variation in trees' growing season humidity. Predictions from isotope theory, confirmed by lab experiments (Roden and Ehleringer, 1999; Roden and Farquhar, 2012), are that leaf water enrichment above the plant source water is small for trees growing in humid conditions, and increases with increasing VPD (Barbour et al., 2002; Barbour et al., 2004; Roden and Siegwolf, 2012). Interestingly, for each species, the tree growing at the drier sites (moist floodplain and moist terra firme) showed stronger correlations between intra-annual $\delta^{18}O_{TR}$ and $\delta^{13}C_{TR}$ variations than the tree growing at the wetter site (wet floodplain and wet terra firme). This provides some indication that growing season water availability/ relative humidity may control the strength of the covariation between both stable isotopes in tree rings of tropical trees. More research is needed to assess how environmental conditions, specifically relative humidity, affect the strength of source water vs. leaf enrichment signals in tree rings.

3.6. Conclusions

We investigated $\delta^{13}C$ and $\delta^{18}O$ in cellulose of two Amazon terra firme and two floodplain trees located along a precipitation gradient. We show here that intra-annual variation in isotopes ($\delta^{13}C_{TR}$ and $\delta^{18}O_{TR}$) in four Amazon trees growing in different environments follow predictions based on isotope theory. Observed intra-annual variation in $\delta^{13}C_{TR}$ agreed well with Farquhar's model of leaf level ^{13}C discrimination considering stomatal responses to seasonal variation in VPD and temperature effects on mesophyll conductance, and suggest a direct transfer of climate signals from leaf to tree ring. We do also find some signatures of post-photosynthetic carbon remobilisation effects on $\delta^{13}C_{TR}$ which are especially clear in

the wet floodplain tree and to a lesser degree in the moist terra firme tree. Intra-annual variation in $\delta^{18}O_{TR}$ closely matched seasonal variation in source water and the predicted effects of leaf water enrichment due to variation in VPD.

The inter-annual variation in $\delta^{13}C_{TR}$ was controlled by local precipitation for trees at the drier growing conditions, but not at the wettest site. Inter-annual variation in $\delta^{18}O_{TR}$ showed different controls in the two species; the floodplain species *M. acaciifolium* recorded variation in leaf water enrichment in response to local climate (cloud cover), while the terra firme species *C. odorata* recorded source water $\delta^{18}O$ variation, which is controlled by large-scale rainout signals (i.e., basin-wide precipitation).

The four trees showed differences in the degree of co-variation between $\delta^{13}C_{TR}$ and $\delta^{18}O_{TR}$ with the strongest covariation in the floodplain tree experiencing the driest growing conditions and lowest covariation for the wet terra firme tree. Higher covariation in the drier sites are most likely the result of stomatal responses to humidity affecting both isotopes in the same way. The four trees represent a continuum from entirely source water dominated $\delta^{18}O_{TR}$ signal (in the wettest site) to primarily leaf level process dominated $\delta^{18}O_{TR}$ signal (in the driest site). Our data cannot reveal whether variation in control of $\delta^{18}O_{TR}$ signals are caused by species-specific differences in physiology (*C. odorata* versus *M. acaciifolium*), or truly reflects a dominant influence of VPD gradients.

Our results provide some clear insights, but also raise new questions. Firstly, we showed that across the four trees, $\delta^{13}C_{TR}$ reflected primarily photosynthetic C-discrimination responses to humidity and temperature. We also found signatures of carbon remobilisation effects but surprisingly these were not linked to species phenology. More research under what circumstances carbon remobilization occurs and how it affects $\delta^{13}C_{TR}$ will help interpreting tree ring isotope signals. Secondly, our results suggest that $\delta^{18}O_{TR}$ can be controlled by very different processes, source water $\delta^{18}O$ variation vs. leaf water enrichment, but it remains unclear which process

dominates when and under what circumstances. Difference in the controls on $\delta^{18}O_{TR}$ have profound implications for the interpretation of $\delta^{18}O_{TR}$ in palaeo-climatic and plant physiological studies. For example, source water $\delta^{18}O$-signals may record large-scale rainout information over continents, (Brienen et al., 2012; Baker et al., 2016), or hurricane influences on coastal sites (Miller et al., 2006), while leaf water enrichment signals are expected to reflect climate variation of a much local nature via VPD (i.e., Kahmen et al., 2008).

Chapter 4 **Effects of hydroclimatic variability on ring-widths of *Macrolobium acaciifolium* floodplain trees from different regions within the Amazon Basin**

Abstract

The annual rise of the river levels in the Amazon Basin causes the flooding of up to 15% of the Amazon region for several months. During the aquatic phase, trees cease growth inducing the formation of annual growth rings in floodplain trees. Previous studies have shown that tree rings of floodplain trees from central Amazon are good proxies for past variability of river levels and length of terrestrial phase, which is related to the dry season over the catchment area of the rivers. To evaluate if the length of the terrestrial phase or other climate variables modulate the growth rate of *Macrolobium acaciifolium*, ring-width chronologies were built at three floodplain sites located in western, central and southwest Amazon. Tree rings were crossdated and their year of formation were verified using radiocarbon analysis. Bomb-peak radiocarbon dates of the tree rings matched closely the estimated dates obtained by cross dating the ring-width series. Ring-widths were strongly associated with the local river hydrology, with negative influences of river level and positive influences of the length of the terrestrial phase on tree growth. In addition, temperature also affected tree growth negatively at the site with the driest conditions during the growing season. Influences of river hydrology and climate were stronger for the two sites located in smaller river basins, where the terrestrial phase coincides with the dry season, at western and southwest Amazonia. These results reveal that despite the presence of false rings which require a laborious crossdating, tree-ring chronologies of *M. acaciifolium* are useful to improve our understanding of the past hydroclimatic variability during the dry season in the Amazon Basin.

4.1. Introduction

The analysis of tree rings is a useful tool to reconstruct past climate variability. Well-dated reconstructions of past environmental conditions require that trees form annual rings. In the past, tree ring analysis was mostly restricted to temperate zones, because it was thought that tropical climate is favourable for tree growth year-round and thus that tropical trees do not form annual rings (Worbes, 2002). During the last decades, studies in the tropics proved the annual formation of growth rings based on both dendrochronological methods and radiocarbon dating for over 200 tree species (Lisi et al., 2008; Brienen et al., 2016; Schöngart et al., 2017). However, not all of these species are useful for climate analysis, as the dendroclimatological approach also requires common growth variability within the population and a strong climate signal in the tree rings.

For most non-flooded tropical environments, the primary cause for the formation of tree rings in most tropical forests is rainfall seasonality (Worbes, 2002; Lisi et al., 2008). Wood production is mostly restricted to the wet season, as prolonged periods of water deficit may reduce or completely stops cambial activity (e.g. Lisi et al., 2008). Thus, tree ring width analysis in tropical regions has been particularly useful to reconstruct past wet season conditions, when most of tree growth occurs (Dünisch et al., 2003; Brienen and Zuidema, 2005; Locosselli et al., 2016; Lopez et al., 2017; Granato-Souza et al., 2018). However, trees may grow during the dry season in seasonally flooded areas, where cambium activity is downregulated by root anoxia during the aquatic phase (Worbes, 2002; Schöngart et al., 2002; Worbes, 2004). These differences in the period of cambium activity bring new possibilities to explore past climate variability during different seasons if seasonally flooded trees from floodplain forests are also probed.

Amazon floodplain forests occur along the banks of Amazonian rivers and are subject to annually recurring floods caused by the seasonal variation of river levels of Amazon rivers (Junk et al., 2014). As the flood duration period is the primary limiting factor for tree growth, pioneering dendro-chronological studies showed that growth of

Amazon floodplain trees is sensitive to the duration of the non-flooded period and may potentially be used to reconstruct past variations in river levels (Schöngart et al., 2004; Schöngart et al., 2005; Assahira et al., 2017; Batista and Schöngart, 2018). Thus, tree ring width of these trees can potentially be used to infer past dry season length in different sub-basins of the Amazon. Although the use of floodplain tree rings is not new, there are still very few published chronologies of Amazon floodplain trees, mostly with the species *Macrolobium acaciifolium*, and existing records are limited to the central region of the Amazon (Schöngart et al., 2004; Schöngart et al., 2005; Assahira et al., 2017; Batista and Schöngart, 2018). In different regions of the Amazon, climate conditions during the terrestrial phase may differ considerably from central Amazon floodplains, with some sites exhibiting a rather wet terrestrial phase, and others receiving very little rainfall amounts. The present study was designed to contrast different sub-basins of the Amazon where rainfall amounts during the terrestrial phase differ considerably, and provide a wider picture of what floodplain trees can tell about past hydroclimatic variability.

In order to know if the tree rings of *M. acaciifolium* record the length of the terrestrial dry phase and river levels across different areas in the Amazon, we developed three ring-width chronologies from three different sites in the Amazon. We used correlation analysis to test the possible effects of local dry season climate on the ring-with chronologies and to evaluate if ring-widths may reflect global sea surface temperatures which influence climate conditions in the Amazon Basin.

4.2. Methods

4.2.1. Study sites and species

Field work was carried out at three seasonal floodplain sites, selected to differ according to the geographic location of their respective drainage basins. The sites are located at a floodplain in the western end of the Amazon Basin, within the catchment of the Marañon River in Peru (74°05'30''W, 4°29'30''S); in the central Amazon within the catchment of the Negro River in Brazil (60°38'45''W, 2°40'10''S), and in southwest Amazon at the floodplains of the Sena River which are within the catchment of the

Madre-de-Dios River in Bolivia (67º20'36''W, 11º40'41''S). The site in southwest Amazon experiences the longest dry season with up to 6 months per year with less than 100mm rainfall, followed by the site in central Amazon with up to 3 months dry season per year, while rainfall at the site in western Amazon rarely drops below 100mm in any month. The river seasonality follows closely the rainfall seasonality at the western and southwest Amazon site, and lag the rainfall seasonality by 3 months in the site from central Amazon. See Chapter 2 (Figure 2.2 and Table 2.1) for a detailed description of the hydrological conditions at each site.

At each site, 40 to 50 *M. acaciifolium* trees with varying diameter were sampled and used to produce one ring-width chronology for each site (Figure 4.1). This species was chosen because it is widespread in Amazon floodplains (Schöngart et al., 2005; ter Steege et al., 2013). Data about *M. acaciifolium* trees growing in central Amazon floodplains indicate this species regularly renews its canopy during the flooded period (Schöngart et al., 2002) and forms very clear rings that have been shown to be annual using dendrochronological methods and radiocarbon dating (Schöngart et al., 2005; Assahira et al., 2017). In addition, ring-widths of *M. acaciifolium* trees from central Amazon are correlated with the duration of the non-flooded period, i.e. the period when the river levels are below the trees' topographic position (Schöngart et al., 2005; Assahira et al., 2017; Batista and Schöngart, 2018).

4.2.2. Development of the chronologies

From each sampled tree, two or three wood cores were taken using increment borers of 5.15mm and 10mm diameter. Samples were shipped to the Dendrochronology Laboratory at University of Leeds, where 100μm thin slices were cut from each core using a core microtome (Gärtner and Nievergelt, 2010). The thin slices were mounted in slides and digitalized as a film (e.g. positive film scanning) with an Epson Scanner V700 with resolution varying from 3200-3500 dpi (~50-20 kilopixel mm^2). The widths of the tree rings were then measured from the scans using the software ImageJ - ObjectJ plugin (version 1.03, Vischer and Nastase, 2017).

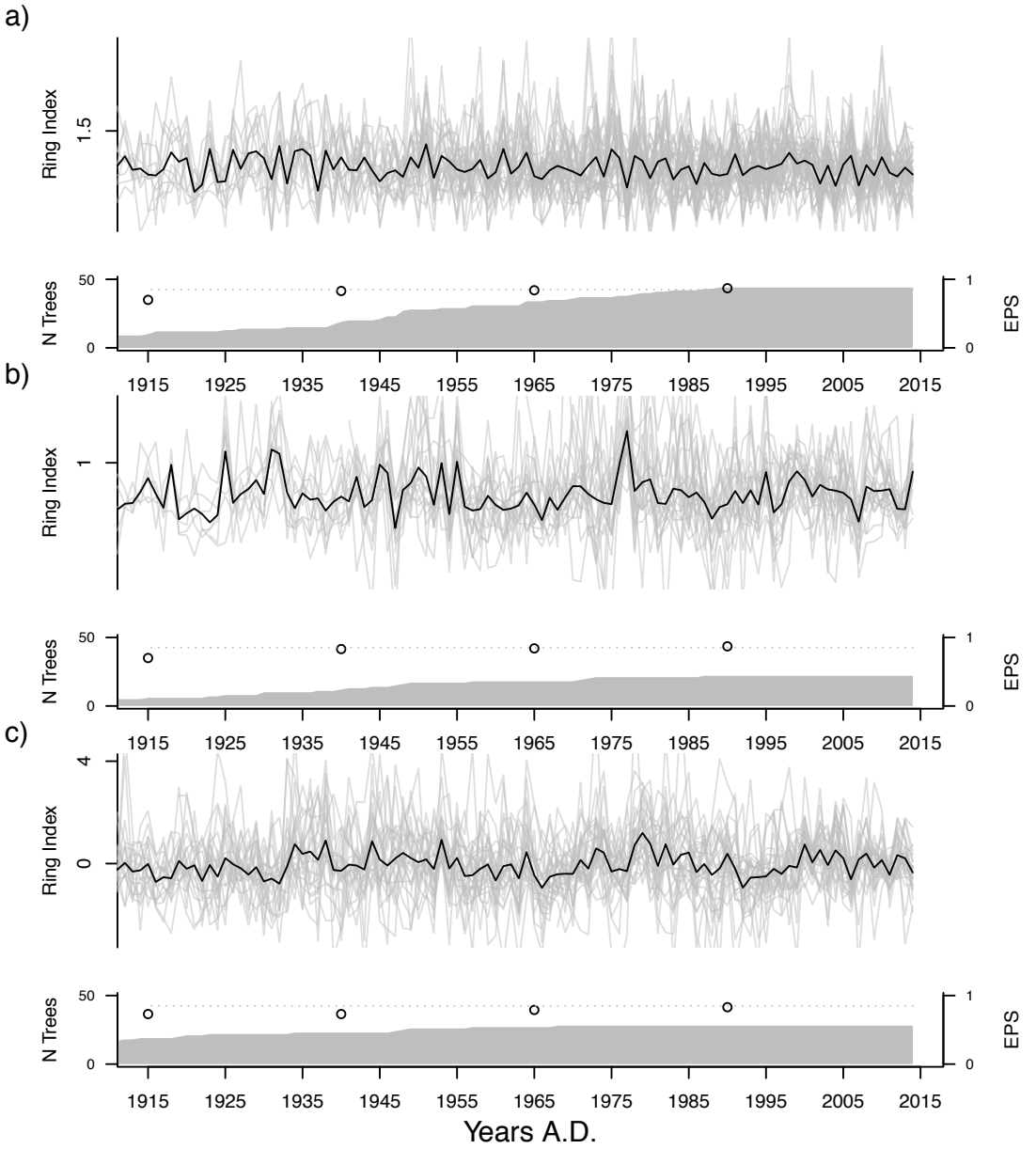

Figure 4.1. Ring-width chronologies produced for each site for the period from 1905 to 2015. Below each chronology the running EPS for 50yr overlapping segments and the number of trees included in different segments are shown. The horizontal dotted gray and black lines indicate the EPS value of 0.85. (a) western Amazon, (b) central Amazon and (c) southwest Amazon.

Wood anatomy and the ring-width measurements of the different cores from each tree were then visually compared from the scans to detect the presence of false rings in the samples. See Chapter 2 for details on the detection of false rings. The series obtained from the radii of each tree were then averaged to produce one mean ring-width series per tree. The mean ring-width series of each tree were dated from bark to pith assigning the sampling year to the outermost ring of the cores. The date of

each ring corresponds to the calendar year when the trees start growing (i.e. Schulman's convention). This is an important convention in cases when the growth season starts in one year and ends in the other year, which is the case for the trees from our site in central Amazon. To verify the dating of the chronologies, we also compared the radiocarbon bomb-peak dates of the wood in the tree rings of the years 1980, 1960 and 1957. This was done for three trees of each site – a total of 27 radiocarbon dates.

To produce the tree-ring chronologies, the ring-width series of each tree were processed to remove growth variations related to trees' ontogenetic development and canopy suppression/release (Brienen and Zuidema, 2006), and to retain only decadal scale climate variability. Each series was first individually standardized by fitting a smooth spline (Cook and Peters, 1981; Cook and Peters, 1997) and retaining the deviations from the curve fit (STN series). We find that for our dataset a relatively stiff spline with 50 percent frequency cutoff over a wave length of half the length of each series was adequate to remove the ontogenetic signal from all trees without removing the decadal variability – see Chapter 2, Figure 2.6 and Table 2.2. for details of other detrending methods tested. Then for each STN tree record an autoregressive model is fitted to remove short-term autocorrelation of up to three years ('pre-whitening') (Cook and Kairiukstis, 1990). In other words, when the ring-width values in a series can be predicted by the ring-widths of 1-3 previous rings in the same series, this predicted variability is estimated using a model and removed from the ring-width series. In many cases removing short term variation based on an autoregressive model improves the common signal of the trees in a population, and potentially isolates most cleanly the climatic signal in the chronology. The residuals of the autoregressive modelling produced one residual (RES) series per tree. Finally, two chronologies were produced for each site, one based on the STN series and one based on the RES series. These chronologies were produced by calculating the robust mean of the ring-widths for each calendar year. From here on this data processing will be referred to as detrending, and any further mention to ring-widths will be referring to the detrended ring-width series.

After RES and STN chronologies were produced for each site, the strength of the common signal in each chronology was assessed by calculating the average of all pairwise correlations of each series ($\bar{R}$), the average of the correlations of each series with the mean of all others (inter series corr.), the expressed population signal (EPS) and the mean sensitivity (Biondi and Qeadan, 2008). Details on the calculation of each of these statistical tools are shown in detail in **Chapter 2: Methods**. All detrending procedure and chronology statistic calculations were done in the software R using the dplR package.

4.2.3. Correlations with climate variables

The effects of climate on the detrended ring-widths were then studied by regression analysis and Pearson's correlation between the ring-width series and time series of hydroclimatic variables. Since the detrending procedure of tree rings removes any long-term trend from tree growth, linear trends present in the environmental data were also removed prior to the regression and correlation analysis. This was done by retaining deviation from the linear fits to the climatic data. Hydroclimatic variables considered were local cloud cover, precipitation and temperature obtained from CRU TS 4.00 (Harris et al., 2014), river levels obtained from the Hidroweb portal of the SNIRH-ANA (Brazil) and from the SENHAMI Peru. For the sites in central and southwest Amazon, we used rainfall data from the nearest stations located in Manaus and Riberalta, respectively. For the site in western Amazon, we used data from a station located in Nauta covering the period from 2000 to 2014 A.D. and also from another station in Tabatinga covering the period from 1985 to 2014. The river records from these two stations are highly correlated (r^2=-088,p<0.001).

Daily rainfall data was used to estimate the dry season length and rainfall at each site. This estimation was based on five-day rainfall averages, or pentads (Marengo et al., 2001). The dry season onset (end) was defined as the first of six out of eight pentads with rainfall below (above) the annual mean, provided that rainfall was above (below) the annual mean for at least six out of the eight previous pentads. Due to the lack of daily station data in the site from western Amazon, for this site the dry season length

and rainfall were calculated using the Tropical Rainfall Measurement Mission (TRMM 3B42 2011, 10.5067/TRMM/TMPA/3H/7).

In addition to these climatic variables, the length of the terrestrial phase of a tree was also estimated. The length of the terrestrial phase may actually be a more precise measure of the dry season length, because it represents the dry season over the whole catchment area of the local river. Based on river level records from local stations, the length of the terrestrial phase was estimated as the number of days the river levels remained below the tree base. For this calculation it was important to know the relative position of the trees to the local river levels. The height of the tree base above the river level was measured in the field and the date of the estimation was recorded. The mean height of the tree bases above the river level was then compared to the river levels recorded on the same date from nearest gauging station. This comparison allowed to determine the exact location of the trees relative to the river levels recorded from the nearest station. As *Macrolobium acaciifolium* trees frequently start growing just before the start of the true terrestrial phase (Schöngart et al., 2002), we considered that the growing period started when the river level dropped below 0.5-1m above the tree base.

4.3. Results and Discussion

4.3.1. Development of the tree ring chronologies

Careful comparison of the wood anatomy and ring-width series of different cores permitted detection of false rings (see Chapter 2, Figure 2.4), leading to correlation values of 0.5 to 0.8 between the ring-width series from different radii of the same tree. Ring-width series of trees that were not significantly correlated with the average of the ring-width series of all other trees from the same site were not included in the chronology. The final chronologies included 90% of all trees sampled in the western Amazon, approximately 75% of the trees sampled in southwest Amazon and only 50% of the trees sampled in central Amazon. Mean diameter increments and tree ages of trees included in the chronologies was 8.04±4.74mm and 76±31 years for the site in

western Amazon, 6.06±3.63mm and 77± 28 years for the site in central Amazon, and 4.99±3.32 mm and 138±68 years for the site in southwest Amazon.

The results from the radiocarbon analysis reveal a close match of year of formation of the tree rings estimated by cross dating the ring widths and by radiocarbon dating of the cellulose in the tree rings (Figure 4.2). For many rings both ages matched precisely. In few cases the pre-dating and the radiocarbon ages were mismatched by up to 2 years before 1980 A.D. These results confirm that this species' tree rings are indeed annual and that well-dated chronologies can be produced by careful analysis of the wood anatomy to identify the presence of false rings.

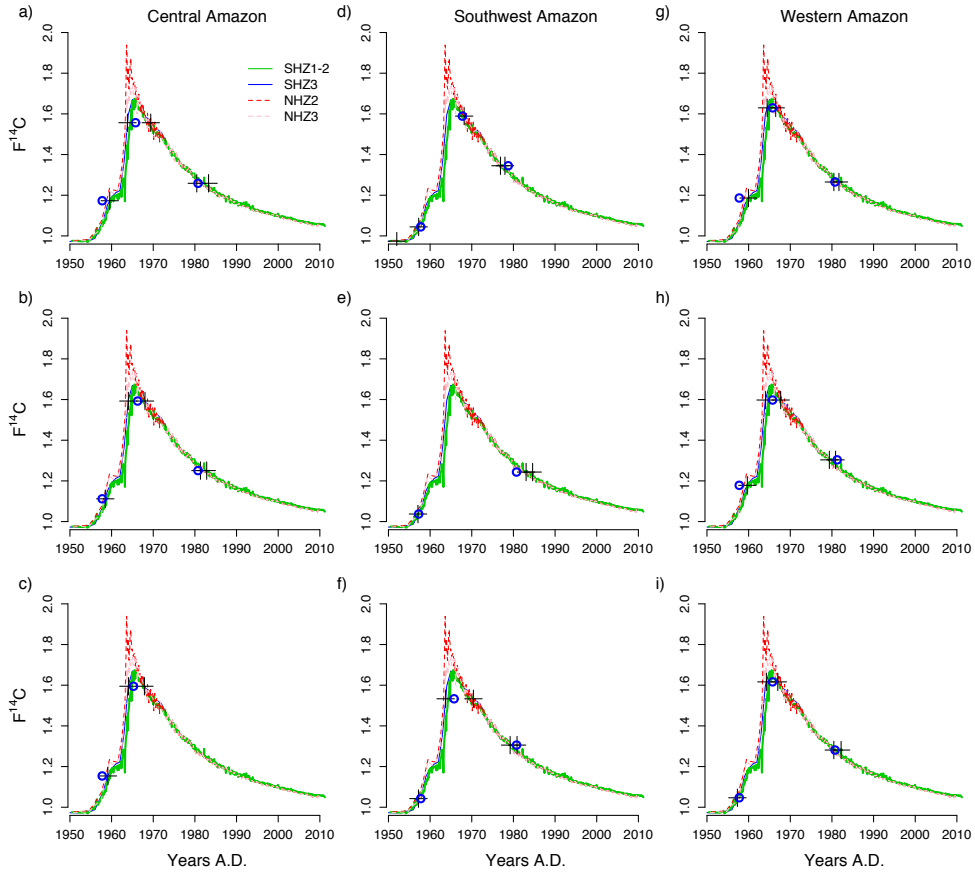

Figure 4.2. Results from the radiocarbon dating of 25 tree rings from 9 of the trees used in this study. Blue circles indicate the ring-dates obtained through wood anatomical analysis and tree-ring cross dating, plotted against their respective measured $F^{14}C$, and back crosses indicate the radiocarbon dates of the tree rings based on their measured $F^{14}C$ and on the $F^{14}C$ bomb-peak curves from the southern Hemisphere Zones 1-2. (a-c) Trees from the site in central Amazon, (d-f) trees from the site in southwest Amazon and (g-i) trees from the site in western Amazon.

As these possible small dating errors may also significantly reduce or even completely dampen correlations with inter-annual climate variability, all inter-annual correlations with climate conditions were done for the period after 1980 A.D., which is the most well dated period for all three sites, and also the period during which climate data is available for most stations.

Investigation of the RES and STN chronologies for each site revealed that for the site in southwest and central Amazon, the RES chronologies had much lower EPS than the STN chronologies. Thus, the chronologies for these sites were produced with the STN series. For the site in western Amazon, the pre-whitening resulted in a significant improvement of the EPS. Thus, for this site the RES chronology were used.

The final chronology with the best signal-strength (EPS) was the chronology of the site from western Amazon which had the highest overall EPS (Table 4.1 and Figure 4.1). EPS values are close or above the threshold of 0.85 in the first 50 years of each chronology. For the sites in central and southwest Amazon, the EPS is significantly reduced for periods prior to 1990, which may be related to small dating errors as revealed by the radiocarbon dating. However, over the most of the period from 1900-2014 their inter-tree correlation remains above 0.3 and their $\bar{R}$ remained stable (Table 1). Thus, the lower EPS values of the chronologies from southwest and central Amazon can likely be attributed to their lower number of replicates (Table 1).

We note that the results of the descriptive statistics (Table 4.1) values and inter-tree correlation of the chronologies from this study are lower than for other tree-ring chronologies of Amazon trees, which also generally are based on a lower number of replicates (Brienen and Zuidema, 2005; Locosselli et al., 2013; Locosselli et al., 2016; Assahira et al., 2017; Granato-Souza et al., 2018). This suggests a relatively weak common variability of the tree growth (or signal coherency) from our sites. This may be due to more variation in the individual tree responses to environmental conditions, or possibly due to lower climate sensitivity of the trees in our datasets compared to other tropical trees.

4.3.2. Correlations with river levels and the length of the terrestrial phase

The tree-ring chronologies from each site correlated significantly with different climate variables (Table 4.2 and Figure II.1 in Appendix II). Tree growth at the sites from southwest and western Amazon is strongly and negatively associated with river levels and positively with the length of the terrestrial phase. At the central Amazon site, there was no relationship with the length of the terrestrial phase, and the correlation value with river levels was lower. We find no significant association with the dry season length estimated from local daily rainfall data.

Table 4.1. Descriptive statistics for the tree-ring chronologies of each study site. $\bar{R}$ is the mean of all pairwise correlations of all series in the dataset. Inter-series corr. is the mean of correlations of each tree with the average series of all other trees. EPS is the expressed population signal. EPS values above 0.85 are expected when the series are well replicated. The total number of sampled trees is shown in parenthesis next to the total number of trees included the chronologies for each site.

western Amazon	Overall	2014-1964	1989-1939	1960-1910	1939-1889
Number of trees	45 (50)				
Mean sensitivity	0.5				
EPS	0.87	0.87	0.84	0.83	0.70
Inter-series corr.	0.33	0.33	0.28	0.36	0.33
$\bar{R}$	0.13	0.13	0.11	0.16	0.18
Oldest tree	176.00				
Length with min. 5 trees	114.00				
southwest Amazon					
Number of trees	30 (40)				
Mean sensitivity	0.5				
EPS	0.79	0.83	0.79	0.73	0.73
Inter-series corr.	0.30	0.33	0.30	0.36	0.30
$\bar{R}$	0.12	0.15	0.12	0.10	0.09
Oldest tree	337.00				
Length with min. 5 trees	214.00				
central Amazon					
Number of trees	22 (45)				
Mean sensitivity	0.44				
EPS	0.86	0.85	0.86	0.87	0.93
Inter-series corr.	0.38	0.36	0.37	0.42	0.46
$\bar{R}$	0.23	0.22	0.23	0.24	0.38
Oldest tree	129.00				
Length with min. 5 trees	108.00				

It is unclear why the relationships with river hydrology were so different for the central Amazon site. This is surprising, as previously published chronologies from floodplain trees (including *M. acaciifolium*) are associated with the length of the terrestrial phase (Schöngart et al., 2004; Schöngart et al., 2005; Batista and Schöngart, 2018). Here we note that some of these chronologies which have approximately the same number of replicates as the number in our chronology from central Amazon were built with cross-sectional disc samples from the tree trunks in addition to wood cores, which can aid the cross-dating of trees.

We also note that for each site, the influence of river level on the ring-width series occurred during different periods within the growing season of each site. For the site in southwest Amazon, the ring-widths are more strongly associated with river levels at the beginning of the growing season. For the site in western Amazon, the correlation is stronger for most of the growing season, but the time series of local river levels is relatively short here (2000-2014). Considering a longer time-series from a station approximately 150 km downstream (Tabatinga), the ring-widths are more strongly influenced by the river levels at end of the growing season, which is also the case for the site in central Amazon. These differences may reflect the different patterns of seasonal fluctuation of the river levels (Figure 4.3).

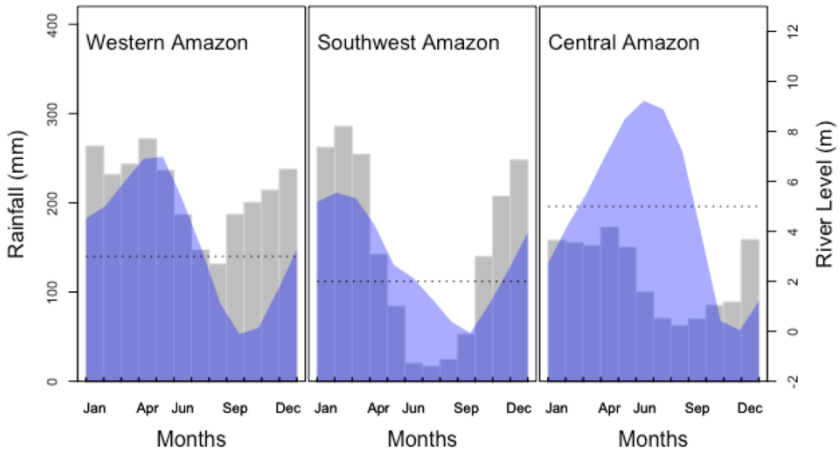

Figure 4.3. Rainfall and river level seasonality for the three studied sites. Note that the river levels recede much more gradually at the site in southwest Amazon.

Table 4.2. Summary of the strongest correlations of the chronologies of each site with climate/environmental variables for periods within the tree's growing seasons. The months of the growing seasons at each site are indicated in parenthesis. For each correlation shown, asterisks indicate the significance levels as p<<0.05*, p<0.01** and p<0.001***. In the Season column, the seasons Dry-wet and Wet-dry stand for inter-season transition periods. The corresponding months used in to calculate the correlations are shown in column Months, while months followed by (-1) indicate periods of previous calendar years. For the terrestrial phase, the location of the station and the river level for the start and end of the non-flooded period are indicated in parenthesis.

Variable	Season	Pearson's *r*	Months	Period
western Amazon (Jul-Dec)				
Rainfall	Dry-wet	-0.38*	Dec.Feb	1983-2014
Cloud cover	Dry	-0.44**	Aug.Nov	1978-2014
River level (Nauta)	Dry-wet	-0.57*	May.Dec	2000-2014
River level (Tabatinga)	Dry-wet	-0.54**	Oct.Dec	1978-2014
Length of the terrestrial phase (Nauta, 7 - 6.5m)	Dry	0.63***		2000-2014
Length of the terrestrial phase (Tabatinga, 8.5-8m)	Dry	0.35***		1985-2014
AMO	Dry	0.46**	Aug.Nov	1978-2014
southwest Amazon (Apr-Nov)				
Rainfall	Wet-dry	-0.53**	Mar.Sep	1990-2014
Temperature	Dry	-0.42*	May.Jul	1978-2014
River level	Wet-dry	-0.42**	Mar-May	1978-2014
Terrestrial Phase (Riberalta, 5-4.5m)	Dry-wet	0.68***		1990-2014
AMO	Dry-wet	0.45**	Feb(-1).Jan	1978-2014
Nino3.4		-0.35*	Jan(-1).Sep(-1)	1978-2014
PDO		-0.51*	May.Jul	1978-2014
central Amazon (Sep-Feb)				
Rainfall	Wet-Dry	-0.39*(-0.38*)	Mar.May	1979-2015
River level	Wet	-0.4*(-0.4*)	Dec.Feb	1979-2015
AMO	Wet-Dry	0.33*	Sep(-2).Aug(-1)	1979-2015

At the site in southwest Amazonia, the river level recedes gradually, and remains close to the height of the tree base for longer during the start of the terrestrial phase compared to the other two sites. In contrast, at the other two sites from western and central Amazon the river levels drop much more sharply, and thus are possibly less limiting for tree growth during the start of the growing season.

4.3.3. Correlations with rainfall and cloud cover

At all sites tree growth was negatively related with local rainfall during the start or end of the trees' growing seasons. For the site in western Amazon this was only significant for the period after 1983. Although rainfall generally has a positive effect on growth of trees from non-flooded environments, this result is consistent with previous chronologies produced for floodplain trees (Schöngart et al., 2004), and may result from the effect of rainfall on the local river hydrology. If more rainfall results in increased river levels, this could lead to reduced length of the trees' growing season. This is possibly the same mechanism that leads to the observed influence of cloud cover on tree growth from the western Amazon site, which were also apparent in the spatial correlation maps (Figure 4.4a and Table 4.2), if cloud cover can be interpreted as an indicator of convection and rainfall. Alternatively, the negative correlations with cloud cover could also be related with more cloud cover being associated with light limitation for tree growth.

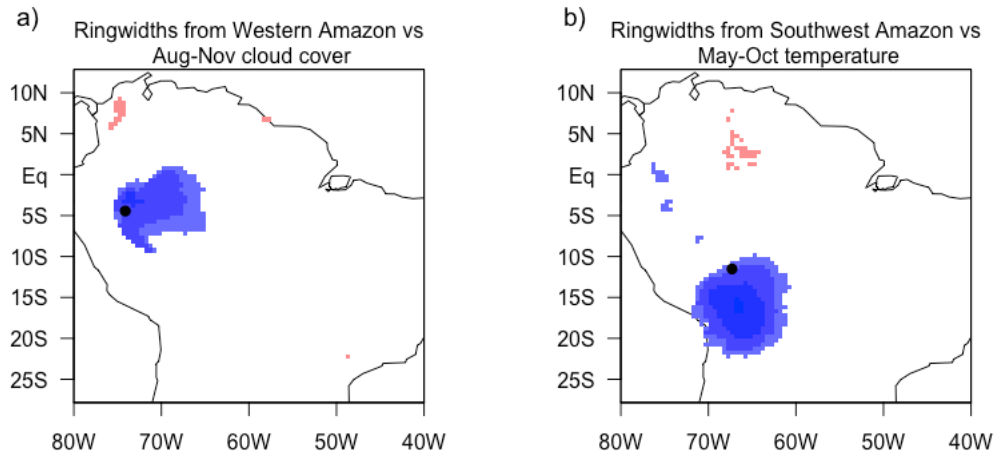

Figure 4.4. Spatial correlation maps of ring-width chronologies with gridded datasets from CRU TS 4.00 climatology. (a) Detrended ring-widths from the site in southwest Amazon and May-Oct temperatures. (b) Detrended ring-widths from the site in western Amazon with Aug-Nov cloud cover. Only correlations significant at the 95% confidence interval are shown. Correlations were calculated for the period from 1980 to 2014 A.D.

4.3.4. Correlation with temperature for the southwest Amazon site

For the southwest Amazon site, we find a relatively strong effect of local and regional temperature on ring-widths, though not as strong as with the length of the terrestrial

phase. This relation is also evident in the spatial correlation maps (Figure 4.4b and Table 2). Temperature may limit tree growth by increasing leaf temperature and thus leaf to air vapour pressure deficit, which may lead to reduced stomatal conductance (Lloyd and Farquhar, 2008; Doughty and Goulden, 2009). Elevated temperatures may also affect the photosynthetic machinery of the leaves (Peñuelas and Llusià, 2002; Allakhverdiev et al., 2008), increasing photorespiration rates by affecting the affinity of RuBisCO for CO_2 and the CO_2 compensation point (Jackson and Volk, 1970; Ogren, 1984), reducing photosynthesis rates, and potentially affecting tree productivity negatively.

Many studies report that temperature is an important driver of inter-annual tree growth variation in tropical forests (Doughty and Goulden, 2009; Dong et al., 2012) and frequently ring-widths are correlated with both rainfall and temperature (Fichtler et al., 2004; Vlam et al., 2013; Locosselli et al., 2016; Locosselli et al. 2016b), as is the case in our study. In some cases this may be simply caused by co-variation of rainfall and temperature leading to statistically significant relations with both these variables (Brienen et al., 2010; Humphrey et al., 2018). In order to separate the effects of rainfall and temperature, we used partial regression to test the effects of each of these variables separately while controlling for the effects of the other. When considering both rainfall and temperature in the same analysis we found that only the effect of temperature remained significant (period 1988-2014, r^2=-0.49, p<0.01). Following the same logic, we also considered both the length of the terrestrial phase and temperature in one analysis, and both variables remained significant, explaining together over 60% of the variability in the ring-width from 1990-2014 (r^2=0.61,p<0.001). In summary these results suggest that both the length of the terrestrial phase and air temperature are the main drivers of tree growth of *Macrolobium acaciifolium* in the floodplains of southwest Amazon. This is consistent with our results from the Chapter 3 of this thesis, where intra-annual isotope variations in the tree rings of *M. acaciifolium* trees also suggest that this species may respond to temperature variations.

The fact that temperature only had a significant effect on tree growth at one site suggests that this may not be entirely related to any specific traits of *Macrolobium acaciifolium,* especially because this species has small and compound leaves, which have lower boundary layer resistance to vapour diffusion and are usually more efficient in reducing leaf temperatures (Jones, 1992; Fauset et al., 2018). Strangely the temperature at this site is not hotter than at the other two sites, nor presents more variability. The hottest temperatures are actually observed at the central Amazon site. The effect of temperature on tree growth at the southwest Amazon site may be related to the dryer growing season and also to different soil properties at this site. While the trees from the sites in western and central Amazon grow on clayey soils, the soils at the site from southwest Amazon are sandy (personal observation) and probably have a lower water retention capacity. Thus, it is possible that the soils at the site in southwest Amazon retain less water, which can increase the water stress of the trees from this site, restricting the thermoregulation capacity of leaves through evapotranspiration (Jones, 1992, Fauset et al., 2018), and ultimately affecting photosynthesis and growth rates. The fact that the trees from this site had the lowest mean diameter increment rates also suggest that the growing conditions are more limiting in this site compared to the other two sites.

4.3.5. Teleconnections with external large scale climate controls

At inter-annual time scales, we find the ring widths of all three sites are significantly related with known controls of large scale climate variability in the Amazon (Figure II.2 in Appendix II). One control that appears to affect all three sites was the Atlantic Multidecadal Oscillation (AMO). The AMO is large scale climate control which is based on the average anomalies of sea surface temperatures in the North Atlantic Ocean region, between 0 and 80 degrees of latitude (Enfield et al., 2001). The positive (warm) phase of the AMO is linked with higher frequencies of droughts in the Amazon (Barichivich et al., 2018), which in turn affect the growth of floodplain trees by increasing the length of the terrestrial phase during dry years. This mechanism is consistent with our results that reveal increased ring-widths in years with high AMO

indices. For the site in central Amazon, it is also interesting to note that there is a negative relation with the SST of the Tropical South Atlantic. Warm SSTs of the South Atlantic may lead to increased wet season rainfall over the northeast Amazon (Yoon and Zeng, 2010). Thus, warm SSTs in these different regions of the Atlantic Ocean are expected to have opposite effects on the length of the terrestrial phase of the trees in central and western Amazon, which is consistent with the opposite sign of the observed correlations with SSTs in each of these regions.

One surprising result is the significant relation between the Pacific Decadal Oscillation and ring-widths of the site in southwest Amazon. The PDO is related to anomalies of sea surface temperatures in the north and Tropical regions of Pacific Ocean, which affect the frequency and strength of El Niño and La Niña events (Zhang et al., 1997; Mantua and Hare, 2002). Pacific Ocean SSTs are known to affect rainfall and river levels in central and northern Amazon (Marengo and Espinoza, 2015), and thus it is surprising that we find evidence for its effect on tree growth at the southwest Amazonian site, but not for the other two sites.

The observed effects of the AMO on tree growth has important implications for the floodplain forests of the Amazon. The AMO plays a central role in the decadal variations of river levels and discharges in the Amazon, which have been increasing over recent decades (Barichivich et al., 2018). As most floodplain tree species are adapted to tolerate different levels of flooding (Wittmann et al., 2006; Wittmann et al., 2012), small changes in the hydrological cycle can lead to large scale death of floodplain trees. This has been observed for example after the construction of dams which cause small increases in the river levels, leading to large scale death of floodplain trees downstream of the dams (Assahira et al., 2017; de Resende et al., 2018).

4.3.6. Potential for climate reconstructions

In this study, we find that the effects of the length of the terrestrial phase on ring-widths of the sites from western and southwest Amazonia have the greatest potential

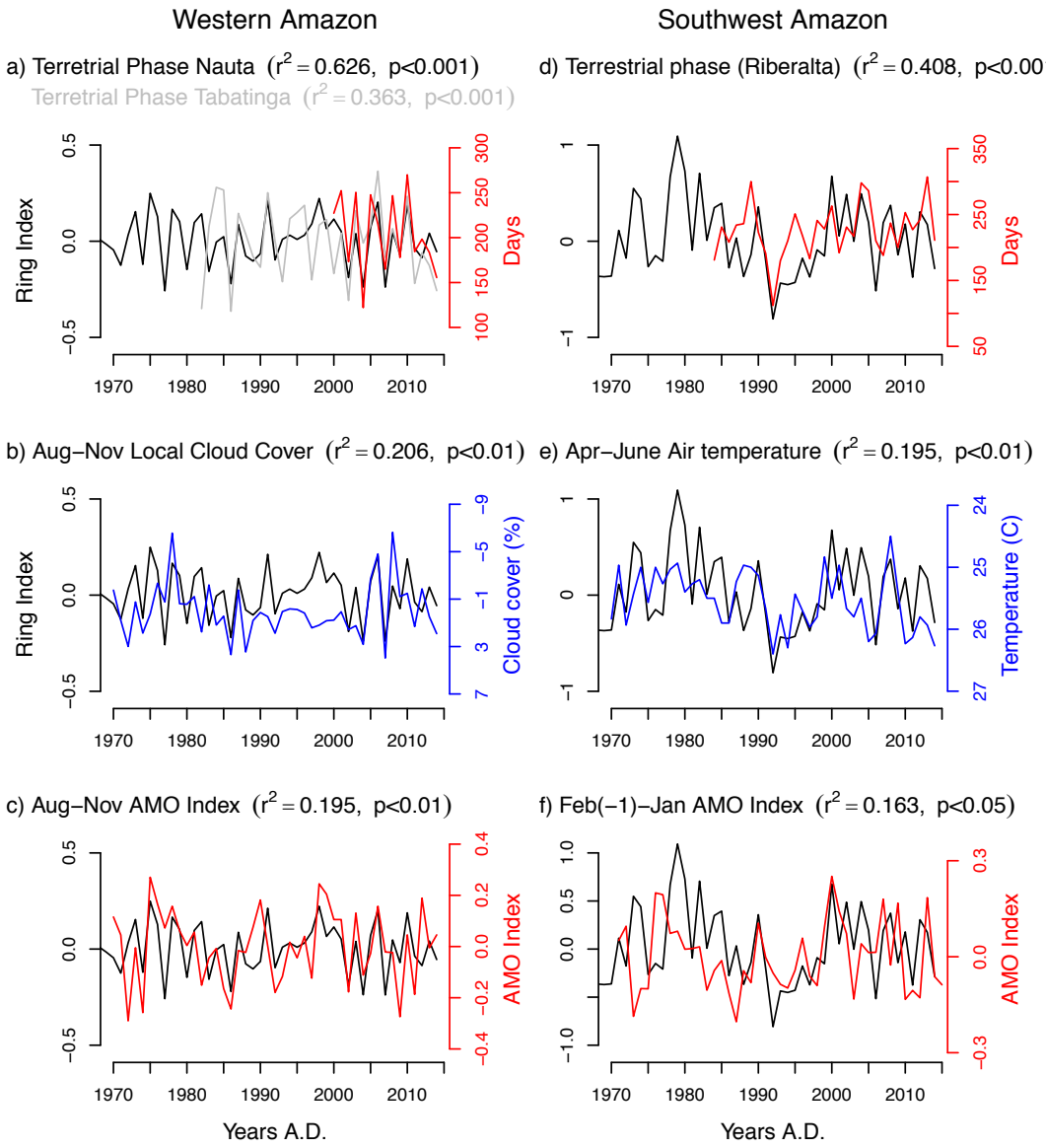

Figure 4.5. Comparison of the time series of the tree ring chronologies of each site with the strongest (significant) correlated environmental variables and teleconnections. (a-c) Site from western Amazon, (d-f) site from southwest Amazon. Note that the time series shown in blue (red) indicate negative (positive) correlations. In the cases when the correlations are negative (b,e), the y-axis of the climate series was inverted. The results of a linear regression between the times series shown in each graph are shown in parenthesis. Note that in (f) it is possible to see that before 1990, the ring-width series lags the AMO indices by two years, which reduces the overall explained variability r-squared of the regression.

for climate reconstruction. This potential is also revealed by the association between the ring-width chronologies from these sites and the length of the terrestrial phase (Figure 4.5ad). For each of these sites, the observed relationships with cloud cover and temperature also seem to explain a significant part of the variability in tree growth (Figure 4.5be). Although all correlations mentioned so far are statistically

significant, the use of tree rings for climate reconstruction requires that these correlations are persistent. In Figure 4.5f, it is also possible to note that prior to 1990, the ring-with series of the site in southwest Amazon lags the time series of the AMO by 2 years. This is possibly an indication for the presence of false or missing rings still in this chronology. That is also the case for the chronology for the site in western Amazon for periods preceding 1970. Thus, inter-annual climate analysis with these chronologies are only possible for periods of 30-50 years, while the variations at decadal time-scales can be used for longer-term climate reconstructions. Some detrending methods can potentially be applied to evaluate multidecadal trends in the ring-width series (Peters et al., 2015), but this would hardly be possible in our study. Most of the trees in our chronologies are less than 100 years old, with less than 10 trees achieving 200 years in all the 140 trees of our dataset. Thus any attempt to detect long term trends with our dataset would inevitably be subject to common biases of tree ring datasets (Brienen et al., 2012; Bowman et al., 2013; Brienen et al., 2016). On the other hand, other floodplain trees may achieve much higher ages of up to 400 years, and may potentially be used for longer term climate reconstructions (Schöngart et al., 2005; Schöngart et al., 2010). Thus, it is recommended that additional floodplain species of wide occurrence in the Amazon are studied.

4.4. Conclusions

The main goal of this study was to produce tree ring chronologies of floodplain trees which could permit to reconstruct the past variability of river levels and dry season climate in different sub-basins of the Amazon. We find both potential and limitations for this approach. The main potential revealed by this study is in the observed correlations with environmental variables, which are as strong as previously reported for floodplain trees and also for trees from non-flooded tropical areas – see Table 4.2. The main limitation revealed by this study is related to the presence of false rings in *M. acaciifolium*, which require time and effort to be detected and accounted for in the chronologies. The presence of false rings in these trees poses a limitation for using these chronologies for long-term climate reconstructions at the inter-annual

scale, and may be the reason the influences of river hydrology were not so strong for the site in central Amazon.

Our results suggest the main driver of inter-annual variations in tree growth is the length of the terrestrial phase. This measure is related to length of the dry season over the catchment area of the river, which corresponds to the local dry season at the sites in western and southwest Amazon. In general, our results are consistent with previous studies that also find the terrestrial phase to be the strongest control on tree growth in central Amazon floodplains. Besides confirming previous findings, our study also reveals two novel results related to the growth of floodplain trees. Firstly, we show that for the site in southwestern Amazon, inter-annual variations in temperature have a significant effect on tree growth, and this effect is independent from rainfall. Secondly, for the first time we show that the Atlantic Multidecadal Oscillation may play a central role for the inter-annual variability of tree growth in floodplain forests, especially for the western Amazon site, likely via its effect on the length of the terrestrial phase.

Chapter 5 Oxygen isotope ratios in tree rings of *Macrolobium acaciifolium* reflect past climate during the dry and transitional seasons

Summary

Climate observations in the Amazon Basin suggest the dry season may have been becoming longer and/or drier over recent decades. However, there are many uncertainties about past dry season climate variability in the Amazon. Here we explored the potential of using oxygen isotopes in tree rings ($\delta^{18}O_{TR}$) of floodplain trees as proxies for past dry season climate variability. As floodplain trees grow mostly during the dry and/or transitional season we expected these to record dry season climate variation. We built $\delta^{18}O_{TR}$ chronologies for three sites located in western, central and southern Amazon. Consistent with our expectations, the $\delta^{18}O_{TR}$ records from western and central Amazon reflected climate conditions during the dry and transitional season, respectively. Both records were negatively affected by large-scale rainfall over the Amazon basin and positively affected by local and large-scale temperatures. The climate influences on $\delta^{18}O_{TR}$ from the southwestern Amazon site were in the opposite direction to our expectations, and thus inconsistent with our understanding of climatic effects on $\delta^{18}O_{TR}$. Of the three $\delta^{18}O_{TR}$ records analyzed here, the western Amazon record showed the greatest potential for reconstruction of past dry season climate. The long-term increase in $\delta^{18}O_{TR}$ from this site is consistent with observed decreasing rainfall amounts during the dry season in the south and east of the Basin and related to long-term warming of sea surface temperatures of the Tropical North Atlantic Ocean. Our results demonstrate the potential and limitations of using $\delta^{18}O_{TR}$ of floodplain trees as unique proxy for past dry season climate variability, and highlight the importance of understanding the causes for an intensification of the dry season in the Amazon, and its consequences for the carbon balance and biodiversity in the region.

5.1. Introduction:

Amazon Forests cover 5 million square km of tropical South America. They provide major ecosystem services by influencing the global redistribution of moisture and heat (Bonan, 2008) and by sequestering ~ 0.38 Pg C $year^{-1}$ over the last decades (Phillips et al., 2009; Beer et al., 2010; Pan et al., 2011; Sleen et al., 2017). The forest vegetation is sensitive to climate variations, and is expected to respond to changes in the hydrological cycle of the region (Phillips et al., 2009; Brienen et al., 2015). In particular, changes in the climate conditions during the dry season could have a strong effect on the forest functioning, and dry season climate has been found to be one of the most important determinants of forest structure and dynamics (Xu et al., 2011; Quesada et al., 2012; Schietti et al., 2016) and species distributions in the Amazon (Esquivel-Muelbert et al., 2017).

Recent analysis of long term climate variability and river discharges in the Amazon suggest that the dry season in the south of the Amazon is possibly becoming longer and more intense over recent decades (Fu et al., 2013; Gloor et al., 2013; Marengo and Espinoza, 2015). There are concerns that this may be due in part to effects of deforestation (Nobre et al., 1991; Butt et al., 2011; Fu et al., 2013; Spracklen and Garcia-Carreras, 2015; Khanna et al., 2017) and down-regulation of plant stomatal conductance in response to increased atmospheric [CO_2] (Wullschleger et al., 2002; Ainsworth and Rogers, 2007; Cernusak et al., 2013), which may lead to reduced evapotranspiration from the forest. As the evapotranspiration from the forest is an important source of rainfall in the region (Salati et al., 1979; Spracklen et al., 2012; Wright et al., 2017), reduced evapotranspiration could lead to drier conditions, especially during the dry season (Spracklen et al., 2012; Zemp et al., 2014; Khanna et al., 2017). This effect has been predicted by many model simulations (Shukla et al., 1990; Werth and Avissar, 2002; Cox et al., 2004; Nobre et al., 2009; Medvigy et al., 2011; Harper et al., 2014), and few studies suggest that drying due to reduced evapotranspiration may already have begun to happen in the south of the Amazon (Fu et al., 2013; Spracklen and Garcia-Carreras, 2015). However, there is much

disagreement between different model predictions for the Amazon region (Flato et al., 2013; Huntingford et al., 2013; Boisier et al., 2015; Friedlingstein, 2015), and there are still many uncertainties about the evolution of the dry season in different regions within the Basin (Boisier et al., 2015). In part, these uncertainties can be attributed to the lack of long long-term climate data for most of the region. Therefore, obtaining more information about past dry season climate variability is potentially useful to clarify how the dry season has been changing in different regions within the Basin over the past century.

One potentially useful approach to obtain more information about past dry season climate variability is through the analysis of tree rings of Amazon floodplain trees, which grow mostly during the dry season when they are not flooded (Schöngart et al., 2002; Schöngart et al., 2004). In Chapter 4 of this thesis we explored the potential of using tree ring-widths of Amazon floodplain trees as proxies for past dry season length in different regions within the Amazon. One additional approach to obtain information from the tree rings is by analyzing the oxygen isotopes ratios ($\delta^{18}O$) in their cellulose tissues ($\delta^{18}O_{TR}$). $\delta^{18}O_{TR}$ reflect the $\delta^{18}O$ of the soil water used by plants, altered by leaf water enrichment during transpiration, which is in turn affected by local climate conditions (Dongmann et al., 1974; Roden and Ehleringer, 1999; Farquhar et al., 2007; Holloway-Phillips et al., 2016). In the Amazon, variations of $\delta^{18}O$ of rainfall water is determined by large scale precipitation patterns within the basin (Salati et al., 1979; Vimeux et al., 2005; Villacís et al., 2008; Baker et al., 2016). As a result, previous studies have shown that $\delta^{18}O$ in tree rings of terra firme trees is an effective tool to reconstruct past wet season climate conditions in the Amazon (Brienen et al., 2012; Baker et al., 2015).

Since floodplain trees grow mostly during the non-flooded period, analyzing oxygen isotope composition in their tree rings may potentially be suited to reconstruct variations in past dry season intensity. This potential was initially explored in the Chapter 3 of this thesis, where we investigated the drivers of intra-annual oxygen and carbon isotope rations within the tree rings of *Macrolobium acaciifolium*. In the

current Chapter, we will explore this further by analyzing the inter-annual variation in oxygen isotopes in tree rings of *Macrolobium acaciifolium* covering the past 80-100 years. Our main aim is to evaluate the relative strength of the signals of local and large-scale climate in $\delta^{18}O$ in tree rings, and the relative strengths of the major controls of the Amazon hydrology (SST of the ENSO 3.4 region, Pacific Decadal/Interdecadal Oscillation, Tropical North Atlantic SSTs and the Atlantic Multidecadal Oscillation) on $\delta^{18}O$ in tree rings.

5.2. Methods

To carry out this study, we analyzed $\delta^{18}O_{TR}$ of the floodplain tree species *Macrolobium acaciifolium.* Sampling was done at the same sites as in Chapter 4 of this thesis: in western, central and southern Amazon. See Chapter 2 for details of the location hydroclimatic features of each site. At each site, we selected 7-8 wood cores (22 cores in total). Cores were selected based on the confidence of the dating of their tree rings and on the width of their tree rings to provide sufficient material for isotopes analysis. All cores which were radiocarbon dated in Chapter 4 were used for the $\delta^{18}O_{TR}$ analyses. We extracted cellulose from the wood of individual rings in the Dendrochronology Laboratory of the University of Leeds using the methods of Wieloch et al. (2011) and Kagawa et al. (2015). The oxygen isotopic ratio in the cellulose extracted from the tree rings ($\delta^{18}O_{TR}$) was then analyzed with an Isotope Ratio Mass Spectrometer (Sercon 20-20 IRMS) in the Environment Isotopes Laboratory of the University of Leicester. All isotopic ratios in this study are expressed relative to the Vienna Standard Mean Ocean Water (V-SMOW), in ‰ units.

5.2.1. Construction and dating of the $\delta^{18}O_{TR}$ time-series

As a first exploratory step of the nature of the potential climate signals in the $\delta^{18}O_{TR}$, we analyzed the $\delta^{18}O_{TR}$ of three sub-samples per ring in 20 rings for three wood cores per site (Figure 5.1). This was done because intra-annual variations in $\delta^{18}O_{TR}$ of this species are large and display different climate signals (see Chapter 3). We thus evaluated first if one or more specific ring segments were most strongly related to

climate (temperature and precipitation) at local and Amazon-wide scales using Pearson's correlations. This initial exploratory analysis revealed large differences in the coherency of the $\delta^{18}O$ signals between the different trees. The trees from the site in western Amazon showed the best common signal, while the trees from the site in central Amazon showed a less coherent signal (Figure 5.1). Despite the differences in coherency, the average $\delta^{18}O_{TR}$ in the tree ring segments showed significant correlations with climatic and environmental variables at all sites (Figure III.1 in Appendix III). For the site in western Amazon, only the $\delta^{18}O_{TR}$ in the middle segment of the tree rings correlated significantly with climate variables (Figures III.6 and III.1 in Appendix III). Thus, for isotopes analyses, the middle ring segment was used for western Amazon site, while the entire ring was used for the trees from the sites in central and southwest Amazon.

We then analyzed the $\delta^{18}O_{TR}$ in 60-100 rings per tree, using only the middle ring segment for the western Amazon site. Each individual $\delta^{18}O_{TR}$ series was dated by assigning the sampling date to the outermost ring of the cores and using the Schulman convention, i.e. the ring is assigned the calendar year in which the trees start growing. For example, if the trees grow from September 2005 to February 2006, the ring is assigned the calendar year of 2005 A.D. Rings previously identified to be false rings in the Chapter 4 were similarly considered false rings here. However, as a precautionary measure, the $\delta^{18}O$ of some presumably false rings were also measured separately. This was done so that if upon later inspection of the $\delta^{18}O_{TR}$ chronology one of these rings appeared to be true, it could still be included in the chronology. The $\delta^{18}O$ series of each core was then visually and statistically compared to produce a mean $\delta^{18}O_{TR}$ series of 80-100 years for each site (Figure 5.2). Statistical comparison to evaluate how well the individual series cross-correlate was done through Pearson's correlation analysis of all pairwise combinations of the series from each site.

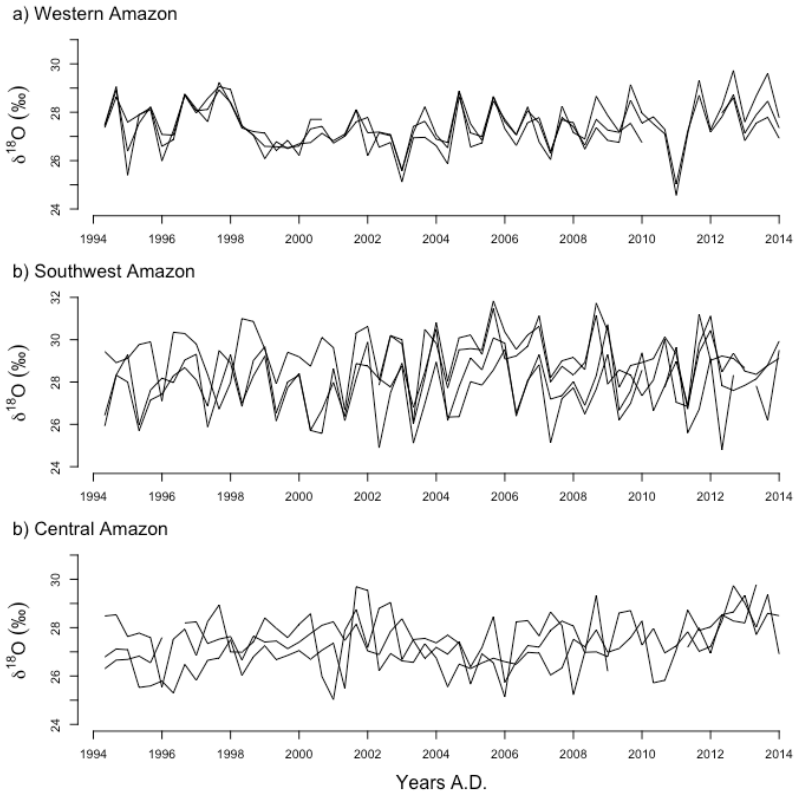

Figure 5.1. Analysis of $\delta^{18}O_{TR}$ in three sub-samples per ring for three trees per site. (a) western Amazon, (b) southwest Amazon and (c) central Amazon.

To assess whether one or more $\delta^{18}O_{TR}$ series did not present a common signal with the others, we repeated the cross-correlations between the series of each site, each time removing one of the $\delta^{18}O$ series – effectively bootstrapping the cross-correlations.

5.2.2. Influence of climate and hydrology over the $\delta^{18}O_{TR}$

Influence of local climate and hydrology on the average $\delta^{18}O_{TR}$ series of each site was evaluated using Pearson's correlation, and regression analyses of the $\delta^{18}O_{TR}$ with local climate conditions. Local climate parameters considered were river levels, rainfall, cloud cover and temperature.

As previous studies show that the amount of wet season rainfall over the trajectories of air masses upwind from the sampling site are a good predictor of the $\delta^{18}O_{TR}$ of Amazon trees that grow during the wet season (Baker et al., 2016), we also evaluated

whether the $\delta^{18}O_{TR}$ were associated to large-scale climate. To assess the possible region of influence of rainout over rainfall $\delta^{18}O$ at these sites during the tree's growing seasons, we calculated for each site, 15 day hourly back-trajectories of the moisture at 800Pa (~2000m) using the HYSPLIT model (Draxler et al. 2011). The regional differences of climate influences on tree ring $\delta^{18}O_{TR}$ were then visualized using spatial correlation maps produced by calculating all pointwise correlations of the $\delta^{18}O_{TR}$ records with gridded precipitation and temperature from CRU TS 4.00 climatology. As a separate measure of large-scale hydrology, we also considered river levels and discharge of the Amazon rivers that drain rainfall over large areas within the Amazon. Temperature was also considered in these analyses because a significant proportion of rainfall during the dry season may originate from forest evapotranspiration (Spracklen et al., 2012; Zemp et al., 2014), which is affected by temperature -dependent vapour pressure deficit (Hasler and Avissar, 2007). Climate tele-connections of the $\delta^{18}O_{TR}$ signal with large-scale climate controls were also assessed by correlating the $\delta^{18}O_{TR}$ series of each site with gridded sea surface temperatures (SST) from Had SST (Rayner et al., 2003).

As we were interested in both trends and interannual variations in $\delta^{18}O_{TR}$, we did all correlations with climate variables using both the observed (raw) data and detrended $\delta^{18}O_{TR}$ and climate data to emphasize the correlations at the inter-annual scales. This detrending consisted of calculating the residuals between the observed data and the long term trends which were estimated by fitting a smoothing spline of half the length of the series and 50% frequency response – see Figure 5.2.

Finally, to assess the sensitivity of the long-term trends in the $\delta^{18}O_{TR}$ records to possible changes in leaf water enrichment caused by local climate conditions or to long-term changes in g_s, we used the tree-ring-isotope model detailed in Chapter 3. For each site, we predicted changes in $\delta^{18}O_{TR}$ using one model with only local changes in temperature and relative humidity and keeping g_s constant, and one where we changed g_s in addition to the climate forcing to simulate a possible change in g_s due

to increasing CO_2. In this latter version of the model, we decreased g_s by 20% (from 0.3 in 1965 A.D. to 0.24 $mol.m^{-2}.s^{-1}$ in 2014 A.D.).

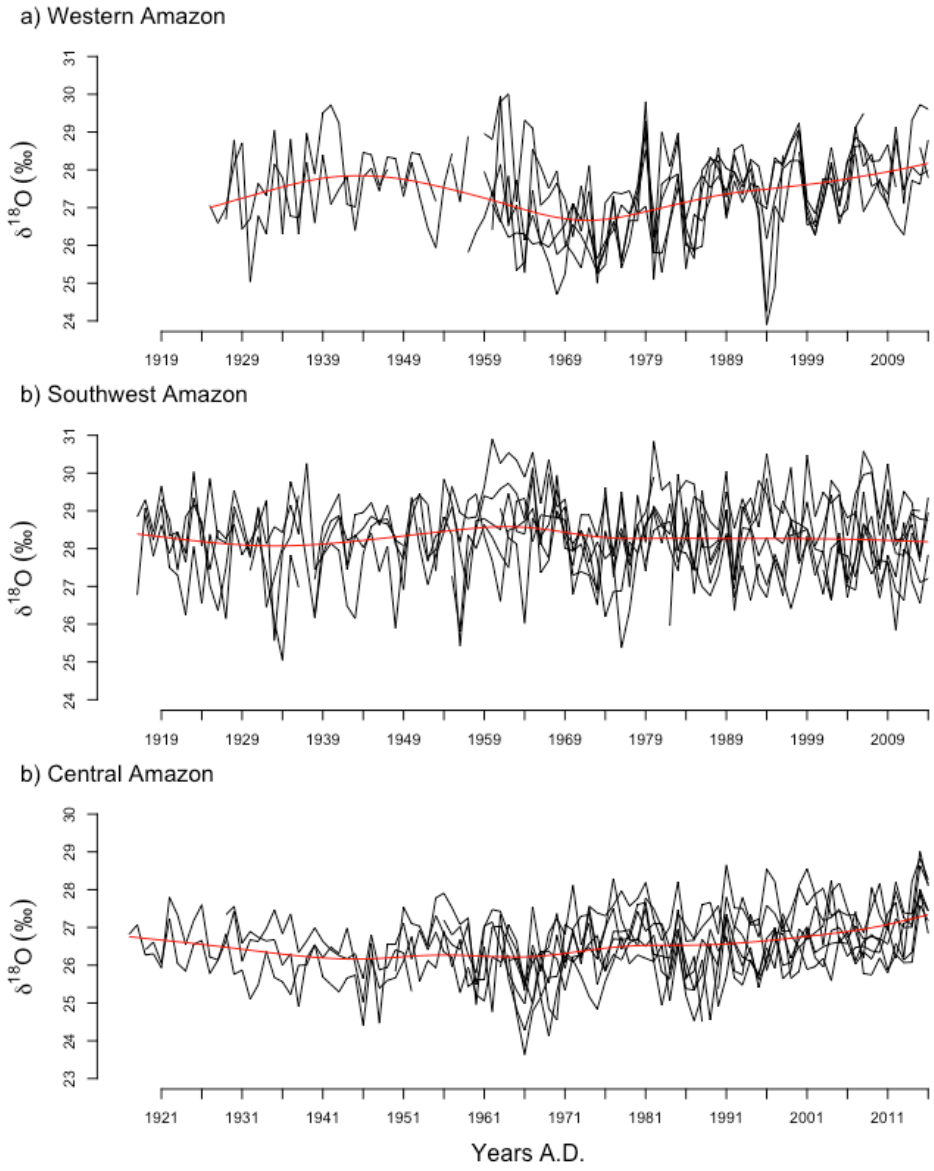

Figure 5.2. Oxygen isotope records ($\delta^{18}O_{TR}$) for each of the sites, showing the multidecadal trends in the average of all trees for each site. (a) western Amazon (*r*=0.47), (b) southwest Amazon (r=0.30) and (c) central Amazon (*r*=0.38).

5.2.3. Data sources

For all sites, temperature and cloud cover were obtained from CRU TS 4.00 (Harris et al., 2014). Rainfall data were obtained from local stations, or from CRU TS 4.00 when where local station data were not available. For the site in southwest Amazon we used rainfall data from a local station in Riberalta, approximately 150km from the sampling site. For the site in central Amazon, we used local station rainfall data from Manaus, approximately 80km downstream from the sampling site. For the site in western Amazon there were no local rainfall stations nearby and therefore we used rainfall data from CRU TS 4.00 for this site.

River level data were obtained from local gauging station records. For the site in southwest Amazon we used river level data from a station in Riberalta. For the site in western Amazon, we considered river data from two stations. One is located in Nauta which is very close to the sampling site, covering the period from 2000-2014 A.D., and another located in Tabatinga, which is located approximately 400km downstream from the sampling site, covering the period from 1985-2014 A.D. Despite this large distance between the two stations, the river levels in Tabatinga closely co-varied with the river records from Nauta (r^2=-088,p<0.001), and are available back to 1985.

For the site in central Amazon, we considered river records from stations both upstream and downstream from the sampling site. The river station from Manaus presents the longest river records available in the Negro river and this station is also the closest to the sampling site in central Amazon, approximately 80Km downstream. However, in Manaus, the Negro river levels reflect mainly the Amazon River levels, because the station is very close where these two rivers join. Thus, the Negro River levels recorded from Manaus may not be the best measure of rainfall over the Negro river catchment area, which may be better represented by river levels recorded from stations upstream from the sampling site. Thus, we considered two additional stations located in Moura and Santa Isabel, where the Negro river levels are not affected by the Amazon River. The integrated rainfall over the Negro catchment area

(estimated from CRU TS 4.00) is better correlated with the Negro recorded in Moura ($r=0.76$, $p<0.01$) and Santa Isabel ($r=0.82$, $p<0.01$) than with Negro levels recorded in Manaus ($r=0.65$, $p<0.001$, 1970-2014 A.D.).

5.3. Results

5.3.1. Construction and dating of $\delta^{18}O_{TR}$ chronologies

Two of the trees from the site in western Amazon and one tree in the site from southwest Amazon were not significantly correlated with most of the other series in the same site. Thus, these series were removed from the analysis. After removing these series, the site with the best cross-correlations was the western Amazon site (average *r*=0.47), followed by the site in central Amazon (average *r*=0.38), with the least coherent signals in the southwest Amazon site (average r=0.30).

5.3.2. Correlations with climate variables

The correlations of each $\delta^{18}O_{TR}$ record with all local and large-scale climate variables and river levels are shown in Figures III.3-5 in Appendix III, and the strongest correlations found are shown in Table 5.1. Our results for the sites in western and central Amazon were similar to each other and in line with our expectations. As the dry season is still relatively humid/wet in these two sites, especially at the western Amazon site, we expected that plant physiological responses to local climate conditions would not be strong. For both sites, we find positive effects of local temperature on $\delta^{18}O_{TR}$, and stronger effects of large-scale climate (Figures II.2 and II.3 in Appendix III). These effects of large-scale climate on the $\delta^{18}O_{TR}$ records are evident in the positive influences of temperature and negative influences of rainfall over large areas of the Amazon Basin, and negative influences of the levels of rivers which drain rainfall over large areas within the basin (Figure 5.3). While the $\delta^{18}O_{TR}$ record of the sites in western and central Amazon were similarly influenced by large-scale temperature and hydrology, there were also differences in the observed climate-relations at each site (Figures III.2-3 in Appendix III). Firstly, the $\delta^{18}O_{TR}$ variations were influenced by climate during the main growing period of each site

which is during the dry season in the western Amazon site and during the dry-wet season transition in the central Amazon. Secondly, the regions of influence of large scale temperature and rainfall over the $\delta^{18}O_{TR}$ records also differed for each site.

Table 5.1. Strongest correlations of the $\delta^{18}O$ chronologies of all sites three sites with local and large-scale environmental variables. For each site, months in parenthesis indicate the growing season. Correlations are for the period 1980-2014. Asterisks indicate the significance levels <0.05*,<0.01**,<0.001***. All correlations shown are within the growing seasons of each site. Only correlations with climate during the growing season period are shown. For each site correlations with sea surface temperatures during months preceding the start of the growing period are also shown, when significant. Sea surfaced temperatures were averaged over the regions of the Tropical North Atlantic (TNA), Tropical South Atlantic (TSA) and Nino 3.4 region in the Tropical Pacific.

Climate Variable	Pearson's r	Season (months)
western Amazon (Jun-Dec)		
Local Temperature	0.43	Dry (Jul.Sep)*
Local rainfall	0.13	Dry(Jul-Nov)
Amazon-wide rainfall	-0.57	Dry (Aug.Oct)***
south and east Amazon Rainfall	-0.62	Dry (Jul.Oct)***
Amazon wide temperature	0.66	Annual mean***
Amazon River discharge in Obidos	-0.5	Annual minimum*
TNA sea surface temperature	0.47	(Feb.Jun)**
TNA sea surface temperature	0.52	(Jun.Oct)**
Nino3.4 sea surface temperature	0.39	(Feb.Jun)*
central Amazon (Sep-Feb)		
Local temperature	0.38	Dry-Wet (Oct.Feb)*
Local rainfall	-0.39	Dry-wet(Aug.Jan)*
Negro River levels in Moura	-0.42	Dry-Wet (Nov.Jan)*
north Amazon Rainfall	-0.4	Dry-wet (Sep.Nov)*
northeast Amazon Rainfall	0.49	Annual mean**
Amazon River level in Obidos	-0.48	Dry-Wet (Dec.Feb)*
TSA sea surface temperature	-0.41	(Feb.Jun)*
southwest Amazon (May-Nov)		
Local Rainfall	0.54	Dry (Jul.Nov)**
Local Temperature	-0.4	Jun.Sep*
south Amazon Rainfall	0.52	Jul.Nov**
Amazon wide temperature	-0.43	Jun.Aug**

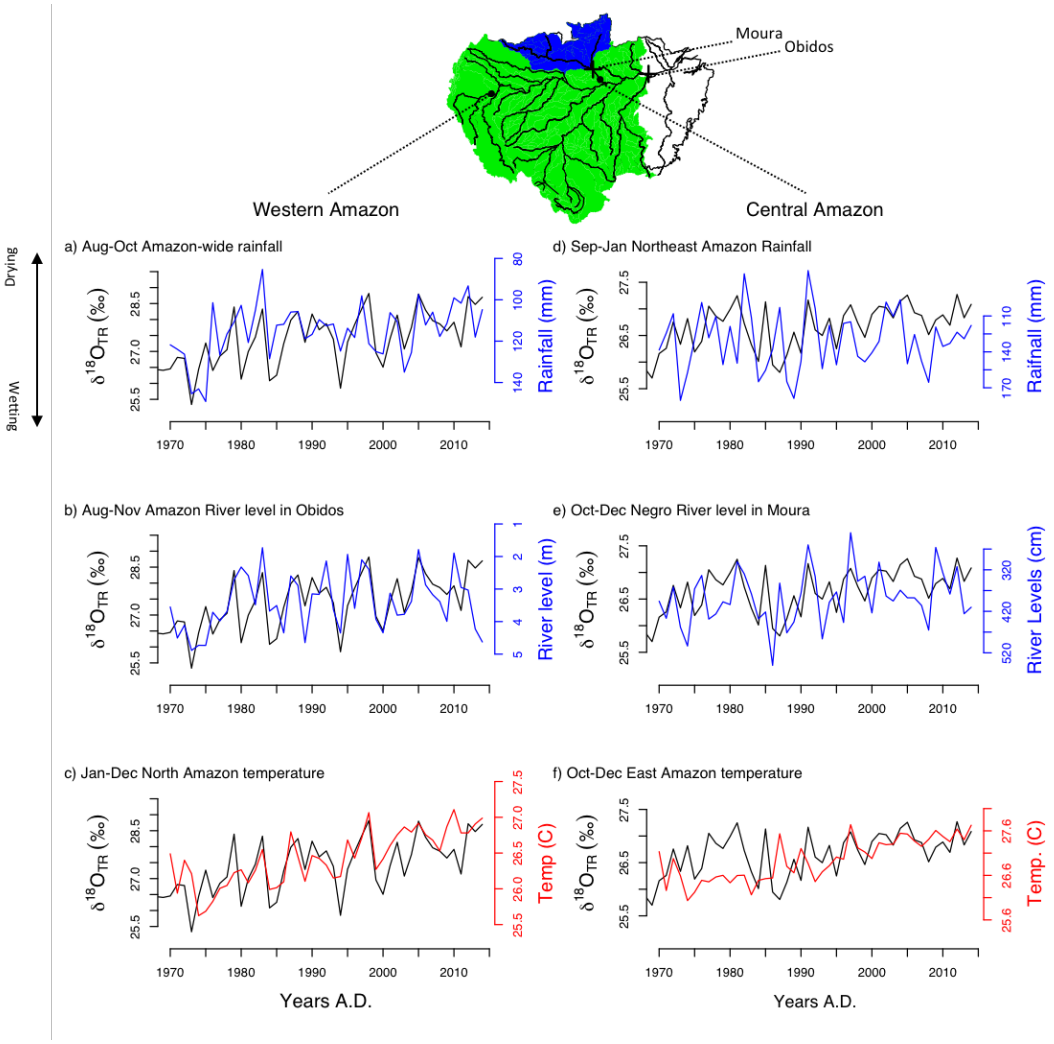

Figure 5.3. Comparison of the time series of the $\delta^{18}O_{TR}$ records from the sites in western (a-c) and central Amazon (d-e) with the environmental variables that showed the strongest correlation with them. Note the inverted axis of rainfall (a,d) and river levels (b,e), which are shown in blue. The map on top shows the location of the sampling sites (black dots), and the drainage areas of the Amazon river in Obidos (green area) and of the Negro River upstream from Moura (blue area).

These differences in the region of influence of the large-scale climate variables on the $\delta^{18}O_{TR}$ record of the central and western Amazon sites are evident in the spatial correlation maps produced for each site (Figure 5.4 and 5.5). However, for the site in central Amazon, they were only evident for the period from 1990-2014. In addition, the region of influence of rainfall on the $\delta^{18}O_{TR}$ record from this site is only evident when the long-term trend is removed from both the $\delta^{18}O_{TR}$ and the climatic data (Figure 5.4d and 5.5d), while the region of influence of temperature is only evident in the raw data (Figure 5.4e and 5.5e).

The differences in the region of influence of climate on the $\delta^{18}O_{TR}$ records from the western and central Amazon sites are also evidenced by the correlations with these records with river levels that integrate rainfall over large areas for these sites (Figures III.2-3 in Appendix III). The $\delta^{18}O_{TR}$ record from the site in central Amazon was more strongly influenced the river levels of the Negro River, which drains rainfall from the north of the Basin. In contrast, the $\delta^{18}O_{TR}$ record from the western Amazon site was more influenced by the river levels of the Amazon River which drains rainfall from the entire Basin (see Figure 5.3).

Surprisingly, the correlations found for the site in southwest Amazon have the opposite sign of the relation found for the other two sites. They were negatively affected by local and large-scale temperatures during the growing season (Figure III.4 in Appendix III), positively affected by local rainfall during the growing (dry) season. The negative influence of large-scale temperature on the $\delta^{18}O_{TR}$ from this site is evident in the spatial correlation maps (Figure 5.4 and 5.5b). The $\delta^{18}O_{TR}$ record from this site was also negatively affected by maximum rainfall during the previous wet season, at the end of the trees' flooded period.

5.3.3. Correlations with global sea surface temperature anomalies

We also found large-scale influences of tropical sea surface temperatures on $\delta^{18}O_{TR}$ for the western and central Amazon sites, but not for the southwest Amazon site. These correlations are shown in the spatial correlation maps between the $\delta^{18}O_{TR}$ records and sea surface temperatures (Figure 5.6). The spatial correlations of the $\delta^{18}O_{TR}$ record from western Amazon with Pacific SSTs showed a very clear El Niño Southern Oscillation influence, and in addition an influence of SST in the northern region of the Tropical Atlantic Ocean. The correlations with the ENSO region are most evident when the long-term trend is removed from the data (Figure 5.6a), while the correlation with the SST of the Tropical North Atlantic are most evident in the raw data without removing long-term trends (Figure 5.6b).

For the central Amazon site, the spatial correlation maps reveal a negative influence of the SST of the Tropical South Atlantic on the $\delta^{18}O_{TR}$. However, these influences were mostly evident when the long-term trends were removed from the data (Figure 5.7c), but not so much when the trends were present in the data (Figure 5.6d).

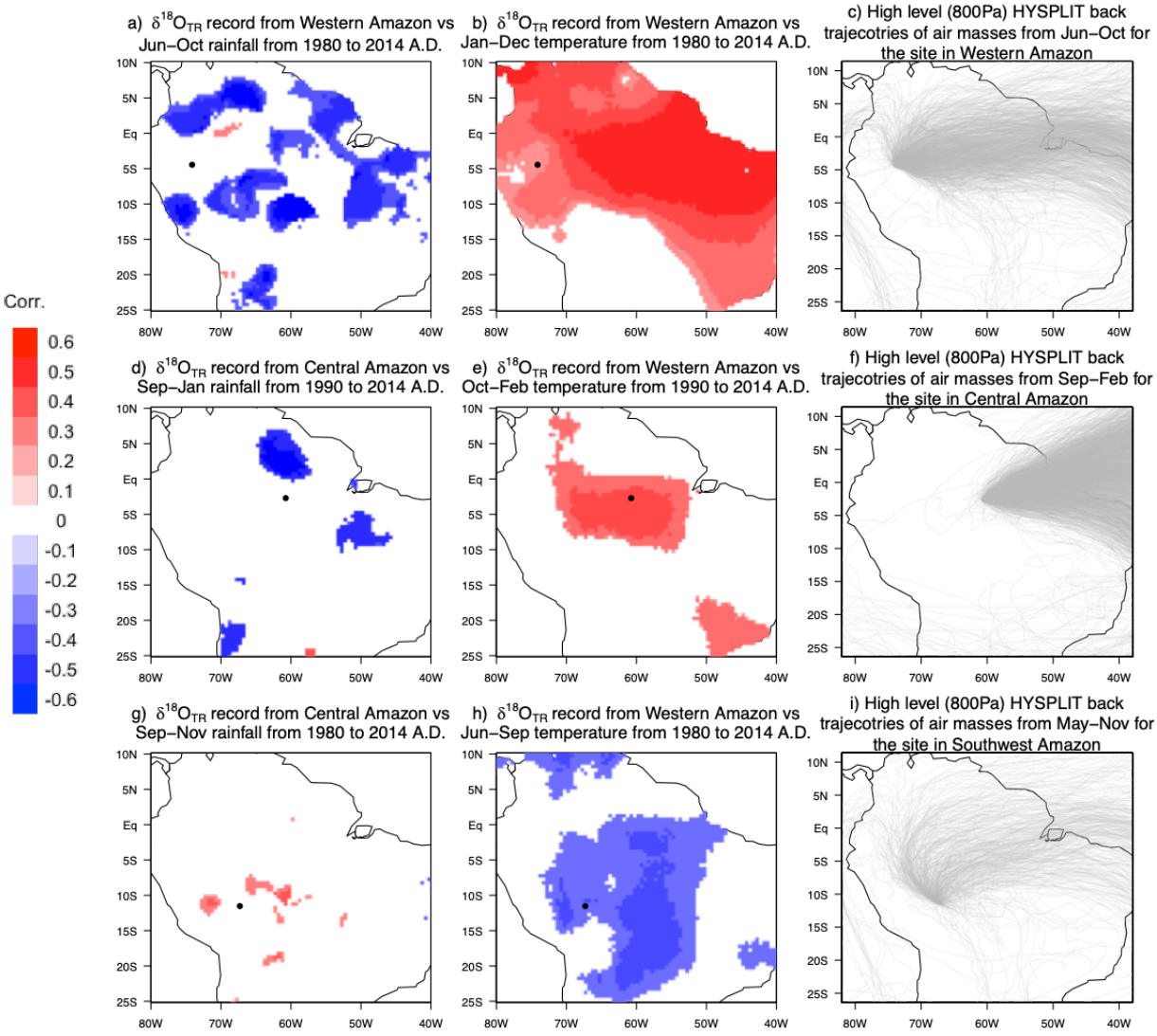

Figure 5.4. Spatial correlation maps of the $\delta^{18}O_{TR}$ of each site with gridded datasets of rainfall (left panels) and temperature (right panels) from CRU TS 4.00. Only significant correlations with 95% confidence level are shown. Only significant correlations are shown ($p<0.05$). (a-c) $\delta^{18}O_{TR}$ from southwest Amazon, (d-f) $\delta^{18}O_{TR}$ from western Amazon and (g-i) $\delta^{18}O_{TR}$ from central Amazon. Note that for the site in central Amazon the correlations are shown for the period from 1990-2014 A.D. Prior to that period, the correlations did not show any evident spatial pattern for this site.

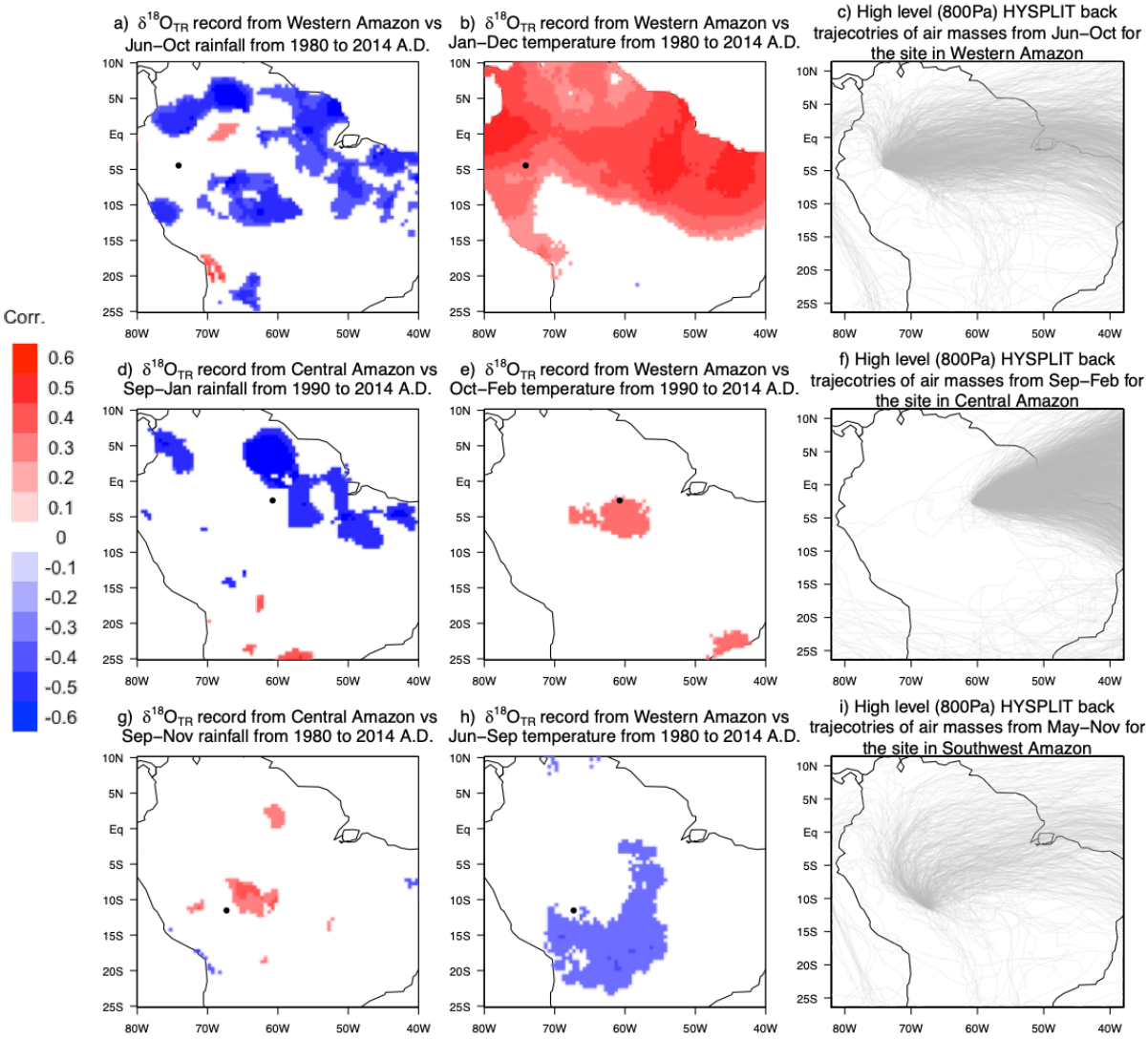

Figure 5.5. Same as Figure 5.4, but removing the long term from both the $\delta^{18}O_{TR}$ records and the climate data.

5.3.1. Sensitivity of the Long-term trends in the $\delta^{18}O$ series to leaf water enrichment

The $\delta^{18}O_{TR}$ records show variations of up to 2‰ on decadal time scales over the last 30 years (Figure 5.2 and 5.3). These decadal-scale trends may result from changes in the source water signal caused by changes in the hydrological cycle, or arise from changes in leaf water enrichment (above source water) due to plant physiological responses to local climate and or atmospheric carbon dioxide concentrations. Specifically, increasing concentrations of atmospheric CO_2 could lead to down-regulation of stomatal conductance (Morison, 1985; Eamus et al., 1993; Ainsworth

and Rogers, 2007; Lammertsma et al., 2011; Cernusak et al., 2011; Franks, 2013; Cernusak et al., 2013; Sleen et al., 2017), and thus affect plant transpiration and leaf water enrichment (e.g. Figure 3.2 in Chapter 3). To help elucidate the possible causes for the long-term trends in the $\delta^{18}O_{TR}$ records, we have compared them to the modelled $\delta^{18}O_{TR}$ trends based on changes in local climate conditions and in changes in g_s.

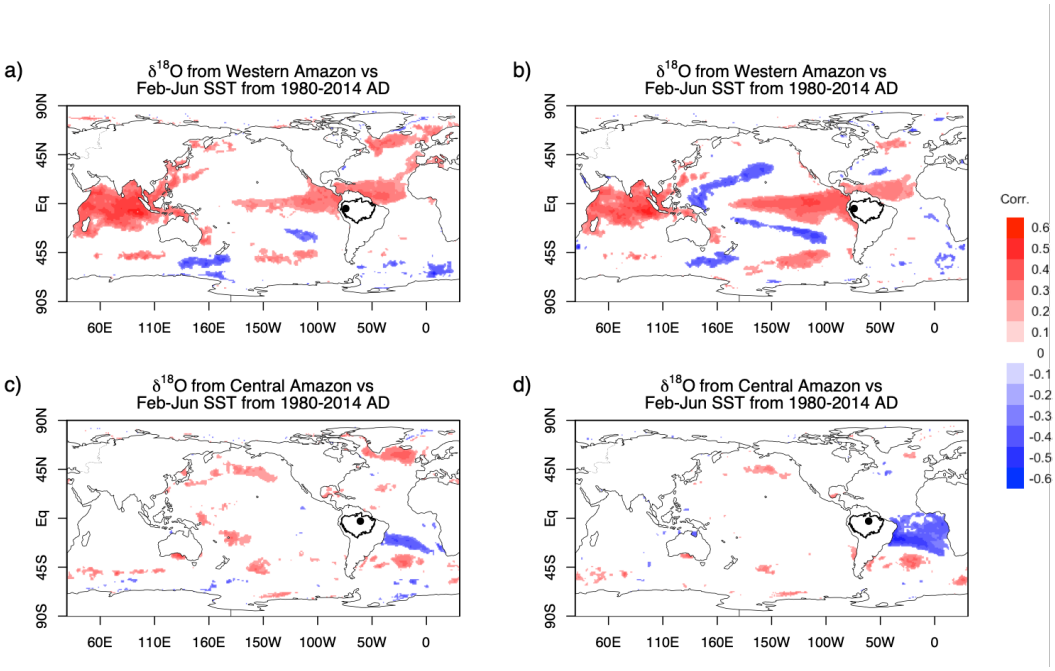

Figure 5.6. Spatial correlation maps of the $\delta^{18}O_{TR}$ records of each site with sea surface temperatures (SST) from Had Climatology. (a,b) western Amazon, (c,d) central Amazon. Correlations the long term trend removed are shown in the left panels, and correlations using the raw data are shown in the right panels. Only significant correlations at the 95% confidence interval are shown.

At all three sites we observed increases in temperature over the period from 1965 to 2014 A.D., while the relative humidity (which is temperature dependent) remained the same. For all three sites, the modelled trends based only on the changes in climate are of smaller magnitude than the observed $\delta^{18}O_{TR}$ trends over the analyzed periods (Figure 5.7b,d,f). Reducing g_s by 20% results in larger increases in $\delta^{18}O_{TR}$ for all sites, but for sites from western and central Amazon predicted trends are still smaller than observed trends in $\delta^{18}O_{TR}$ (Figure 5.7bf). For the site in southwest Amazon, 20% g_s reduction leads to a trend in the opposite direction of the observed, because the observed $\delta^{18}O_{TR}$ trend at this site is negative (Figure 5.7d). These results

may be sensitive to the various assumptions used in the isotope model. For example, one of the factors influencing the magnitude of leaf water enrichment is the effective path length — for water movement from of the veins to the stomata in the leaves see section 3.2.2 in Chapter 3) . A change of the path length (from 0.05m to 0.01m) made however very little difference to the outcome of the predictions (see Figure III.5 in Appendix III for a path length of 0.01m).

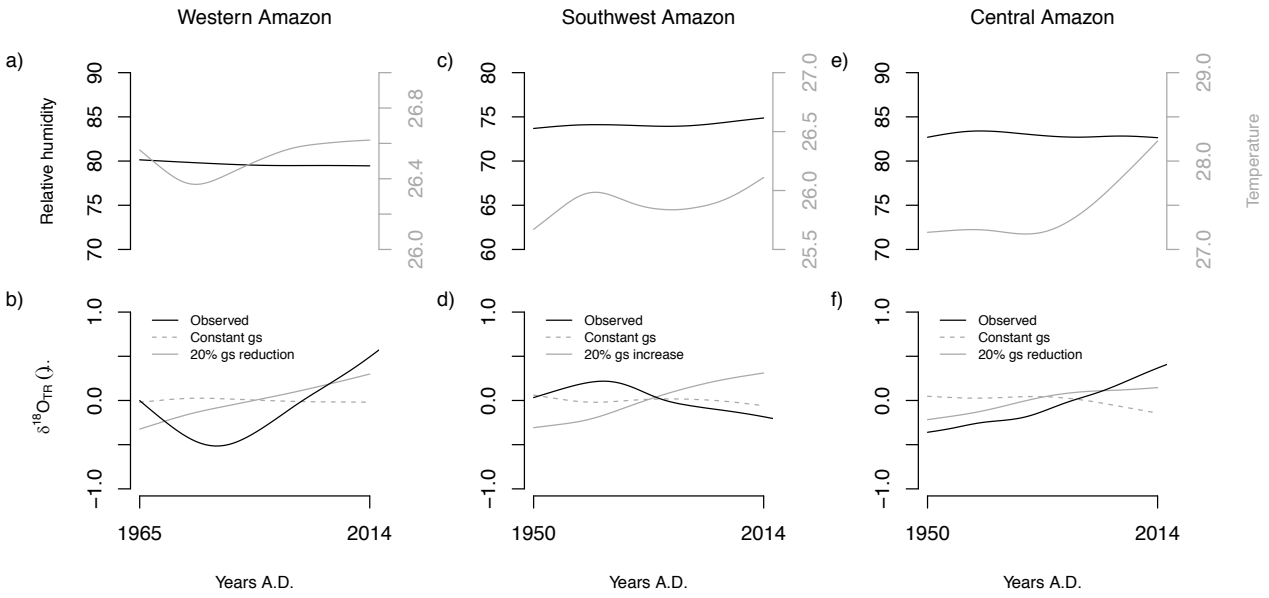

Figure 5.7. Predicted vs observed trends in tree ring $\delta^{18}O$ at each of the sampled sites. (a,b) Site from Peru, (b,c) site from Bolivia, (c,d) site from Brazil. Top panels (a,c,e) show changes in relative humidity and temperature during the periods for which trends are observed in the tree ring $\delta^{18}O$. Bottom panels (b,d,f) show the observed trends in tree ring $\delta^{18}O$ (black lines), and the predicted trend (grey lines) modelled with tree-ring-isotope models.

5.4. Discussion

In the following sections we will first discuss the observed climate influences on each of the $\delta^{18}O_{TR}$ records, and then discuss the implications of the long-term trends observed in the $\delta^{18}O_{TR}$ of each site.

5.4.1. Climate influences on the inter-annual $\delta^{18}O_{TR}$ variations since 1980 A.D – western and central Amazon sites

Our results show that the $\delta^{18}O_{TR}$ records of the sites from western and central Amazon are mainly negatively influenced by the amount of rainfall and river

levels/discharge, and positively influenced by local and large-scale temperature variations in the Amazon Basin (Figures 5.4 and 5.5). These results are consistent with our findings from Chapter 3. While the influence of local temperature suggest these records may reflect leaf water enrichment effects to some extent, the close relations with large scale hydrology suggest these records are also strongly associated with variations in plant source-water $\delta^{18}O$, which is in turn affected by precipitation amounts and Rayleigh rainout processes upwind from the sampling site (Salati et al., 1979; Vimeux et al., 2005; Vuille and Werner, 2005). The influences of large-scale hydrology on tree ring $\delta^{18}O$ are consistent with our expectations, and in line with previous studies (Brienen et al., 2012; Baker et al., 2016). Additional support for this interpretation can obtained looking at the regional influences of climate found on $\delta^{18}O_{TR}$ at each of these sites, which match approximately the region of the trajectories of air mass from the Ocean to each of the sampling sites (Figure 5.4 and 5.5). Note also that the trajectories of the air masses from the Ocean to western Amazon cover a wide area within the Basin and comprise the entire area covered by the trajectories to the central Amazon site. This is possibly the reason why the spatial correlation maps reveal a wider the region of influence of climate on the $\delta^{18}O_{TR}$ of the western Amazon site, which integrates almost entirely the region of climate influences on the $\delta^{18}O_{TR}$ record from the central Amazon site.

5.4.2. Climate influences on the inter-annual $\delta^{18}O_{TR}$ variations of the southwest Amazon site

Our results from the site in southwest Amazon were inconsistent with our expectations, and even showed the opposite relationships from expected as the $\delta^{18}O_{TR}$ was positively influenced by local rainfall and negatively influenced by temperature (Figure 5.4, 5.5 and Figure III.4 in Appendix III). However, the $\delta^{18}O_{TR}$ from this site shows also a negative influence of large-scale rainfall over south-eastern Amazon during the end of the wet season (preceding the growing season), and by local and large-scale maximum monthly rainfall from the previous wet season (Figure III.4e,g,h in Appendix III). These negative influences of previous wet season

rainfall are consistent with the effect of rainfall amount on $\delta^{18}O_{TR}$ in rain. This signal from the preceding rainy season then be transferred to the tree rings due to a lagging effect between actual rainfall and runoff to river water, and the subsequent use of river water by trees after flood levels have receded. As there is very little rainfall during the dry season at this site, river water left in the soils after the river levels recede may indeed be the only or main source of water available for these trees. That is not necessarily the case for the trees from the western and central Amazon sites, where there is much more rainfall during the dry season, and thus trees may use mainly water derived from dry season rainfall.

Additional support that the $\delta^{18}O_{TR}$ from the southwest Amazon site indeed reflects wet season rainfall $\delta^{18}O$ to some extent can be obtained by comparing it with the $\delta^{18}O_{TR}$ record from a non-flooded tree species that grows in a nearby site, which is closely related to wet season rainfall $\delta^{18}O$ (Brienen et al. 2012, Baker et al. 2015).

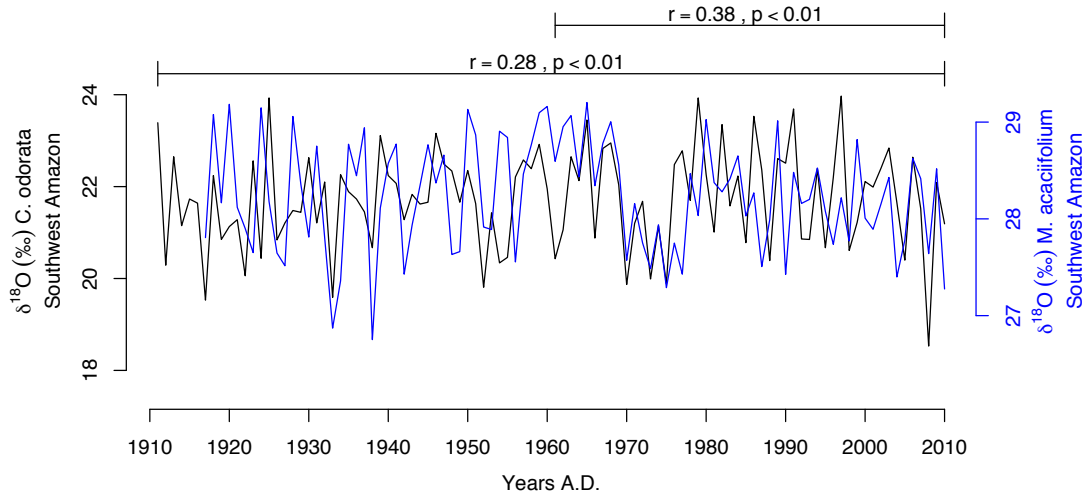

Figure 5.8. Comparison of the $\delta^{18}O_{TR}$ record of *M. acaciifolium* trees from southwest Amazon floodplain forests (blue line) and the $\delta^{18}O_{TR}$ record of *C. odorata* trees from southwest Amazon terra firme forests (black line, Brienen et al., 2012). The correlation between these two records is indicated above for two different intervals, 1910 to 2010 and 1960 to 2010 A.D.

The two records show some remarkable similarities (Figure 5.8), but their correlation coefficient is actually much lower than expected. This low correlation can possibly arise from (1) the influence of remobilization of carbohydrates from previous year to

the $\delta^{18}O_{TR}$, or (2) by methodological issues related to the dating of the tree rings from the southwest Amazon site, which could also lead to the unexpected positive correlations with rainfall (see Figure 4.3 from Chapter 4). In all, we cannot reach a solid conclusion about the climate influences on $\delta^{18}O_{TR}$ record from the western Amazon site, especially because the positive influences of rainfall on the $\delta^{18}O_{TR}$ from this site remains a puzzle. Therefore, we will now focus the remainder of the discussion on the long term trends from the western and central Amazon sites.

5.4.3. Long term trends in the $\delta^{18}O_{TR}$ of the western and central Amazon sites

The $\delta^{18}O_{TR}$ records of the sites in western and central Amazon both show an increasing trend of up to 2‰ over the past 30-50 years. Such trends can arise both from long-term changes in (1) plant source water $\delta^{18}O$, or (2) from changes in leaf water enrichment. Our modelling approach of the expected effects of plant physiological effects on the leaf water enrichment at these sites suggests that very large reduction of 35-50% in plant stomatal conductance (g_s) would be necessary to explain the long-term trends in $\delta^{18}O_{TR}$ (Figure 5.7). Possible mechanisms that would allow for such g_s reductions are changes in climate and increases in atmospheric CO_2.

The most important climate factor that may affect g_s and thus $\delta^{18}O_{TR}$ is the temperature dependent relative humidity (Barbour, 2007). As the local relative humidity in our sites has remained stable/does not show long term trends over the entire period (Figure 5.7), it is unlikely that local climate conditions have led to a long term reduction in g_s of this magnitude. Alternatively, down regulations of plant stomatal conductance (g_s) caused by increasing atmospheric CO_2 concentrations are another possible cause for the observed $\delta^{18}O_{TR}$ trends in the sites from central and western Amazon. Evidence from sub-fossil leaf material (Lammertsma et al., 2011) and from carbon isotope measurements in tree-rings of tropical trees (Sleen et al., 2015) suggest that increasing atmospheric [CO_2] could have led to a long-term down-regulations of g_s over the past 150yr. However, under such a scenario of a CO_2 induced change in g_s affecting the long-term trends in $\delta^{18}O_{TR}$ at our sites, we would

expect to continuous increases in $\delta^{18}O_{TR}$ over the full record, which is not the case (Figure 5.7). The observed increasing $\delta^{18}O_{TR}$ trends only start from ca. 1950 and 1970 for the sites in central and western Amazon, respectively. Prior these periods, the $\delta^{18}O_{TR}$ trends were declining (Figure 5.2). Moreover, carbon isotope ratios in tree rings (Sleen et al., 2015) and free air [CO_2] fertilization experiments (Wullschleger et al., 2002; Ainsworth and Rogers, 2007; Cernusak et al., 2011; Cernusak et al., 2013) suggest that g_s would not be reduced by more than 35% per 100ppm CO_2 increase. From 1960 to 2014 A.D., atmospheric [CO_2] increased by about 85ppm. Thus, we would expect to see g_s reductions of approximately 30% - although there may be a lot of variation between species (Lammertsma et al., 2011). To reproduce the increasing trends observed in the sites from western and central Amazon, larger g_s reductions in the order of 35-50% during the last ~ 50 years would be necessary.

In all, comparison of our modelling approach and the observed $\delta^{18}O_{TR}$ trends suggests that it is unlikely that the observed long-term $\delta^{18}O_{TR}$ trends in the western and central Amazon sites are caused by leaf water enrichment related to long-term changes in local climate or due to g_s reductions in response to atmospheric CO_2 growth. As we have shown that the $\delta^{18}O_{TR}$ records from these two sites are closely associated with large scale climate signals via $\delta^{18}O$ in plant source water, the long term trends in $\delta^{18}O_{TR}$ seem to primarily reflect changes in plant source water $\delta^{18}O$ and are thus indicative for changes in the hydrological cycle. The implication of this result are discussed in the next section.

5.4.4. Implications of the observed $\delta^{18}O_{TR}$ trends for large-scale climate in the Amazon

If the increasing $\delta^{18}O_{TR}$ trends observed for the sites in western and central Amazon are indeed influenced by changes in plant source water $\delta^{18}O$, then the records suggest a generally drying and warming trend during the trees' growing seasons since approximately 1950-1970.

Surprisingly, the increasing $\delta^{18}O_{TR}$ trend is more pronounced in western Amazon (Figure 5.7), where $\delta^{18}O_{TR}$ is most strongly influenced by dry season climate. As we find a close association between the $\delta^{18}O_{TR}$ record from the western Amazon site and rainfall/Amazon river levels during the dry season, the $\delta^{18}O_{TR}$ trend in this record is a strong indication of a drying trend during the dry season in the Amazon.

In contrast, the $\delta^{18}O_{TR}$ trend is less pronounced in the record from central Amazon. As the growing season in this site is during the transition season, this $\delta^{18}O_{TR}$ record is also influenced by rainfall during the start of the rainy season. The influence of early wet season rainfall is one possible cause for the less pronounced trend in the $\delta^{18}O_{TR}$ record from central Amazon. Nonetheless, this record does show an increasing trend, which can arise either from a dominant signal of dry season climate on this record, or may signify that climate during the transitional season is also becoming slightly dryer and warmer, possibly as a consequence of a long-term lengthening of the dry season in the Amazon.

Another possible explanation for the difference in the slope of the $\delta^{18}O_{TR}$ trends of the central and western Amazon sites may be related to the spatial differences in the region of climate influences observed for each site (Figures 5.4 and 5.5). The $\delta^{18}O_{TR}$ from the site in central Amazon is more strongly influenced by rainfall in the Negro basin and in the northeast of the Amazon (Figure 5.3). In contrast, the $\delta^{18}O_{TR}$ record from the western Amazon site is more influenced by rainfall in most of the Amazon region (Figure 5.4 and 5.5). Thus, it is possible that the different trends in $\delta^{18}O_{TR}$ of each of these records reflect differences in climatic trends between geographical regions in the Basin.

The possible differences in both the regional and seasonal influences of climate in the $\delta^{18}O_{TR}$ trends of each of these sites would be somewhat consistent with recent changes in the hydrological cycle of the Amazon Basin. Such recent changes show generally increasing rainfall during the wet season of the north and northwest of the Basin, while the dry season south of the Amazon has become slightly drier (Gloor et

al., 2013; Gloor et al., 2015; Barichivich et al., 2018) and possibly longer (Fu et al., 2013; Marengo and Espinoza, 2015). Climate observations in the Amazon suggest that there may have been small reductions in rainfall during the 3 driest months in the order of 100mm from 1990-2010, and mostly in the central, east and south of the Basin (Gloor et al., 2013, their Figure 3a; Gloor et al., 2015, their Figure 3). The magnitude of such observations is similar to the climatic trends observed in this study and reflected in the $\delta^{18}O_{TR}$ record from western Amazon.

In all, these results from the western and central Amazon sites reveal the potential of using these records to assess long term trends in the climate of different regions and during different seasons in the Amazon. The $\delta^{18}O_{TR}$ of different sites seems to reflect climate during the trees' growing seasons, which is not exactly the same in floodplains of different regions in the Amazon. Nevertheless, our results suggest a dominant signal of dry season climate and low river levels in the in the $\delta^{18}O_{TR}$ records of western and central Amazon floodplains. This contrasts with the climatic in the $\delta^{18}O_{TR}$ records from non-flooded forests, for example records of *Cedrela odorata* trees, which show a dominant signal of wet season climate and high river levels (Brienen et al., 2012, Baker et al., 2015).

5.4.5. Possible effects of large scale temperature on the $\delta^{18}O_{TR}$ records

We also find influences of large-scale temperature variations on these records (Figures 5.4 and 5.5), which is surprising as temperature variations are not thought to be an important driver of inter-annual rainfall $\delta^{18}O$ in the Amazon (Vimeux et al., 2005) or in other tropical areas (Schubert and Jahren, 2015). Temperature has increased by approximately 2 ^{o}C over the period for which we observe an increase in $\delta^{18}O_{TR}$ (Figure 5.4 and 5.5). These persistent increases in temperature could nonetheless affect the ^{18}O fractionation during the condensation of rain drops, weaken the condensation of heavy water (with respect to normal water) and weaken Rayleigh rainout effects resulting in long term increases in rainfall $\delta^{18}O$ at the end of water vapour trajectories. Thus, we cannot rule out that the observed trends in

$\delta^{18}O_{TR}$ in the records from central and western Amazon may reflect long term increases in large-scale temperature over the Amazon.

In addition, large-scale changes in temperature could affect the $\delta^{18}O_{TR}$ records indirectly by affecting the large-scale rainfall recycling through evapotranspiration from the forest, which can also influence the $\delta^{18}O$ in rainfall (Salati et al., 1979). The forest's evapotranspiration is an important source of rainfall in the Amazon, especially during the dry season (Salati et al., 1979; Spracklen et al., 2012; Zemp et al., 2014; Spracklen and Garcia-Carreras, 2015). Rising temperatures increase the saturated vapour pressure of the air, leading to increased vapour pressure deficit. Increasing vapour pressure would lead to higher transpiration if plants do not adjust g_s, but it is generally observed/expected that due to water stress during the dry season, plants will limit water loss by reducing g_s and transpiration (Cox et al., 1998). Thus, it is possible that, to some extent, the increasing trends in the $\delta^{18}O_{TR}$ records from the western and central Amazon sites reflect changes in the forest evapotranspiration caused by g_s reductions of the forests in response to large-scale temperature changes in the Amazon.

5.4.6. Influences of global sea surface temperatures

Additional insights on the long term $\delta^{18}O_{TR}$ trends observed in the western and central Amazon may be gained from the spatial correlation maps of the $\delta^{18}O_{TR}$ of these sites with sea surface temperatures. The maps of spatial correlation between the $\delta^{18}O_{TR}$ record from the western Amazon site and sea surface temperatures show influences of SSTs of both the Pacific and of the Tropical North Atlantic Region (Figure 5.6). The influence of SST's in the Pacific are more pronounced when the long-term trends in the data are removed from both the SST data and the $\delta^{18}O_{TR}$. Thus, it seems that the inter-annual variability of this $\delta^{18}O_{TR}$ record may be mainly influenced by the effects of Pacific SSTs on Amazon climate, more specifically by El Niño and La Niña events. On the other hand, the influence of the SST of the Atlantic is most pronounced in the long-term trend (Figure 5.6). It is interesting that this increasing $\delta^{18}O_{TR}$ trend in the western Amazon site only started after roughly 1980, which

coincides with the start of a pronounced increase in SST of the Tropical North Atlantic (Gloor et al., 2013). In addition, sea surface temperatures of the Tropical North Atlantic are known to influence climate in the Amazon mainly during the dry season and over the southern portion of the Basin (Yoon and Zeng, 2010), which is consistent with the region and season of climate influences on the $\delta^{18}O_{TR}$ from this site (Figure 5.4 and 5.5). (Gloor et al., 2013; Barichivich et al., 2018). A long term warming of the SST in the Tropical North Atlantic Ocean could indeed lead to warmer temperatures or reduced rainfall amounts during the dry season in the Amazon, which could lead to increased source water $\delta^{18}O$ and thereby affect the $\delta^{18}O_{TR}$ records. Thus, the long-term increase in $\delta^{18}O_{TR}$ from the western Amazon site is consistent with the expected effects of increasing temperatures in the Tropical North Atlantic Ocean on climate during the dry season in the Amazon.

In contrast, the $\delta^{18}O_{TR}$ record of the central Amazon site seems to be mainly influenced by the SSTs of Tropical South Atlantic region (Figure 5.6), which is known to affect climate mainly in southeast South America and in part of northeast Amazon (Yoon and Zeng, 2010). In the study from Yoon and Zeng (2010), their Figure 8 shows a similar pattern to the observed in the correlations of the $\delta^{18}O_{TR}$ of central Amazon with rainfall (Figure 5.5d). Thus, it is possible that influences of sea surface temperatures found for this site arise from the influence of the sea surface temperatures of the Tropical South Atlantic on the rainfall over the catchment area of the Negro River.

5.5. Conclusions

We analyzed interannual and long-term variations of oxygen isotope ratios in the tree rings of *M. acaciifolium* trees from three floodplain sites located in western, southwest and central Amazon. We expected that the $\delta^{18}O_{TR}$ records would be related to climate conditions during the dry season, and possibly allow for an assessment of the evolution of dry season Amazon precipitation over the past century. Our results revealed some potential for this approach but also leave some unanswered questions.

The observed climate influences on the $\delta^{18}O_{TR}$ from the sites in central and western Amazon are largely consistent with our expectations. They are both negatively influenced by large-scale rainfall upwind from the sampling sites and positively influenced by local and large-scale temperatures. Our results suggest that while these records may be to some degree influenced by temperature effects on leaf water enrichment, the main control seems to be variation in plant source water $\delta^{18}O_{TR}$. In contrast, our results from the southwest Amazon site were not consistent with our expectations and cannot be explained mechanistically at the moment.

One of the most distinct features of the $\delta^{18}O_{TR}$ records analyzed here is that they all present decadal variations of up to 2‰ over the last 50 years. Our analyses suggest that, at least in the sites from western and central Amazon, these trends are not so much related to plant physiological effects over leaf water enrichment, and more likely reflect a drying trend during the dry season of the south and east of the Amazon. Such drying trend is observed in the data and is consistent with previous studies that suggest the dry season in the south of the Amazon is possibly becoming drier (Fu et al., 2013; Gloor et al., 2013; Marengo and Espinoza, 2015). Our results also suggest that the sea surface temperatures of Tropical North Atlantic may play a central role in these climate changes.

Chapter 6 **Synthesis and Conclusions**

In this thesis I examined whether/how floodplain tree-ring data could improve our understanding of past variability of two aspects of the hydrological cycle in the Amazon, the length and intensity (i.e. amount of rainfall) of the dry season. I did this combining ring-width and oxygen isotope ratios in the tree rings of the floodplain tree species *Macrolobium acaciifolium* as a proxy for past variability of the dry season length over the drainage basin of different Amazonian rivers (e.g. Schöngart et al., 2004) and for large-scale dry season climate conditions (i.e. precipitation amounts, e.g. Brienen et al. 2012; Baker et al. 2015). My focus was on the dry season because it is one of the key controls of forest vegetation (Malhi et al., 2008), influencing tree mortality rates and thereby the Amazon carbon balance (Lewis et al., 2011; Philips et al., 2009), and because climate observations in the region suggest that the dry season is becoming dryer and longer, especially in the south of the Amazon (Fu et al., 2013; Gloor et al., 2013; Marengo et al., 2015; Spracklen and García-Carreras, 2015; Barichivich et al., 2018). This is the first time that isotope ratios of tropical tree rings were used to obtain information about past dry season conditions, and thus the records presented in this thesis are unique in this regard. For this reason, it was also necessary to make a thorough assessment of the potentials and limitations of using these records, which were explored in the Chapters 3 and 4 of this thesis.

In the Chapter 3 of this thesis, I first explored in detail what type of information can be obtained from the oxygen isotopes ($\delta^{18}O$) in the tree rings of *Macrolobium acaciifolium*. This was done by comparing the intra-annual isotopic ratios of both $\delta^{18}O$ and carbon isotope ratios ($\delta^{13}C$). Specifically, it was expected that *M. acaciifolium* tree rings would carry mainly a dry season rainfall $\delta^{18}O$ signal, which would complement other tree-ring records from terra firme tree species (see Brienen et al. 2012, Baker et al., 2015). In the Chapter 4 of this thesis, I then explored the potential of using ring-width chronologies of *M. acaciifolium* from different regions within the Amazon Basin to reconstruct past climate variability for the terrestrial phase of the

trees. The research conducted in Chapter 4 builds up on the pioneering tree ring work with floodplain tree species from central Amazon (Schöngart et al., 2004; Schöngart et al., 2005), and expands to other regions within the Basin. The main purpose here was to examine the potential of floodplain ring-widths of floodplain trees growing in different regions and climatic/flooding conditions to reconstruct past variability of river levels and the length of the dry season over the river's catchment area. Finally, in Chapter 5 of this Thesis I constructed tree ring $\delta^{18}O$ chronologies from chronologies revealed the potential of this approach to reconstruct past dry season climate variation in the Amazon. In the next section, I will detail the main findings of each of these Chapters, and then discuss the main implications of my findings, and the possibility for additional research to improve this field.

6.1. Contrasting controls on tree ring isotope variation for Amazon floodplain and terra firme trees

In Chapter 3 I examined the of the main controls of seasonal variation in $\delta^{18}O$ variation in the tree rings of *Macrolobium acaciifolium* from seasonally flooded forests, and compared these with the controls of the $\delta^{18}O$ in the tree rings of *Cedrela odorata* from non-flooded environments, which records mainly wet season rainfall $\delta^{18}O$ (Brienen et al., 2012; Baker et al., 2015; Baker et al., 2018). The study consisted in the analysis of the co-variations of oxygen and carbon isotope ratios within tree rings (i.e. intra-ring variations) as a measure of the strength of leaf physiological effects on both isotopes (Scheidegger et al., 2000; Roden and Siegwolf, 2012; Barbour and Song, 2014). In addition, I used a modelling approach to compare the observed variations of the isotope ratios within the tree rings with model predictions of the expected effects of source water $\delta^{18}O$ variation leaf physiology on the isotope ratios in the tree rings (Barbour, 2007; Sternberg, 2008). This combination of a dual-isotope (Scheidegger et al., 2000) and modelling approaches permitted to evaluate in detail the relative contributions of source water $\delta^{18}O$ and leaf water enrichment for trees growing in different environmental conditions. The results of these analyses supported previous studies that suggest that $\delta^{18}O$ in tree rings of *C. odorata* mainly

reflect source water $\delta^{18}O$, and show that the $\delta^{18}O$ in the tree rings of *M. acaciifolium* are more strongly affected by leaf water enrichment than *C. odorata* likely due to differences in plant physiological responses and local climate conditions during the growing season. I then made a first exploration of the climate signals recorded $\delta^{18}O$ in the tree rings of *M. acaciifolium*. This showed that the average $\delta^{18}O$ the tree rings of *M. acaciifolium* recorded local climate influences on leaf water enrichment, especially in sites where the dry season is longer and drier. This analysis also revealed that different climate signals may be recorded in different parts of the tree rings. Specifically, $\delta^{18}O$ of specific tree ring segments *M. acaciifolium* trees growing in wetter conditions recorded large-scale climate signals that likely originates from plant's source water $\delta^{18}O$.

6.2. Are the tree rings of *Macrolobium acaciifolium* trees from floodplain forests good proxies for past climate variability in the Amazon Basin?

In Chapters 4 and 5, I explored the potential of using ring-width and oxygen isotopes chronologies of *M. acaciifolium* as proxies for past climate conditions during the tree's growing seasons. For these Chapters, I sampled wood cores from approximately 140 trees located in three sites in western Amazon (Peru), southwest Amazon (Bolivia) and central Amazon (Brazil). To develop the ring-width chronologies, the wood anatomy and ring-widths of all samples were analyzed. Correct dating and measuring of the ring-widths of *M. acaciifolium* was challenging because most of the trees presented frequent false rings. Because of the presence of false rings, it was necessary to verify the ages of the tree rings by analyzing the bomb-peak radiocarbon ages of the tree rings. The estimated ages by cross-dating the ring-widths matched closely with bomb-peak radiocarbon ages of the wood in the tree rings. This analysis confirmed that the tree rings of *M. acaciifolium* were mostly dated correctly, which is a prerequisite for their use as proxies for past climatic variability. However, these analyses also revealed that the tree ring series may present dating errors of 1 in 30 years. I then selected a subset of 7-8 samples per site for oxygen

isotope analysis and to explore their potential as proxies for past dry season climate variability in the Amazon. Despite these possible dating errors present in the tree rings, both the ring-width and isotopes records from each site reflected climate variability during the tree's growing seasons, but with differences between the three sites. For this reason, I will now summarize the findings of each of the sites separately.

6.3. Tree ring records from the western Amazon site

The trees from the western Amazon site revealed the best potential for reconstruction of past dry season climate variability. As the trees for this site grow mainly during the dry season, it was expected that their tree rings would reflect past variability of dry season climate. The ring-widths of most of the sampled trees from this site could be crossdated, and the main driver of tree growth in this site is the length of the terrestrial phase of the trees, which had a positive effect on the ring-widths. While the ring-width chronologies reflect the local hydrological variability during the tree's growing seasons, the $\delta^{18}O_{TR}$ chronology from this site reflected past dry season climate over large-areas in the Amazon, especially in the south of the Basin. This result is consistent with our findings from the analyses of Chapter 3, which indicates that $\delta^{18}O_{TR}$ of *M. acaciifolium* trees growing in wetter conditions may reflect the $\delta^{18}O$ of the source water used in the tree rings, which in turn reflects the total precipitation along the trajectory of air parcels over the continent (Salati et. al., 1979, Vuille and Werner, 2005; Vimeux et al., 2005; Baker et a., 2016). This $\delta^{18}O_{TR}$ chronology also presents a long term trend of up to 2 ‰ which seems to mainly related to a drying trend in the south of the Amazon Basin. This result is consistent with recent observations which suggest a long term decrease in rainfall during the dry season in the Amazon (Fu et al., 2013; Gloor et al., 2015). Interestingly, both the $\delta^{18}O_{TR}$ and the ring-widths of the trees from this site seem to be influenced by sea surface temperatures of the Atlantic Ocean. The ring-widths of the trees from this site are closely related to the Atlantic Multidecadal Oscillation index, and their $\delta^{18}O_{TR}$ reflects the sea surface temperatures of the Tropical North Atlantic Region. While

these two measures are not the same, these results are consistent with the central role to the SST of North Atlantic Ocean for the dry season climate of the Amazon Basin (Barichivich et al., 2018).

6.4. Tree ring records from the central Amazon site

Crossdating the tree rings from the site in central Amazon site was not as successful as for the other sites. Approximately 50% of the trees could not be cross-dated, which shows the limitation of this approach due to the presence of false rings in these trees. The ring-widths from this site were also not affected by the length of the terrestrial phase, and showed only weak negative effects of river levels. This is the most surprising results of the analyses from Chapter 4, as it is not consistent with previously published ring-width chronologies from central Amazon floodplains (Schöngart et al., 2004; Schöngart et al., 2005). The reason for the lack of a clear environmental signal in the ring-with record from this site remains unclear, but probably reflects, at least partially, the weak cross-dating of the ring-widths of this site. Despite this lack of a clear climate signal in the ring-width record, the radiocarbon analysis indicate that the tree rings from this site are as well dated, and the $\delta^{18}O_{TR}$ record from this site revealed significant influenced of large-scale climate conditions. The climate influences in the $\delta^{18}O_{TR}$ record of this site were similar to the results for the western Amazon site, but the long term trend in the $\delta^{18}O_{TR}$ record from this site was not as pronounced in as in the western Amazon site. This is probably because the $\delta^{18}O_{TR}$ record from this site reflects mainly past climate conditions during the transition from the wet to the dry season, which corresponds to the growing season at this site. As climate observations in the Amazon suggest opposing trends during the wet and dry seasons (Gloor et al., 2013; Gloor et al., 2015), it is possible that rainfall during the growing season at this site shows no long-term trend. On the other hand, it is noteworthy that the $\delta^{18}O_{TR}$ record from this site does actually present an increasing trend, which could be consistent with previous studies that suggest a lengthening of the dry season (Fu et al., 2013; Marengo et al. 2015). However, the analyses carried out in this Thesis do not allow to for a conclusion with

this regard. In all, the results of the $\delta^{18}O_{TR}$ record from are consistent with the results from the $\delta^{18}O_{TR}$ record from western Amazon site, and the long-term increasing trends in the $\delta^{18}O_{TR}$ records from both these sites likely reflect a dry trend during the dry season in the Amazon.

6.5. Tree ring records from the southwest Amazon site

The results of the tree ring records from the southwest Amazon also showed potentials and limitations for their use as proxies for past climatic variability. The main potential revealed for records from this site is in the positive influences of the length of the terrestrial phase on the ring-width chronologies, which was almost as strong as observed in the western Amazon site. Surprisingly, the ring-widths at this site were also negatively influenced by local temperatures during the beginning of the terrestrial phase, which has not been seen in any other floodplains. The negative influence of temperature on tree growth probably reflects the water-limiting conditions imposed by the very low rainfall amounts during the growing season, and to low water retention capacity of the sandy soils at this site. In such water-limiting conditions, leaves may have a lower thermoregulation capacity through evaporative cooling, and thus be more sensitive to the effects of temperature on leaf transpiration and photosynthesis rates (Jones et al., 1992; Fauset et al. 2018).

In contrast to the results from the ring-width chronologies, the results of the $\delta^{18}O_{TR}$ record from this site were more puzzling. Based on the analyses of Chapter 3 which were done with trees from this same site, the long and dry growing season should have a strong effect on leaf water enrichment, which in turn should be the main factor driving the $\delta^{18}O_{TR}$ in this site. Thus, I expected that the $\delta^{18}O_{TR}$ record from this site would mainly reflect local climate conditions during the dry season, which corresponds to the terrestrial phase. Contrary to these expectations, the $\delta^{18}O_{TR}$ record from this site seemed to contain a climate signal recorded in the source water $\delta^{18}O$ of the end of the previous wet season, as is indicated by its remarkable similarities with a $\delta^{18}O_{TR}$ record of *C. odorata* from a nearby site, which is a good proxy for past wet season rainfall $\delta^{18}O$ (Brienen et. al., 2012; Baker et al., 2015).

This apparent indication that the $\delta^{18}O_{TR}$ from the southwest Amazon site may reflect $\delta^{18}O$ in rainfall from the previous wet season was puzzling for two reasons. Firstly, the results from Chapter 3 suggest the $\delta^{18}O_{TR}$ from these trees is mainly determined by leaf water enrichment, which in turn should reflect local climate conditions and plant regulation of stomatal conductance. As all leaf water enrichment occurs above source water $\delta^{18}O$, it can be argued that including additional trees in the chronology may enhance the source water signal, especially if physiological responses to climate differ strongly between individual trees. Secondly, during the wet season the trees from this site are flooded and are not expected to grow. However, as there is very little rainfall during the growing season of these trees, it can be argued that all or most water available for the trees for this site is the water left by the river, which is runoff water from the end of the previous wet season. In essence, this argument then implies that floodplain trees may use different sources of water depending on the climate conditions during the growing season and on the local soil properties. Thus, in the next section I will discuss some of the available literature about the use of different sources of water by trees, and explain how this may apply for the floodplain sites studied in this Thesis.

6.6. Use of different sources of water by trees

Information about the use of different sources of water provides valuable information for interpreting isotope rations in tree rings (Treydte et al., 2014), provides insights on the strategies of different species and life forms to cope with water-limiting conditions (Stahl et al., 2013; Schwendenmann et al., 2015; Wang et al., 2017; Barbeta and Peñuelas, 2017; De Deurwaerder et al., 2018) and can potentially improve our understanding of how forests feedback on climate conditions through evapotranspiration during periods of drought (Da Rocha et al., 2009; Miguez-Macho and Fan, 2012). Water available for trees in different sites and seasons may differ in relation to its source, i.e. rainfall, snow melt or even fog (Ehleringer and Dawson, 1992; Dawson, 1996; Roden et al., 2009; Scholl et al., 2011) and in relation to the depth from which water is taken up from the soils by the roots. Use of water

from deep vs shallow soil layers depends on species traits such as canopy phenology, rooting depth and vessel architecture (Köcher et al., 2013; Schwendenmann et al., 2015; De Deurwaerder et al., 2018) and on the height of the ground water table (Geris et al., 2017; Barbeta and Peñuelas, 2017).

When considering the possible sources of water of floodplain trees, a central discussion is be related to the hydrological processes involved in the infiltration and percolation of water through soils. Data from several ecosystem types across the world suggest there is a complete hydrological separation between water used by plants and water that percolates to the water table and rivers (Brooks et al., 2010; Evaristo et al., 2015). According to this "two water world" hypothesis (Brooks et al., 2010; Phillips, 2010; McDonnel, 2014), soil pores are filled up with the first water they get, and subsequent rainfall does not mix with the water previously in the soil, but rather percolates as mobile water to ground and streams. If this the case for Amazon floodplain trees, then most water used by the trees in any floodplains would originate from river runoff from the end of the previous flooded season. As our study shows that the $\delta^{18}O_{TR}$ records from the sites in central and western Amazon actually record climate conditions during the terrestrial phase, our results do not agree with this mechanism.

While few studies of plant water uptake support the two water world hypothesis (Goldsmith et al., 2011; Bowling et al., 2017), others also find evidence that plants may use ground water (O'Grady et al., 2005; Bertrand et al., 2012; Barbeta and Peñuelas, 2017), percolating mobile water (Treydte et al., 2014) or even a mix of bound and mobile water in the soils (Gazis et al., 2003; Vargas et al., 2017). The possibility of a mixing of percolating and soil bound water, and that trees may be able to make use of both these sources is much more consistent with the climate influences observed in all $\delta^{18}O_{TR}$ records produced in this Thesis. If this is the case, then is indeed plausible that the trees from the sites in central and western Amazon may be able to use rainfall water throughout their respective growing seasons, while

in the southwest Amazon the trees mainly use river water, as rainfall during their growing season is scarce.

6.7. Summary of conclusions and main implications of results

6.7.1. What can the ring-width chronologies tell us about past climate conditions?

- Tree growth at all studied sites is mainly driven by the local river hydrology. Trees are more productive in years with shorter flooding periods related to less rainfall amounts over the catchment area of the rivers.
- The climatic signal provided by these chronologies is highly dependable the level water-stress of the trees. For trees that grow under water-limiting conditions, temperature may increase the trees' water stress and represent an additional limitation for tree growth, which is also reflected in ring width chronologies.
- Ring-width chronologies of trees growing in floodplains of smaller river catchments seem to present more potential for climate reconstructions.
- Ring-width chronologies of *M. acaciifolium* can be used a proxies for past dry season conditions, even though such trees present frequent false rings which require labor-intensive wood anatomical analysis and ring-width crossdating.

6.7.2. What type of information can be obtained from oxygen isotope ratios in the tree rings of *M. acaciifolium*?

- Seasonally, oxygen isotopes in tree rings of individual *M. acaciifolium* can be strongly influenced by leaf water enrichment effects. This effect is particularly strong for trees growing in water-limiting conditions, but less so for trees growing under wetter conditions.
- At inter-annual and longer time scales, variations in plant source water $\delta^{18}O$ are reflected in the $\delta^{18}O_{TR}$, especially at wetter sites.
- Climate influences the $\delta^{18}O_{TR}$ during the growing season of the trees. $\delta^{18}O_{TR}$ records of Amazon floodplain trees can be used to reconstruct dry season

conditions, provided that: (1) the growing season of the trees is entirely during this season, which is generally the case for smaller river basins, and (2) trees are able to use rainfall as one main source of water during the growing season.

6.8. Final considerations and directions for future research

The research presented here proves that tree rings of floodplain trees can be used as proxies for past dry season climate variability. Crossdating ring-widths of *M. acaciifolium* results in climate-sensitive chronologies that reflect past dry season length over the catchment area of the rivers, but also requires a high number samples, and is labour-intensive and time consuming. When possible, the analysis of oxygen isotopes ratios in the tree rings may be used as the best approach for reconstruction of past dry season climate conditions. Our study supports climate observations that suggest that the dry season climate is becoming drier and warmer in the Amazon, with a central role of the warming sea surface temperatures of the North Atlantic Ocean. Obtaining a proxy for the dry season represents an important advance in the field, because most proxy records that permit to improve our understanding of past climate variability mainly provide information about climate conditions during the wet season only. The use of $\delta^{18}O_{TR}$ of floodplain trees and of trees from non-flooded areas may be combined to provide climate reconstructions at the seasonal scale. As recent climate observations in the Amazon suggest that climate changes may differ between seasons, it would be very interesting to develop more $\delta^{18}O_{TR}$ records of floodplain and non-flooded trees from nearby sites in future studies. I recommend a focus on floodplains sites from small river basins and with a rather moist dry season climate in order to obtain the best climatic signals from $\delta^{18}O_{TR}$ chronologies.

To further improve this field, it would be interesting to examine in detail the physiological and biochemical pathway that leads to the final isotopic composition of cellulose in *M. acaciifolium* and also additional floodplain species in future studies. Specifically, significant improvements in the field may be achieved by direct

measurement of leaf water $\delta^{18}O$ for species with different leaf traits (e.g. Holloway Phillips et al., 2016) and by exploring the proportion and the isotopic signal of oxygen from cellulose that is labelled with oxygen from stem water (e.g. Sternberg, 2008; Cheesman and Cernusak., 2017). Studies comparing the $\delta^{18}O_{TR}$ and $\delta^{13}C_{TR}$ variations and modelling approaches such as the approach from Chapter 3 of this Thesis are also highly recommendable to understand the climate signals in $\delta^{18}O_{TR}$ chronologies. Finally, given the lack of information about the possible sources of water of floodplain trees, future studies should also investigate how different floodplain species growing in different climate conditions may uptake water from different sources and soil depths.

References

Aceituno, P. 1988. On the Functioning of the Southern Oscillation in the South American Sector. Part I: Surface Climate. *Monthly Weather Review*. **116**(3), pp.505–524.

Ainsworth, E.A. and Rogers, A. 2007. The response of photosynthesis and stomatal conductance to rising [CO_2]: Mechanisms and environmental interactions. *Plant, Cell and Environment*. **30**(3), pp.258–270.

Alencar, A., Nepstad, D. and Diaz, M. del C.V. 2005. Forest Understory Fire in the Brazilian Amazon in ENSO and Non-ENSO Years : Area Burned and Committed Carbon Emissions. Earth Interactions. **10**(6), pp. 1–17..

Allakhverdiev, S.I., Kreslavski, V.D., Klimov, V.V., Los, D.A., Carpentier, R. and Mohanty, P. 2008. Heat stress: An overview of molecular responses in photosynthesis. *Photosynthesis Research*. **98**(1–3), pp.541–550.

Allen, C.D., Macalady, A.K., Chenchouni, H., Bachelet, D., McDowell, N., Vennetier, M., Kitzberger, T., Rigling, A., Breshears, D.D., Hogg, E.H. Ted., Gonzalez, P., Fensham, R., Zhang, Z., Castro, J., Demidova, N., Lim, J.H., Allard, G., Running, S.W., Semerci, A. and Cobb, N. 2010. A global overview of drought and heat-induced tree mortality reveals emerging climate change risks for forests. *Forest Ecology and Management*. **259**(4), pp.660–684.

Anderson, W.T., Bernasconi, S.M. and Mckenzie, J. a 1998. Oxygen and carbon isotopic record of climatic variability in tree ring cellulose (Picea abies)' An example from central Switzerland (1913-1995). *Journal of Geophysical Research*, **103**(24) pp. 31,625-31,636.

Anderson, L.O., Trivedi, M., Queiroz, J., Aragão, L.E.O.C., Marengo, J., Young, C. and Meir, P., Counting the costs of the 2005 Amazon drought: A preliminary assessment, 2011. *Ecosystem Services for Poverty Alleviation in Amazonia*, pp.97-103.

Andreae, M.O., Rosenfeld, D., Artaxo, P.Frank, G.P., Costa, A.A., Longo, K.M. and Silva-Dias, M.A.F. 2004. Smoking rain clouds over the Amazon. *Science*. **303**, pp.1337–1342.

Antonelli, A., Zizka, A., Antunes, F. and Scharn, R. 2018. Amazonia is the primary source of Neotropical biodiversity. *Proceedings of the National Academy of Sciences*, **115**(23), pp.6034–6039.

Aragão, L.E.O.C., Anderson, L.O., Fonseca, M.G., Rosan, T.M., Vedovato, L.B., Wagner, F.H., Silva, C.V.J., Silva Junior, C.H.L., Arai, E., Aguiar, A.P., Barlow, J., Berenguer, E., Deeter, M.N., Domingues, L.G., Gatti, L., Gloor, M., Malhi, Y., Marengo, J.A., Miller, J.B., Phillips, O.L. and Saatchi, S. 2018. 21st Century drought-related fires counteract the decline of Amazon deforestation carbon emissions. *Nature Communications*. **9**(1), pp.1–12.

Aragão, L.E.O.C., Malhi, Y., Roman-Cuesta, R.M., Saatchi, S., Anderson, L.O. and Shimabukuro, Y.E. 2007. Spatial patterns and fire response of recent Amazonian droughts. *Geophysical Research Letters*. **34**(7), p.L07701.

Araguás-Araguás, L., Froehlich, K. and Rozanski, K. 2000. Deuterium and oxygen-18 isotope composition of precipitation and atmospheric moisture. *Hydrological Processes*. **14**, pp.1341–1355.

Arneth, A., Harrison, S.P., Zaehle, S., Tsigaridis, K., Menon, S., Bartlein, P.J., Feichter, J., Korhola, A., Kulmala, M., O'Donnell, D., Schurgers, G., Sorvari, S. and Vesala, T. 2010. Terrestrial biogeochemical feedbacks in the climate system. *Nature Geoscience*. **3**(8), pp.525–532.

Assahira, C., Resende, A.F. de, Trumbore, S.E., Wittmann, F., Cintra, B.B.L. and Batista, E.S. 2017. Tree mortality of a flood-adapted species in response of hydrographic changes caused by an Amazonian river dam. *Forest Ecology and Management*. **396**, pp.113–123.

Assis, R.L., Haugaasen, T., Schöngart, J., Montero, J.C., Piedade, M.T.F. and Wittmann, F. 2015. Patterns of tree diversity and composition in Amazonian floodplain paleo-várzea forest. *Journal of Vegetation Science*. **26**(2), pp.312–322.

Avissar, R. and Werth, D. 2005. Global Hydroclimatological Teleconnections Resulting from Tropical Deforestation. *Journal of Hydrometeorology*. 6(2), pp.134–145.

Bailey-Serres, J. and Voesenek, L.A.C.J. 2008. Flooding Stress: Acclimations and Genetic Diversity. *Annual Review of Plant Biology*. **59**(1), pp.313–339.

Baker, J.C.A., Gloor, M., Spracklen, D. V., Arnold, S.R., Tindall, J.C., Clerici, S.J., Leng, M.J. and Brienen, R.J.W. 2016. What drives interannual variation in tree ring oxygen isotopes in the Amazon? *Geophysical Research Letters*. **43**(22), 11,831-11,840.

Baker, J.C.A., Hunt, S.F.P., Clerici, S.J., Newton, R.J., Bottrell, S.H., Leng, M.J., Heaton, T.H.E., Helle, G., Argollo, J., Gloor, M. and Brienen, R.J.W. 2015. Oxygen isotopes in tree rings show good coherence between species and sites in Bolivia. *Global and Planetary Change*. **133**, pp.298–308.

Baker, J.C.A., Santos, G.M., Gloor, M. and Brienen, R.J.W. 2017. Does Cedrela always form annual rings? Testing ring periodicity across South America using radiocarbon dating. *Trees - Structure and Function*. **31**(6), pp.1999–2009.

Baker, P.A., Dunbar, R.B., Cross, S.L., Seltzer, G.O., Grove, M.J., Rowe, H.D., Fritz, S.C., Tapia, P.M. and Broda, J.P. 2001. The History of South American Tropical Precipitation for the Past 25,000 Years. *Science*. **291**, pp.640–643.

Ballantyne, A.P., Baker, P.A., Chambers, J.Q., Villalba, R. and Argollo, J. 2011. Regional differences in south american monsoon precipitation inferred from the growth and isotopic composition of tropical trees. *Earth Interactions*. **15**(5), pp.1–35.

Barbour, M.M. 2007. Stable oxygen isotope composition of plant tissue: a review. *Global Biogeochemical Cycles*. **34**, pp.83–94.

Barbour, M.M. and Farquhar, G.D. 2000. Relative humidity- and ABA-induced variation in carbon and oxygen isotope ratios of cotton leaves. *Plant, Cell and Environment*. **23**(5), pp.473–485.

Barbour, M.M., Fischer, R.A., Sayre, K.D. and Farquhar, G.D. 2000. Oxygen isotope ratio of leaf and grain material correlates with stomatal conductance and grain yield in irrigated wheat. *Australian Journal of Plant Physiology*. **27**(7), pp.625–637.

Barbour, M.M., Roden, J.S., Farquhar, G.D. and Ehleringer, J.R. 2004. Expressing leaf water and cellulose oxygen isotope ratios as enrichment above source water reveals evidence of a Péclet effect. *Oecologia*. **138**(3), pp.426–435.

Barbour, M.M., Walcroft, a S. and Farquhar, G.D. 2002. Seasonal variation in $\delta^{13}C$ and $\delta^{18}O$ of cellulose from growth rings of Pinus radiata. *Plant, cell & environment*. **25**, pp.1483–1499.

Barichivich, J., Gloor, E., Peylin, P., Brienen, R.J.W., Schöngart, J., Espinoza, J.C. and Pattnayak, K.C. 2018. Recent intensification of Amazon flooding extremes driven by strengthened Walker circulation. *Science Advances*. **4**(9), p.eaat8785.

Barnard, H.R., Brooks, J.R. and Bond, B.J. 2012. Applying the dual-isotope conceptual model to interpret physiological trends under uncontrolled conditions. *Tree Physiology*. **32**(10), pp.1183–1198.

Batista, E.S. and Schöngart, J. 2018. Dendroecology of Macrolobium acaciifolium (Fabaceae) in Central Amazonian floodplain forests. *Acta Amazonica*. **48**(4), pp.311–320.

Beer, C., Reichstein, M., Tomelleri, E., Ciais, P., Jung, M., Carvalhais, N., Rödenbeck, C., Arain, M.A., Baldocchi, D., Bonan, G.B., Bondeau, A., Cescatti, A., Lasslop, G., Lindroth, A., Lomas, M., Luyssaert, S., Margolis, H., Oleson, K.W., Roupsard, O., Veenendaal, E., Viovy, N., Williams, C., Woodward, F.I. and Papale, D. 2010. Terrestrial gross carbon dioxide uptake: Global distribution and covariation with climate. *Science*. **329**, pp.834–838.

Belger, L., Forsberg, B.R. and Melack, J.M. 2011. Carbon dioxide and methane emissions from interfluvial wetlands in the upper Negro River basin, Brazil. *Biogeochemistry*. **105**(1-3), pp.171-183.

Berlage, H.P., 1931. On the relationship between thickness of tree rings of Djati (teak) trees and rainfall on Java. *Tectona*, **24**, pp.939-953.

Betts, R.A., Malhi, Y. and Roberts, J.T. 2008. The future of the Amazon: New perspectives from climate, ecosystem and social sciences. *Philosophical Transactions of the Royal Society B: Biological Sciences*. **363**(1498), pp.1729–1735.

Biastoch, A. and Böning, C.W. 2013. Anthropogenic impact on Agulhas leakage. *Geophysical Research Letters*. **40**(6), pp.1138–1143.

Biastoch, A., Böning, C.W., Schwarzkopf, F.U. and Lutjeharms, J.R.E. 2009. Increase in Agulhas leakage due to poleward shift of Southern Hemisphere westerlies. *Nature*. **462**, pp.495–498.

Biastoch, A., Durgadoo, J. V., Morrison, A.K., Van Sebille, E., Weijer, W. and Griffies, S.M. 2015. Atlantic multi-decadal oscillation covaries with Agulhas leakage. *Nature Communications*. **6**, pp.1–7.

Biondi, F. and Qeadan, F. 2008. Inequality in paleorecords. *Ecology*. **89**(4), pp.1056–1067.

Bird, B.W., Abbott, M.B., Vuille, M., Rodbell, D.T., Stansell, N.D. and Rosenmeier, M.F. 2011. A 2,300-year-long annually resolved record of the South American summer monsoon from the Peruvian Andes. *Proceedings of the National Academy of Sciences*. **108**(21), pp.8583–8588.

Black, D.E., Abahazi, M.A., Thunell, R.C., Kaplan, A., Tappa, E.J. and Peterson, L.C. 2007. An 8-century tropical Atlantic SST record from the Cariaco Basin: Baseline variability, twentieth-century warming, and Atlantic hurricane frequency. *Paleoceanography*. **22**(4), pp.1–10.

Bloom, A.A., Palmer, P.I., Fraser, A. and Reay, D.S. 2012. Seasonal variability of tropical wetland CH 4 emissions: the role of the methanogen-available carbon pool. *Biogeosciences*. **9**(8), pp.2821-2830.

Boisier, J.P., Ciais, P., Ducharne, A. and Guimberteau, M. 2015. Projected strengthening of Amazonian dry season by constrained climate model simulations. *Nature Climate Change*. **5**(7), pp.656–660.

Bonan, G.B. 2008. Forests and climate change: Forcings, feedbacks, and the climate benefits of forests. *Science*. **320**(5882), pp.1444–1449.

Borchert, R. 1999. Climatic Periodicity, Phenology, and Cambium Activity in Tropical Dry Forest Trees. *IAWA Journal*. **20**(3), pp.239–247.

Bormann, F.H. and Berlyn, G. 1981. Age and growth of Tropical Trees: New directions for future research. *Yale School of Forestry & Environmental Studies Bulletin*, Series. 6.

Bottinga, Y. and Craig, H. 1969. Oxygen isotope fractionation between CO_2 and water, and the isotopic composition of marine atmospheric CO_2. *Earth and Planetary Science Letters*. **5**, pp.285–295.

Bowman, D.M.J.S., Brienen, R.J.W., Gloor, E., Phillips, O.L. and Prior, L.D. 2013. Detecting trends in tree growth: Not so simple. *Trends in Plant Science*. **18**(1), pp.11–17.

Brendell, O., Ianetta, P.P.M. and Stewart, D. 2000. A Rapid and Simple Method to Isolate Pure Alpha-Cellulose. *Phytochemical Analysis*. **11**, pp.7–10.

van Breukelen, M.R., Vonhof, H.B., Hellstrom, J.C., Wester, W.C.G. and Kroon, D. 2008. Fossil dripwater in stalagmites reveals Holocene temperature and rainfall variation in Amazonia. *Earth and Planetary Science Letters*. **275**(1–2), pp.54–60.

Brienen, R.J.W., Gloor, E. and Zuidema, P.A. 2012. Detecting evidence for CO_2 fertilization from tree ring studies: The potential role of sampling biases. *Global Biogeochemical Cycles*. **26**(1), pp1-13.

Brienen, R.J.W., Gloor, M. and Ziv, G. 2016. Tree demography dominates long-term growth trends inferred from tree rings. *Global Change Biology*. **23**(2), pp.474–484.

Brienen, R.J.W., Helle, G., Pons, T.L., Guyot, J.-L. and Gloor, M. 2012. Oxygen isotopes in tree rings are a good proxy for Amazon precipitation and El Nino-Southern Oscillation variability. *Proceedings of the National Academy of Sciences*. **109** (42), 16957–16962.

Brienen, R.J.W., Lebrija-Trejos, E., Zuidema, P.A. and Martínez-Ramos, M. 2010. Climate-growth analysis for a Mexican dry forest tree shows strong impact of sea surface temperatures and predicts future growth declines. *Global Change Biology*. **16**(7), pp.2001–2012.

Brienen, R.J.W., Phillips, O.L., Feldpausch, T.R., Gloor, E., Baker, T.R., Lloyd, J., Lopez-Gonzalez, G., Monteagudo-Mendoza, A., Malhi, Y., Lewis, S.L., Vásquez Martinez, R., Alexiades, M., Álvarez Dávila, E., Alvarez-Loayza, P., Andrade, A.,

Aragaõ, L.E.O.C., Araujo-Murakami, A., Arets, E.J.M.M., Arroyo, L., Aymard C., G.A., Bánki, O.S., Baraloto, C., Barroso, J., Bonal, D., Boot, R.G.A., Camargo, J.L.C., Castilho, C. V., Chama, V., Chao, K.J., Chave, J., Comiskey, J.A., Cornejo Valverde, F., Da Costa, L., De Oliveira, E.A., Di Fiore, A., Erwin, T.L., Fauset, S., Forsthofer, M., Galbraith, D.R., Grahame, E.S., Groot, N., Hérault, B., Higuchi, N., Honorio Coronado, E.N., Keeling, H., Killeen, T.J., Laurance, W.F., Laurance, S., Licona, J., Magnussen, W.E., Marimon, B.S., Marimon-Junior, B.H., Mendoza, C., Neill, D.A., Nogueira, E.M., Núñez, P., Pallqui Camacho, N.C., Parada, A., Pardo-Molina, G., Peacock, J., Penã-Claros, M., Pickavance, G.C., Pitman, N.C.A., Poorter, L., Prieto, A., Quesada, C.A., Ramírez, F., Ramírez-Angulo, H., Restrepo, Z., Roopsind, A., Rudas, A., Salomaõ, R.P., Schwarz, M., Silva, N., Silva-Espejo, J.E., Silveira, M., Stropp, J., Talbot, J., Ter Steege, H., Teran-Aguilar, J., Terborgh, J., Thomas-Caesar, R., Toledo, M., Torello-Raventos, M., Umetsu, R.K., Van Der Heijden, G.M.F., Van Der Hout, P., Guimarães Vieira, I.C., Vieira, S.A., Vilanova, E., Vos, V.A. and Zagt, R.J. 2015. Long-term decline of the Amazon carbon sink. *Nature*. **519**(7543), pp.344–348.

Brienen, R.J.W., Schöngart, J. and Zuidema, P.A. 2016. Tree rings in the tropics: Insights into the Ecology and Climate Sensitivity of Tropical Trees. In: Tropical Tree Physiology. *Springer*, Switzerland, pp.439–461.

Brienen, R.J.W., Wanek, W. and Hietz, P. 2011. Stable carbon isotopes in tree rings indicate improved water use efficiency and drought responses of a tropical dry forest tree species. *Trees*. **25**(1), pp.103–113.

Brienen, R.J.W. and Zuidema, P.A. 2007. Incorporating persistent tree growth differences increases estimates of tropical timber yield. *Frontiers in Ecology and the Environment*. **5**(6), pp.302–306.

Brienen, R.J.W. and Zuidema, P.A. 2006. Lifetime growth patterns and ages of Bolivian rain forest trees obtained by tree ring analysis. *Journal of Ecology*. **94**(2), pp.481–493.

Brienen, R.J.W. and Zuidema, P.A. 2005. Relating tree growth to rainfall in Bolivian rain forests: A test for six species using tree ring analysis. *Oecologia*. **146**(1), pp.1–12.

Briffa, K.R. and Jones, P.D. 1990. Basic chronology statistics and assessment. In: Methods of Dendrochronology: Applications in the Environmental Sciences. *Kluwer Academic Publishers*. pp. 137-152.

Brondízio, E.S., de Lima, A.C.B., Schramski, S. and Adams, C. 2016. Social and health dimensions of climate change in the Amazon. *Annals of Human Biology*. **43**(4), pp.405–414.

Brondizio, E.S. and Moran, E.F. 2008. Human dimensions of climate change: The vulnerability of small farmers in the Amazon. *Philosophical Transactions of the Royal Society B: Biological Sciences*. **363**(1498), pp.1803–1809.

Brooks, J.R., Barnard, H.R., Coulombe, R. and McDonnell, J.J. 2010. Ecohydrologic separation of water between trees and streams in a Mediterranean climate. *Nature Geoscience*. **3**(2), pp.100–104.

Brugnoli, E., Hubick, K.T., von Caemmerer, S., Wong, S.C. and Farquhar, G.D. 1988. Correlation between the Carbon Isotope Discrimination in Leaf Starch and

Sugars of C(3) Plants and the Ratio of Intercellular and Atmospheric Partial Pressures of Carbon Dioxide. *Plant physiology*. **88**(4), pp.1418–24.

Buckley, B.M., Palakit, K., Duangsathaporn, K., Sanguantham, P. and Prasomsin, P. 2007. Decadal scale droughts over northwestern Thailand over the past 448 years: Links to the tropical Pacific and Indian Ocean sectors. *Climate Dynamics*. **29**(1), pp.63–71.

Burk, R.L. and Stuiver, M. 1981. Oxygen Isotope Ratios in Trees Reflect Mean Annual Temperature and Humidity. *Science*. **211**, pp.1417–1419.

Butt, N., De Oliveira, P.A. and Costa, M.H. 2011. Evidence that deforestation affects the onset of the rainy season in Rondonia, Brazil. *Journal of Geophysical Research Atmospheres*. **116**(11), pp.2–9.

von Caemmerer, S. and Evans, J.R. 2015. Temperature responses of mesophyll conductance differ greatly between species. *Plant, Cell and Environment*. **38**, pp.629–637.

Callede, J., Cochonneau, G., Vieira Alves, F., Guyot, J.L., Santos Guimaraes, V. and De Oliveira, E. 2010. The river amazon water contribution to the Atlantic Ocean. *Revue des sciences de l'eau*. **23**(3).

Cernusak , L.A., Pate, J.E., Farquhar G.D. 2002. Diurnal variation in the stable isotope composition of water and dry matter in fruiting *Lupinus angustifolius* under field conditions. *Plant, cell and environment*. **25**, pp.893–907.

Cernusak, L.A., Barbour, M.M., Arndt, S.K., Cheesman, A.W., English, N.B., Feild, T.S., Helliker, B.R., Holloway-Phillips, M.M., Holtum, J.A.M., Kahmen, A., Mcinerney, F.A., Munksgaard, N.C., Simonin, K.A., Song, X., Stuart-Williams, H., West, J.B. and Farquhar, G.D. 2016. Stable isotopes in leaf water of terrestrial plants. *Plant Cell and Environment*. **39**(5), pp.1087–1102.

Cernusak, L.A., Farquhar, G.D. and Pate, J.S. 2005. Environmental and physiological controls over oxygen and carbon isotope composition of Tasmanian blue gum, Eucalyptus globulus. *Tree Physiology*. **25**(2), pp.129–146.

Cernusak, L.A. and Kahmen, A. 2013. The multifaceted relationship between leaf water ^{18}O enrichment and transpiration rate. *Plant, Cell and Environment*. **36**(7), pp.1239–1241.

Cernusak, L.A., Tcherkez, G., Keitel, C., Cornwell, W.K., Santiago, L.S., Knohl, A., Barbour, M.M., Williams, D.G., Reich, P.B., Ellsworth, D.S., Dawson, T.E., Griffith, H.G., Farquhar, G.D. and Wright, I.J. 2009. Why are non-photosynthetic tissues generally ^{13}C enriched compared with leaves in C3 plants ? Review and synthesis of current hypotheses. *Functional Plant Biology*. **36**, pp.199–213.

Cernusak, L.A., Winter, K., Dalling, J.W., Holtum, J.A.M., Jaramillo, C., Körner, C., Leakey, A.D.B., Norby, R.J., Poulter, B., Turner, B.L. and Wright, S.J. 2013. Tropical forest responses to increasing atmospheric CO_2: Current knowledge and opportunities for future research. *Functional Plant Biology*. **40**(6), pp.531–551.

Cernusak, L.A., Winter, K., Martínez, C., Correa, E., Aranda, J., Garcia, M., Jaramillo, C. and Turner, B.L. 2011. Responses of Legume Versus Nonlegume Tropical Tree Seedlings to Elevated CO_2 Concentration. *Plant Physiology*. 157(1), pp.372–385.

Chambers, J.Q., Higuchi, N. and Schimel, J.P. 1998. Ancient trees in Amazonia. *Nature*. **391**, pp.135–136.

Chaumont, F., Moshelion, M. and Daniels, M.J. 2005. Regulation of plant aquaporin activity. *Biology of the Cell*. **97**(10), pp.749–764.

Chen, G., Powers, R.P., de Carvalho, L.M.T. and Mora, B. 2015. Spatiotemporal patterns of tropical deforestation and forest degradation in response to the operation of the Tucuruí hydroelectricdam in the Amazon basin. *Applied Geography*. **63**, pp.1–8.

Chiessi, C.M., Mulitza, S., P??tzold, J., Wefer, G. and Marengo, J.A. 2009. Possible impact of the Atlantic Multidecadal Oscillation on the South American summer monsoon. *Geophysical Research Letters*. **36**(21), pp.1–5.

China, S., Burrows, S., Wang, B., Harder, T., Weis, J., Tanarhte, M., Rizzo, L., Brito, J., Cirino, G.G., Ma, P.-L., Cliff, J., Artaxo, P., Gilles, M.K. and Laskin, A. 2018. Non marine sources of sodium salt particles in the Amazon basin. *Nature communications*. **9**(1), p. 4793.

Cintra, B.B.L., Schietti, J., Emillio, T., Martins, D., Moulatlet, G., Souza, P., Levis, C. and Quesada, C.A. 2013. Soil physical restrictions and hydrology regulate stand age and wood biomass turnover rates of Purus – Madeira interfluvial wetlands in Amazonia. *Biogeosciences*, **10**, pp.7759–7774.

Coe, M.T., Latrubesse, E.M., Ferreira, M.E. and Amsler, M.L. 2011. The effects of deforestation and climate variability on the streamflow of the Araguaia River, Brazil. *Biogeochemistry*. **105**(1), pp.119–131.

Condit, R., Hubbel, S.P. and Foster, R.B. 1995. Mortality Rates Of 205 Neotropical Tree And Shrub Species And The Impact Of A Severe Drought. *Ecological Monographs*. **65**(4), pp.419–439.

Cook, E.R. and Peters, K. 1997. Calculating unbiased tree-ring indices for the study of climatic and environmental change. *The Holocene*. **7**(3), pp.361–370.

Cook, E.R. and Peters, K. 1981. The smoothing spline: a new approach to standardizing forest interior tree-ring width series for dendroclimatic studies. *Tree-Ring Bulletin*. **41**, pp.45–53.

Cook ER, Kairiukstis L (1990) Methods of dendrochronology: applications in the environmental science. *Springer, Berlin*.

Costa, A.C.L. da, Galbraith, D., Almeida, S., Takeshi, B., Portela, T., Athaydes, D., Junior, S., Braga, A.P., Gonc, P.H.L. De, Oliveira, A.A.R. De, Fisher, R., Phillips, O.L., Metcalfe, D.B., Levy, P. and Meir, P. 2010. Effect of 7 yr of experimental drought on vegetation dynamics and biomass storage of an eastern Amazonian rainforest. *New Phytologist*. **187**, pp.579–591.

Costa, M.H., Botta, A. and Cardille, J.A. 2003. Effects of large-scale changes in land cover on the discharge of the Tocantins River, Southeastern Amazonia. *Journal of Hydrology*. **283**(1–4), pp.206–217.

Costa, M.H. and Foley, J.A. 2000. Combined effects of deforestation and doubled atmospheric CO_2 concentrations on the climate of Amazonia. *Journal of Climate*. **13**(1), pp.18–34.

Costa, M.H. and Foley, J.A. 1999. Trends in the hydrologic cycle of the Amazon basin. *Journal of Geophysical Research*. **104**(12), pp. 14,189-14,198.

Costa, M.H. and Pires, G.F. 2010. Effects of Amazon and Central Brazil deforestation scenarios on the duration of the dry season in the arc of deforestation. *International Journal of Climatology*. **30**(13), pp.1970–1979.

Costa, M.H., Yanagi, S.N.M., Souza, P.J.O.P., Ribeiro, A. and Rocha, E.J.P. 2007. Climate change in Amazonia caused by soybean cropland expansion, as compared to caused by pastureland expansion. *Geophysical Research Letters*. **34**(7), pp.2–5.

Costa, M.S., Vasconcellos, T.J. de, Barros2, C.F. and Callado, C.H. 2013. Does growth rhythm of a widespread species change in distinct growth sites? *IAWA Journal*. **34**(4), pp.498–509.

Cox, P.M., Betts, R.A., Collins, M., Harris, P.P., Huntingford, C. and Jones, C.D. 2004. Amazonian forest dieback under climate-carbon cycle projections for the 21st Century. *Theoretical and Applied Climatology*. **78**, pp.137–156.

Cox, P.M., Betts, R.A., Jones, C.D. and Spall, S.A. 2000. Acceleration of global warming due to carbon cycle feedbacks in a coupled climate model Peter. *Nature*. **408**, pp.184–187.

Cox, P.M., Harris, P.P., Huntingford, C., Betts, R.A., Collins, M., Jones, C.D., Jupp, T.E., Marengo, J.A. and Nobre, C.A. 2008. Increasing risk of Amazonian drought due to decreasing aerosol pollution. *Nature*. **453**, pp.212–215.

Cox, P.M., Huntingford, C. and Harding, R.J. 1998. A canopy conductance and photosynthesis model for use in a GCM land surface scheme. *Journal of Hydrology*. **212–213**(1–4), pp.79–94.

Craig, H., 1961. Standard for reporting concentrations of deuterium and oxygen-18 in natural waters. *Science*. **133**(3467), pp.1833-1834.

Craig, H. and Gordon, L. 1965. Deuterium and oxygen 18 variations in the ocean and the marine atmosphere In: Stable Isotopes in Oceanographic Studies and Paleotemperatures. *Spoleto*, Italy. pp.9–130.

Cruz, F.W., Burns, S.J., Karmann, I., Sharp, W.D. and Vuille, M. 2006. Reconstruction of regional atmospheric circulation features during the late Pleistocene in subtropical Brazil from oxygen isotope composition of speleothems. *Earth and Planetary Science Letters*. **248**(1–2), pp.494–506.

Cruz, F.W., Burns, S.J., Karmann, I., Sharp, W.D., Vuille, M., Cardoso, A.O., Ferrari, J.A., Silva Dias, P.L. and Jr, O.V. 2005. Insolation-driven changes in atmospheric circulation over the past 116,000 years in subtropical Brazil. *Journal of Geophysical Research: Solid Earth*. **434**, pp.63–65.

Cruz, F.W., Vuille, M., Burns, S.J., Wang, X., Cheng, H., Werner, M., Lawrence Edwards, R., Karmann, I., Auler, A.S. and Nguyen, H. 2009. Orbitally driven east-west antiphasing of South American precipitation. *Nature Geoscience*. **2**(3), pp.210–214.

Dai, K.M. and Fan, C., 1986. Bomb produced ^{14}C content in tree rings grown at different latitudes. *Radiocarbon*. **28**(2A), pp.346-349.

D'Almeida, C., Vörösmarty, C.J., Hurtt, G.C., Marengo, J.A., Dingman, S.L. and Keim, B.D. 2007. The effects of deforestation on the hydrological cycle in Amazonia: a review on scale and resolution. *International Journal of Climatology*. **27**, pp.633–647.

Damesin, C. and Lelarge, C. 2003. Carbon isotope composition of current-year shoots from Fagus sylvatica in relation to growth, respiration and use of reserves. *Plant, Cell and Environment*. **26**(2), pp.207–219.

Danis, P.A., Masson-Delmotte, V., Stievenard, M., Guillemin, M.T., Daux, V., Naveau, P. and von Grafenstein, U. 2006. Reconstruction of past precipitation $\delta^{18}O$ using tree-ring cellulose $\delta^{18}O$ and $\delta^{13}C$: A calibration study near Lac d'Annecy, France. *Earth and Planetary Science Letters*. **243**(3–4), pp.439–448.

Dansgaard, W. 1964. Stable isotopes in precipitation. *Tellus*. **16**(4), pp.436–468.

Davidson, E.A., De Araüjo, A.C., Artaxo, P., Balch, J.K., Brown, I.F., Mercedes, M.M., Coe, M.T., Defries, R.S., Keller, M., Longo, M., Munger, J.W., Schroeder, W., Soares-Filho, B.S., Souza, C.M. and Wofsy, S.C. 2012. The Amazon basin in transition. *Nature*. **481**, pp.321–328.

Dawson, T.E. and Ehleringer, J.R. 1993. Isotopic enrichment of water in the 'woody' tissues of plants: Implications for plant water source, water uptake, and other studies which use the stable isotopic composition of cellulose. *Geochimica et Cosmochimica Acta*. **57**(14), pp.3487–3492.

DeNiro, M.J. and Cooper, L.W. 1989. Post-photosynthetic modification of oxygen isotope ratios of carbohydrates in the potato: Implications for paleoclimatic reconstruction based upon isotopic analysis of wood cellulose. *Geochimica et Cosmochimica* Acta. **53**(10), pp.2573–2580.

Dezzeo, N., Worbes, M., Ishii, I. and Herrera, R. 2003. Annual Tree Rings Revealed by Radiocarbon Dating in Seasonally Flooded Forest of the Mapire River, a Tributary of the Lower Orinoco River , Venezuela Author. *Plant Ecology*. **168**(1), pp.165–175.

Dixon, J., Brown, R.K., Houghton, R.A., M.C., Solomon, Trexier, A.M. and Wisniewski, S. 1994. Carbon Pools and Flux of Global Forest Ecosystems. *Science*. **263**(5144), pp.185–190.

Dong, S.X., Davies, S.J., Ashton, P.S., Bunyavejchewin, S., Nur Supardi, M.N., Kassim, A.R., Tan, S. and Moorcroft, P.R. 2012. Variability in solar radiation and temperature explains observed patterns and trends in tree growth rates across four tropical forests. *Proceedings of the Royal Society B: Biological Sciences*. **279**(1744), pp.3923–3931.

Dongmann, G., Nürnberg, H.W., Förstel, H. and Wagener, K. 1974. On the enrichment of $H_2{}^{18}O$ in the leaves of transpiring plants. *Radiation and Environmental Biophysics*. **11**(1), pp.41–52.

Doughty, C.E. and Goulden, M.L. 2009. Are tropical forests near a high temperature threshold? Journal of Geophysical Research: *Biogeosciences*. **114**(1), pp.1–12.

Douglass, A.E. 1914. A method of estimating rainfall by the growth of trees. *Bulletin of the American Geographical Society*. **46**(5), pp.321-335.

Dubreuil, V., Debortoli, N., Funatsu, B., Nédélec, V. and Durieux, L. 2012. Impact of land-cover change in the Southern Amazonia climate: A case study for the region of Alta Floresta, Mato Grosso, Brazil. *Environmental Monitoring and Assessment*. **184**(2), pp.877–891.

Dünisch, O., Montóia, V.R. and Bauch, J. 2003. Dendroecological investigations on Swietenia macrophylla King and Cedrela odorata L. (Meliaceae) in the central Amazon. *Trees - Structure and Function*. **17**(3), pp.244–250.

Dünisch, O. and Puls, J. 2003. Changes in content of reserve materials in an evergreen, a semi-deciduous, and a deciduous Meliaceae species from the Amazon. *Journal of Applied Botany*. **77**, pp.10–16.

Eamus, D., Berryman, C.A. and Duff, G.A. 1993. Assimilation, stomatal conductance, specific leaf area and chlorophyll responses to elevated CO2 of *Maranthes corymbosa*, a tropical monsoon rain forest species. *Australian Journal of Plant Physiology*. **20**(6), pp.741–755.

Edwards, T.W.D., Birks, S.J., Luckman, B.H. and MacDonald, G.M. 2008. Climatic and hydrologic variability during the past millennium in the eastern Rocky Mountains and northern Great Plains of western Canada. *Quaternary Research*. **70**(2), pp.188–197.

Eglin, T., Francois, C., Michelot, A., Delpierre, N. and Damesin, C. 2010. Linking intra-seasonal variations in climate and tree-ring $\delta^{13}C$: A functional modelling approach. *Ecological Modelling*. **221**(15), pp.1779–1797.

Ehleringer, J.R. and Dawson, T.E. 1992. Water uptake by plants: perspectives from stable isotope composition. Plant Cell Environ. 15(9), pp.1073–1082.

Enfield, D.B., Mestas-Nuñez, A.M. and Trimble, P.J. 2001. The Atlantic multidecadal oscillation and its relation to rainfall and river flows in the continental U.S. *Geophysical Research Letters*. **28**(10), pp.2077–2080.

Engel, Z., Skrzypek, G., Chuman, T., Šefrna, L. and Mihaljevič, M. 2014. Climate in the Western Cordillera of the Central Andes over the last 4300 years. *Quaternary Science Reviews*. **99**, pp.60–77.

van der Ent, R.J., Savenije, H.H.G., Schaefli, B. and Steele-Dunne, S.C. 2010. Origin and fate of atmospheric moisture over continents. *Water Resources Research*. **46**(9), pp.1–12.

Epstein, S., Thompson, P. and Yapp, C.J. 1977. Oxygen and hydrogen isotopic ratios in plant cellulose. Science. **198**(4323), pp.1209–15.

Espinoza, J.C., Ronchail, J., Guyot, J.L., Junquas, C., Vauchel, P., Lavado, W., Drapeau, G. and Pombosa, R. 2011. Climate variability and extreme drought in the upper Solimões River (western Amazon Basin): Understanding the exceptional 2010 drought. *Geophysical Research Letters*. **38**(13), pp.1–6.

Espinoza Villar, J.C., Guyot, J.L., Ronchail, J., Cochonneau, G., Filizola, N., Fraizy, P., Labat, D., de Oliveira, E., Ordoñez, J.J. and Vauchel, P. 2009. Contrasting regional discharge evolutions in the Amazon basin (1974-2004). *Journal of Hydrology*. **375**(3–4), pp.297–311.

Esquivel-Muelbert, A., Baker, T.R., Dexter, K.G., Lewis, S.L., ter Steege, H., Lopez-Gonzalez, G., Monteagudo Mendoza, A., Brienen, R., Feldpausch, T.R., Pitman, N., Alonso, A., van der Heijden, G., Peña-Claros, M., Ahuite, M., Alexiaides, M., Álvarez Dávila, E., Murakami, A.A., Arroyo, L., Aulestia, M., Balslev, H., Barroso, J., Boot, R., Cano, A., Chama Moscoso, V., Comiskey, J.A., Cornejo, F., Dallmeier, F., Daly, D.C., Dávila, N., Duivenvoorden, J.F., Duque Montoya, A.J., Erwin, T., Di Fiore, A., Fredericksen, T., Fuentes, A., García-Villacorta, R., Gonzales, T.,

Guevara Andino, J.E., Honorio Coronado, E.N., Huamantupa-Chuquimaco, I., Killeen, T.J., Malhi, Y., Mendoza, C., Mogollón, H., Jørgensen, P.M., Montero, J.C., Mostacedo, B., Nauray, W., Neill, D., Vargas, P.N., Palacios, S., Palacios Cuenca, W., Pallqui Camacho, N.C., Peacock, J., Phillips, J.F., Pickavance, G., Quesada, C.A., Ramírez-Angulo, H., Restrepo, Z., Reynel Rodriguez, C., Paredes, M.R., Sierra, R., Silveira, M., Stevenson, P., Stropp, J., Terborgh, J., Tirado, M., Toledo, M., Torres-Lezama, A., Umaña, M.N., Urrego, L.E., Vasquez Martinez, R., Gamarra, L.V., Vela, C.I.A., Vilanova Torre, E., Vos, V., von Hildebrand, P., Vriesendorp, C., Wang, O., Young, K.R., Zartman, C.E. and Phillips, O.L. 2017. Seasonal drought limits tree species across the Neotropics. *Ecography*. **40**(5), pp.618–629.

Esquivel-Muelbert, A., Galbraith, D., Dexter, K.G., Baker, T.R., Lewis, S.L., Meir, P., Rowland, L., Da Costa, A.C.L., Nepstad, D. and Phillips, O.L. 2017. Biogeographic distributions of neotropical trees reflect their directly measured drought tolerances. *Scientific Reports*. **7**(1), pp.1–11.

Evans, J.R. and von Caemmerer, S. 2013. Temperature response of carbon isotope discrimination and mesophyll conductance in tobacco. *Plant, Cell and Environment*. **36**, pp.745–756.

Evaristo, J., Jasechko, S. and McDonnell, J.J. 2015. Global separation of plant transpiration from groundwater and streamflow. *Nature*. **525**, pp.91–94.

Farquhar, G.D. and Cernusak, L.A. 2012. Ternary effects on the gas exchange of isotopologues of carbon dioxide. *Plant, Cell and Environment*. **35**(7), pp.1221–1231.

Farquhar, G.D., Cernusak, L.A. and Barnes, B. 2007. Heavy Water Fractionation during Transpiration. *Plant Physiology*. **143**(1), pp.11–18.

Farquhar, G.D., Ehleringer, R. and Hubic, K.T. 1989. Carbon Isotope Discrimination and Photosynthesis. *Annual Review of Plant Biology*. **40**, pp.503–537.

Farquhar, G.D., O'Leary, M.H. and Berry, J.A. 1982. On the relationship between carbon isotope discrimination and the intercellular carbon dioxide concentration in leaves. *Australian Journal of Plant Physiology*. **9**(2), pp.121–137.

Farquhar, G.D. and Lloyd, J., 1993. Carbon and oxygen isotope effects in the exchange of carbon dioxide between terrestrial plants and the atmosphere. In *Stable isotopes and plant carbon-water relations*. pp. 47-70. Academic Press.

Farquhar, G.D. and Sharkey, T.D. 1982. Stomatal Conductance and Photosynthesis. *Annual Review of Plant Physiology*. **33**(1), pp.317–345.

Fauset, S., Marcos, P.M., Gloor, M.U., Joly, C.A., Galbraith, D.R., Sullivan, M.J.P., Vieira, S.A. and Phillips, O.L. 2018. Differences in leaf thermoregulation and water use strategies between three co - occurring Atlantic forest tree species. *Plant, Cell and Environment*. **41**, pp.1618–1631.

Fearnside, P. 2005. Deforestation in Brazilian Amazonia : History , Rates and Consequences. *Conservation Biology*. **19**(3), pp.728–733.

Feldpausch, T.R., Lloyd, J., Lewis, S.L., Brienen, R.J.W., Gloor, M., Monteagudo Mendoza, A., Lopez-Gonzalez, G., Banin, L., Abu Salim, K., Affum-Baffoe, K., Alexiades, M., Almeida, S., Amaral, I., Andrade, A., Aragão, L.E.O.C., Araujo

Murakami, A., Arets, E.J.M., Arroyo, L., Aymard C., G.A., Baker, T.R., Bánki, O.S., Berry, N.J., Cardozo, N., Chave, J., Comiskey, J.A., Alvarez, E., De Oliveira, A., Di Fiore, A., Djagbletey, G., Domingues, T.F., Erwin, T.L., Fearnside, P.M., França, M.B., Freitas, M.A., Higuchi, N., Honorio C., E., Iida, Y., Jiménez, E., Kassim, A.R., Killeen, T.J., Laurance, W.F., Lovett, J.C., Malhi, Y., Marimon, B.S., Marimon-Junior, B.H., Lenza, E., Marshall, A.R., Mendoza, C., Metcalfe, D.J., Mitchard, E.T.A., Neill, D.A., Nelson, B.W., Nilus, R., Nogueira, E.M., Parada, A., S.-H. Peh, K., Pena Cruz, A., Peñuela, M.C., Pitman, N.C.A., Prieto, A., Quesada, C.A., Ramírez, F., Ramírez-Angulo, H., Reitsma, J.M., Rudas, A., Saiz, G., Salomão, R.P., Schwarz, M., Silva, N., Silva-Espejo, J.E., Silveira, M., Sonké, B., Stropp, J., Taedoumg, H.E., Tan, S., Ter Steege, H., Terborgh, J., Torello-Raventos, M., Van Der Heijden, G.M.F., Vásquez, R., Vilanova, E., Vos, V.A., White, L., Willcock, S., Woell, H. and Phillips, O.L. 2012. Tree height integrated into pantropical forest biomass estimates. *Biogeosciences*. **9**(8), pp.3381–3403.

Feldpausch, T.R., Phillips, O.L., Brienen, R.J.W., Gloor, E., Lloyd, J., Malhi, Y., Alarcón, A., Dávila, E.Á., Andrade, A., Aragao, L.E.O.C., Arroyo, L., Aymard, G.A.C., Baker, T.R., Baraloto, C., Barroso, J., Bonal, D., Castro, W., Chama, V., Chave, J., Domingues, T.F., Fauset, S., Groot, N., Coronado, E.H., Laurance, S., Laurance, W.F., Lewis, S.L., Licona, J.C., Marimon, B.S., Bautista, C.M., Neill, D.A., Oliveira, E.A., Santos, C.O., Camacho, N.C.P., Prieto, A., Quesada, C.A., Ramírez, F., Rudas, A., Saiz, G., Salomão, R.P., Silveira, M., Steege, H., Stropp, J., Terborgh, J., Heijden, G.M.F., Martinez, R.V., Vilanova, E. and Vos, V.A. 2016. Amazon forest response to repeated droughts. *Global Biogeochemical Cycles*. **30**(7), pp.964–982.

Ferrio, J.P. and Voltas, J. 2005. Carbon and oxygen isotope ratios in wood constituents of *Pinus halepensis* as indicators of precipitation, temperature and vapour pressure deficit. *Tellus*. **57B**, 164–173.

Fernandes, K., Giannini, A., Verchot, L., Baethgen, W. and Pinedo-Vasquez, M. 2015. Decadal covariability of Atlantic SSTs and western Amazon dry-season hydroclimate in observations and CMIP5 simulations. *Geophysical Research Letters*. **42**(16), pp.6793–6801.

Fichtler, E., Clark, D.A. and Worbes, M. 2003. Age and Long-term Growth of Trees in an Old-growth Tropical Rain Forest, Based on Analyses of Tree Rings and 14C1. *Biotropica*. **35**(3), p.306.

Fichtler, E., Helle, G. and Worbes, M. 2010. Stable-Carbon Isotope Time Series from Tropical Tree Rings Indicate a Precipitation Signal. *Tree-Ring Research*. **66**(1), pp.35–49.

Fichtler, E., Trouet, V., Beeckman, H., Coppin, P. and Worbes, M. 2004. Climatic signals in tree rings of Burkea africana and Pterocarpus angolensis from semiarid forests in Namibia. *Trees - Structure and Function*. **18**(4), pp.442–451.

Fichtler, E. and Worbes, M. 2012. Wood anatomical variables in tropical trees and their relation to site conditions and individual tree morphology. *IAWA Journal*. **33**(2), pp.119–140.

Flato, G., Marotzke, J., Abiodun, B., Braconnot, P., Chou, S.C., Collins, W., Cox, P., Driouech, F., Emori, S., Eyring, V., Forest, C., Gleckler, P., Guilyardi, E., Jakob, C.,

Kattsov, V., Reason, C. and Rummukainen, M. 2013. Evaluation of Climate Models. *Climate Change 2013: The Physical Science Basis. Contribution of Working Group I to the Fifth Assessment Report of the Intergovernmental Panel on Climate Change*. pp.741–866.

Flores, B.M., Holmgren, M., Xu, C., van Nes, E.H., Jakovac, C.C., Mesquita, R.C.G. and Scheffer, M. 2017. Floodplains as an Achilles' heel of Amazonian forest resilience. *Proceedings of the National Academy of Sciences*. **114**(17), pp.4442–4446.

Foley, J.A., Botta, A., Coe, M.T. and Costa, M.H. 2002. El Niño-Southern oscillation and the climate, ecosystems and rivers of Amazonia. *Global Biogeochemical Cycles*. **16**(4), pp.79-1-79–20.

Fonti, P., Solomonoff, N., García-González, I. 2007. Earlywood vessels of Castanea sativa record temperature before their formation. *New Phytologist*. **173**(3), pp. 562–570.

Franks, P.J. 2013. Tansley review Sensitivity of plants to changing atmospheric CO 2 concentration : from the geological past to the next century. *New Phytologist*. **197**, pp.1077–1094.

Friedlingstein, P. 2015. Carbon cycle feedbacks and future climate change. *Philosophical Transactions of the Royal Society A*. **373**(2054), 20140421.

Fritts, H.C., 1971. Dendroclimatology and dendroecology. *Quaternary Research*. **1**(4), pp.419-449.

Fu, R., Yin, L., Li, W., Arias, P.A., Dickinson, R.E., Huang, L., Chakraborty, S., Fernandes, K., Liebmann, B., Fisher, R. and Myneni, R.B. 2013. Increased dry-season length over southern Amazonia in recent decades and its implication for future climate projection. *Proceedings of the National Academy of Sciences*. **110**(45), pp.18110–18115.

Garreaud, R.D., Vuille, M., Compagnucci, R. and Marengo, J. 2009. Present-day South American climate. *Palaeogeography, Palaeoclimatology, Palaeoecology*. **281**(3–4), pp.180–195.

Garreaud, R.D. and Wallace, J.M. 1998. Summertime Incursions of Midlatitude Air into Subtropical and Tropical South America. *Monthly Weather Review*. **126**, pp.2713–2733.

Gärtner, H. and Nievergelt, D. 2010. The core-microtome: A new tool for surface preparation on cores and time series analysis of varying cell parameters. *Dendrochronologia*. **28**(2), pp.85–92.

Gash, J.H.C. and Nobre, C.A. 1997. Climatic effects of Amazonian deforestation- Some results from ABRACOS. *Bulletin of the American Meteorological Society*. **78**(5), pp.823–830.

Gat, J.R. and Matsui, E. 1991. Atmospheric water balance in the Amazon basin: An isotopic evapotranspiration model. *Journal of Geophysical Research*. **96**(D7), p.13179.

Gatti, L. V, Gloor, M., Miller, J.B., Doughty, C.E., Malhi, Y., Domingues, L.G., Basso, L.S., Martinewsky, A., Correia, C.S.C., Borges, V.F., Freitas, S., Braz, R., Anderson, L.O., Rocha, H., Grace, J., Phillips, O.L. and Lloyd, J. 2014. Drought sensitivity of

Amazonian carbon balance revealed by atmospheric measurements. *Nature*. **506**, pp.76–80.

Gebrekirstos, A., Bräuning, A., Sass-Klassen, U. and Mbow, C. 2014. Opportunities and applications of dendrochronology in Africa. *Current Opinion in Environmental Sustainability*. **6**(1), pp.48–53.

Gebrekirstos, A., Worbes, M., Teketay, D., Fetene, M. and Mitlöhner, R. 2009. Stable carbon isotope ratios in tree rings of co-occurring species from semi-arid tropics in Africa: Patterns and climatic signals. *Global and Planetary Change*. **66**(3–4), pp.253–260.

Gedney, N. and Valdes, P.J. 2000. The effect of Amazonian deforestation on the northern hemisphere circulation and climate. *Geophysical Research Letters*. **27**(19), pp.3053–3056.

Gentry, A.H. and Lopez-Parodi, J. 1980. Deforestation and Increased Flooding of the Upper Amazon. *Science*. **210**, pp.1354–1356.

Gessler, A., Ferrio, J.P., Hommel, R., Treydte, K., Werner, R.A. and Monson, R.K. 2014. Stable isotopes in tree rings: Towards a mechanistic understanding of isotope fractionation and mixing processes from the leaves to the wood. *Tree Physiology*. **34**(8), pp.796–818.

Gessler, A. and Treydte, K. 2016. The fate and age of carbon - insights into the storage and remobilization dynamics in trees. *New Phytologist*. **209**(4), pp.1338–1340.

Gloor, M., Barichivich, J., Ziv, G., Brienen, R., Schöngart, J. and Peylin, P. 2015. Recent Amazon climate as background for possible ongoing and future changes of Amazon Humid Forests. *Global Biogeochemical Cycles*. **29**, pp. 1384–1399.

Gloor, M., Brienen, R.J.W., Galbraith, D., Feldpausch, T.R., Schöngart, J., Guyot, J.L., Espinoza, J.C., Lloyd, J. and Phillips, O.L. 2013. Intensification of the Amazon hydrological cycle over the last two decades. *Geophysical Research Letters*. **40**(9), pp.1729–1733.

Gonfiantini, R. 1978. Standards for stable isotope measurements in natural compounds. *Nature*. **271**(5645), p.534.

Granato-Souza, D., Stahle, D.W., Barbosa, A.C., Feng, S., Torbenson, M.C.A., de Assis Pereira, G., Schöngart, J., Barbosa, J.P. and Griffin, D. 2019. Tree rings and rainfall in the equatorial Amazon. *Climate Dynamics*. **52**(3-4), pp.1857–1869.

Griffiths, H. and Helliker, B.R. 2013. Mesophyll conductance : internal insights of leaf carbon exchange. *Plant, cell and environment*. **36**, pp.733–735.

Gulbranson, E.L. and Ryberg, P.E. 2013. Paleobotanical and Geochemical Approaches To Studying Fossil Tree Rings: Quantitative Interpretations of Paleoenvironment and Ecophysiology. *Palaios*. **28**(3), pp.137–140.

Harper, A., Baker, I.T., Denning, A.S., Randall, D.A., Dazlich, D. and Branson, M. 2014. Impact of evapotranspiration on dry season climate in the Amazon forest. *Journal of Climate*. **27**(2), pp.574–591.

Harris, I., Jones, P.D., Osborn, T.J. and Lister, D.H. 2014. Updated high-resolution grids of monthly climatic observations - the CRU TS3.10 Dataset. *International Journal of Climatology*. **34**(3), pp.623–642.

Harris, S.E. and Mix, A.C. 1999. Pleistocene precipitation balance in the Amazon Basin recorded in deep sea sediments. *Quaternary Research*. **51**(1), pp.14–26.

Hasler, N. and Avissar, R. 2007. What Controls Evapotranspiration in the Amazon Basin? *Journal of Hydrometeorology*. **8**(3), pp.380–395.

Hastenrath, S. and Heller, L. 1977. Dynamics of Climate Hazards in northeast Brazil. *Quarterly Journal of the Royal Meteorological Society*. **103**, pp.77–92.

Haug, G.H., Hughen, K.A., Sigman, D.M., Peterson, L.C. and Röhl, U. 2001. Southward Migration of the Intertropical Convergence Zone Through the Holocene. *Science*. **293**(5533), pp.1304–1308.

Hayles, A., Santos, G.M., Herrera-Ramírez, D.A., Martin-Fernandez, M., Ruiz-Carrascal, D., Boza-Espinoza, T.E., Fuentes, A.F. and Jørgensen, P.M. Matching dendrochonological dates with the southern hemisphere ^{14}C bomb curve to confirm annual tree rings in *Pseudolmedia rigida* from Bolivia. 2015. *Radiocarbon*. **51**(1), pp. 1–13.

Helle, G. and Schleser, G.H. 2004. Beyond CO2-fixation by Rubisco - An interpretation of$^{13}C/^{12}C$ variations in tree rings from novel intra-seasonal studies on broad-leaf trees. *Plant, Cell and Environment*. **27**(3), pp.367–380.

Henderson-Sellers, A., Dickinson, R.E., Durbidge, T.B., Kennedy, P.J., McGuffie, K. and Pitman, J. 1993. Tropical Deforestation ' Modeling Local- to Regional-Scale Climate Change. *Journal of Geophysical Research*. **98**(92), pp.7289–7315.

Henderson-Sellers, A., McGuffie, K. and Zhang, H. 2002. Stable isotopes as validation tools for global climate model predictions of the impact of Amazonian deforestation. *Journal of Climate*. **15**(18), pp.2664–2677.

Hietz, P., Wanek, W. and Dünisch, O. 2005. Long-term trends in cellulose $\delta^{13}C$ and water-use efficiency of tropical Cedrela and Swietenia from Brazil. *Tree Physiology*. **25**(6), pp.745–752.

Hoffmann, G., Ramirez, E., Taupin, J.D., Francou, B., Ribstein, P., Delmas, R., Dürr, H., Gallaire, R., Simoes, J., Schotterer, U., Stievenard, M. and Werner, M. 2003. Coherent isotope history of Andean ice cores over the last century. *Geophysical Research Letters*. **30**(4), pp.1–4.

Holloway-Phillips, M., Cernusak, L.A., Barbour, M., Song, X., Cheesman, A., Munksgaard, N., Stuart-Williams, H. and Farquhar, G.D. 2016. Leaf vein fraction influences the Péclet effect and18O enrichment in leaf water. *Plant Cell and Environment*. **39**(11), pp.2414–2427.

Holmes, R. L. 1983 Computer -assisted quality control in tree -ring dating and measurement. *Tree -Ring Bulletin.* **43**: 69 -78.

Hua, W., Dai, A., Zhou, L., Qin, M. and Chen, H. 2019. An externally-forced decadal rainfall seesaw pattern over the Sahel and southeast Amazon. *Geophysical Research Letters*. **46**, pp.1–10.

Humphrey, V., Zscheischler, J., Ciais, P., Gudmundsson, L., Sitch, S. and Seneviratne, S.I. 2018.Oobserved changes in terrestrial water storage. *Nature*. **560**, pp.628-632.

Huntingford, C., Zelazowski, P., Galbraith, D., Mercado, L.M., Sitch, S., Fisher, R., Lomas, M., Walker, A.P., Jones, C.D., Booth, B.B.B., Malhi, Y., Hemming, D., Kay, G., Good, P., Lewis, S.L., Phillips, O.L., Atkin, O.K., Lloyd, J., Gloor, E., Zaragoza-castells, J. and Meir, P. 2013. Simulated resilience of tropical rainforests to CO_2 -induced climate change. *Nature Geoscience*. **6**(4), pp.268–273.

Hurley, J. V., Vuille, M. and Hardy, D.R. 2016. Forward modeling of δ18O in Andean ice cores. *Geophysical Research Letters*. **43**(15), pp.8178–8188.

Hut, G. 1987. Consultants' group meeting on stable isotope reference samples for geochemical and hydrological investigations. *Internacional Atomic Energy Agency*. Vienna.

Jackson, W.A. and Volk, R.J. 1970. Photorespiration. *Annual Reviews of Plant Physiology*. **21**, pp385-432.

Jones, H. G. (1992). Plants and microclimate. Cambridge, UK: *Cambridge University Press*.

Junk, W.J. 1989. The flood pulse concept in River-Floodplain systems *Canadian special publication of fisheries and aquatic sciences*. **106(**1), pp.110-127.

Junk, W.J., Piedade, M.T.F., Lourival, R., Wittmann, F., Kandus, P., Lacerda, L.D., Bozelli, R.L., Esteves, F.A., Nunes da Cunha, C., Maltchik, L., Schöngart, J., Schaeffer-Novelli, Y. and Agostinho, A.A. 2014. Brazilian wetlands: Their definition, delineation, and classification for research, sustainable management, and protection. *Aquatic Conservation: Marine and Freshwater Ecosystems*. **24**(1), pp.5–22.

Junk, W.J., Piedade, M.T.F., Parolin, P., Wittmann, F. and Schongart, J. 2010. Ecophysiology, Biodiversity and Sustainable Management of Central Amazonian Floodplain Forests: A Synthesis In: Amazonian Floodplain Forests: Ecophysiology, Biodiversity and Sustainable Management. *Springer*, Dordrecht. pp.747–748.

Junk, W.J., Piedade, M.T.F., Schöngart, J., Cohn-Haft, M., Adeney, J.M. and Wittmann, F. 2011. A classification of major naturally-occurring amazonian lowland wetlands. *Wetlands*. **31**(4), pp.623–640.

Junk, W.J., Wittmann, F., Schöngart, J. and Piedade, M.T.F. 2015. A classification of the major habitats of Amazonian black-water river floodplains and a comparison with their white-water counterparts. *Wetlands Ecology and Management*. **23**(4), pp.677–693.

Kagawa, A., Sano, M., Nakatsuka, T., Ikeda, T. and Kubo, S. 2015. An optimized method for stable isotope analysis of tree rings by extracting cellulose directly from cross-sectional laths. *Chemical Geology*. **393**, pp.16–25.

Kahmen, A., Sachse, D., Arndt, S.K., Tu, K.P., Farrington, H., Vitousek, P.M. and Dawson, T.E. 2011. Cellulose $\delta^{18}O$ is an index of leaf-to-air vapour pressure difference (VPD) in tropical plants. *Proceedings of the National Academy of Sciences*. **108**(5), pp.1981–1986.

Kahmen, A., Simonin, K., Tu, K.P., Merchant, A., Callister, A., Siegwolf, R., Dawson, T.E. and Arndt, S.K. 2008. Effects of environmental parameters, leaf physiological properties and leaf water relations on leaf water $\delta^{18}O$ enrichment in different Eucalyptus species. *Plant, Cell and Environment*. **31**(6), pp.738–751.

Kanner, L.C., Burns, S.J., Cheng, H., Edwards, R.L. and Vuille, M. 2013. High-resolution variability of the South American summer monsoon over the last seven millennia: Insights from a speleothem record from the central Peruvian Andes. *Quaternary Science Reviews*. **75**, pp.1–10.

Kerr, R.A., 2000. A North Atlantic climate pacemaker for the centuries. *Science*, **288**(5473), pp.1984-1985.

Khanna, J., Medvigy, D., Fueglistaler, S. and Walko, R. 2017. Regional dry-season climate changes due to three decades of Amazonian deforestation. *Nature Climate Change*. **7**(3), pp.200–204.

Kirschke, S., Bousquet, P., Ciais, P., Saunois, M., Canadell, J.G., Dlugokencky, E.J., Bergamaschi, P., Bergmann, D., Blake, D.R., Bruhwiler, L. and Cameron-Smith, P. 2013. Three decades of global methane sources and sinks. *Nature geoscience*. **6**(10), p.813.

Kitoh, A., Endo, H., Krishna Kumar, K., Cavalcanti, I.F.A., Goswami, P. and Zhou, T. 2013. Monsoons in a changing world: A regional perspective in a global context. *Journal of Geophysical Research: Atmospheres*. **118**(8), pp.3053–3065.

Lammertsma, E.I., Wagner-Cremer, F., Wassen, M.J., de Boer, H.J., Dilcher, D.L. and Dekker, S.C. 2011. Climate forcing due to optimization of maximal leaf conductance in subtropical vegetation under rising CO_2. *Proceedings of the National Academy of Sciences*. **108**(10), pp.4041–4046.

Leavittt, S.W. and Long, A. 1991. Seasonal stable-carbon isotope variability in tree rings: possible paleoenvironmental signals. *Chemical Geology (Isotope Geoscience Section)*. **87**, pp. 59–70.

Lee, J.E. and Fung, I. 2008. "Amount effect" of water isotopes and quantitative analysis of post-condensation processes. *Hydrological Processes*. 22, pp.1–8.

Lewis, S.L., Brando, P.M., Phillips, O.L., Van Der Heijden, G.M.F. and Nepstad, D. 2011. The 2010 Amazon drought. *Science*. **331**(6017), p.554.

Li, X., Xie, S.P., Gille, S.T. and Yoo, C. 2016. Atlantic-induced pan-tropical climate change over the past three decades. *Nature Climate Change*. **6**(3), pp.275–279.

Li, Z.H., Labbé, N., Driese, S.G. and Grissino-Mayer, H.D. 2011. Micro-scale analysis of tree-ring $\delta^{18}O$ and $\delta^{13}C$ on α-cellulose spline reveals high-resolution intra-annual climate variability and tropical cyclone activity. *Chemical Geology*. **284**(1–2), pp.138–147.

Libby, L.M., Pandofili, L.J., Payton, P.H., Marshall, J., Becker, B. and Giertz-Siebenlist, V. 1976. Isotopic tree thermometers. *Nature*. **261**, pp.284–288.

Liebmann, B. 2011. The South American Monsoon System In: The Global Monsoon System: Research and Forecast., pp.137–157.

Lisi, C.S., F, M.T., Botosso, P.C., Roig, F.A., Maria, V.R.B., Ferreira-fedele, L., Voigt, A.R.A. and Filho, M.T. 2008. Tree-Ring Formation, Radial Increment Periodicity, and Phenology of Tree Species From a Seasonal Semi-Deciduous Forest in Southeast Brazil. *IAWA Journal*. **29**(2), pp.189–207.

Liu, X., An, W., Treydte, K., Shao, X., Leavitt, S., Hou, S., Chen, T., Sun, W. and Qin, D. 2012. Tree-ring $\delta^{18}O$ in southwestern China linked to variations in regional cloud cover and tropical sea surface temperature. *Chemical Geology*. **291**, pp.104–115.

Lloyd, J. and Farquhar, G.D. 2008. Effects of rising temperatures and [CO_2] on the physiology of tropical forest trees. *Philosophical Transactions of the Royal Society B: Biological Sciences*. **363**(1498), pp.1811–1817.

Loader, N.J., Robertson, I. and McCarroll, D. 2003. Comparison of stable carbon isotope ratios in the whole wood, cellulose and lignin of oak tree-rings. *Palaeogeography, Palaeoclimatology, Palaeoecology*. **196**(3–4), pp.395–407.

Locosselli, G.M., Buckeridge, M.S., Moreira, M.Z. and Ceccantini, G. 2013. A multi-proxy dendroecological analysis of two tropical species (Hymenaea spp., Leguminosae) growing in a vegetation mosaic. *Trees - Structure and Function*. **27**(1), pp.25–36.

Locosselli, G.M., Schöngart, J. and Ceccantini, G. 2016. Climate/growth relations and teleconnections for a Hymenaea courbaril (Leguminosae) population inhabiting the dry forest on karst. *Trees - Structure and Function*. **30**(4), pp.1127–1136.

Locosselli, G.M., Cardim, R.H. and Ceccantini, G., 2016. Rock outcrops reduce temperature-induced stress for tropical conifer by decoupling regional climate in the semiarid environment. *International Journal of Biometeorology*, **60**(5), pp.639-649.

Lopez, L., Stahle, D., Villalba, R., Torbenson, M., Feng, S. and Cook, E. 2017. Tree ring reconstructed rainfall over the southern Amazon Basin. *Geophysical Research Letters*. 44(14), pp.7410–7418.

López, L. and Villalba, R. 2011. Climate Influences on the Radial Growth of *Centrolobium microchaete*, a Valuable Timber Species from the Tropical Dry Forests in Bolivia. *Biotropica*. **43**(1), pp.41–49.

Lorenz, R., Pitman, A.J. and Sisson, S.A. 2016. Does Amazonian deforestation cause global effects: Can we be sure? *Journal of Geophysical Research*. **121**(10), pp.5567–5584.

Luo, Y.-H. and Sternberg, L. da S.L. 1992. Hydrogen and Oxygen Isotopic Fractionation During Heterotrophic Cellulose Synthesis. *Journal of Experimental Botany*. **43**(1), pp.47–50.

Magrin, G.O., Marengo, J.A., Boulanger, J.P., Buckeridge, M.S., Castellanos, E., Poveda, G., Scarano, F.R. and Vicuña, S., 2014. Central and South America. *Climate Change*, pp.1499-1566.

Malhi, Y., Baker, T.R., Phillips, O.L., Almeida, S., Alvarez, E., Arroyo, L., Chave, J., Czimczik, C.I., Di Fiore, A., Higuchi, N., Killeen, T.J., Laurance, S.G., Laurance, W.F., Lewis, S.L., Montoya, L.M.M., Monteagudo, A., Neill, D.A., Vargas, P.N., Patino, S., Pitman, N.C.A., Quesada, C.A., Salomao, R., Silva, J.N.M., Lezama, A.T., Martínez, R.V., Terborgh, J., Vinceti, B. and Lloyd, J. 2004. The above-ground coarse wood productivity of 104 Neotropical forest plots. *Global Change Biology*. **10**(5), pp.563–591.

Malhi, Y., Roberts, J.T., Betts, R. a, Killeen, T.J., Li, W. and Nobre, C. a 2008. The Fate of the Amazon. *Science*. **319** (5860), pp.169–172.

Managave, S.R., Sheshshayee, M.S., Bhattacharyya, A. and Ramesh, R. 2011. Intra-annual variations of teak cellulose $\delta^{18}O$ in Kerala, India: Implications to the reconstruction of past summer and winter monsoon rains. *Climate Dynamics*. **37**(3), pp.555–567.

Mantua, N.J. and Hare, S.R. 2002. The pacific decadal oscillation. *Journal of Oceanography*. **58**(1991), pp.35–44.

Manyari, W.V. and de Carvalho, O.A. 2007. Environmental considerations in energy planning for the Amazon region: Downstream effects of dams. *Energy Policy*. **35**(12), pp.6526–6534.

Marengo, J.A. 2005. Characteristics and spatio-temporal variability of the Amazon river basin water budget. *Climate Dynamics*. **24**(1), pp.11–22.

Marengo, J.A. 2004. Interdecadal variability and trends of rainfall across the Amazon basin. *Theoretical and Applied Climatology*. **78**(1–3), pp.79–96.

Marengo, J.A. 2009. Long-term trends and cycles in the hydrometeorology of the Amazon basin since the late 1920s. *Hydrological Processes: An International Journal,* **23**(22), pp.3236-3244.

Marengo, J.A., Borma, L.S., Rodriguez, D.A., Pinho, P., Soares, W.R. and Alves, L.M. 2013. Recent Extremes of Drought and Flooding in Amazonia: Vulnerabilities and Human Adaptation. *American Journal of Climate Change*. 2(02), pp.87–96.

Marengo, J.A. and Espinoza, J.C. 2015. Extreme seasonal droughts and floods in Amazonia : causes, trends and impacts. *International Journal of Climatology*. **36**(3), pp.1033-1050.

Marengo, J.A., Liebmann, B., Kousky, V.E., Filizola, N.P. and Wainer, I.C. 2001. Onset and end of the rainy season in the Brazilian Amazon Basin. *Journal of Climate*. **14**(5), pp.833–852.

Marengo, J.A., Nobre, C.A., Tomasella, J., Cardoso, M.F. and Oyama, M.D. 2008. Hydro-climatic and ecological behaviour of the drought of Amazonia in 2005. *Philosophical Transactions of the Royal Society B: Biological Sciences*. **363**(1498), pp.1773–1778.

Marengo, J.A., Soares, W.R., Saulo, C. and Nicolini, M. 2004. Climatology of the Low-Level Jet east of the Andes as derived from the NCEP reanalyses. *Journal of Climate*. **17**, pp.2261–2280.

Marengo, J.A., Tomasella, J., Soares, W.R., Alves, L.M. and Nobre, C.A. 2012. Extreme climatic events in the Amazon basin. *Theoretical and Applied Climatology*. **107**(1–2), pp.73–85.

Marengo, J.A., Tomasella, J. and Uvo, C.R. 1998. Trends in streamflow and rainfall in tropical South America: Amazonia, eastern Brazil, and northwestern Peru. *Journal of Geophysical Research Atmospheres*. **103**(D2), pp.1775–1783.

Maslin, M.A. and Burns, S.J. 2000. Reconstruction of the Amazon basin effective moisture availability over the past 14,000 years. *Science.* **290**, pp.2285–2287.

Masson-Delmotte, V., Raffalli-Delerce, G., Danis, P.A., Yiou, P., Stievenard, M., Guibal, F., Mestre, O., Bernard, V., Goosse, H., Hoffmann, G. and Jouzel, J. 2005. Changes in European precipitation seasonality and in drought frequencies revealed by a four-century-long tree-ring isotopic record from Brittany, western France. *Climate Dynamics*. **24**(1), pp.57–69.

Matsui, E., Salati, E., Ribeiro, M.N.G., Reis, C.., Tancredi, A.C.S.N.F. and Gat, J.R. 1983. Precipitation in the Central Amazon Basin: The isotopic composition of rain and atmospheric moisture at Belem and Manaus. *Acta Amazonica*. **13**(2), pp.307–369.

McCarroll, D. and Loader, N.J. 2004. Stable isotopes in tree rings. Q*uaternary Science Reviews*. **23**(7–8), pp.771–801.

McDermitt, D.K. 1990. Sources of error in the estimation of stomatal conductance and transpiration from porometer data. *HortScience*. **25**(12), pp.1538–1548.

McGregor, S., Timmermann, A., Stuecker, M.F., England, M.H., Merrifield, M., Jin, F.F. and Chikamoto, Y. 2014. Recent walker circulation strengthening and pacific cooling amplified by Atlantic warming. *Nature Climate Change*. **4**(10), pp.888–892.

Medvigy, D., Walko, R.L. and Avissar, R. 2011. Effects of deforestation on spatiotemporal distributions of precipitation in South America. *Journal of Climate*. **24**(8), pp.2147–2163.

Melack, J.M. and Wang, Y. 1998. Delineation of flooded area and flooded vegetation in Balbina Reservoir (Amazonas, Brazil) with synthetic aperture radar. *Internationale Vereinigung für theoretische und angewandte Limnologie: Verhandlungen*. **26**, pp.2374–2377.

Melack, J.M. and Hess, L.L., 2010. Remote sensing of the distribution and extent of wetlands in the Amazon basin. In Amazonian floodplain forests. *Springer*, Dordrecht. pp. 43-59.

Mendivelso, H.A., Camarero, J.J., Gutiérrez, E. and Zuidema, P.A. 2014. Time-dependent effects of climate and drought on tree growth in a Neotropical dry forest: Short-term tolerance vs. long-term sensitivity. *Agricultural and Forest Meteorology*. **188**, pp.13–23.

Mendivelso, H.A., Camarero, J.J., Royo Obregón, O., Gutiérrez, E. and Toledo, M. 2013. Differential Growth Responses to Water Balance of Coexisting Deciduous Tree Species Are Linked to Wood Density in a Bolivian Tropical Dry Forest. *PLoS ONE*. **8**(10), p.e73855.

Miller, D.L., Mora, C.I., Grissino-Mayer, H.D., Mock, C.J., Uhle, M.E. and Sharp, Z. 2006. Tree-ring isotope records of tropical cyclone activity. *Proceedings of the National Academy of Sciences of the United States of America*. **103**(39), pp.14294–14297.

Moran, E.F., Adams, R., Bakoyéma, B., F, S. and Boucek, B. 2006. Human strategies for coping with El Niño related drought in Amazônia. *Climatic Change*. **77**(3–4), pp.343–361.

Morison, J.I.L. 1985. Sensitivity of stomata and water use efficiency to high CO_2. *Plant, Cell & Environment*. **8**(6), pp.467–474.

Motzer, T., Munz, N., Küppers, M., Schmitt, D. and Anhuf, D. 2005. Stomatal conductance, transpiration and sap flow of tropical montane rain forest trees in the southern Ecuadorian Andes. *Tree Physiology*. **25**(10), pp.1283–1293.

Muscarella, R., Bacon, C.D., Faurby, S., Antonelli, A., Kristiansen, S.M., Svenning, J. and Balslev, H. 2018. Soil Fertility and flood regime are correlated with phylogenetic structure of Amazonian palm communities. *Annals of Botany*. *123*(4), pp.641-655.

Nebel, G., Kvist, L.P., Vanclay, J.K., Christensen, H., Freitas, L. and Ruíz, J. 2001. Structure and floristic composition of flood plain forests in the Peruvian Amazon I. Overstorey. *Forest Ecology and Management*. **150**(1–2), pp.27–57.

Nepstad, D., McGrath, D., Stickler, C., Alencar, A., Azevedo, A., Swette, B., Bezerra, T., DiGiano, M., Shimada, J., Da Motta, R.S., Armijo, E., Castello, L., Brando, P.,

Hansen, M.C., McGrath-Horn, M., Carvalho, O. and Hess, L. 2014. Slowing Amazon deforestation through public policy and interventions in beef and soy supply chains. *Science*. **344**(6188), pp.1118–1123.

Nepstad, D.C., Tohver, I.M., Ray, D., Moutinho, P. and Cardinot, G. 2007. Mortality Of Large Trees And Lianas Following Experimental Drought In An Amazon Forest. *Ecology*. **88**(9), pp.2259–2269.

Nobre, C.A., Sampaio, G., Borma, L.S., Castilla-Rubio, J.C., Silva, J.S. and Cardoso, M. 2016. Land-use and climate change risks in the Amazon and the need of a novel sustainable development paradigm. *Proceedings of the National Academy of Sciences.* **113**(39), pp.10759–10768.

Nobre, C.A., Sellers, P.J. and Shukla, J. 1991. Amazonian deforestation and regional climate change. *Journal of Climate*. **4**, pp.957–988.

Nobre, P., Malagutti, M., Urbano, D.F., De Almeida, R.A.F. and Giarolla, E. 2009. Amazon deforestation and climate change in a coupled model simulation. *Journal of Climate*. **22**(21), pp.5686–5697.

Nock, C.A., Baker, P.J., Wanek, W., Leis, A., Grabner, M., Bunyavejchewin, S. and Hietz, P. 2010. Long-term increases in intrinsic water-use efficiency do not lead to increased stem growth in a tropical monsoon forest in western Thailand. *Global Change Biology*. **17**(2), pp.1049–1063.

Novello, V.F., Vuille, M., Cruz, F.W., Stríkis, N.M., De Paula, M.S., Edwards, R.L., Cheng, H., Karmann, I., Jaqueto, P.F., Trindade, R.I.F., Hartmann, G.A. and Moquet, J.S. 2016. Centennial-scale solar forcing of the South American Monsoon System recorded in stalagmites. *Scientific Reports*. **6**(24762), pp.1–8.

Ogren, W.L. Photorespiration: Pathways, regulation and modification. 1984. *Annual Reviews of Plant Physiology*. **35**, pp415-442.

Ohashi, S., Durgante, F.M., Kagawa, A., Kajimoto, T., Trumbore, S.E., Xu, X., Ishizuka, M. and Higuchi, N. 2015. Seasonal variations in the stable oxygen isotope ratio of wood cellulose reveal annual rings of trees in a Central Amazon terra firme forest. *Oecologia*. **180**(3), pp.685–696.

Ohashi, S., Okada, N., Nobuchi, T., Siripatanadilok, S. and Veenin, T. 2009. Detecting invisible growth rings of trees in seasonally dry forests in Thailand: Isotopic and wood anatomical approaches. *Trees - Structure and Function*. **23**(4), pp.813–822.

Ovando, A., Tomasella, J., Rodriguez, D.A., Martinez, J.M., Siqueira-Junior, J.L., Pinto, G.L.N., Passy, P., Vauchel, P., Noriega, L. and von Randow, C. 2016. Extreme flood events in the Bolivian Amazon wetlands. *Journal of Hydrology: Regional Studies*. **5**, pp.293–308.

Pan, Y., Burdsey, R.A., Fang, J., Houghton, R., Kauppi, P.E., Kurz, W.A., Phillips, O.L., Shvidenko, A., Lewis, S.L., Canadell, J.G., Ciais, P., Jackson, R.B., Pacala, S.W., McGuire, A.D., Piao, S., Rautiainen, A., Sitch, S. and Hayes, D. 2011. A large and persistent carbon sink in the world's forests. *Science*. **333**(6045), pp.988–93.

Pangala, S.R., Moore, S., Hornibrook, E.R. and Gauci, V. 2013. Trees are major conduits for methane egress from tropical forested wetlands. *New Phytologist*. **197**(2), pp.524-531.

Pangala, S.R., Enrich-Prast, A., Basso, L.S., Peixoto, R.B., Bastviken, D., Hornibrook, E.R., Gatti, L.V., Marotta, H., Calazans, L.S.B., Sakuragui, C.M. and Bastos, W.R. 2018. Large emissions from floodplain trees close the Amazon methane budget. *Nature*. **553**(7688), p.366.

Parolin, P. 2009. Submerged in darkness: Adaptations to prolonged submergence by woody species of the Amazonian floodplains. *Annals of Botany*. **103**(2), pp.359–376.

Parolin, P., Simone, O. de, Haase, K., Waldhoff, D., Rottenberger, S., Kuhn, U., Kesselmeier, J., Kleiss, B., Schmidt, W. and Piedade, M.T.F. 2004. Central Amazon Floodplain Forests: TreeAdaptations in a Pulsing System. *The Botanical Review*. **70**(3), pp.357–380.

Parolin, P. and Wittmann, F. 2010. Struggle in the flood: tree responses to flooding stress in four tropical floodplain systems. *AoB Plants*. **2010**, pp. 1-19.

Peters, R.L., Groenendijk, P., Vlam, M. and Zuidema, P.A. 2015. Detecting long-term growth trends using tree rings: A critical evaluation of methods. *Global Change Biology*. **21**(5), pp.2040–2054.

Peñuelas, J. and Llusià, J. 2002. Linking photorespiration, monoterpenes and thermotolerance in Quercus. *New Phytologist*. **155**, pp.227-237.

Phillips, O.L., Aragão, L.E.O.C., Lewis, S.L., Fisher, J.B., Lloyd, J., López-González, G., Malhi, Y., Monteagudo, A., Peacock, J., Quesada, C.A., Van Der Heijden, G., Almeida, S., Amaral, I., Arroyo, L., Aymard, G., Baker, T.R., Bánki, O., Blanc, L., Bonal, D., Brando, P., Chave, J., De Oliveira, Á.C.A., Cardozo, N.D., Czimczik, C.I., Feldpausch, T.R., Freitas, M.A., Gloor, E., Higuchi, N., Jiménez, E., Lloyd, G., Meir, P., Mendoza, C., Morel, A., Neill, D.A., Nepstad, D., Patiño, S., Peñuela, M.C., Prieto, A., Ramírez, F., Schwarz, M., Silva, J., Silveira, M., Thomas, A.S., Steege, H. Ter, Stropp, J., Vásquez, R., Zelazowski, P., Dávila, E.A., Andelman, S., Andrade, A., Chao, K.J., Erwin, T., Di Fiore, A., Honorio, E.C., Keeling, H., Killeen, T.J., Laurance, W.F., Cruz, A.P., Pitman, N.C.A., Vargas, P.N., Ramírez-Angulo, H., Rudas, A., Salamão, R., Silva, N., Terborgh, J. and Torres-Lezama, A. 2009. Drought sensitivity of the amazon rainforest. *Science*. **323**(5919), pp.1344–1347.

Phillips, O.L., Baker, T.R., Arroyo, L., Higuchi, N., Killeen, T.J., Laurance, W.F., Lewis, S.L., Lloyd, J., Malhi, Y., Monteagudo, A., Neill, D.A., Nüñez Vargas, P., Silva, J.N.M., Terborgh, J., Vásquez Martínez, R., Alexiades, M., Almeida, S., Brown, S., Chave, J., Comiskey, J.A., Czimczik, C.I., Di Fiore, A., Erwin, T., Kuebler, C., Laurance, S.G., Nascimento, H.E.M., Olivier, J., Palacios, W., Patiño, S., Pitman, N.C.A., Quesada, C.A., Saldias, M., Torres Lezama, A. and Vinceti, B. 2004. Pattern and process in Amazon tree turnover, 1976-2001. *Philosophical Transactions of the Royal Society B: Biological Sciences*. **359**(1443), pp.381–407.

Pinho, P.F., Marengo, J.A. and Smith, M.S. 2015. Complex socio-ecological dynamics driven by extreme events in the Amazon. *Regional Environmental Change*. **15**(4), pp.643–655.

Pons, T.L. and Helle, G. 2011. Identification of anatomically non-distinct annual rings in tropical trees using stable isotopes. *Trees - Structure and Function*. **25**(1), pp.83–93.

Pöschl, U., Martin, S.T., Sinha, B., Chen, Q., Gunthe, S.S., Huffman, J.A., Borrmann, S., Farmer, D.K., Garland, R.M., Helas, G., Jimenez, J.L., King, S.M., Manzi, A., Mikhailov, E., Pauliquevis, T., Petters, M.D., Prenni, A.J., Roldin, P., Rose, D., Schneider, J., Su, H., Zorn, S.R., Artaxo, P. and Andreae, M.O. 2010. Rainforest aerosols as biogenic nuclei of clouds and precipitation in the Amazon. *Science*. **329**(5998), pp.1513–1516.

Poussart, P.F., Evans, M.N. and Schrag, D.P. 2004. Resolving seasonality in tropical trees: Multi-decade, high-resolution oxygen and carbon isotope records from Indonesia and Thailand. *Earth and Planetary Science Letters*. **218**(3–4), pp.301–316.

Poussart, P.F. and Schrag, D.P. 2005. Seasonally resolved stable isotope chronologies from northern Thailand deciduous trees. *Earth and Planetary Science Letters*. **235**(3–4), pp.752–765.

Poussart, P.M., Myneni, S.C.B. and Lanzirotti, A., 2006. Tropical dendrochemistry: A novel approach to estimate age and growth from ringless trees. *Geophysical Research Letters*. **33**(17), pp. L17711 1–5.

Prance, G.T. 1979. Notes on the Vegetation of Amazonia III. The Terminology of Amazonian Forest Types Subject to Inundation. *Brittonia*. **31**(1), p.26.

Pumijumnong, N., Eckstein, D. and Sass, U. 2014. Tree-Ring Research on Tectona Grandis in Northern Thailand. *IAWA Journal*. **16**(4), pp.385–392.

Quaas, J. 2012. Evaluating the 'critical relative humidity' as a measure of subgrid-scale variability of humidity in general circulation model cloud cover parameterizations using satellite data. *Journal of Geophysical Research Atmospheres*. **117**(9), pp.1–10.

Quéré, C. Le, Moriarty, R., Andrew, R.M., Peters, G.P., Ciais, P., Friedlingstein, P. and Jones, S.D. 2015. Global carbon budget 2014. *Earth System Sciences*. **7**, pp.47–85.

Quesada, C.A., Phillips, O.L., Schwarz, M., Czimczik, C.I., Baker, T.R., Patiño, S., Fyllas, N.M., Hodnett, M.G., Herrera, R., Almeida, S., Alvarez Dávila, E., Arneth, A., Arroyo, L., Chao, K.J., Dezzeo, N., Erwin, T., Di Fiore, A., Higuchi, N., Honorio Coronado, E., Jimenez, E.M., Killeen, T., Lezama, A.T., Lloyd, G., Löpez-González, G., Luizão, F.J., Malhi, Y., Monteagudo, A., Neill, D.A., Núñez Vargas, P., Paiva, R., Peacock, J., Peñuela, M.C., Peña Cruz, A., Pitman, N., Priante Filho, N., Prieto, A., Ramírez, H., Rudas, A., Salomão, R., Santos, A.J.B., Schmerler, J., Silva, N., Silveira, M., Vásquez, R., Vieira, I., Terborgh, J. and Lloyd, J. 2012. Basin-wide variations in Amazon forest structure and function are mediated by both soils and climate. *Biogeosciences*. **9**(6), pp.2203–2246.

Ramesh, R., Bhattacharya, S.K. and Gopalan, K. 1986. Climatic correlations in the stable isotope records of silver fir (*Abies pindrow*) trees from Kashmir, India. *Earth and Planetary Science Letters*. **79**(1–2), pp.66–74.

Ramírez, J.A. and del Valle, J.I. 2012. Local and global climate signals from tree rings of Parkinsonia praecox in La Guajira, Colombia. *International Journal of Climatology*. **32**(7), pp.1077–1088.

Ramos da Silva, R. and Avissar, R. 2006. The Hydrometeorology of a Deforested Region of the Amazon Basin. *Journal of Hydrometeorology*. **7**(5), pp.1028–1042.

Randow, C. von, Manzi, A.O., Kruijt, B., Oliveira, P.J. de, Zanchi, F.B., Silva, R.L. da, Hodnett, M.G., Gash, J.H., Elbers, J.A., Waterloo, M.J., Cardoso, F.L. and Kabat, P. 2015. Comparative measurements and seasonal variations in energy and carbon exchange over forest and pasture in South West Amazonia. *International Journal of Economic Research*. **12**(4), pp.885–899.

Rebetez, M., Saurer, M. and Cherubini, P. 2003. To what extent can oxygen isotopes in tree rings and precipitation be used to reconstruct past atmospheric temperature? A case study. *Climatic Change*. **61**(1–2), pp.237–248.

Resende, A.F., Schöngart, J., Streher, A.S., Ferreira-Ferreira, J., Piedade, M.T.F. and Silva, T.S.F. 2018. Massive tree mortality from flood pulse disturbances in Amazonian floodplain forests: The collateral effects of hydropower production. *Science of The Total Environment*. **659**, pp.587–598.

Reuter, J., Stott, L., Khider, D., Sinha, A., Cheng, H. and Edwards, R.L. 2009. A new perspective on the hydroclimate variability in northern South America during the Little Ice Age. *Geophysical Research Letters*. **36**(21), pp.1–5.

Reynolds-Henne, C.E., Siegwolf, R.T.W., Treydte, K.S., Esper, J., Henne, S. and Saurer, M. 2007. Temporal stability of climate-isotope relationships in tree rings of oak and pine (Ticino, Switzerland). *Global Biogeochemical Cycles*. **21**(4), pp.1–12.

Richey, J.E., Meade, R.H., Salati, E., Devol, A.H., Nordin, C.F. and Santos, U. Dos 1986. Water Discharge and Suspended Sediment Concentrations in the Amazon River: 1982–1984. *Water Resources Research*. **22**(5), pp.756–764.

De Ridder, M., Van Den Bulcke, J., Van Acker, J. and Beeckman, H. 2013. Tree-ring analysis of an African long-lived pioneer species as a tool for sustainable forest management. *Forest Ecology and Management*. **304**, pp.417–426.

Risi, C., Bony, S. and Vimeux, F. 2008. Influence of convective processes on the isotopic composition ($\delta^{18}O$ and δD) of precipitation and water vapour in the tropics: 2. Physical interpretation of the amount effect. *Journal of Geophysical Research Atmospheres*. **113**(19), pp.1–12.

Robertson, I., Waterhouse, J.S., Barker, A.C., Carter, A.H.C. and Switsur, V.R. 2001. Oxygen isotope ratios of oak in east England: Implications for reconstructing the isotopic composition of precipitation. *Earth and Planetary Science Letters*. **191**(1–2), pp.21–31.

Roden, J. and Siegwolf, R. 2012. Is the dual-isotope conceptual model fully operational? *Tree Physiology*. **32**(10), pp.1179–1182.

Roden, J.S. and Ehleringer, J.R. 1999. Hydrogen and oxygen isotope ratios of tree-ring cellulose for riparian trees grown under hydroponically controlled environments. *Oecologia*. **121**, pp. 467–477.

Roden, J.S. and Ehleringer, J.R. 2007. Summer precipitation influences the stable oxygen and carbon isotopic composition of tree-ring cellulose in Pinus ponderosa. *Tree Physiology*. **27**(4), pp.491–501.

Roden, J.S. and Farquhar, G.D. 2012. A controlled test of the dual-isotope approach for the interpretation of stable carbon and oxygen isotope ratio variation in tree rings. *Tree Physiology*. **32**(4), pp.490–503.

Roden, J.S., Johnstone, J.A. and Dawson, T.E. 2009. Intra-annual variation in the stable oxygen and carbon isotope ratios of cellulose in tree rings of coast redwood (Sequoia sempervirens). *Holocene*. **19**(2), pp.189–197.

Roden, J.S., Lin, G. and Ehleringer, J.R. 2000. A mechanistic model for interpretation of hydrogen and oxygen isotope ratios in tree-ring cellulose. *Geochimica et Cosmochimica Acta*. **64**(1), pp.21–35.

Röpke, C.P., Amadio, S., Zuanon, J., Ferreira, E.J.G., De Deus, C.P., Pires, T.H.S. and Winemiller, K.O. 2017. Simultaneous abrupt shifts in hydrology and fish assemblage structure in a floodplain lake in the central Amazon. *Scientific Reports*. **7**(40170), pp.1–10.

Rosa, S.A., Barbosa, A.C.M.C., Junk, W.J., da Cunha, C.N., Piedade, M.T.F., Scabin, A.B., Ceccantini, G.C.T. and Schöngart, J. 2017. Growth models based on tree-ring data for the Neotropical tree species Calophyllum brasiliense across different Brazilian wetlands: implications for conservation and management. *Trees - Structure and Function*. **31**(2), pp.729–742.

Roy, S.B. and Avissar, R. 2002. Impact of land use/land cover change on regional hydrometeorology in Amazonia. *Journal of Geophysical Research D: Atmospheres*. **107**(20), pp.1–12.

Rozanski, K., Araguás-Araguás, L. and Gonfiantini, R. 1993. Isotopic Patterns in Modern Global Precipitation. *Climate change in Continental isotopic records.* pp.1–36.

Rozendaal, D.M.A., Brienen, R.J.W., Soliz-Gamboa, C.C. and Zuidema, P.A. 2010. Tropical tree rings reveal preferential survival of fast-growing juveniles and increased juvenile growth rates over time. *New Phytologist*. **185**(3), pp.759–769.

Salati, E., Dall'Olio, A., Matsui, E. and Gat, J.R. 1979. Recycling of Water in the Amazon Basin: An isotopic study. *Water Resources Research*. **15**(5), pp.1250–1258.

Salati, E. and Nobre, C.A. 1991. Possible climatic impacts of tropical deforestation. *Climatic Change*. **19**(1–2), pp.177–196.

Salati, E. and Vose, P.B. 1984. Amazon Basin: A system in equilibrium. *Science*. **225**(4658), pp.129–138.

Sampaio, G., Nobre, C., Costa, M.H., Satyamurty, P., Soares-Filho, B.S. and Cardoso, M. 2007. Regional climate change over eastern Amazonia caused by pasture and soybean cropland expansion. *Geophysical Research Letters*. **34**(17), pp.1–7.

Saurer, M., Borella, S. and Leuenberger, M. 1997. $\delta^{18}O$ of tree rings of beech (Fagus silvatica) as a record of $\delta^{18}O$ of the growing season precipitation. *Tellus, Series B: Chemical and Physical Meteorology*. **49**(1), pp.80–92.

Saurer, M., Cherubini, P., Reynolds-Henne, C.E., Treydte, K.S., Anderson, W.T. and Siegwolf, R.T.W. 2008. An investigation of the common signal in tree ring stable isotope chronologies at temperate sites. *Journal of Geophysical Research: Biogeosciences*. **113**(4), pp.1–11.

Saurer, M., Kress, A., Leuenberger, M., Rinne, K.T., Treydte, K.S. and Siegwolf, R.T.W. 2012. Influence of atmospheric circulation patterns on the oxygen isotope ratio

of tree rings in the Alpine region. *Journal of Geophysical Research Atmospheres*. **117**(5), pp.1–12.

Saurer, M., Siegwolf, R.T.W. and Schweingruber, F.H. 2004. Carbon isotope discrimination indicates improving water-use efficiency of trees in northern Eurasia over the last 100 years. *Global Change Biology*. **10**(12), pp.2109–2120.

Scheidegger, Y., Saurer, M., Bahn, M. and Siegwolf, R. 2000. Linking stable oxygen and carbon isotopes with stomatal conductance and photosynthetic capacity: A conceptual model. *Oecologia*. **125**(3), pp.350–357.

Schietti, J., Martins, D., Emilio, T., Souza, P.F., Levis, C., Baccaro, F.B., Pinto, J.L.P. da V., Moulatlet, G.M., Stark, S.C., Sarmento, K., de Araújo, R.N.O., Costa, F.R.C., Schöngart, J., Quesada, C.A., Saleska, S.R., Tomasella, J. and Magnusson, W.E. 2016. Forest structure along a 600 km transect of natural disturbances and seasonality gradients in central-southern Amazonia. *Journal of Ecology*. **104**(5), pp.1335–1346.

Schleser, G.H., Anhuf, D., Helle, G. and Vos, H. 2015. A remarkable relationship of the stable carbon isotopic compositions of wood and cellulose in tree-rings of the tropical species Cariniana micrantha (Ducke) from Brazil. *Chemical Geology*. **401**, pp.59–66.

Schneider, T., Bischoff, T. and Haug, G.H. 2014. Migrations and dynamics of the intertropical convergence zone. *Nature*. **513**(7516), pp.45–53.

Schollaen, K., Heinrich, I., Neuwirth, B., Krusic, P.J., D'Arrigo, R.D., Karyanto, O. and Helle, G. 2013. Multiple tree-ring chronologies (ring width, $\delta^{13}C$ and $\delta^{18}O$) reveal dry and rainy season signals of rainfall in Indonesia. *Quaternary Science Reviews*. **73**, pp.170–181.

Schongart, J., Arieira, J., Fortes, C.F., Arruda, E.C. de and Nunes-da-Cunha, C. 2008. Carbon dynamics in aboveground coarse wood biomass of wetland forests in the northern Pantanal , Brazil. *Biogeosciences Discussions*. **5**, pp.2103–2130.

Schöngart, J., Bräuning, A., Carolina, A., Campos, M., Lisi, C.S. and De Oliveira, J.M. 2017. Dendroecological studies in the Neotropics: History, status and future challenges. In: Dendroecology. *Springer*, Cham. pp.35–69.

Schöngart, J., Junk, W.J., Piedade, M.T.F., Ayres, J.M., Hüttermann, A. and Worbes, M. 2004. Teleconnection between tree growth in the Amazonian floodplains and the El Niño-Southern Oscillation effect. *Global Change Biology*. **10**(5), pp.683–692.

Schöngart, J., Orthmann, B., Hennenberg, K.J., Porembski, S. and Worbes, M. 2006. Climate-growth relationships of tropical tree species in West Africa and their potential for climate reconstruction. *Global Change Biology*. **12**(7), pp.1139–1150.

Schöngart, J., Piedade, M.T.F., Ludwigshausen, S., Horna, V. and Worbes, M. 2002. Phenology and stem-growth periodicity of tree species in Amazonian floodplain forests. *Journal of Tropical Ecology*. **18**(4), pp.581–597.

Schöngart, J., Piedade, M.T.F., Wittmann, F., Junk, W.J. and Worbes, M. 2005. Wood growth patterns of Macrolobium acaciifolium (Benth.) Benth. (Fabaceae) in Amazonian black-water and white-water floodplain forests. *Oecologia*. **145**(3), pp.454–461.

Schöngart, J., Wittmann, F., Junk, W.J. and Piedade, M.T.F. 2017. Vulnerability of Amazonian floodplains to wildfires differs according to their typologies impeding generalizations. *Proceedings of the National Academy of Sciences*. **114**(41), pp.E8550-E8551.

Schöngart, J., Wittmann, F. and Worbes, M. 2010. Biomass and net primary production of Central Amazonian Floodplain Forests In: Amazonian Floodplain Forests: Ecophysiology, Biodiversity and Sustainable Management. *Springer*, Dordrecht. pp.347–388.

Schubert, B.A. and Jahren, A.H. 2015. Seasonal temperature and precipitation recorded in the intra-annual oxygen isotope pattern of meteoric water and tree-ring cellulose. *Quaternary Science Reviews*. **125**, pp.1–14.

Schweingruber, F.H., Eckstein, D., Serre-Bachet, F. and Bräker O.U. 1990. Identification, presentation and interpretation of event years and pointer years in dendrochronology. *Dendrochronologia*. **8**, pp.15–38

Seibt, U., Rajabi, A., Griffiths, H. and Berry, J.A. 2008. Carbon isotopes and water use efficiency: Sense and sensitivity. *Oecologia*. **155**(3), pp.441–454.

Servain, J., Caniaux, G., Kouadio, Y.K., McPhaden, M.J. and Araujo, M. 2014. Recent climatic trends in the tropical Atlantic. *Climate Dynamics*. **43**(11), pp.3071–3089.

Shukla, J., Nobre, C. and Sellers, P. 1990. Amazon deforestation and climate change. *Science*. **247**(4948), pp.1322–1325.

Singer, B.H. and Castro, M.C.D.E. 1995. Agricultural Colonization and Malaria on the Amazon Frontier. *Annals New York Academy of Sciences*. **954**(1), pp.184-222.

Skomarkova, M. V., Vaganov, E.A., Mund, M., Knohl, A., Linke, P., Boerner, A. and Schulze, E.D. 2006. Inter-annual and seasonal variability of radial growth, wood density and carbon isotope ratios in tree rings of beech (Fagus sylvatica) growing in Germany and Italy. *Trees - Structure and Function*. **20**(5), pp.571–586.

Skrzypek, G., Engel, Z., Chuman, T. and Šefrna, L. 2011. Distichia peat - A new stable isotope paleoclimate proxy for the Andes. *Earth and Planetary Science Letters*. **307**(3–4), pp.298–308.

van der Sleen, P., Groenendijk, P., Vlam, M., Anten, N.P.R., Bongers, F. and Zuidema, P.A. 2017. Trends in tropical tree growth: re-analyses confirm earlier findings. *Global Change Biology*. **23**(5), pp.1761–1762.

van der Sleen, P., Groenendijk, P., Vlam, M., Anten, N.P.R., Boom, A., Bongers, F., Pons, T.L., Terburg, G. and Zuidema, P.A. 2015. No growth stimulation of tropical trees by 150 years of CO2 fertilization but water-use efficiency increased. *Nature Geoscience*. **8**(1), pp.24–28.

van der Sleen, P., Zuidema, P.A. and Pons, T.L. 2017. Stable isotopes in tropical tree rings: theory, methods and applications. *Functional Ecology*. **31**(9), pp.1674–1689.

Slik, J.W.F., Arroyo-Rodríguez, V., Aiba, S.-I., Alvarez-Loayza, P., Alves, L.F., Ashton, P., Balvanera, P., Bastian, M.L., Bellingham, P.J., van den Berg, E., Bernacci, L., da Conceição Bispo, P., Blanc, L., Böhning-Gaese, K., Boeckx, P., Bongers, F., Boyle, B., Bradford, M., Brearley, F.Q., Breuer-Ndoundou Hockemba, M.,

Bunyavejchewin, S., Calderado Leal Matos, D., Castillo-Santiago, M., Catharino, E.L.M., Chai, S.-L., Chen, Y., Colwell, R.K., Chazdon, R.L., Clark, C., Clark, D.B., Clark, D.A., Culmsee, H., Damas, K., Dattaraja, H.S., Dauby, G., Davidar, P., DeWalt, S.J., Doucet, J.-L., Duque, A., Durigan, G., Eichhorn, K.A.O., Eisenlohr, P. V., Eler, E., Ewango, C., Farwig, N., Feeley, K.J., Ferreira, L., Field, R., de Oliveira Filho, A.T., Fletcher, C., Forshed, O., Franco, G., Fredriksson, G., Gillespie, T., Gillet, J.-F., Amarnath, G., Griffith, D.M., Grogan, J., Gunatilleke, N., Harris, D., Harrison, R., Hector, A., Homeier, J., Imai, N., Itoh, A., Jansen, P.A., Joly, C.A., de Jong, B.H.J., Kartawinata, K., Kearsley, E., Kelly, D.L., Kenfack, D., Kessler, M., Kitayama, K., Kooyman, R., Larney, E., Laumonier, Y., Laurance, S., Laurance, W.F., Lawes, M.J., Amaral, I.L. do, Letcher, S.G., Lindsell, J., Lu, X., Mansor, A., Marjokorpi, A., Martin, E.H., Meilby, H., Melo, F.P.L., Metcalfe, D.J., Medjibe, V.P., Metzger, J.P., Millet, J., Mohandass, D., Montero, J.C., de Morisson Valeriano, M., Mugerwa, B., Nagamasu, H., Nilus, R., Ochoa-Gaona, S., Onrizal, Page, N., Parolin, P., Parren, M., Parthasarathy, N., Paudel, E., Permana, A., Piedade, M.T.F., Pitman, N.C.A., Poorter, L., Poulsen, A.D., Poulsen, J., Powers, J., Prasad, R.C., Puyravaud, J.-P., Razafimahaimodison, J.-C., Reitsma, J., dos Santos, J.R., Roberto Spironello, W., Romero-Saltos, H., Rovero, F., Rozak, A.H., Ruokolainen, K., Rutishauser, E., Saiter, F., Saner, P., Santos, B.A., Santos, F., Sarker, S.K., Satdichanh, M., Schmitt, C.B., Schöngart, J., Schulze, M., Suganuma, M.S., Sheil, D., da Silva Pinheiro, E., Sist, P., Stevart, T., Sukumar, R., Sun, I.-F., Sunderland, T., Suresh, H.S., Suzuki, E., Tabarelli, M., Tang, J., Targhetta, N., Theilade, I., Thomas, D.W., Tchouto, P., Hurtado, J., Valencia, R., van Valkenburg, J.L.C.H., Van Do, T., Vasquez, R., Verbeeck, H., Adekunle, V., Vieira, S.A., Webb, C.O., Whitfeld, T., Wich, S.A., Williams, J., Wittmann, F., Wöll, H., Yang, X., Adou Yao, C.Y., Yap, S.L., Yoneda, T., Zahawi, R.A., Zakaria, R., Zang, R., de Assis, R.L., Garcia Luize, B. and Venticinque, E.M. 2015. An estimate of the number of tropical tree species. *Proceedings of the National Academy of Sciences*. **112**(24), pp.7472–7477.

Smith, L.T., Aragão, L.E.O.C., Sabel, C.E. and Nakaya, T. 2014. Drought impacts on children's respiratory health in the Brazilian Amazon. *Scientific Reports*. **4**, pp.1–8.

Soares-Filho, B.S., Nepstad, D.C., Curran, L.M., Cerqueira, G.C., Garcia, R.A., Ramos, C.A., Voll, E., McDonald, A., Lefebvre, P. and Schlesinger, P. 2006. Modelling conservation in the Amazon basin. *Nature*. **440**(7083), pp.520–523.

Sombroek, W. 2001. Spatial and Temporal Patterns of Amazon Rainfall. *AMBIO: A Journal of the Human Environment*. **30**(7), pp.388–396.

Sorribas, M.V., Paiva, R.C.D., Melack, J.M., Bravo, J.M., Jones, C., Carvalho, L., Beighley, E., Forsberg, B. and Costa, M.H. 2016. Projections of climate change effects on discharge and inundation in the Amazon basin. *Climatic Change*. **136**(3–4), pp.555–570.

de Sousa Lobo, G., Wittmann, F. and Piedade, M.T.F.. 2019. Response of black-water floodplain (igapó) forests to flood pulse regulation in a dammed Amazonian river. *Forest Ecology and Management*. 434, pp.110-118.

Souza, F.C. De, Dexter, K.G., Phillips, O.L., Brienen, R.J.W., Chave, J., Galbraith, D.R., Gonzalez, G.L., Mendoza, A.M., Pennington, R.T., Poorter, L., Andrade, A., Alexiades, M., Esteban, A., C, G.A.A., Baraloto, C., Barroso, J.G., Camargo, L.C., Bonal, D., Boot, R.G.A., Comiskey, A., Valverde, F.C., Fiore, A. Di, Elias, F., Erwin, T.L., Feldpausch, T.R., Ferreira, L., Fyllas, N.M., Gloor, E., Herault, B., Coronado, N.H., Herrera, R., Higuchi, N., Killeen, J., Laurance, W.F., Laurance, S., Lloyd, J., Lovejoy, E., Malhi, Y., Maracahipes, L., Marimon, B.S., Oliveira, E.A., Lenza, E., Neill, A., Nu, P., Iii, J.J.P., Palacios, A., Pen, M.C., Pitman, C.A., Prieto, A., Quesada, C.A., Ramirez-, H., Rudas, A., Ruokolainen, K., Saloma, R.P., Silveira, M., Stropp, J., Steege, H., Thomas-, R., Hout, P. Van Der, Heijden, G.M.F. Van Der, Van, P.J., Meer, D., Vasquez, R. V, Vieira, S.A., Vilanova, E., Vos, V.A., Wang, O., Young, K.R., Zagt, R.J. and Baker, T.R. 2016. Evolutionary heritage influences Amazon tree ecology. *Proceedings of the Royal Society B*. **283**, pp. 20161587.

Spracklen, D. V., Arnold, S.R. and Taylor, C.M. 2012. Observations of increased tropical rainfall preceded by air passage over forests. *Nature*. **489**(7415), pp.282–285.

Spracklen, D.V. and Garcia-Carreras, L. 2015. The impact of Amazonian deforestation on Amazon basin rainfall. *Geophysical Research Letters*. **42**(21), pp.9546–9552.

ter Steege, H., Pitman, N.C.A., Sabatier, D., Baraloto, C., Salomão, R.P., Guevara, J.E., Phillips, O.L., Castilho, C. V., Magnusson, W.E., Molino, J.F., Monteagudo, A., Vargas, P.N., Montero, J.C., Feldpausch, T.R., Coronado, E.N.H., Killeen, T.J., Mostacedo, B., Vasquez, R., Assis, R.L., Terborgh, J., Wittmann, F., Andrade, A., Laurance, W.F., Laurance, S.G.W., Marimon, B.S., Marimon, B.H., Vieira, I.C.G., Amaral, I.L., Brienen, R., Castellanos, H., López, D.C., Duivenvoorden, J.F., Mogollón, H.F., Matos, F.D.D.A., Dávila, N., García-Villacorta, R., Diaz, P.R.S., Costa, F., Emilio, T., Levis, C., Schietti, J., Souza, P., Alonso, A., Dallmeier, F., Montoya, A.J.D., Piedade, M.T.F., Araujo-Murakami, A., Arroyo, L., Gribel, R., Fine, P.V.A., Peres, C.A., Toledo, M., Aymard C., G.A., Baker, T.R., Cerón, C., Engel, J., Henkel, T.W., Maas, P., Petronelli, P., Stropp, J., Zartman, C.E., Daly, D., Neill, D., Silveira, M., Paredes, M.R., Chave, J., Lima Filho, D.D.A., Jørgensen, P.M., Fuentes, A., Schöngart, J., Valverde, F.C., Di Fiore, A., Jimenez, E.M., Mora, M.C.P., Phillips, J.F., Rivas, G., Van Andel, T.R., Von Hildebrand, P., Hoffman, B., Zent, E.L., Malhi, Y., Prieto, A., Rudas, A., Ruschell, A.R., Silva, N., Vos, V., Zent, S., Oliveira, A.A., Schutz, A.C., Gonzales, T., Nascimento, M.T., Ramirez-Angulo, H., Sierra, R., Tirado, M., Medina, M.N.U., Van Der Heijden, G., Vela, C.I.A., Torre, E.V., Vriesendorp, C., Wang, O., Young, K.R., Baider, C., Balslev, H., Ferreira, C., Mesones, I., Torres-Lezama, A., Giraldo, L.E.U., Zagt, R., Alexiades, M.N., Hernandez, L., Huamantupa-Chuquimaco, I., Milliken, W., Cuenca, W.P., Pauletto, D., Sandoval, E.V., Gamarra, L.V., Dexter, K.G., Feeley, K., Lopez-Gonzalez, G. and Silman, M.R. 2013. Hyperdominance in the Amazonian tree flora. *Science*. **342**(6156), p.1243092.

Sternberg, L. da S.L.O. 2008. Oxygen stable isotope ratios of tree-ring cellulose: The next phase of understanding. *New Phytologist*. **181**(3), pp.553–562.

Sternberg, L., Pinzon, M.C., Anderson, W.T. and Jahren, A.H. 2006. Variation in oxygen isotope fractionation during cellulose synthesis: Intramolecular and biosynthetic effects. *Plant, Cell and Environmen*t. **29**(10), pp.1881–1889.

Stickler, C.M., Coe, M.T., Costa, M.H., Nepstad, D.C., McGrath, D.G., Dias, L.C.P., Rodrigues, H.O. and Soares-Filho, B.S. 2013. Dependence of hydropower energy generation on forests in the Amazon Basin at local and regional scales. *Proceedings of the National Academy of Sciences*. **110**(23), pp.9601–9606.

Stríkis, N.M., Cruz, F.W., Cheng, H., Karmann, I., Edwards, R.L., Vuille, M., Wang, X., de Paula, M.S., Novello, V.F. and Auler, A.S. 2011. Abrupt variations in South American monsoon rainfall during the Holocene based on a speleothem record from central-eastern Brazil. *Geology*. **39**(11), pp.1075–1078.

Thompson, L.G., Mosley-Thompson, E., Davis, M.E., Lin, P.N., Henderson, K., Cole-Dai, J., Bolzan, J.F. and Liu, K. 1995. Late glacial stage and holocene tropical ice core records from Huascarán, Peru. *Science*. **269**, pp.46–50.

Thompson, L.G., Mosley-Thompson, E., Davis, M.E., Zagorodnov, V.S., Howat, I.M., Mikhalenko, V.N. and Lin, P.N. 2013. Annually resolved ice core records of tropical climate variability over the past ~1800 years. *Science*. **340**(6135), pp.945–950.

Thompson, L.G., Mosley-thompson, E. and Henderson, K.A. 2000. Ice-core palaeoclimate records in tropical America. *Journal of Quaternary Science.* **15**(4), pp.377–394.

Tournaire-Roux, C., Sutka, M., Javot, H., Gout, E., Gerbeau, P., Luu, D.T., Bligny, R. and Maurel, C. 2003. Cytosolic pH regulates root water transport during anoxic stress through gating of aquaporins. *Nature*. **425**(6956), pp.393–397.

Treydte, K., Boda, S., Graf Pannatier, E., Fonti, P., Frank, D., Ullrich, B., Saurer, M., Siegwolf, R., Battipaglia, G., Werner, W. and Gessler, A. 2014. Seasonal transfer of oxygen isotopes from precipitation and soil to the tree ring: Source water versus needle water enrichment. *New Phytologist*. **202**(3), pp.772–783.

Treydte, K., Frank, D., Esper, J., Andreu, L., Bednarz, Z., Berninger, F., Boettger, T., D'Alessandro, C.M., Etien, N., Filot, M., Grabner, M., Guillemin, M.T., Gutierrez, E., Haupt, M., Helle, G., Hilasvuori, E., Jungner, H., Kalela-Brundin, M., Krapiec, M., Leuenberger, M., Loader, N.J., Masson-Delmotte, V., Pazdur, A., Pawelczyk, S., Pierre, M., Planells, O., Pukiene, R., Reynolds-Henne, C.E., Rinne, K.T., Saracino, A., Saurer, M., Sonninen, E., Stievenard, M., Switsur, V.R., Szczepanek, M., Szychowska-Krapiec, E., Todaro, L., Waterhouse, J.S., Weigl, M. and Schleser, G.H. 2007. Signal strength and climate calibration of a European tree-ring isotope network. *Geophysical Research Letters*. **34**(24), pp.2–7.

Treydte, K.S., Schleser, G.H., Helle, G., Frank, D.C., Winiger, M., Haug, G.H. and Esper, J. 2006. The twentieth century was the wettest period in northern Pakistan over the past millennium. *Nature*. **440**, pp.1179–1182.

Tropical Rainfall Measuring Mission (TRMM). 2011. TRMM (TMPA) Rainfall Estimate L3 3 hour 0.25 degree x 0.25 degree V7, Greenbelt, MD, Goddard Earth Sciences Data and Information Services Center (GES DISC), Accessed: 24/01/2017, 10.5067/TRMM/TMPA/3H/7

Tundisi, J.G., Goldemberg, J., Matsumura-Tundisi, T. and Saraiva, A.C.F. 2014. How many more dams in the Amazon. *Energy Policy*. **74**, pp.703–708.

Vargas, A.I., Schaffer, B., Yuhong, L. and Sternberg, L. da S.L. 2017. Testing plant use of mobile vs immobile soil water sources using stable isotope experiments. *New Phytologist*. **215**(2), pp.582–594.

Vera, C., Higgins, W., Amador, J., Ambrizzi, T., Garreaud, R., Gochis, D., Gutzler, D., Lettenmaier, D., Marengo, J., Mechoso, C.R., Nogues-Paegle, J., Silva Dias, P.L. and Zhang, C. 2006. Toward a unified view of the American monsoon systems. *Journal of Climate*. **19**(20), pp.4977–5000.

Victoria, R.L., Martinelli, L. a, Mortatti, J. and Richey, J. 1991. Mechanisms of Water Recycling in the Amazon Basin - Isotopic Insights. *Ambio - A Journal of the Human Environment*. **20**(8), pp.384–387.

Villacís, M., Vimeux, F. and Taupin, J.D. 2008. Analysis of the climate controls on the isotopic composition of precipitation ($\delta^{18}O$) at Nuevo Rocafuerte, 74.5°W, 0.9°S, 250 m, Ecuador. *Comptes Rendus - Geoscience*. **340**(1), pp.1–9.

Vimeux, F., Gallaire, R., Bony, S., Hoffmann, G. and Chiang, J.C.H. 2005. What are the climate controls on δD in precipitation in the Zongo Valley (Bolivia)? Implications for the Illimani ice core interpretation. *Earth and Planetary Science Letters*. **240**(2), pp.205–220.

Vimeux, F., Ginot, P., Schwikowski, M., Vuille, M., Hoffmann, G., Thompson, L.G. and Schotterer, U. 2009. Climate variability during the last 1000 years inferred from Andean ice cores: A review of methodology and recent results. *Palaeogeography, Palaeoclimatology, Palaeoecology*. **281**(3–4), pp.229–241.

Vischer and Nastase 2017. ObjectJ: Non-destructive marking and linked results in ImageJ. University of Amsterdam. Available at https://sils.fnwi.uva.nl/bcb/objectj/index.html.

Vittor, A.Y., Gilman, R.H., Tielsch, J., Glass, G., Shields, T., Lozano, W.S., Pinedo-Cancino, V. and Patz, J.A. 2006. The Effect Of Deforestation On The Human-Biting Rate Of Anopheles Darlingi, The Primary Vector Of Falciparum Malaria In The Peruvian Amazon. *American Journal of Tropical Medicine and Hygiene*. **74**(1), pp.3–11.

Vlam, M., Baker, P.J., Bunyavejchewin, S., Mohren, G.M.J. and Zuidema, P.A. 2014. Understanding recruitment failure in tropical tree species: Insights from a tree-ring study. *Forest Ecology and Management*. **312**, pp.108–116.

Vlam, M., Baker, P.J., Bunyavejchewin, S. and Zuidema, P.A. 2013. Temperature and rainfall strongly drive temporal growth variation in Asian tropical forest trees. *Oecologia*. **174**(4), pp.1449–1461.

Voelker, S.L., Brooks, J.R., Meinzer, F.C., Roden, J., Pazdur, A., Pawelczyk, S., Hartsough, P., Snyder, K., Plavcová, L. and Šantruček, J. 2014. Reconstructing relative humidity from plant $\delta^{18}O$ and δD as deuterium deviations from the global meteoric water line. *Ecological Applications*. **24**(5), pp.960–975.

Vuille, M. and Werner, M. 2005. Stable isotopes in precipitation recording South American summer monsoon and ENSO variability: Observations and model results. *Climate Dynamics*. **25**(4), pp.401–413.

Wang, J., Chagnon, F.J.F., Williams, E.R., Betts, A.K., Renno, N.O., Machado, L.A.T., Bisht, G., Knox, R. and Bras, R.L. 2009. Impact of deforestation in the Amazon basin on cloud climatology. *Proceedings of the National Academy of Sciences*. **106**(10), pp.3670–3674.

Wang, X., Edwards, R.L., Auler, A.S., Cheng, H., Kong, X., Wang, Y., Cruz, F.W., Dorale, J.A. and Chiang, H.W. 2017. Hydroclimate changes across the Amazon lowlands over the past 45,000 years. *Nature*. **541**(7636), pp.204–207.

Werth, D. and Avissar, R. 2002. The local and global effects of Amazon deforestation. *Journal of Geophysical Research*. **107**, pp.551–558.

Wieloch, T., Helle, G., Heinrich, I., Voigt, M. and Schyma, P. 2011. A novel device for batch-wise isolation of α-cellulose from small-amount wholewood samples. *Dendrochronologia*. **29**(2), pp.115–117.

Wigley, T.M.L., Briffa, R. and Jones, P.D. 1984. On the average value of correlated time series, with applications in Dendroclimatology and Hydrometeorology. *Journal of Climate and Applied Meteorology*. **23**, pp.201–213.

Wills, T.H.G., Robertson, I., Eshetu, Z., Touchan, R., Sass-Klaassen, U. and Koprowski, M. 2011. Crossdating *Juniperus procera* from North Gondar, Ethiopia. *Trees – Structure and Function*. **25**, pp. 71–82.

Wittmann, F., Anhuf, D. and Funk, W.J. 2002. Tree species distribution and community structure of central Amazonian várzea forests by remote-sensing techniques. *Journal of Tropical Ecology*. **18**(6), pp.805–820.

Wittmann, F., Householder, E., Piedade, M.T.F., De Assis, R.L., Schöngart, J., Parolin, P. and Junk, W.J. 2012. Habitat specifity, endemism and the neotropical distribution of Amazonian white-water floodplain trees. *Ecography*. **36**(6), pp.690–707.

Wittmann, F., Junk, W.J. and Piedade, M.T.F. 2004. The várzea forests in Amazonia: Flooding and the highly dynamic geomorphology interact with natural forest succession. *Forest Ecology and Management*. **196**(2–3), pp.199–212.

Wittmann, F., Schöngart, J., Montero, J.C., Motzer, T., Junk, W.J., Piedade, M.T.F., Queiroz, H.L. and Worbes, M. 2006. Tree species composition and diversity gradients in white-water forests across the Amazon Basin. *Journal of Biogeography*. **33**(8), pp.1334–1347.

Wolfe, B.B., Aravena, R., Abbott, M.B., Seltzer, G.O. and Gibson, J.J. 2001. Reconstruction of paleohydrology and paleohumidity from oxygen isotope records in the Bolivian Andes. *Palaeogeography, Palaeoclimatology, Palaeoecology*. **176**(1–4), 177-192.

Worbes, M., 1997. The forest ecosystem of the floodplains. In The central Amazon floodplain. *Springer,* Berlin, Heidelberg. pp. 223-265

Worbes, M. 1999. Annual growth rings , and growth patterns of tropical trees from the in Venezuela Caparo Forest Reserve. *Journal of Ecology*. **87**(3), pp.391–403.

Worbes M. 2002. One hundred years of tree-ring research in the tropics-a brief history and an outlook to future challenges. *Dendrochronologia*. **20**, pp.217–231.

Worbes, M. 2004. MENSURATION| Tree-Ring Analysis.

Wright, J.S., Fu, R., Worden, J.R., Chakraborty, S., Clinton, N.E., Risi, C., Sun, Y. and Yin, L. 2017. Rainforest-initiated wet season onset over the southern Amazon. *Proceedings of the National Academy of Sciences*. **114**(32), pp.8481–8486.

Wullschleger, S.D., Gunderson, C.A., Hanson, P.J., Wilson, K.B. and Norby, R.J. 2002. Sensitivity and canopy conductance to - interacting elevated CO_2 concentration variables and of scale perspectives. *New Phytologist*. **153**(3), pp.485–496.

Xu, L., Samanta, A., Costa, M.H., Ganguly, S., Nemani, R.R. and Myneni, R.B. 2011. Widespread decline in greenness of Amazonian vegetation due to the 2010 drought. *Geophysical Research Letters*. **38**(7), pp.2–5.

Yoon, J.H. and Zeng, N. 2010. An Atlantic influence on Amazon rainfall. *Climate Dynamics*. **34**(2), pp.249–264.

Zhang, Y., Wallace, J.M. and Battisti, D.S. 1997. ENSO-like interdecadal variability: 1900-93. *Journal of Climate*. **10**(5), pp.1004–1020.

Zemp, D.C., Schleussner, C.F., Barbosa, H.M.J., Van Der Ent, R.J., Donges, J.F., Heinke, J., Sampaio, G. and Rammig, A. 2014. On the importance of cascading moisture recycling in South America. *Atmospheric Chemistry and Physics*. **14**(23), pp.13337–13359.

Zemp, D.C., Schleussner, C.F., Barbosa, H.M.J., Hirota, M., Montade, V., Sampaio, G., Staal, A., Wang-Erlandsson, L. and Rammig, A. 2017. Self-amplified Amazon forest loss due to vegetation-atmosphere feedbacks. *Nature Communications*. **8**, pp.1–10.

Zhang, W.-H. and Tyerman, S.D. 1999. Inhibition of Water Channels by $HgCl_2$ in Intact Wheat Root Cells1. *Plant physiology*. **120**, pp.849–858.

Zhang, W.H. and Tyerman, S.D. 1991. Effect of low O2 concentration and azide on hydraulic conductivity and osmotic volume of the cortical-cells of wheat roots. *Australian Journal of Plant Physiology*. **18**(6), pp.603–613.

Zhou, J. and Lau, K.M. 1998. Does a monsoon climate exist over South America? *Journal of Climate*. **11**(5), pp.1020–1040.

Appedinx I
Supporting Information for Chapter 3

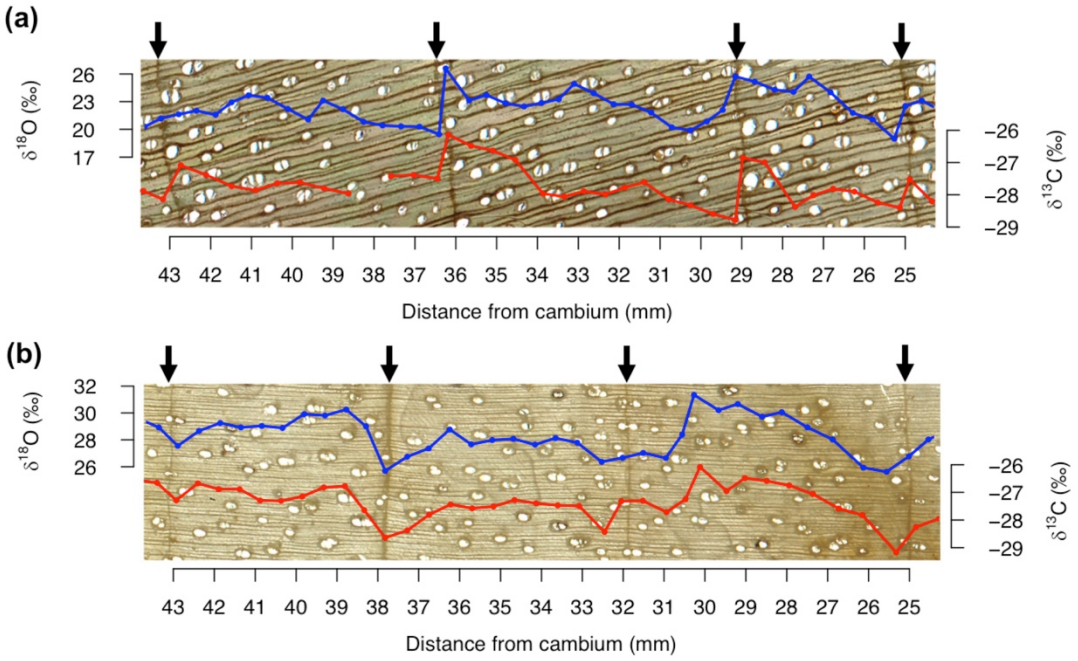

Figure I. 1 Anatomical wood structure of *Macrolobium acaciifolium* (panel a) and *Cedrela odorata* (panel b) with in blue the intra-ring resolution $\delta^{18}O_{TR}$ and in red the $\delta^{13}C_{TR}$ (red lines) series. Arrows indicate the ring boundaries. $\delta^{18}O$ and $\delta^{18}O$ values shown are from α-cellulose.

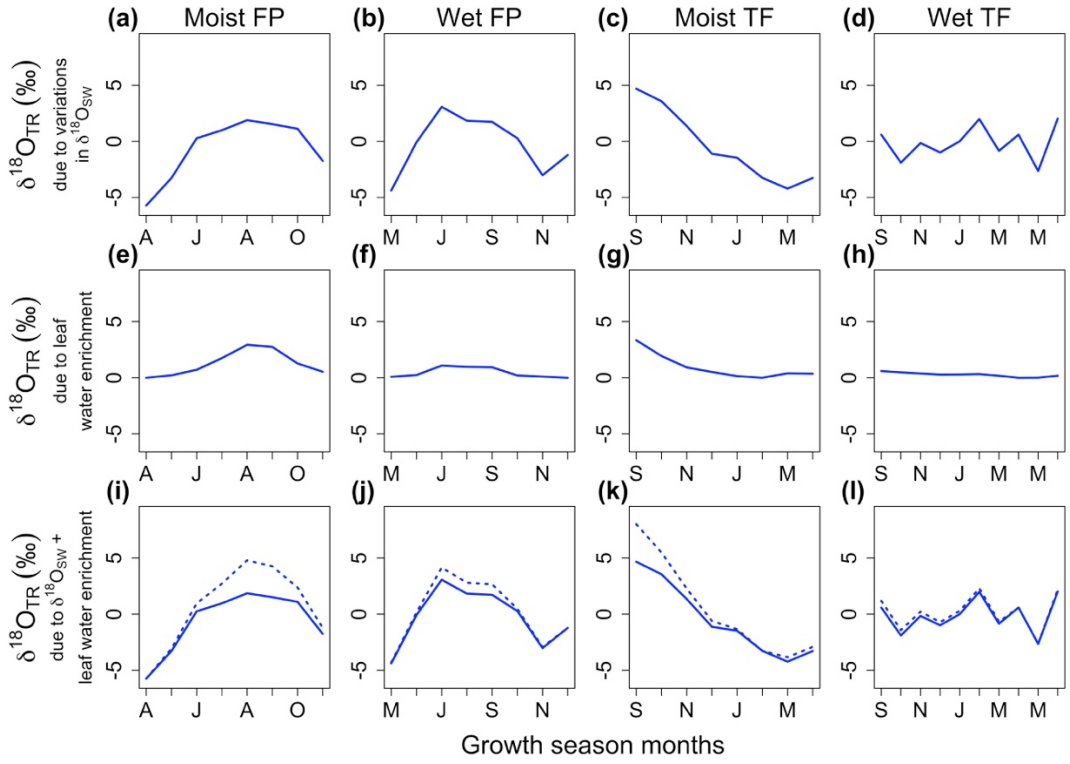

Figure I. 2. Predicted seasonal patterns of tree ring $\delta^{18}O$ ($\delta^{18}O_{TR}$) due to only source water $\delta^{18}O$ effect (top panels), only leaf water enrichment (middle panels), and the combined effect (lower panels). The stippled line in the lower panels indicates the leaf water enrichment above source water $\delta^{18}O$ (solid line). Panels (a,e,i) give the predictions for the Moist Floodplain site, (b,f,j) for the Wet Floodplain site, (c,g,k) for the Moist Terra firme site and (d,h,l) for the Wet terra firme site.

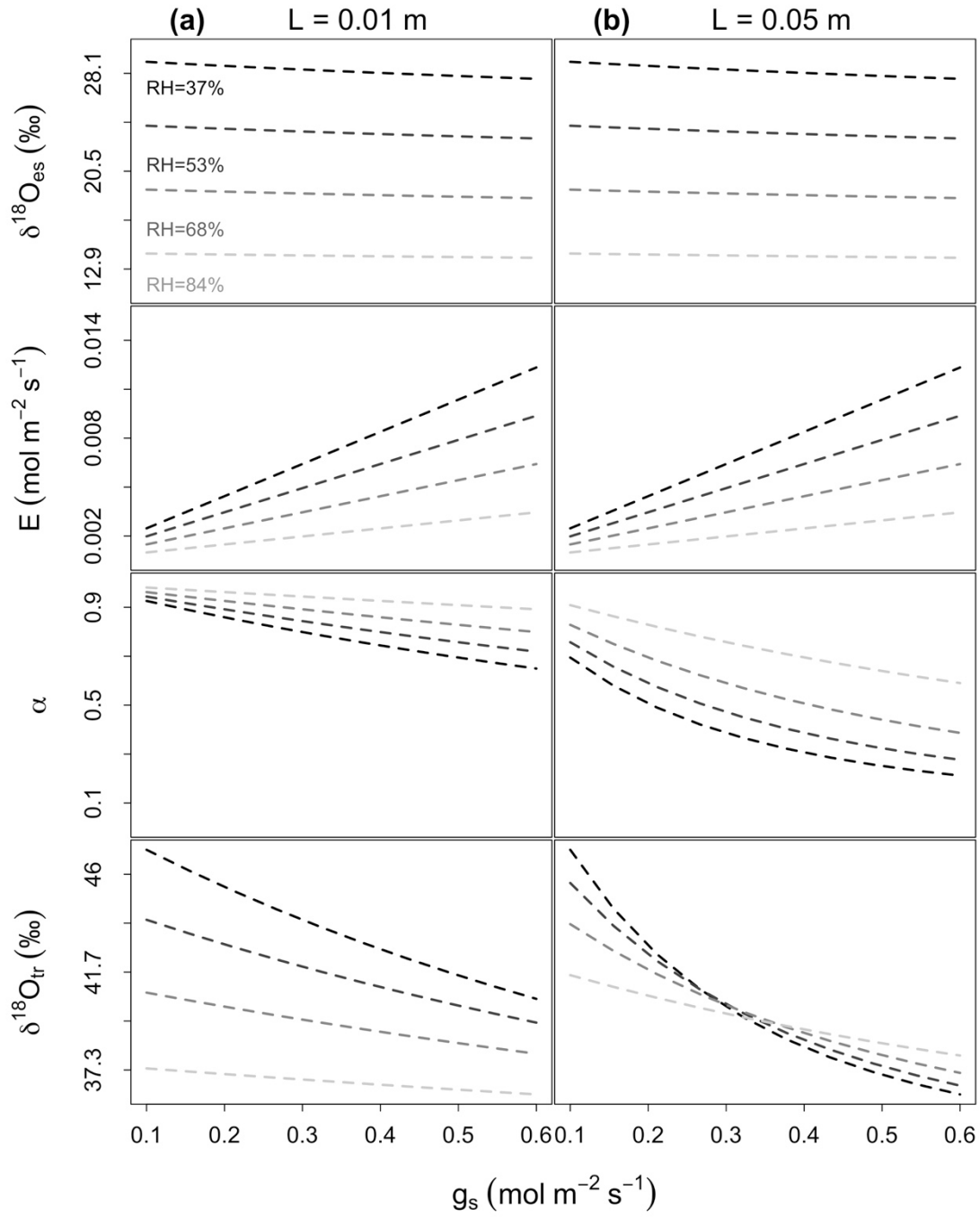

Figure I. 3. Predicted effects of stomatal conductance (g_s) on leaf $\delta^{18}O$ at four different levels of relative humidity (RH) and for two different path lengths. Left panels show effects for short path lengths of L=0.01, and right panels for L=0.05m, and from top to bottom showing the modelled relationship between g_s and d18O of water at the sites of evaporation ($\delta^{18}O_{es}$) (panel a,b), g_s and leaf transpiration (E) (panel c,d), g_s and "admixture" of source water with water from the sites of evaporation (alpha=$\left(\frac{(1-e^{-\wp})}{\wp}\right)$ (panel e,f), and g_s and mean leaf water $\delta^{18}O$ ($\delta^{18}O_{lw}$) (panel g,h).

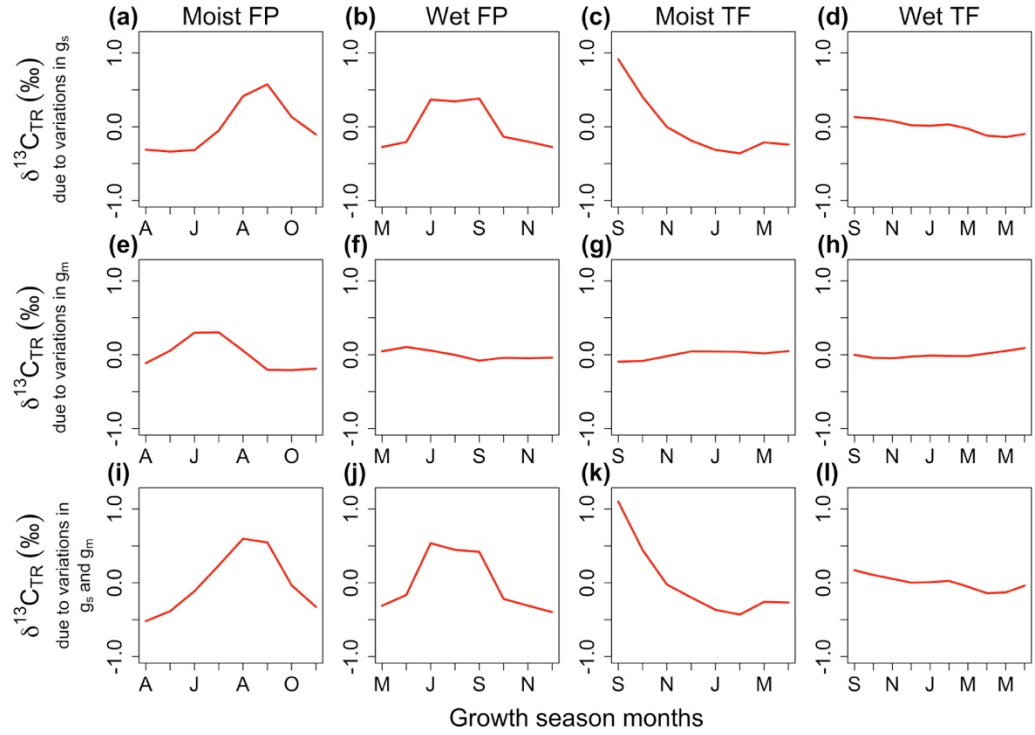

Figure I. 4. Predicted seasonal patterns of tree ring $\delta^{13}C$ ($\delta^{13}C_{TR}$) due to only g_s variations (top panels), only g_m variations (middle panels), and the combined effect (lower panels). Panels (a,e,i) give the predictions for the Moist Floodplain site, (b,f,j) for the Wet Floodplain site, (c,g,k) for the Moist Terra firme site and (d,h,l) for the Wet terra firme site.

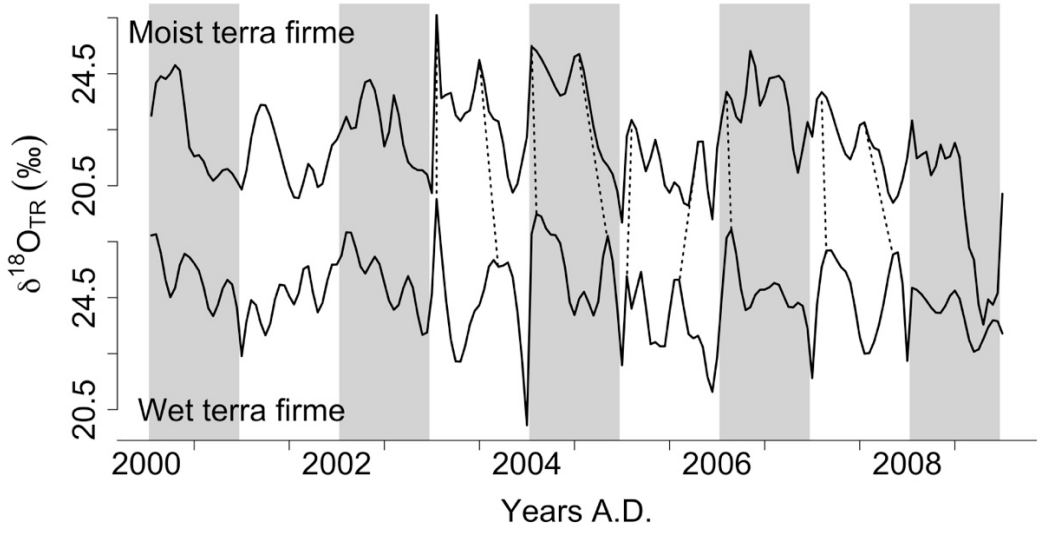

Figure I. 5. Covariation of tree ring $\delta^{18}O$ patterns in Cedrela odorata trees from the two firme sites. Dashed lines indicate common feature in the two series. The sites are 1000 km apart, located in northern Bolivia and Peru (see map in Fig, 1).

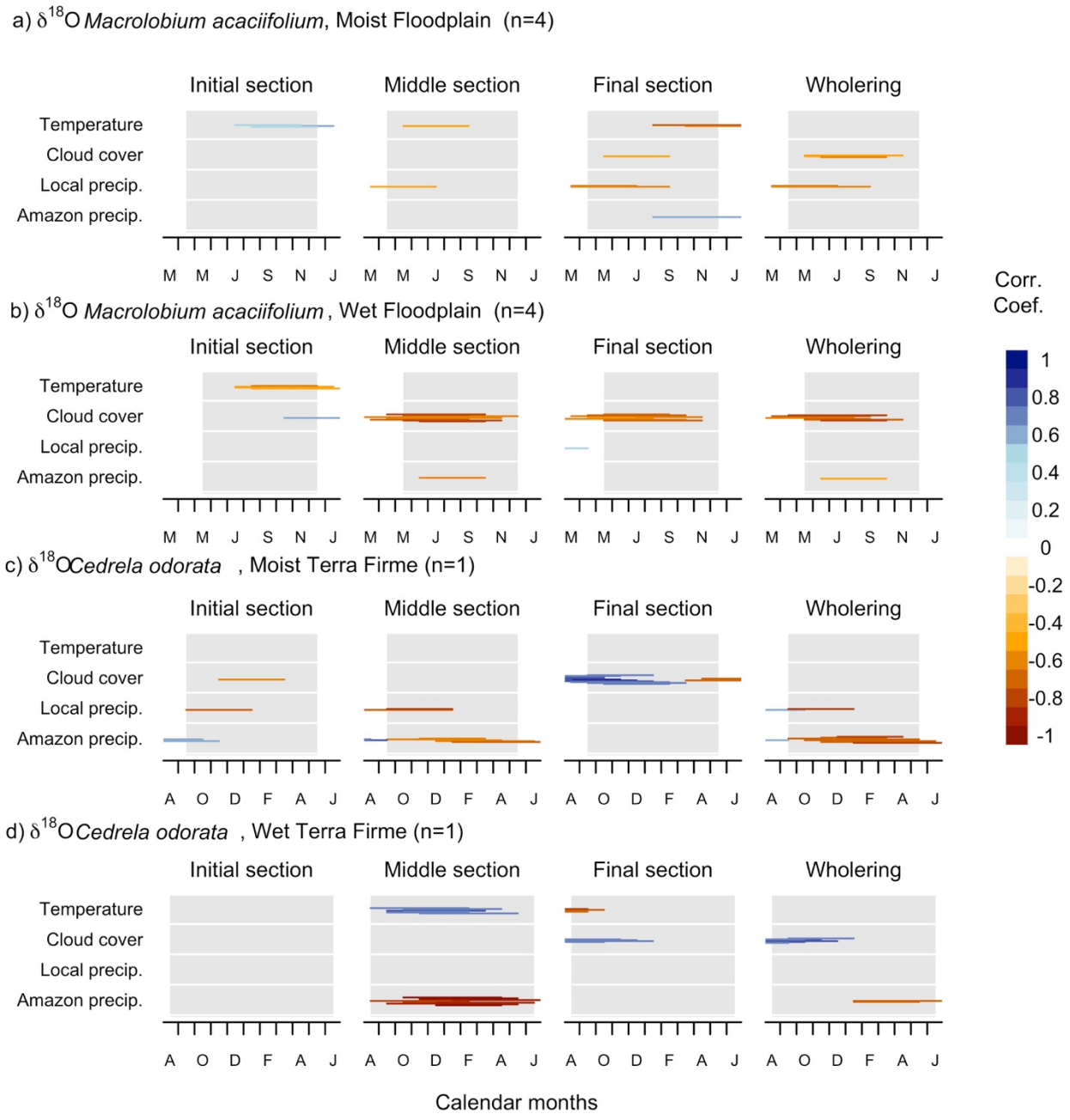

Figure I. 6. Heatmap of the correlations of the inter-annual isotope series with climate variables for the four sites. Panels a-d show the correlations observed for $\delta^{18}O_{TR}$, panels e-h show the correlations for $\delta^{13}C_{TR}$. Correlations are shown for isotopes values of three ring sections and for the whole ring. Pearson correlations were performed using annual mean isotope values against climate variables averaged over running periods of 4 and 6 months lengths. Only statistically significant correlations ($p < 0.05$) are shown. Grey shaded areas indicate the current growing season (right) and the previous growing season (left).

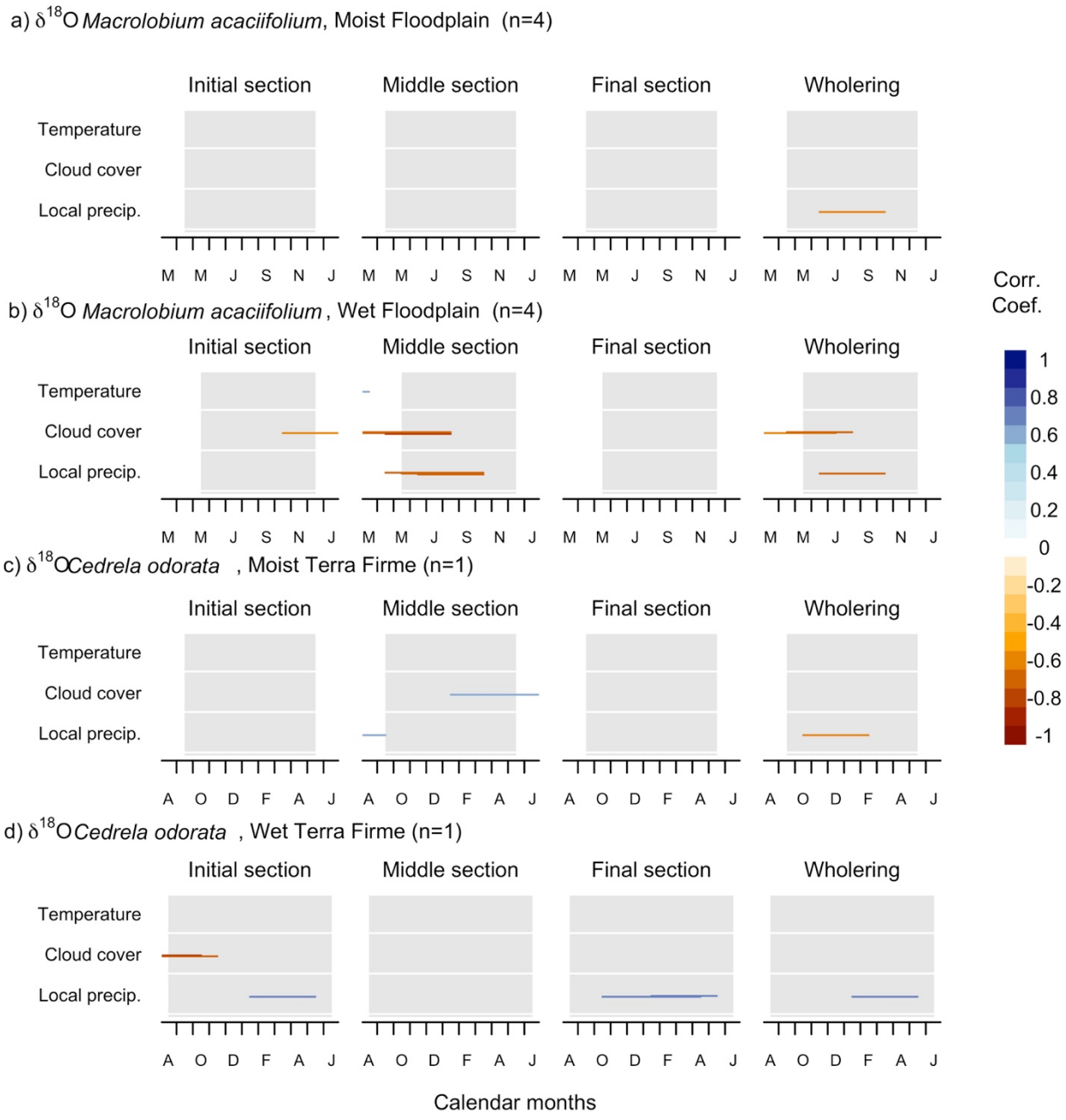

Figure I. 6 Continued.

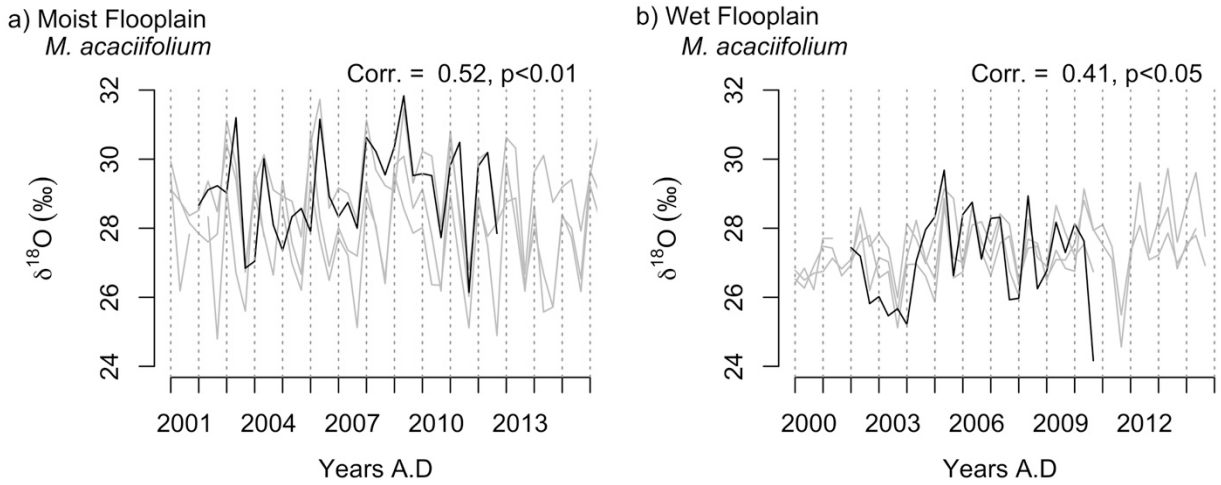

Figure I. 7. Time series of intra-annual tree-ring oxygen isotopes series ($\delta^{18}O_{TR}$) of Macrolobium acaciifolium with 3 samples per ring. a) 4 trees from the Moist floodplain site including the tree shown in the main text (black) (eps=0.78, mean interseries correlation = 0.47). b) 4 trees including the tree from the Wet Floodplain site shown in the main text (black) and 3 trees from a wet floodplain site approximately 500km upstream (eps= 0.77, mean interseries correlation=0.43). Mean interseries correlations are the mean of all pairwise correlations between all series. The coefficients shown in the top of each panel indicate the correlations between the trees with intra-ring high resolution data shown in the main text and the average series of the other 3 trees with 3 samples per ring.

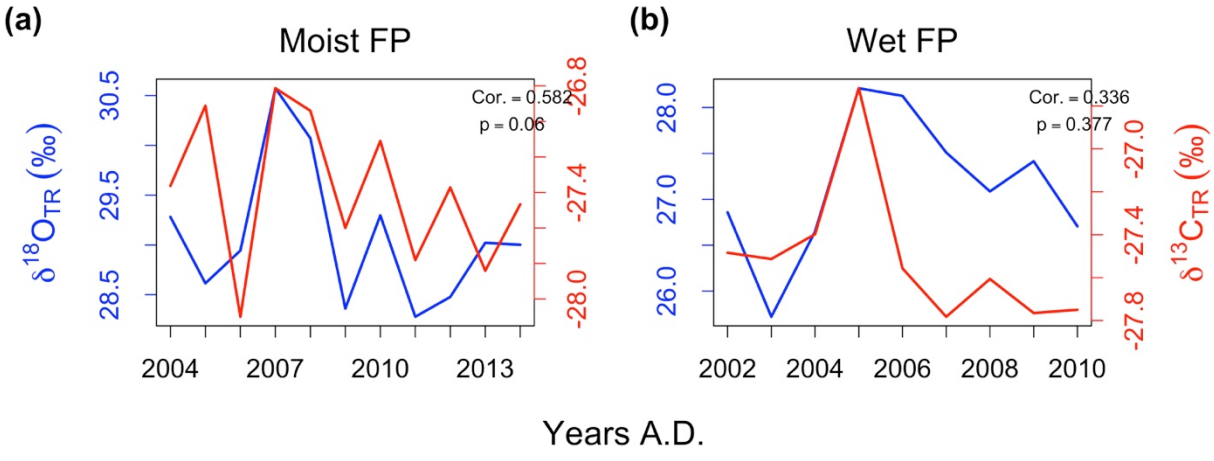

Figure I. 8. Time series of annual $\delta^{18}O$ and $\delta^{13}C$ for the two floodplain trees. Numbers indicate the Pearsons correlation coefficient and p-level. $\delta^{18}O$ and $\delta^{13}C$ values are from α-cellulose, except for the $\delta^{13}C$ series from Wet FP, which is from wholewood.

Table I. 1. List of symbols and abbreviations used in this study.

Symbol	Description	Units
$\delta^{13}C_{plant}$	Carbon isotope composition in plant tissues	‰
$\delta^{13}C_{atm}$	Carbon isotopes composition of atmospheric CO_2	‰
$\delta^{18}O_{es}$	Oxygen isotope com position at the evaporative sites in the leaf (e.g. stomata and mesophyll spaces)	‰
$\delta^{18}O_{lw}$	Oxygen isotope composition of the leaf lamina water	‰
$\delta^{18}O_{\mathrm{tr}}$	Average oxygen isotope composition of tree ring cellulose	‰
$\delta^{18}O_{sw}$	Oxygen isotope composition of rainfall water	‰
$\delta^{18}O_{air}$	Oxygen isotope composition atmospheric vapour	‰
ε^{+}	Equilibrium fractionation during evaporation of $H_2{}^{18}O$	‰
ε_k	Kinetic fractionation factor during diffusion of H_2O from stomata to the atmosphere	‰
ε_{wc}	Fractionation of oxygen during synthesis of sugars in the leaf	‰
a	Fractionation during CO_2 diffusion through stomata	‰
b	Fractionation due to isotopic discrimination during carboxylation	‰
c_i	Leaf internal CO_2 partial pressure	kPa
c_a	Atmospheric CO_2 partial pressure	kPa
e_a	Atmospheric vapour pressure	kPa
e_i	Leaf internal saturated vapour pressure	kPa
e_{sat}	Saturated vapour pressure	kPa
VPD	Atmospheric vapour pressure deficit	kPa
VPD_0	Average vapour pressure deficit over the growing season	kPa
P	Atmospheric pressure	kPa
$p_x p_{ex}$	Proportion of enriched water in the cell (p_x) and proportion of oxygen exchanged with water in the cell during cellulose synthesis (p_{ex})	%
$\wp$	Péclet number	Dimentionless
W	Leaf lamina diameter	m
L	Path length from leaf veins to stomata through the mesophyll	m
D	Diffusion rate of $H_2{}^{18}O$ in water	$m^2 s^{-1}$
u	Velocity of the advective transport of water from leaf veins to stomata	$m\ s^{-1}$
U	Wind speed	$m\ s^{-1}$
C	Molar concentration of water	$mol\ m^{-3}$
E	Leaf transpiration	$mol\ m^{-2} s^{-1}$
A	Assimilation rate of CO_2 during photosynthesis	$mol\ m^{-2} s^{-1}$
g_s	Leaf stomatal conductance	$mol\ m^{-2} s^{-1}$
g_{s0}	Maximum stomatal conductance	$mol\ m^{-2} s^{-1}$
g_b	Leaf boundary layer conductance	$mol\ m^{-2} s^{-1}$
T_{leaf}	Leaf temperature = air temperature	Celsius
T_{air}	Air temperature	Celsius

Table I. 2. Mechanistic models and inputs used in the calculation of the expected patterns of isotopic variation within tree-rings.

Carbon Isotopes fractionation
$\boldsymbol{\delta^{13}C_{plant} \approx \delta^{13}C_{atm} - a\left(\frac{c_a - c_i}{c_a}\right) - b\left(1 - \frac{c_a - c_i}{c_a}\right) \sim -27 \pm 3}$ ‰ (Farquhar et al., 1989)
$a = 4.4$ ‰; $b = 27$ ‰ (Farquhar et al., 1989); $\delta^{13}C_{atm} = 7.7$ ‰ (NOAA)
$\boldsymbol{c_i = c_a - \left(\frac{A}{g_s}\right) P}$ kPa (Farquhar *et al.* 1989)
$P = 101.325$ kPa; $c_a = 0.04154325$ kPa (NOAA, ~410ppm in July 2018) ; $A = 1x10^{-6}$ mol m^{-2}s^{-1} (assumed)
$\boldsymbol{g_s = g_{s0}\left(\frac{1}{1+\frac{VPD}{VPD_0}}\right) \sim 0.2 \pm 1}$ **mol m^{-2}s^{-1}** (assumed)
$g_{s0} = 0.3$ mol m^{-2}s^{-1} (assumed); $VPD = e_{sat} - e_a \sim 0.8 \pm 0.4$ kPa (CRU TS 4.00); $e_a \sim 2.6 \pm 0.4$ kPa (CRU TS 4.00); $e_{sat} = 0.61121\, exp\left(18.678 - \frac{T_{leaf}}{234.5}\right)\left(\frac{T_{leaf}}{257.14+T_{leaf}}\right) \sim 3.4 \pm 0.3$ kPa; $T_{leaf} = T_{air} \sim 26 \pm 2$ Celsius (CRU TS 4.00); $VPD_0 =$ growing season long term mean $\sim 1 \pm 0.5$ kPa (CRU TS 4.00)
Oxygen Isotopes Fractionation
$\boldsymbol{\delta^{18}O_{tr} = \delta^{18}O_{sw} + (\delta^{18}O_{lw} - \delta^{18}O_{sw})(1 - p_x p_{ex}) + \varepsilon_{wc}}$ ‰ (Barbour and Farquhar, 2000)
$\delta^{18}O_{sw} = -5 \pm 6$ ‰ GNIP, Brienen & Gloor (unpublished data); $\delta^{18}O_{air} = \delta^{18}O_{sw}$ ‰ (assumed); $\varepsilon_{wc} = 27$ ‰ (Cernusak and Kahmen, 2013)
$\boldsymbol{\delta^{18}O_{lw} = \delta^{18}O_{sw} + (\delta^{18}O_{es} - \delta^{18}O_{sw}) * \frac{(1 - e^{-\wp})}{\wp}}$ ‰
$\wp \equiv \frac{Advection}{Diffusion} = \frac{u}{D/L}$; $L = 0.02$ m (assumed); $D = 2.3\ x\ 10^{-9}$ m^{-2}s^{-1}; $u = \frac{E}{C}$ m^{2}s^{-1}; $E = g_s \frac{VPD}{atm} \sim 0.003$ mol m^{-2}s^{-1}; $C = 55\ x\ 10^3$ mol m^{-3}

$\boldsymbol{g_s = g_{s0}\left(\frac{1}{1+\frac{VPD}{VPD_0}}\right) \sim 0.2 \pm 1\ \mathrm{mol\ m^{-2}s^{-1}}}$ (assumed)

$g_{s0} = 0.3\ \mathrm{mol\ m^{-2}s^{-1}}$ (assumed); $VPD = e_{sat} - e_a \sim 0.8 \pm 0.4$ kPa (CRU TS 4.00); $e_a \sim 2.6 \pm 0.4$ kPa; $e_{sat} = 0.61121\ exp\left(18.678 - \frac{T_{leaf}}{234.5}\right)\left(\frac{T_{leaf}}{257.14+T_{leaf}}\right) \sim 3.4 \pm 0.3$ kPa; $T_{leaf} = T_{air} \sim 26 \pm 2$ Celsius; $VPD_0 =$ growing season long term mean $\sim 1 \pm 0.5$ kPa (CRU TS 4.00)

$\boldsymbol{\delta^{18}O_{es} = (\delta^{18}O_{sw} + \varepsilon_k)\left(\frac{e_i - e_a}{e_i}\right) + \varepsilon^{+} + \delta^{18}O_a\left(\frac{e_a}{e_i}\right)}$ ‰ (Dongmann et al., 1974)

$\varepsilon^{+} = 2.644 - 3.206\left(\frac{10^3}{T_K}\right) + 1.534\left(\frac{10^6}{{T_K}^2}\right) \sim 9.57$ ‰ (Bottinga and Craig, 1969); $T_K = T_{leaf} = 299 \pm 4$ Kelvin; $\varepsilon_k = \frac{32g_s^{-1} + 21g_b^{-1}}{g_s^{-1} + g_b^{-1}} \sim 26.5 \pm 5$ ‰ (Farquhar et al., 1989); $g_b = 0.0105\left(\frac{U}{W}\right)^{-0.5} = 1.2 \pm 0.5\ \mathrm{mol\ m^{-2}s^{-1}}$ (McDermitt, 1990; Motzer et al., 2005); $U = 0.5\ \mathrm{m\ s^{-1}}$(assumed); $W = 0.05$ (*Cedrela odorata*); $W = 0.01$ (*Macrolobium acaciifolium*)

Appedinx II
Supporting Information for Chapter 4

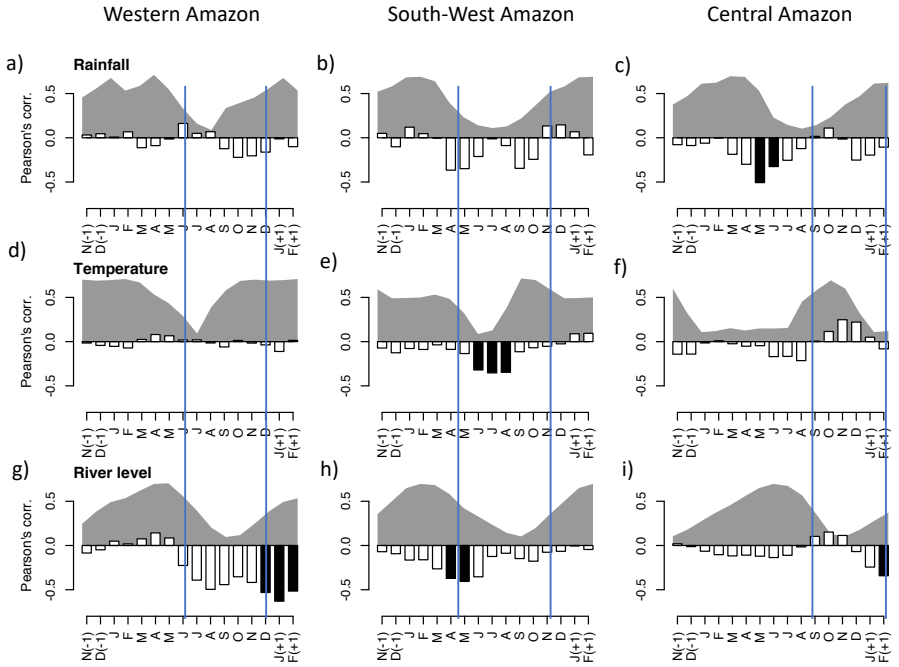

Figure II. 1. Monthly correlations between local rainfall (a-c), temperature (d-f) and river levels (g-i) for each of the chronologies. Correlations were computed for the period from 1968-2014 using 3-month averages. Significant correlations ($p<0.05$) are shown in black. Left panels (a,d,g) show relations for the site in western Amazon, middle panels (b,e,h) for the site in southwest Amazon and right panels (c,f,i) for the site in Central Amazon. Vertical blue lines indicate the start and the end of the growing season of the trees for each site. The growing season is estimated based on the topographic position of the trees on the river bank and the seasonal variation of the river levels locally.

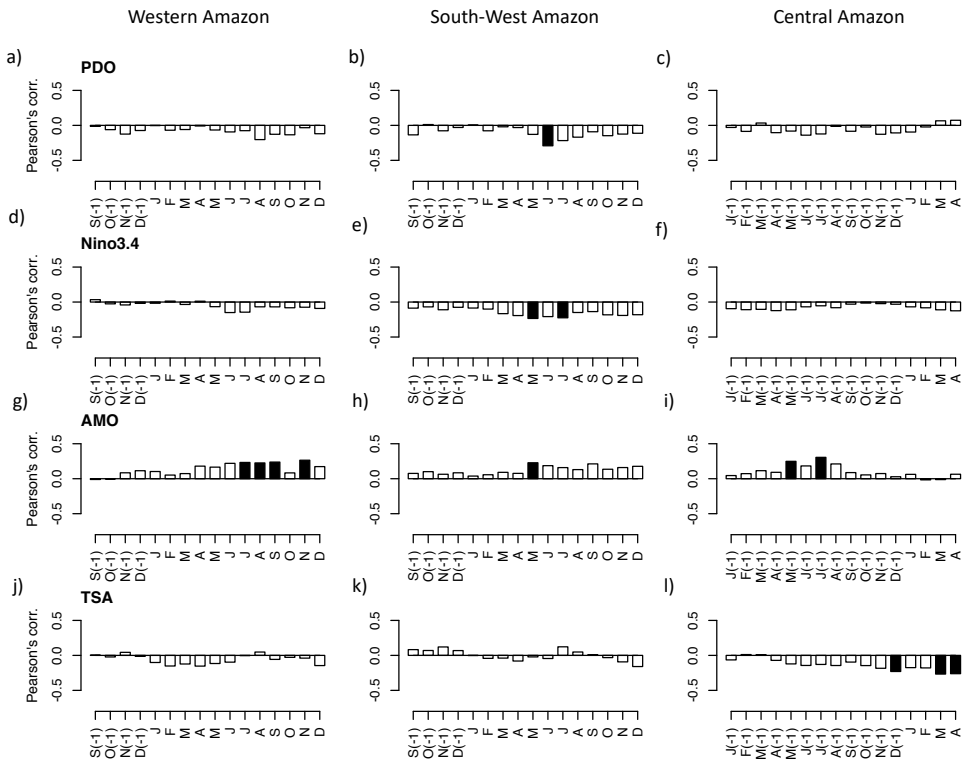

Figure II. 2. Same as before but for known controls of large scale climate variations within the Amazon Basin: Pacific decadal oscillation (PDO), sea surface temperature of the Nino 3.4 region in the Tropical Pacific Ocean (Nino 3.4), Atlantic Multidecadal Oscillation Index (AMO) and sea surface temperatures of the Tropical South Atlantic. Here the correlations were computed for monthly values rather than for 3 month averages. All correlations computed for the period from 1938 to 2014.

Appedinx III
Supporting information for Chapter 5

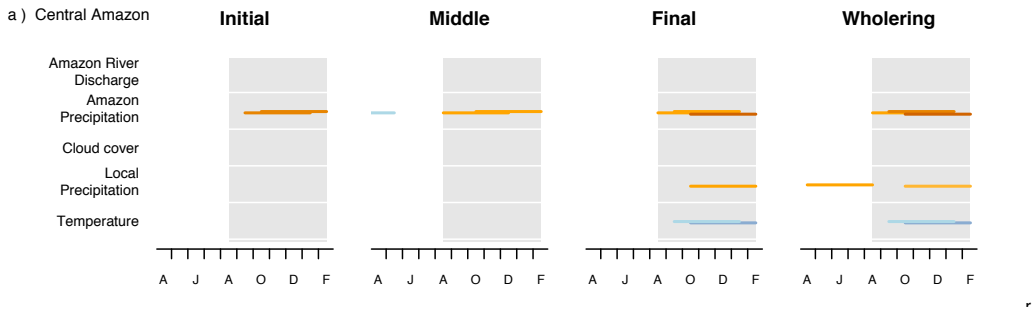

FIgure III. 1. Diagram showing the correlations of $\delta^{18}O_{TR}$ in different ring segments with 3-month means of climatic variables for the Central Amazon site. The results for the other two sites are shown in Appendix I. Each horizontal line represents one significant correlation ($p<0.05$). Grey shaded areas indicate the non-flooded season at each site. For this analyses the rings were cut into three segments prior to the analyses of the oxygen isotope ratios. Each of the three segments are displayed as *Initial, Middle* and *Final*. The correlations for the average ring $\delta^{18}O$ (*Wholering*) are also shown.

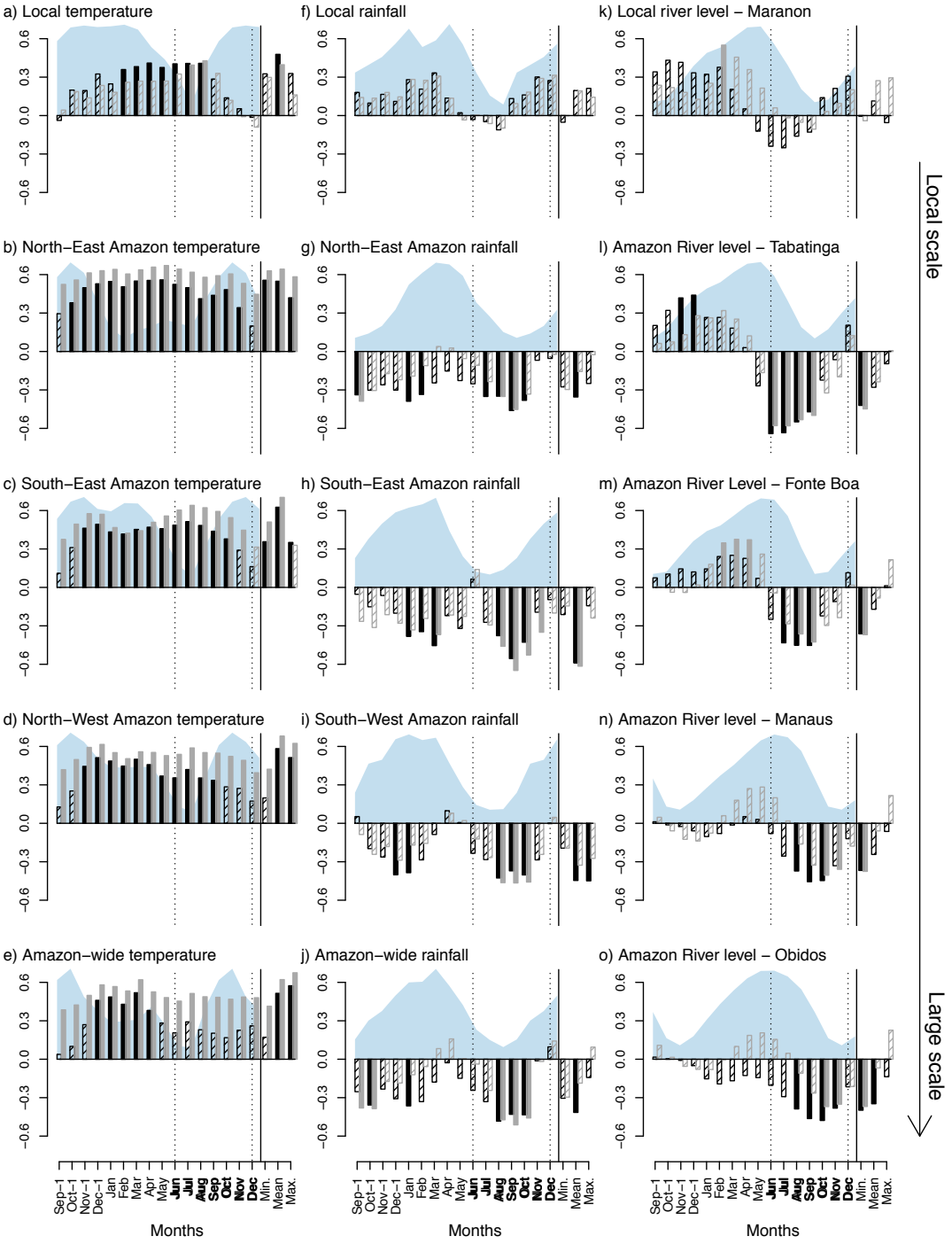

FIgure III. 2. Correlation functions for the $\delta^{18}O_{TR}$ record of the site in western Amazon and 3-montl means of environmental variables at local and large scales. Local scale variables are shown in the top row (a,f,k), and the largest scale variables are shown in the bottom row (e,j,o). Shadings indicate the seasonality (not to scale) of the variable in each graph. The start and end of growing season are indicated by the dotted lines. The growing season is also indicated by the months in bold in the x-axis. Each month correspond to the middle of 3 month averages.

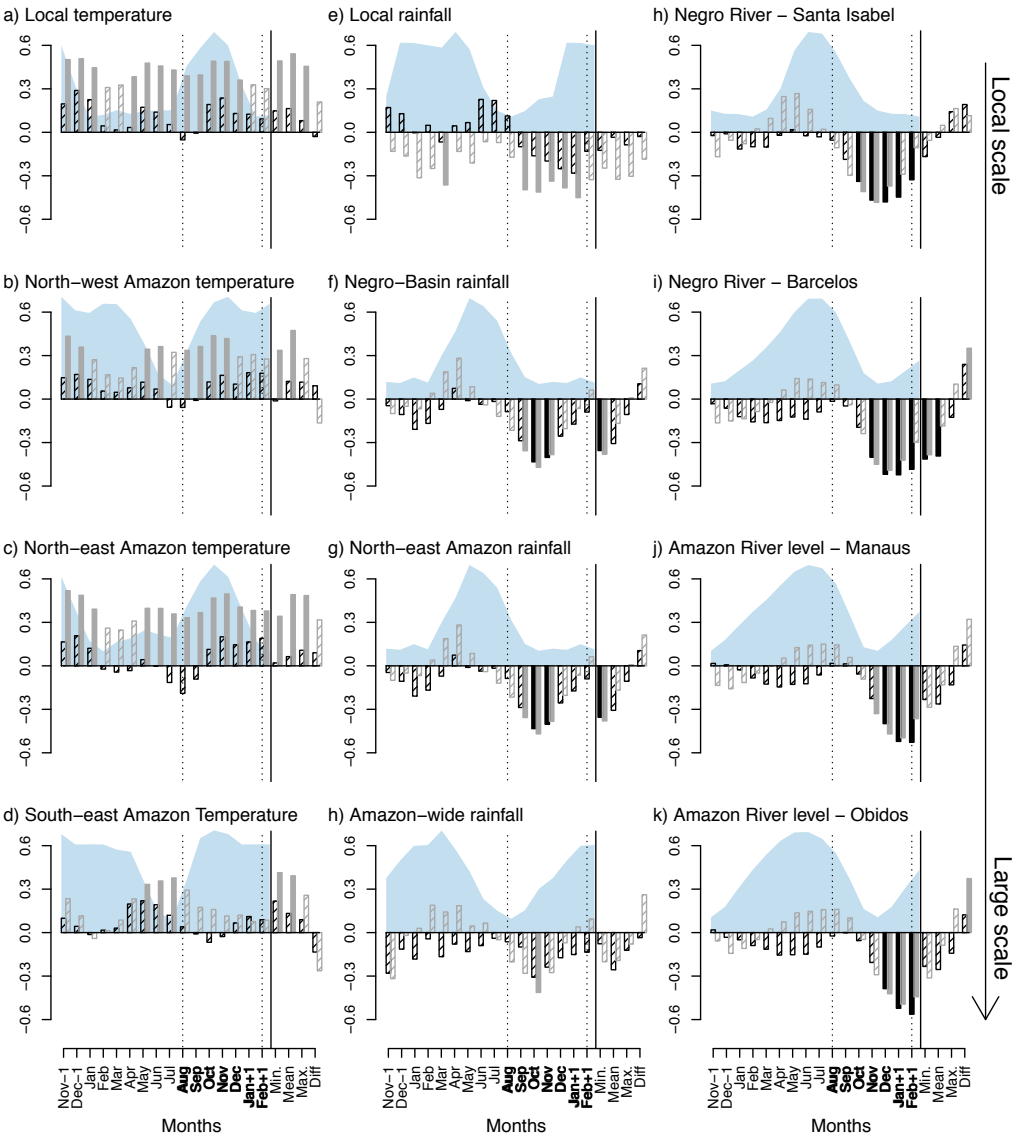

FIgure III. 3. Same as Figure 5.3.2., but for the site in central Amazon. The start and end of growing season are indicated by the dotted lines. The growing season is also indicated by the months in bold in the x-axis.

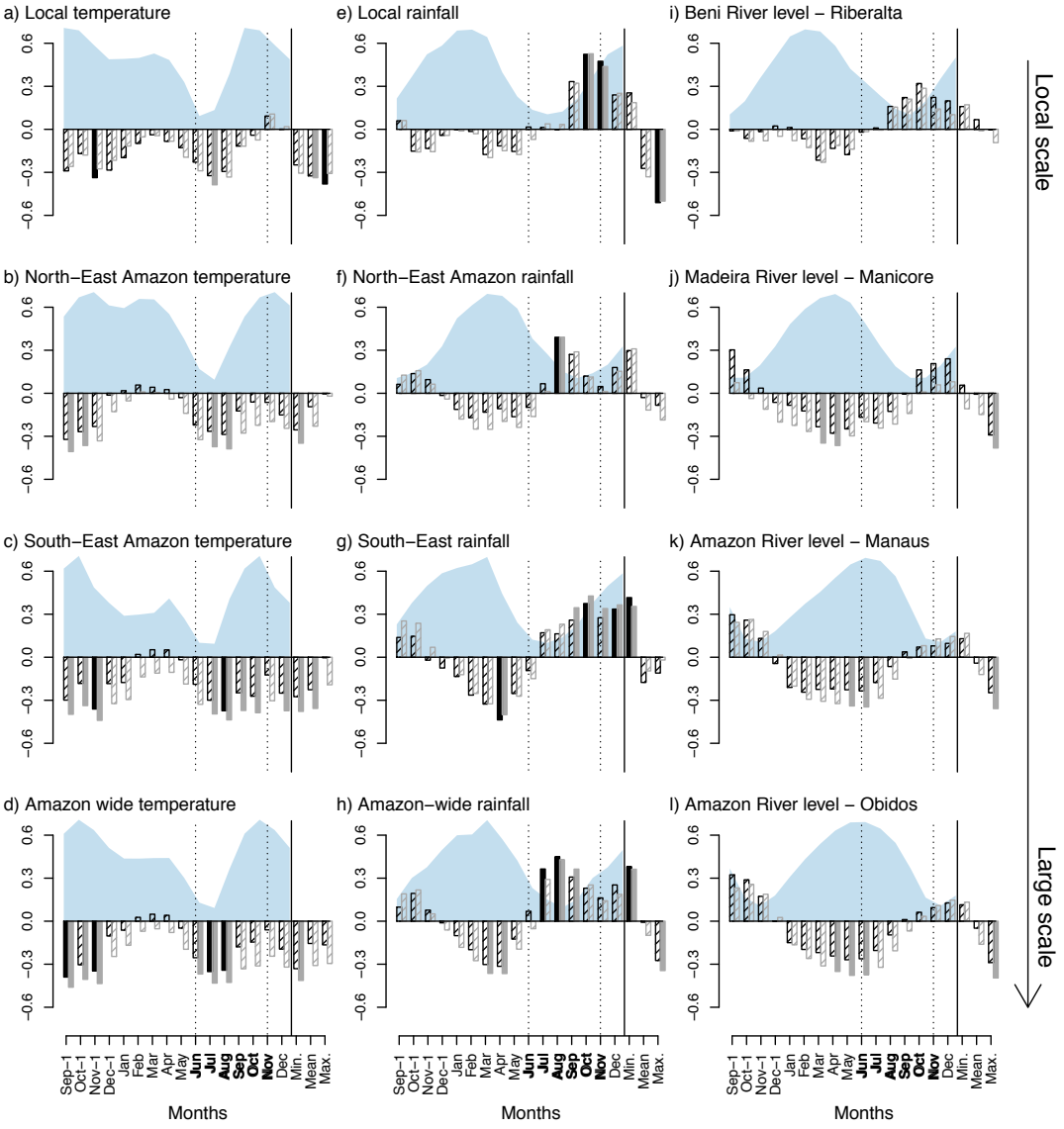

FIgure III. 4. Same as Figure S.3.2, but for the site in southwest Amazon. The start and end of growing season are indicated by the dotted lines. The growing season is also indicated by the months in bold in the x-axis.

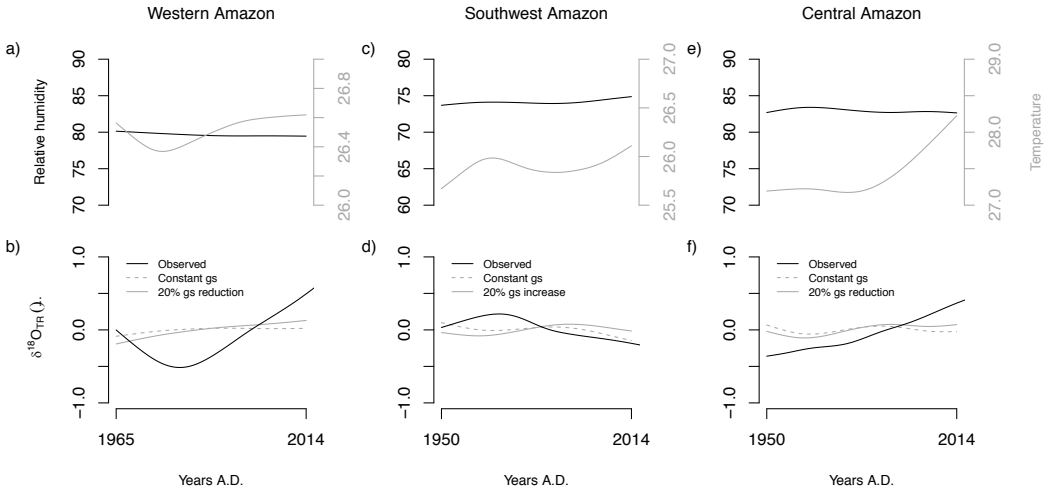

FIgure III. 5. Same as Figure 5.3 but using a path length of 0.01.